Departamento de Electromagnetismo y Física de la Materia
& Institute Carlos I for Theoretical and Computational Physics
University of Granada, Spain

Universality in Self-Organized Criticality

Juan Antonio Bonachela Fajardo
e-mail: jabonachela@onsager.ugr.es

PhD Thesis
Advisor: Prof. D. Miguel Ángel Muñoz Martínez

Granada, 2008

Editor: Editorial de la Universidad de Granada
Autor: Juan Antonio Bonachela Fajardo
D.L.: Gr. 2850-2008
ISBN: 978-84-691-8344-1

Agradecimientos

Si para cualquier persona es importante agradecer la ayuda recibida en su camino, para un estudiante ésto es sin duda algo fundamental. La formación de toda persona está apoyada siempre en el trabajo de mucha gente que sirve como fuente de conocimiento, ya sea a través de conversaciones, charlas, clases o libros.

Quizás no en lo académico, sino en lo personal, para el autor éste es a todas luces el capítulo más importante de la tesis. Aquí, en un humilde intento de agradecer profunda y sinceramente a cada uno su papel desempeñado, es mencionada toda la gente que ha aportado algo a lo largo de los años precedentes que han desembocado en el trabajo resumido en este libro.

Comenzando por el plano profesional, primero quisiera agradecer al Instituto Carlos I de Física Teórica y Computacional su apoyo para recibir la beca que ha cubierto la mayor parte del trabajo realizado en esta tesis. Más especialmente, al Departamento de Electromagnetismo y Física de la Materia de la Universidad de Granada y, en concreto, al grupo de Física Estadística y a su director, Joaquín Marro, pues no sólo me han proporcionado un sitio y un ambiente excelente de trabajo, sino que de cada uno de sus miembros he aprendido cosas que, por grandes o pequeñas que puedan parecer ahora, han supuesto algo importante para mi formación como doctor.

Gracias, pues, a Ramón Contreras, Jorge Mejías, Samuel Johnson, Carlos Pérez, Jesús del Pozo, Pablo Sartori, Paco Ramos, Jesús Biel, Antonio López Lacomba... A José Manuel, por su gestión del clúster que tan frecuentemente monopolizo. A mis antiguos compañeros de despacho, Jesús Cortés y Omar Al Hammal, por todas esas conversaciones (académicas y no académicas) que tan bien me vinieron cuando empezaba. A Pedro L. Garrido, por sus clases, su ayuda y los consejos sobre mi futuro que intentaré aprovechar en la nueva etapa que se me abre ahora. A Joaquín J. Torres y Sebastiano de Franciscis, por su sabiduría neurocientífica. A Pablo Hurtado y Paco de los Santos, que han sido en mayor o menor grado colaboradores en los artículos y, en

cualquier caso, fuentes de apoyo y conocimiento muy importantes durante estos años.

En cuanto a la gente que, tanto en sus visitas como en la distancia, ha colaborado conmigo para sacar adelante parte de esta tesis, quisiera agradecer su esfuerzo a Ivan Dornic, Hugues Chaté, José J. Ramasco, Carlos E. Fiore y Mikko Alava.

También quiero agradecer su hospitalidad a aquellos científicos que me acogieron en sus centros durante mis estancias en el extranjero: Matteo Marsili, Ginestra Bianconi y, muy especialmente, a Haye Hinrichsen: el periodo que pasé en Alemania fue clave para mi formación como investigador (aunque el tema en el que trabajé no tuviera mucho que ver con el de esta tesis).

Por último, y como transición entre el plano profesional y personal, quiero expresar mi más profundo agradecimiento a Miguel A. Muñoz, mi director de tesis y, en mi opinión, uno de los más brillantes físicos teóricos de su generacion. Él ha sabido guiarme por los caminos tortuosos de la Física Estadística del no-equilibrio, y confeccionar el esquema inicial de trabajo que luego daría como fruto esta tesis. Su paciencia infinita, entusiasmo y espoleantes conversaciones han sido clave para llegar al final de un trayecto que, en ocasiones, no sólo se me ha hecho difícil, sino que a veces ha parecido inalcanzable. Su manera de exponer y comprender hasta sus últimas consecuencias cualquier problema que se plantea y su manera de entender la Ciencia hacen que sea el ejemplo de científico en el que me gustaría llegar a convertirme algún dia.

Si para la formación de un científico es importante la gente con la que convive en el plano profesional, más importante todavía es la gente con la que convive en el plano personal. Muchas veces ambos aspectos están mezclados, y uno tiene la fortuna de trabajar con compañeros a los que puede considerar amigos. Aunque no cabe duda de que el ambiente de trabajo que he disfrutado responde a esta descripción, en un merecido apartado especial he de considerar a Manuel Diez Minguito. No sólo por las horas de charla sobre la Física, la vida (presente y futura), etc., sino por los muchos momentos divertidos, desde aquella maratón de "El Señor de los Anillos" hasta las carreras con el "Re-Volt" y las clases magistrales sobre pintura de figuritas.

Otra gente por la que no puedo tener más que palabras de agradecimiento es por mis compañeros de carrera. Diego Salas y Dani Partal ya demostraron su paciencia como pareja de prácticas o de grupo de trabajo. David Navidad, que a ésto debe sumarle un extra por los primeros años de doctorado. Pero una mención honorífica se merece Pablo Sánchez Moreno, que no sólo ha compartido conmigo horas de trabajo (in situ, online o incluso via telefónica)

en estos diez últimos años, sino que ha sido compañero de aventuras inolvidables (aquel primer Linux, la maratón de "La Guerra de las Galaxias"...) y las que quedan!!.

No sería justo dejar de agradecer a los grandes maestros, de cuya inspiración ha salido la banda sonora de las muchas (muchísimas) horas de programación, cálculo y escritura que conforman mi formación como licenciado y doctor. Así pues, debo nombrar a John Williams, Howard Shore, Hans Zimmer... por un lado, y a Dream Theater, Symphony X, Rage, Harem Scarem, Guns'n'Roses, Helloween, Estigia... por otro, porque sin ellos todas estas tareas habrían sido un poco más aburridas.

Pero sin duda, a quien más tiene que agradecer toda persona que logra algo en su vida es a su familia. Desde mis padres, que me enseñaron con su ejemplo cómo debe comportarse y trabajar un buen profesional, a mi hermano, mis tias, mi tio, mis primos, mis abuelos ... toda esa gente, que siempre está y estará apoyándome incondicionalmente, por el "simple" hecho de quererme. En ésto tiene especial mérito mi familia política, porque aunque soy un "agregado" a ella, siempre me han hecho sentir que fuese uno más de ellos (sin ir más lejos, gracias a mi cuñado Armando la mitad de esta tesis ha llegado a buen puerto; sólo alguien que te quiere como a un hermano es capaz de prestarte su portátil durante casi dos meses!!).

Y por último (lugar de honor, precisamente por ser la persona que más merece mi agradecimiento), quiero nombrar a mi mujer, Irene. Tan sólo ella ha sido capaz de hacerme continuar cuando me han faltado las fuerzas, tanto en lo personal como en lo profesional. A ella le debo todo, lo que soy y lo que sé, porque ella ha sido, es y será sin duda el motivo por el que merece la pena luchar hasta alcanzar cualquier objetivo que uno se marque en esta vida.

A todos vosotros, mi más sincero agradecimiento.

Dedicated to Irene

Preface

One of the most fascinating and important phenomena studied by Statistical Physics is the so-called Self-Organized Criticality (SOC). Since Bak, Tang and Wiesenfeld (BTW) coined this term in 1987, more than 3000[1] articles written in these last 21 years about the topic validate the statement which this thesis start with.

The concept of Self-Organized Criticality was introduced with the ambitious aim of being the explanation of the ubiquity of certain mathematical functions which describe some properties of real systems in Nature. Due to the initial impact of the work of BTW, SOC has been able to go beyond the frontiers, not only of its original discipline (Statistical Physics), but also of Physics itself, being a concept used on articles in Biology, Geology, Neuroscience, Ingeneering, Chemistry, Mathematics and even in Social Sciences like Psychology and Humanities.

This burst of works and the broad range of fields in which SOC can be applied have made difficult to find one general and broadly accepted vision about what SOC really is; in fact, there is not *a* definition of SOC in literature, but (and depending on the discipline used to study it) there are many different definitions, sometimes mutually incompatible, of the term.

The aim of this thesis is *not* to review all the work published about the topic up to date. This thesis tries to cover some general aspects of SOC from the perspective of phase transitions and their associated universal features, and this is what the reader should expect from the book.

In **chapter 1**, the basic ideas about this topic are presented. After justifying its importance, the difference between self-organization, criticality and Self-Organized Criticality is clarified. It is pointed out under which conditions the latter is expected, and a preliminary definition for SOC, established.

[1] Source: ISI Web of Knowledge, http://www.isiwebofknowledge.com/

Also, it is introduced the paradigmatic example of SOC, the sandpiles, with the original model of BTW as well as its stochastic version by Manna, and the more realistic Oslo ricepile model. These examples allow to understand how the features defined in the first part of the chapter as characteristic of SOC are applied to specific models.

Meanwhile, the usual observables used in the study of these models are introduced, recalling the concept of critical exponent, which allows to talk about universality classes in SOC. The basic concepts related with phase transitions can also be found in appendix A.

In **chapter 2**, SOC is treated from the point of view of a non-equilibrium phase transition with many absorbing states. This allows to use the typical observables defined in these systems to analyze SOC systems. Next, it is built a bridge connecting these magnitudes with the ones defined in the previous chapter, and *conservation* is used to define a universality class embracing both stochastic sandpiles and absorbing state systems: the Conserved Directed Percolation (C-DP) class.

After that, similarities and differences between this universality class, which this thesis is focused on, and the absorbing-state-system paradigmatic class (Directed Percolation, DP) are pointed out.

In the end, a continuous equation is deduced in order to describe at a mesoscopic level the behavior of the already defined C-DP universality class.

Chapter 3 is devoted to compare the two above mentioned universality classes, as well as to justify the importance of the availability of tools able to distinguish clear and simply whether a system under suspect belongs to one or the other universality class.

Two novel and conceptually simple criteria are presented for differentiation, and their performance is tested by using two models historically missclassified as representatives of DP among sandpiles.

A different perspective from which SOC can be seen is by using elastic interfaces in random media. This is the scope of **chapter 4**.

It is shown how to translate the SOC language into the interfaces one, and the opposite procedure. Next, the apparent incompatibilities between the observables measured in each description are explained. Thus, it is stated that certain types of SOC and interface models are just two different ways to observe the very same phenomenon. This last assertion is also justified by means of Renormalization Group (RG) arguments and RG functions measurements.

Chapter 5 addresses the controversial topic of non-conservation in SOC, confirming its essential part in the existence of Self-Organized Criticality. Hence, an ultimate definition of SOC can be made.

Also, examples in Nature, historically claimed to be SOC, are analyzed in this chapter, to determine whether they are critical or not. It is shown that a very concrete degree of dissipation can be present for a system to continue being critical, stating in this way up to which point the condition of conservation can be relaxed in SOC.

The last chapter (**chapter 6**) is devoted to present some of the experiments showing the features of SOC theoretical models. Some of the earliest experiments, which did not observe the critical behavior of SOC, are studied. But also those which successfully exhibited real scale invariance, becoming the paradigmatic experimental realization of SOC.

On the other hand, the circumstances and conditions under which SOC can be expected in a real system are studied.

In the appendices, the above mentioned summary of some basic concepts about phase transitions and universality can be found (appendix A). But also the steps necessary to map a microscopic reaction-diffusion set of equations into a mesoscopic description of the same problem (appendix B), and the set of tables embracing the results exposed in this thesis (appendix C).

This thesis is written in English, but a summary in Spanish is also included (appendix D) with the purpose to fulfill the requirements to obtain the degree of Philosophy Doctor in Physics with European level, as ruled by the regulations of the University of Granada.

Also, a list of publications of the author is in the last pages of the thesis (see appendix E). The work content in this book is not, of course, all the made by its author. There is much work which has formed part of the learning necessary to obtain the results of some of the parts of this thesis, as well as other published work which, as it is not directly related to this topic, is not explicitely cited. Nonetheless, it can be found in the list of publications above mentioned.

Granada, December 2008.

Contents

Chapter 1

Introduction

Consider one of the tectonic plates forming the crust of the Earth. In a rough sketch of its complicated real behavior, it can be said that a plate travels floating on the internal magma (molten rock) of the planet, in a slow motion in which different plates can converge or clash. When two plates are in contact, the different geologycal processes occurring in the proximity of the contact zone (a fault) can be represented, in such an oversimplified scenario, by only two relevant events: a long-termed process of accumulation of the stress produced by the friction between plates, and an instantaneous relaxation of all the stored stress in a phenomenon referred to as an **earthquake**.

When the intensity of the numerous different earthquakes taking place at different zones of the Earth is collected, and the frequency of occurrence of the intensities is depicted in a graphic with logarithmic axes, the resulting curve (see Fig.1.1) follows with reasonable accuracy, the so-called *Gutenberg-Richter law* [1, 2]:

$$P(I) \sim I^{-\gamma}, \tag{1.1}$$

where the logarithm of the intensity I is called the **magnitude** of the earthquake.

The special mathematical shape of the Gutenberg-Richter law, a *power law*, entails some underlying physical consequences (see appendix A.1.2). As can be observed in Fig.1.1, many different intensities I are measured, up to a certain magnitude M ($M \sim \log(I)$); in an ideal case in which the system under consideration is infinite, it could be said that all intensities

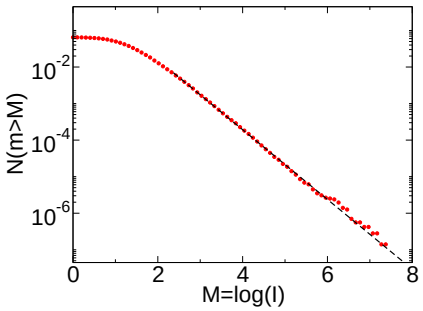

Figure 1.1: Normalized accumulated frequency of occurrence N of earthquakes with magnitude $M \sim \log(I)$, Southern California Catalog, from year 1932 up to the present. As M is already a logarithm, when the N axis is taken in logarithmic scale the Gutenberg-Richter power-law (Eq.(1.1)) is shown as a straight line. Source: Southern California Earthquake Data Base, http://www.data.scec.org.

are possible and, therefore, that there is no *characteristic length* into the system: the behavior described by this law is **scale free**. Moreover, when the distribution of epicenters of the considered earthquakes is observed, very sharp spatial structures or patterns appear.

These features are the hallmark of **complexity**, which implies the existence of a certain hierarchical internal structure, i.e. organization. To be more specific, **self-organization**, because the complex structures (also called *fractals*[1] [3]) appear spontaneously due to the cooperative behavior between the components of the system (short interactions giving rise to long range effects, that is **emergence** of complexity). Along with the mentioned spatial scale-free behavior, complexity entails temporal scale-free behavior as well which, in many cases, arises in form of $1/f$ noise[1].

In Nature, many different systems share the non-trivial spatial and temporal scale-invariant behavior of earthquakes. The examples are countless and cover all the levels of observation, from the nanoscopic structures of carbon nanotubes to the kilometric surface of river networks; and the inert matter as well as the very foundations of life (see Fig.1.2).

The presence of fractals and power laws can be the result of many mechanisms interacting to build them: a combination of exponentials, the result of certain relations between stochastic variables, the presence of some degree of preferential selection, chaos... [4, 5]. But when the power law is associated

[1]See appendix A.3

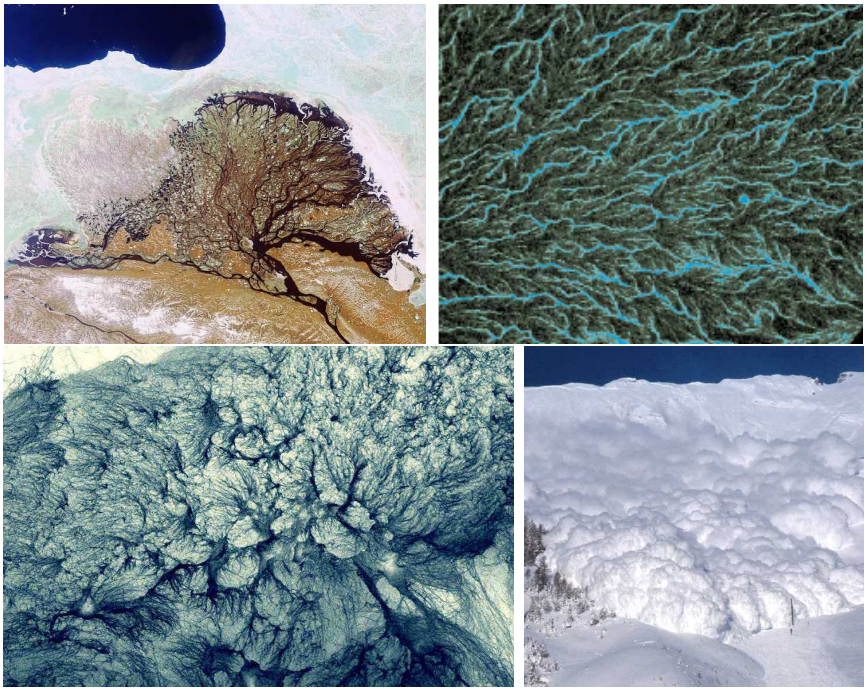

Figure 1.2: Fractals in Nature. Anti-clockwise: Delta of Lena River, Russia; Growth pattern of carbon nanotubes; Avalanche of Snow; Fluorescence optical microscopy image of highly condensated DNA.

with the divergence of correlations, it is signature of **criticality**[2]. Consider the case of the above mentioned fractal structure of the epicenters of earthquakes or any of the examples depicted in Fig.1.2; the formation of such patterns implies that an interaction between the different parts of the system exists, and it is able to be transmitted through all its extent, i.e. the *correlation length/time* is only limited by the size of the system, and therefore it may diverge in the *thermodynamic limit*[2].

The ubiquity of scale-free behavior and self-organization in Nature led Bak, Tang and Wiesenfeld (BTW) to coin the term **Self-Organized Criticality (SOC)** to explain the emergence of complexity in dynamical systems with many interacting degrees of freedom without the presence of any external agent [1, 6]; SOC was devised to be a sort of supergeneral *theory of complexity*.

As we will see, neither all self-organized systems in Nature are critical nor all power laws in there are caused by SOC. Regardless of the cause of this complex behavior, the truth is that power laws are frequent in Nature. This is an observational fact. Maybe the claim of BTW was excessive, and the aim of the original article too ambitious, but it opened a door and attracted the attention of the scientific community towards a very fascinating phenomenon that, in a greater or lesser extent, could be the cause of the scale-invariance of many systems in Nature[3].

It is important to note that SOC is not a new way to label the scale invariance observed in Nature. It involves many more requirements, which many natural systems displaying scale-free properties do not fulfill. In the following sections, the common parts of the dynamics of SOC systems, as well as the basic conditions for a system to exhibit SOC, are presented.

1.1 Avalanche Dynamics

In the more technical language of Statistical Physics, the above mentioned tectonic plates of the crust are systems out of the equilibrium, spatially extended, with many degrees of freedom interacting between them as the response to an external local perturbation, being this response highly nonlinear: in the simplified scenario used up to now, the contact zone between

[2] See appendix A.1.2.

[3] See [7, 8] for a discrepant point of view.

plates (the fault) could be seen as a discrete two-dimensional lattice whose positions interact by means of a certain force, which can be accumulated by the sites until an instantaneous relaxation involving all the system occurs (the earthquake). This kind of evolution, common to all SOC systems, will be here referred to as **avalanche dynamics**. The basics of such dynamics are usually represented by means of the following simple steps:

- **Driving**: An input of information, energy... is introduced into the system. In the case of earthquakes, the input is stress or, ultimately, energy. This magnitude will be used, for simplicity, hereinafter.
- **Activation**: Each site receiving energy, either by the external input or by means of the interaction with its neighborhood, accumulates it until certain **threshold** is exceeded. Then, the site is declared *active*.
- **Relaxation**: An active site redistributes (all or a fraction of) its accumulated energy between its neighbors. This local relaxation (or *toppling*) rule may differ for each system. It is the starting point of a chain reaction or **avalanche** (the *hypocenter* and the earthquake, respectively, in the initial example). The relaxation of a site can, of course, cause more activations into the avalanche.
- **Dissipation**: When redistribution events reach the boundaries of the system (the surface of the crust[4], for instance), energy is dropped off[5].
- **Resting**: When there are no more active sites in the system, the avalanche stops, and a new external input is added.

Avalanches are supposed to occur instantaneously, in contrast to perturbation events. This is the case of earthquakes, where sites accumulate the stress caused by the friction between the tectonic plates of the crust through hundreds of years, and release it during an event which lasts only a few seconds (minutes, at most).

With this type of dynamics, the system under consideration steadily evolves towards a state in which, on average, outgoing energy balances ingoing one, and a scale-free behavior only limited by the system size is observed; it is the *stationary critical state*. The Gutenberg-Richter law, Eq.(1.1), is one example; but other observables behave in a similar way. The **lifetime** of an

[4]The epicenter is the first point of the surface reached by the earthquake.

[5]Other types of dissipation can be defined; see chapter 5 for further discussion.

avalanche is defined as the time interval between the first activation and the time at which there are no active sites left. The **size** of an avalanche is the number of topplings produced during this lifetime. Thus, in the stationary critical regime, all sizes and lifetimes are possible, small events as well as large ones, with the only limitation of the system size.

This critical behavior is manifested, for instance, in the probability distribution of these magnitudes. In this self-organized critical state, the probability for the number of topplings involved during an avalanche to be s is:

$$P(s) \sim s^{-\tau} \mathcal{F}\left(\frac{s}{s_\xi}\right) \tag{1.2}$$

where $\mathcal{F}(x)$ is a *scaling function*, and behaves like:

$$\mathcal{F}\left(\frac{s}{s_\xi}\right) = e^{-s/s_\xi} \tag{1.3}$$

where s_ξ is the characteristic size of an avalanche. Recalling the concept of characteristic length[6], Eq.(1.2)-Eq.(1.3) mean that this probability distribution follows a power law for sizes $s < s_\xi$, and decays exponentially fast from there after. In other words, s_ξ establishes a **cutoff** in the power law behavior, a characteristic length ξ. As the stationary state is supposed to be critical, this cutoff is expected to be a **finite size effect**[6] (i.e. $s_\xi = s_\xi(L)$, where L is the linear size of the system), with the form of a power law, like in ordinary phase transitions:

$$s_\xi(L) \sim L^{D_f} \tag{1.4}$$

where D_f is the so-called **fractal dimension**. Thus, the distribution function can be written as:

$$P(s) \sim s^{-\tau} e^{-s/s_\xi(L)}. \tag{1.5}$$

This is called the **finite-size scaling ansatz** (FSS ansatz), and involves that the deviation from the critical behavior of the distribution function $P(s)$ is due only to a finite size effect. $P(s)$ can be seen as a *spatial response function*. In the very same way, it can be defined its temporal counterpart.

[6]See appendix A.1.2.

The distribution function of the duration of an avalanche (i.e. its lifetime; t, from now on), fulfills:

$$P(t) \sim t^{-\tau_t} e^{-t/t_\xi(L)} \tag{1.6}$$

where:

$$t_\xi(L) \sim L^z \tag{1.7}$$

that is, the only deviations of lifetime probability distribution from the power-law behavior are caused by finite size effects[7]. z is the *dynamic exponent*, which relates space and time. Although many more observables can be defined, for the moment only probability distributions will be used, as an illustrative example of critical observable to be applied to the systems studied in this chapter.

1.2 Basic Ingredients

The phenomenological description of the dynamics made so far is the only characterization of SOC given in most of the articles in the literature. In fact, the minimal set of necessary and sufficient conditions for a system to display it is still an unsolved problem. In what follows, are analyzed one by one the most important features of SOC, with the aim of finding a general definition of it.

The Threshold

As seen above, in the dynamics of a SOC system there is a *threshold*, i.e. a condition for toppling. In SOC models, it is one quantity that, when exceeded by the stored energy of a site, turns it into active.

But the presence of a threshold is more than a condition for instability; it is a condition for *stability*: the threshold allows the system to accumulate some energy during a period of time; if it would not exist, a site receiving

[7] As this distribution is related with the power spectrum $S(f)$ (see appendix A.3), a cutoff in $P(t)$ is translated into a crossover in $S(f)$ from non-trivial behavior to trivial white noise.

energy would be active, regardless of its history (stored energy), and the system would be indefinitely in a regime of avalanches involving many sites, but only a few energy. Without a threshold, in a finite conservative system the initial energy would be transported from the initial seed to the border in a trivial strictly diffusive motion, in which the boundary dissipation is the only way for avalanches to die; but in the thermodynamic limit, all avalanches would be infinite.

On the opposite extreme, an infinite threshold would make each site store the initial received energy, without any possible interaction nor energy transport; the system would be trapped into an infinite series of unitary size avalanches.

In addition, the existence of a non-trivial threshold, along with a conservative redistribution rule, allow the system to develop a *long-term memory*, responsible for the correlations between sites which, in the end, give rise to the scale-free behavior of the system (see below).

The Adiabatic Driving

To procure the independence of avalanche events observed in real SOC systems, in SOC models it is also present an **adiabatic driving**: each input is to be introduced in the pile only when all activity has ceased. This condition is also called **slow driving**.

If a slow driving is not performed, one avalanche would start while another one is running, and it would be impossible to define what such event is, blurring the real behavior of the system. In the thermodynamic limit, each initial perturbation must be applied at only one of the sites, which ensures a clear definition of individual avalanche.

Separation of Time Scales

At this point, it is useful to distinguish between *driving time* and *avalanche internal time*, i.e. lifetime. The time between two perturbations is represented by τ_P and, only for this discussion, lifetime (t) is represented by τ_R.

As said in the overview of the dynamics, avalanches are supposed to occur instantaneously (i.e. $\tau_R \to 0$) as compared with perturbations, and therefore $\tau_R \ll \tau_P$. It is natural, thus, to define a parameter to express conveniently this relation. Let κ be the ratio between both time scales [9]. Then, the condition fulfilled by SOC systems is:

$$\kappa = \frac{\tau_R}{\tau_P} \to 0. \tag{1.8}$$

This parameter will be called **Grinstein parameter** hereinafter. Eq.(1.8) entails an **infinite separation of time scales**. $\kappa = 0$ is only fulfilled in the thermodynamic limit; in a finite system, Eq.(1.8) leads to a finite correlation length, given by the system size.

In a standard nonequilibrium system, relaxation and perturbation time scales are comparable; therefore, this novel feature is specific of SOC systems. In fact, it is a key ingredient of these systems, and it requires the existence of a threshold[8].

Metastability

The requirement of such limit for the Grinstein parameter and the existence of a threshold lead to another essential feature of SOC systems: **metastability**. When the stable state of a real SOC system is perturbed, eventually an avalanche is triggered, after which the system arrives to another metastable configuration.

In SOC models, the system remains stable, accumulating energy, until one site exceeds the threshold; then, an activation event occur, and an avalanche takes the system to another metastable state.

The evolution of SOC systems could be sketched as a hopping series from one metastable state to another, and the detonators of these jumps are the perturbation events.

Self-Organization

A key feature of a SOC system is the self-organized character of its dynamics. But in their modelization, the existence of an external driving is necessary to reach the stationary state. It implies that there is a mechanism which is only activated at a very specific moment of the evolution; it is, in some sense, as if the system would need a *supervisor* [11]. This would make criticality in SOC systems as restrictive as equilibrium or standard nonequilibrium phase transitions are. Contrarily to those cases, in SOC, apparently, no fine-tuning

[8] In [10], an example of violation of this feature and its consequences can be found.

of a parameter is present, but the systems needs the control of an external agent.

As will be discussed in chapter 2, this supervisor can be replaced by a driving which is always present, but in a rate h so small that perturbations are not expected to occur in the course of an avalanche; then, $\tau_P = 1/h$. There would be, thus, a condition for driving, $h \to 0$, that must be put together with the dissipation condition: as dissipation is limited to the boundaries, if a dissipation rate ϵ is defined, it would be a function inversely proportional to the system size (L) and, therefore, would vanish ($\epsilon \to 0$) in the thermodynamic limit. These two conditions, together with $h/\epsilon \to 0$, are equivalent to the time scale separation condition, represented by Eq.(1.8). Now, there is no supervisor, but a sort of tuning would be necessary for criticality.

SOC is usually presented in the literature as a theory which explains scale-free behavior without any parameter tuning. Even if the requirement $\kappa \to 0$, which constitutes the tuning of the Grinstein parameter to a vanishing value, seems to contradict the "self-organized" part of the term "SOC", the fact is that this condition is naturally satisfied by many real systems. For example, it is blatantly obvious that the scale separation is present in earthquakes, where the external supervisor is just the natural slow motion of plates in the crust. *SOC is not, thus, a supergeneral theory* (time scale separation, for instance, is a restrictive condition), but it can be naturally achieved by a system interacting with its environment.

The Control Parameter

A related confusion stems from the affirmation that SOC entails **generic scale invariance** or a lack of **control parameter**[9].

In a standard critical point, there is only one set of values for the parameters of the system which makes it critical; in generic scale invariance, *any* set of values makes the system critical. In a SOC system the latter is also true, but at least one of the parameters is dynamic, that is, it evolves as driving events succeed. Thus, for a predefined choice of the rest of parameters, the dynamic parameter is driven towards its critical value without any apparent external tuning of it. **The critical point is an attractor of the dynamics**, reached due to the necessary time scale separation, given by Eq.(1.8)

But how is the control parameter attracted to its critical value [11]?.

[9] See appendix A.1.2

Consider a system whose dynamics is the defined in the previous section. Energy $E(\vec{x},t)$ is stored at each site of the system, being $\overline{E}$ its density. Consider as initial state the one in which $E(\vec{x},0)=0 \ \ \forall\vec{x}$. In each driving event (whether it be with the slow-driving process or with a constant rate h), $\overline{E}$ is increased a fixed amount dE. At the first stages of the evolution of the system, energy density is not large and driving events trigger only a few activations; moreover, the first avalanches cannot propagate a long distance, and activity decays exponentially fast to zero. The system is in a **subcritical regime**. Driving goes on. When $\overline{E}$ is large enough, any perturbation triggers a reaction; all avalanches spread over all system, and the boundaries are the only limit for them; there is a characteristic size (and activity density) for these events given by the size of the system, which is now in a **supercritical regime**. But when activity reaches the border during large events, energy is dissipated and $\overline{E}$ decreases a (non-fixed) quantity $d\overline{E}$. As energy is lowered, so it is the activity during an avalanche, and the system enters again a subcritical state. Then, a driving is performed and the cycle starts again.

In this way, after an initial transient, $\overline{E}$ is maintained around a specific value $\overline{E}_c$, with fluctuations which disappear in the thermodynamic limit[10]. Driving ($d\overline{E}/dn>0$, where n is the number of driving events) and dissipation ($d\overline{E}/dn<0$) events drive the system towards a balance of energy outflow and inflow, a stationary state in which all avalanche sizes or durations are possible, and correlation length or time span throughout the system. All the response functions become scale free. The system reaches a stationary **critical** state: the SOC stationary state (see Fig.1.3).

It is obvious that, in this discussion, energy density is *the* control parameter. On the other hand, activity density would be the **order parameter**[11] because, when energy is low, activity decays exponentially to zero, and when is large, a stationary value for it could be defined if finite size would not stop the avalanches. *The coupling between order and control parameter is the mechanism of the dynamics responsible for attracting the control parameter to its critical value.*

In summary, fine-tuning or "supervisors" are implicit but hidden by the natural evolution of systems exhibiting SOC, which leads the control parameter to fluctuate around its critical value. Is in this sense how *self-organization* must be understood here.

[10] As these fluctuations are due to the increasing and decreasing of the density, they are inversely proportional to the size of the system.

[11] See appendix A.1.

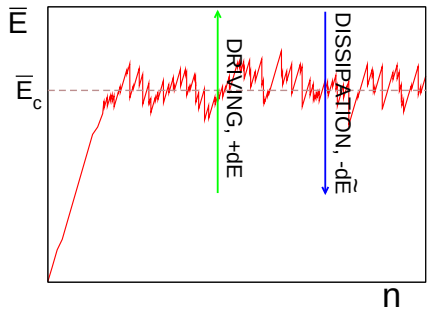

Figure 1.3: Route to criticality. Driving and dissipation of energy keep the system around the critical value of the density, $\overline{E}_c$, with infinitesimal fluctuations inversely proportional to the system size.

Conservation in SOC

So far, it has been shown that the existence of a threshold and slow driving can be summarized in the time scale separation condition and metastability. This two features are essential for SOC. Also, the fact that the critical point is an attractor of the dynamics of the system, to ensure "spontaneous" criticality. The last feature under discussion is **local conservation**[12].

Many of the most prominent systems claimed to be SOC are clearly non-conserved, in the sense that during every redistribution of the physical quantity stored at a site, part of it leaves the system. That is, dissipation is local and not only limited to the boundaries of the system.

The following heuristic argument allows to understand why local conservation implies scale-free behavior in systems with avalanche dynamics [9]. Consider a system whose dynamics is the described in section 1.1, using energy as the stored quantity at its sites. If the system reaches a stationary state for the energy density is because, on average, the amount of energy introduced with the driving can be dissipated (global conservation). If redistribution rules are conservative (local conservation), the only way in which this condition is fulfilled is by transporting any energy excess from the initial seed to the borders. In this way, large amount of energy excess is related with large avalanches, and therefore these large events are not frequent as compared with small events. Thus, the distribution of size/duration of avalanches should reflect this, and the fact that a characteristic size/time

[12] At this point, it is clear that for the SOC stationary state to be reached it is necessary a *global* conservation in the dynamics.

(like the one appearing in an exponential distribution, see Eq.(1.2)-Eq.(1.7)) is not possible because then it would be impossible in the thermodynamic limit to transport energy to the borders and, hence, to fulfill the stationary state condition. Power laws might be, thus, expected.

In summary, SOC is expected for a system with avalanche dynamics and a conservative relaxation rule. It leads to the conclusion that, together with this dynamics, conservation is a sufficient condition for SOC. Thus far, we have not provided arguments to discern whether conservation is a necessary condition; this discussion is delayed until the chapter 5, where nonconservative systems are deeply analyzed.

All the models of SOC to be studied in this chapter and in chapters 2-4 are locally conserved and ruled by dynamics similar to the described in section 1.1, which ensures their scale-free behavior in the stationary state.

1.3 Different Mechanisms to Reach the SOC State

So far, the basic ingredients necessary to exhibit SOC have been scrutinized. They have been exposed by using one concrete approach to the SOC stationary state. But, indeed, there exist two different mechanisms to achieve such state: the already explained mechanism of "integration and fire" (to which the most part of this thesis is devoted) and the extremal dynamics mechanism. These mechanisms can be sharply distinguished by means of their representative models, which are here briefly summarized.

i) *Integration and Fire*.- This generic term embraces the SOC models following exactly the avalanche dynamics explained in detail above. To this group of systems belong the examples in which a physical quantity is stored at the sites of the system until the threshold is overcome at one of them, which triggers an avalanche.

   The paradigmatic model of such systems is the original proposed by BTW: the **sandpile** model [6]. In this model, the sites of the system accumulate grains of sand, and redistribution rules are deterministic and conserved. This example and some variations of it will be discussed in section 1.4 and chapters 2-3, and therefore we do not enter in details now.

   The initial example of this section, the **earthquake**, also follows this

dynamics to reach the SOC state. In the accepted as archetypical model of such systems, the Olami-Feder-Christensen (OFC) model [12], each site accumulates stress until a certain threshold is exceeded. Then, a fraction α of the energy of this site is redistributed among its neighbors. As α is fixed to a value into $(0, 1/2d]$, the system presents a controversial feature: the lack of conservation in relaxation events. A nonconservative relaxation rule can be found also in models of **forest-fires** [13, 14], in which trees grow with probability p until hit by a thunder (with probability f) or reached by a neighboring fire front; the fires devastate any tree in the neighborhood and, in a certain special limit of its parameters, the fire fronts can propagate throughout the system forming fractal patterns. In chapter 5, the consequences of these local dissipative relaxation rules for the SOC behavior will be discussed.

In models of **superconductors**, avalanches are initiated due to an external field which fosters the creation of vortices, which pile up at the sites of the system. Under this mechanism, also **neural networks** can be found; models of some parts of the brain consider the transmission of signal between neurons as an avalanche, triggered by one site after a period in which incoming potentials are stored. When the accumulated potential overtakes a certain threshold, the signal is transmitted in form of pulses throughout the network. These two examples will be extensively treated in chapter 6.

ii) *Extremal dynamics.*- **Evolution** models, like the Bak-Sneppen model [15], use *extremal dynamics* to achieve the self-organized critical state. In this model, each site of a d-dimensional hypercubic lattice represents to a species into an ecosystem; each species i has a random number $x_i \in [0, 1]$ associated with it, which represents its fitness into the environment. The avalanche-triggering event is the selection of the minimum of all these numbers, x_{min}, which marks as active the site with $x_i = x_{min}$. Active sites represent species extinguished and them and their neighbors have to be replaced by another new one, with a new random fitness. When all the active sites have disappeared, the condition is checked again for the whole system. This is how an avalanche is defined; small avalanches represent small adjustments of species, and large events, massive extintions. Avalanches reorganize the system increasing the fitness of all species (like a Darwinian selection rule) above a critical one, x_c; when this happens, the stationary value is reached and critical properties arise.

These are the usual examples of SOC models, but there are many more claimed to be SOC [5, 16, 17]: interface growth models [18], low-temperature dislocation creep [19], atmospheric precipitation [20,21], stock-market crashes [22], solar flares [23], droplet formation [24], river patterns due to water erosion [25–27], landslides and turbidities [28–30], lattice gases [31], electric conduction in random media [32]...

The next section is devoted to the archetypical examples of SOC models, on which most of the work, both analytical and numerical, at the literature has been focused.

1.4 Piles of Sand and Rice

The concept of SOC was, for the first time, used during the study of the behavior of coupled pendulums [1]. However, this system (also present in the first, seminal work [6]) was considered by the authors not an intuitive example to introduce the concept of SOC. Instead, in the description of BTW's new concept, it was used the metaphor of a pile of sand, more accessible to non-trained readers (after all, who has never played with sand or observed a hourglass?).

A *real* sandpile is an open system in which grains of sand are introduced at a low rate. When a grain is posed at the center of the pile, a column of sand is formed at this site, the pile grows, and so it does its slope. While the slope is below its **angle of repose**, it remains stable, and behaves like a solid, because each component of the system is fixed at its position. When it is over this angle, the pile becomes metastable; and, when a critical angle is exceeded, any grain addition can trigger a chain reaction in which the grains in the pile are reorganized in order to reduce the slope again (avalanche). If the avalanche reaches the border of the pile, grains are consequently dropped off. During this fluid-like period, in which a flow of grains can be defined, no new grain is added.

When the pile is driven from a random site, an homogeneous landscape of grains is formed instead. However, the related physics does not change. An added grain makes the pile gain potential energy, which is accumulated. When the potential energy is high enough to overcome stability condition, the pile becomes unstable and an avalanche is triggered. During the chain reaction, the grains with largest potential energy fall to lower levels, transforming their potential energy into kinetic energy; this energy is lost in collisions with other grains (friction), dissipated in form of heat. When a grain loses

all its kinetic energy, it stops. During the avalanche, then, potential energy is transformed into kinetic energy and dissipated in order to gain stability; thus, in the course of an avalanche there is an energy flow with which the pile is rearranged to reduce its slope.

Is in this sense in which the first sandpile models were described as "dissipative" [6, 10, 33]. But, here, grains[13] are identified as discrete units of energy, ideal *quanta*[14]. In this way, a conservation in the total number of grains of the pile means a conservation in its total energy, and a rule breaking this conservation is what we call dissipative in this text. From now on, we will talk indistinctly about sand grains or energy.

How does a sandpile reach the SOC stationary state? When the density of grains is small, only small local events happen; they have no consequence in other parts of the pile: the pile is still a collection of independent, isolated parts. Small avalanches usually stop before reaching the boundaries, increasing the density of energy of the pile. As the pile grows, so it do the events, and when the density is large enough, any small perturbation can be felt in any part of the pile, transmitted in the form of large event. Large avalanches reach the border and, in consequence, dissipate energy. By means of driving and dissipation and small and large avalanches, the pile is driven towards a stationary state in which all sizes of avalanche are possible, and correlations span through all the pile: the self-organized stationary critical state has been reached. In this state, the behavior of an individual grain or part of the pile cannot be understood in isolation, but only the behavior of the complete system. The whole pile is the minimal observational unit.

In the rest of this chapter, three of the most studied models of sandpiles will be introduced.

The BTW sandpile

It is time to define a specific set of rules for the dynamics of the system described above. In the model presented in [6], each site of a d-dimensional system stores an abstract quantity, which could represent the force of a pendulum, the slope of the pile or the height, indistinctly, at this point of the system. Let i be the label which distinguishes a position on a d-dimensional

[13] In theoretical models, "ideal grains", all identical, which can be piled up, are considered.

[14] As will be seen, a continuous definition of energy is also possible in sandpiles.

hypercubic lattice, whose cartesian coordinates are given by $\vec{r}_i$, and z_i the variable which represents, e.g. the height of the pile at this site.

The common part of the dynamics of all SOC models proceed in this pile as described in section 1.1: driving events are performed until the height of one site exceeds the threshold, z_c; when this happens, the site becomes unstable (active) and relaxes the excess of energy by toppling grains to its neighbors; if this toppling triggers more activations, relaxation events are performed until no more active sites are in the system; then, a new grain is added, and the cycle starts again.

The specific part of the rules for this model are described by:

1. Driving: A randomly chosen site i receives one single grain:

$$z_i \to z_i + 1. \tag{1.9}$$

2. Toppling: When a site fulfills the condition $z_i \geq z_c$, a *fixed amount* of grains is equally distributed to *each* of its nearest neighbors (n.n.) in order to recover stability:

$$\begin{cases} z_i \to & z_i + \Delta_{i,i} \\ z_j \to & z_j + \Delta_{i,j} \quad \forall j. \end{cases} \tag{1.10}$$

   where Δ is, with a notation similar to the used in [34], a generic operator which describes the number of grains involved in any of these steps:

$$\Delta_{i,j} = \begin{cases} -2d & \text{for } i = j \\ 1 & \text{for } j \text{ n.n. of } i \\ 0 & \text{elsewhere.} \end{cases} \tag{1.11}$$

3. Dissipation: The grains toppled out of the pile, due to the relaxation of an active site at the border, are lost; this is equivalent to the condition:

$$z_{i_{out}} = 0, \tag{1.12}$$

With the definition of the matrix Δ given by Eq.(1.11), the conservation in the toppling rules is ensured by the condition:

$$\sum_j \Delta_{i,j} \leq \ 0 \qquad \forall i. \tag{1.13}$$

Due to the open boundaries, the left hand side is always negative. If they were closed, the inequality would be saturated.

Note that the dynamical rules for this sandpile are extraordinary simple, but, as we will see, the underlying behavior is extremely complex. It is another example of the *emergence of complexity* from simple interactions. The mathematics involved in updating rules are only sums and substractions, but the mathematics needed to analyze the critical behavior is very complicated. Thus, even this simple, *deterministic*, isotropic model cannot be analytically solved[15].

In a subsequent article [33], BTW define other set of rules specific for the slope, which is defined as $z_i - z_{i+1}$ in one dimension. Both sets of rules, the one which uses heights and the one which uses slopes, are very common in the literature. Hereinafter, the original height rules will be used [6], which entail certain advantages:

- The idea of height is more intuitive and allows to visualize immediately the configuration of the pile.
- Due to the relation between them, the isotropic rules defined for the slope becomes anisotropic for the height. This could cause confussion if one works with both at once.
- Heights are univoquely defined in all dimensions, while slopes need a convention for any d.
- Using heights, the condition for instability depends only on one site, and not on its neighborhood.

Moreover, the use of heights confers special properties to the model. In [34], Dhar studied many interesting properties of the BTW model defined with heights instead of slopes. This model has a property called **Abelianity**, reason why it is also called **Abelian Sandpile Model** (ASM). This reflects the fact that, in this sandpile, when it is defined using heights, the order in which toppling events are performed into the same avalanche does not change its final configuration.

The author also defines the evolution to the SOC state as a route through non-critical metastable states (**transient states**) until the critical metastable

[15] Other anisotropic variants are easier to treat analytically. See chapter 3.

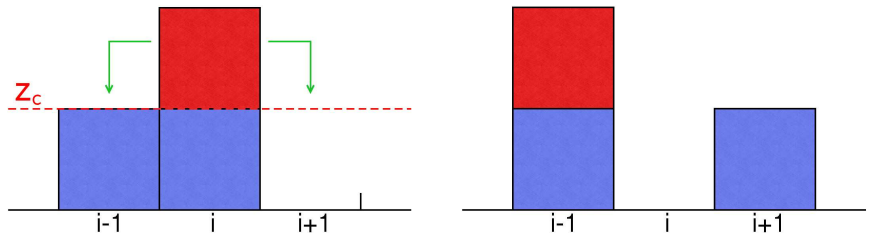

Figure 1.4: Small avalanche in the $d = 1$ BTW sandpile model. Left: Height at site i is above the threshold z_c, and therefore a toppling is necessary to recover stability. Right: After the toppling, site i and $i + 1$ are stable, but site $i - 1$ is unstable; the avalanche ensues.

configurations characteristic of SOC (**recurrent states**) are reached. Although the number of metastable configurations grows exponentially with the system size, only recurrent states have non-zero probability of occurrence in the SOC regime. This probability is equal for all these states. The number of recurrent configurations is given by $N_R = \mathrm{Det}(\Delta)$[16], and it is possible to know whether an arbitrary configuration is one of the N_R allowed by using the **burning algorithm** [34, 35].

Moreover, this isotropic sandpile can be related with spanning-trees by using the burning algorithm, as well as with the $q \to 0$ limit of the Potts model [36]. This allows to obtain a deeper knowledge of the sandpile albeit, unfortunately, not to solve it analytically. For most of the critical exponents (for instance, probability distribution ones), computer simulations are still needed.

BTW in $d = 1$

Following Eq.(1.11), for the one-dimensional version of the model, the toppling rules are:

$$\begin{cases} z_i \to z_i - 2 \\ z_j \to z_j + 1 \end{cases} \qquad \text{for } j \text{ n.n. of } i, \tag{1.14}$$

and the threshold is fixed at $z_c = 2$. When a site is active ($z_i \geq 2$), it topples one grain to each nearest neighbor. If one of these neighbors is out of the pile,

[16] The inverse of the Δ matrix (see Eq.(1.11)) is also related with the two-point correlation function [34, 35].

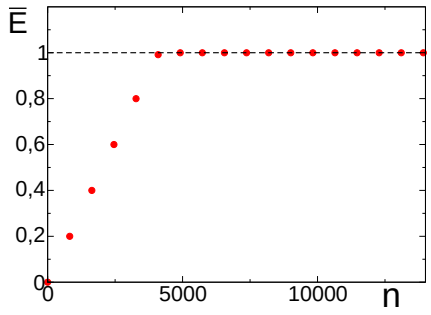

Figure 1.5: Evolution of the energy density $\overline{E}$ as a function of the number of driving events, n, in the $d = 1$ BTW model. For $n < 5000$, all final configurations, whose energy is here represented, are transients. For $n \geq 5000$, the only recurrent final configuration is achieved, and $\overline{E} = z_c - 1$ remains unchanged.

the grain is dissipated. An illustrative example can be observed in Fig.1.4.

For $d = 1$ this model has a trivial "critical" behavior [16, 33, 37]. Let the initial state of the sandpile be the empty one. As grains are added and stored, some small avalanches occur, and some transient configurations are visited. But after a few driving steps, the configuration in which all sites fulfill $z_i = z_c - 1$ is reached; this state, called the *minimally stable configuration*, is the only recurrent configuration possible. Therefore, $N_R = 1$, and the measured density of energy $\overline{E} = \sum_i z_i/L$ takes a fixed value $\overline{E} = z_c - 1$, with no fluctuations (see Fig.1.5). Any perturbation to this state ends in this same state, after a few avalanche steps to recover stability.

Consider, for example, a system of size $L = 5$ (see Fig.1.6). Starting from the minimally stable configuration (step 0, not shown), a new grain is added to the central site (step 1); then, a non-linear diffusive motion starts in the pile until, after six updating steps of the avalanche (lifetime $t = 6$) and nine toppling events ($s = 9$), stability is recovered: the pile is again in the minimally stable state.

In this way, as all avalanches start from the same initial state, the size of the avalanche depends only on the site at which the initial grain is added. As the position of the seed is an integer randomly selected from an uniform distribution in $[1, L]$, all sizes and lifetimes are equally probable. The exponents are trivial (see Table 1.1), as well as the spatial and temporal structures. The system is "critical" in the sense that any perturbation is propagated throughout all the system, but not in the usual meaning of the term.

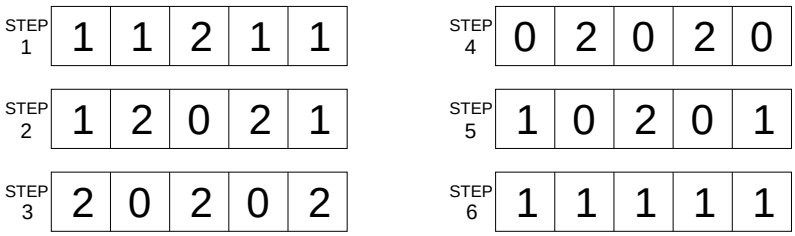

Figure 1.6: Avalanche in a $L = 5$ one-dimensional system starting from the only stationary state: the minimally state configuration. The central site is perturbed, and the final configuration is again the minimally stable one.

BTW model	τ	τ_t
$d = 1$	0(0)	0(0)
$d = 2$	1.13(3)	1.16(3)

Table 1.1: Critical exponents for the size/lifetime probability distributions in the BTW sandpile model. Figures in parentheses represent the statistical error in the last digit of the measurement. The case $d = 1$ is trivial. Own measurements, but in agreement with, for instance, [46].

BTW in $d = 2$

For $d = 2$, the toppling rules are not much different from the one-dimensional case; now, $z_c = 4$, and:

$$\begin{cases} z_i \to & z_i - 4 \\ z_j \to & z_j + 1 \qquad \text{for } j \text{ n.n. of } i \end{cases} \tag{1.15}$$

A sketch of a relaxation event can be observed in Fig.1.7. Redistribution rules are as simple as the one-dimensional ones, but the behavior of the system in the stationary state is much richer. Now, there is more than one stable configuration in the stationary state ($N_R > 1$)[17], and therefore the energy density $\overline{E}$ remains fluctuating around a non-trivial stationary value ($\overline{E}_c = 2.1235(2)$), with fluctuations given by a power of the inverse of the system size[18]. Activity is able to form non-trivial spatial structures, as can be

[17] As mentioned above, indeed the number of recurrent states increases exponentially with system size.

[18] Due to the finite size of the system, there exist a size correction to the thermodynamic limit energy density $\overline{E}_{c_L} - \overline{E}_{c_\infty} \sim L^{-\gamma}$ [45].

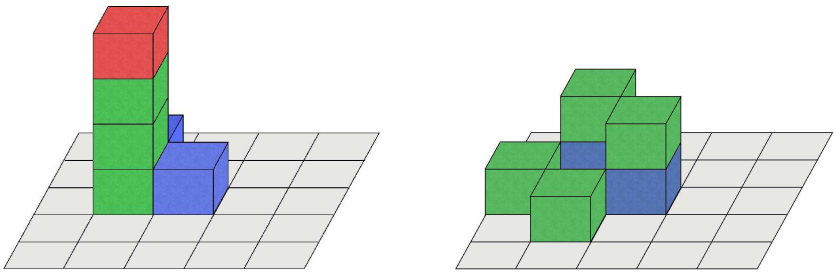

Figure 1.7: Small avalanche in the $d = 2$ BTW sandpile model. Left: The red grain, site i, is exceeding the threshold, making this site unstable. Right: One grain is given to each nearest neighbor; now all sites are stable.

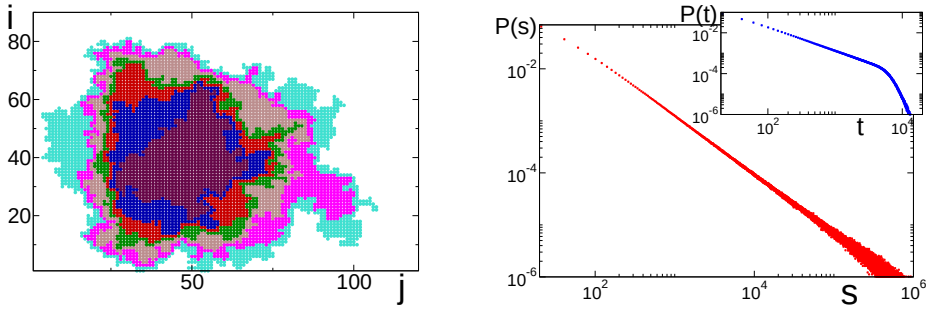

Figure 1.8: Left: Example of activity pattern in a 150x150 BTW sandpile. Each color labels a number of topplings per site: the darker the color, the larger the number of topplings. Right: Size and lifetime probability distributions in a $d = 2$ BTW sandpile with $L = 1000$ as linear size; the exponents, measured by using a least squares fit, are in table 1.1.

seen in the left part of Fig.1.8. The bulk of the figure is compact (due to the deterministic relaxation rules), while the border is fractal; also, waves into avalanches can be distinguished [38, 39], regions of sites which have toppled an identical number of times.

This model is still controversial due to the fault to FSS ansatz in the simple form of distributions as $P(s)$. The BTW sandpile presents **multifractal scaling** instead [40,41], and the waves into each avalanche are the only single events in which usual FSS can be observed for all quantities [38, 39, 42]. The cause for this anomalous scaling was claimed to be in the strong difference of dissipative (i.e. which reach the border) and non-dissipative avalanches [43].

Although extensive studies have been done about this $d = 2$ sandpile (see [44] for a review, but also [45, 46] for numerical simulations, [47–49] for a continuous modification of the model...), the values of the critical exponents

need still to be obtained with simulations and, as can be deduced by reading a few of the articles proposed above, there is not even an accepted reliable set of observables to be used. The result of the simple measurement of size and lifetime probability distributions can be observed in the right part of Fig.1.8 and also in table 1.1. In the plot of the lifetime probability distribution (inset), a clear example of the cutoff due to finite size (Eq.(1.7)) can be seen around $t = 12000$. The duration of an avalanche here is much smaller than its size because, as said above, a site can topple many times (*multiple topplings*).

In any case, the non-trivial values of the exponents show, thus, non-trivial behavior in the stationary state, which can be called critical in the strict sense of the term.

BTW in $d = \infty$

As dimensionality increases, the effect of the underlying spatial structure of any system disappears. When this happens, long range interactions replace to local rules, breaking the concept of "space". Then, no spatial structure nor spatial correlations are present in the model, and mean-field theory can be applied. Mean field behavior is also present for a regular d-dimensional hypercubic lattice when d is over an upper-critical dimension, d_c which for BTW [45, 48, 50] and the rest of piles of this chapter is $d_c = 4$.

Apart from increasing dimensionality, there are many other forms to achieve the mean-field regime. For example, to put all dynamical rules in a Bethe lattice; due to the special properties of these lattices, mean-field BTW can be solved analytically and their critical exponents, deduced [51].

It is possible also to use the so-called *random-neighbor* ensemble, where connections between random distant sites are allowed in a system which is usually defined in a regular lattice; this is equivalent to an infinite spatial dimensionality on the system, and therefore mean-field exponents are recovered. Boundary conditions can be replaced by sink sites, at which sand grains are lost.

By using any of these ensembles, the mean-field system is able to reach the stationary critical state. In it, and for large enough systems, activity of the avalanches cannot pass twice through the same site, and therefore the avalanche propagates by means of a *branching process* (see [46,52], or chapter 5) with certain details which allows to map the problem to *self-avoiding random walks* or more complicated walkers [50], for which the associated critical exponents are well known.

For all these different paths to mean field, the exponents expected for size and lifetime probability distribution are $\tau = 3/2$ and $\tau_t = 1/2$ (see [51], for instance).

The Manna Model

The BTW model has been described and characterized by means of its exponents. In $d = 1$, its behavior is trivial, and for $d > 1$ anomalous scaling properties are observed. It would be interesting to analyze a non-trivial example of sandpile with no anomalous properties, able to show complex behavior at any dimension below the upper critical one.

Many non-trivial one-dimensional models were proposed at first moment (as the ones introduced in [53], and other variants of it). But due to the simplicity of the rules of the BTW sandpile, it is better to focus our attention on a similar example with non-trivial behavior in $d = 1$. The most simple example is the so-called **Manna model** [54].

The Manna model is a sandpile in which a hard-core repulsion among the different particles stored at a same position is introduced. In this way, any site storing more than one particle becomes unstable and, as a result of the repulsion, all its grains are distributed in an uncontrolled way among the neighboring sites.

The evolution rules of this sandpile in d-dimensions are very similar to the ones defined for the BTW model. In fact, the driving rule, Eq.(1.9), and the dissipation rule, Eq.(1.12), remain the same. But during a toppling, an active site redistributes *all its energy* between sites randomly chosen among its $2d$ nearest neighbors. Thus, a Δ matrix cannot be predefined in this model, because it changes each time of each avalanche. In fact, as the repulsion is identical in any dimension, the toppling rules coincide for any d:

$$\begin{cases} z_i \to & 0 \\ z_j \to & z_j + 1 \end{cases} \qquad \text{for } z_i \text{ sites, random n.n. of } i \tag{1.16}$$

This model is apparently slightly different from the BTW sandpile, but this difference in the relaxation rule is a key detail. In the BTW model, there is only a source of stochasticity: the random choice of the initial seed. In the Manna model, stochasticity is not only in the initial seed, but also during

Manna model	τ	τ_t
$d = 1$	1.11(5)	1.17(5)
$d = 2$	1.27(3)	1.48(3)

Table 1.2: Critical exponents for the size/lifetime probability distributions in the Manna sandpile model. Own measurements; the results coincide with any of the measured in the literature (see, for instance, [55]).

the avalanches, present in the random choice of the target of the toppling[19].

To be more precise, the stochastic rule in the BTW pile only influences the initial state, not the avalanches. The critical behavior of a non-chaotic system does not depend on the initial condition, and therefore any noise present only in this stage is irrelevant. But, in the Manna model, the noise is present on the evolution rules in a non-trivial way, making this noise relevant, and affects to the critical behavior of the pile[20].

The differences between the two models become fairly evident in simulations: in $d = 1$, the Manna model has a complex behavior in the stationary state, in which $N_R \neq 1$, recurrent states are not equally probable, and the energy density reaches a non-trivial value ($\overline{E}_c = 0.8913(2)$) around which remains fluctuating. Correlation functions and the rest of observables are scale free. As can be seen in table 1.2, the critical exponents measured are not trivial, which is a reflection of the power law behavior of the probability distributions (see left part of Fig.1.9).

The complex behavior is, thus, present in any dimension, and makes extremely difficult any analytical treatment of the isotropic model[21].

Another evidence of the differences between these models is the activity pattern (Fig.1.9) which, unlike in the BTW model, is not compact, but now both the bulk and the border of it are fractal. The bulk is much richer, and the avalanches are much more heterogeneous. Moreover, contrarily to the BTW model, the behavior of the Manna sandpile fulfills the FSS ansatz [49].

Nonetheless, as the dimension increases, the differences are less remark-

[19] As each site chooses between its nearest neighbors of a regular lattice, spatial correlations are present and the situation is very different from the random neighbor ensemble.

[20] Also different is the case of varying boundary conditions, see chapter 3.

[21] Due to its rules, the Manna model is not Abelian, although a "stochastic Abelian" variant, in which *two grains* are toppled, and each of these grains is delivered to one random n.n., can be also defined [56].

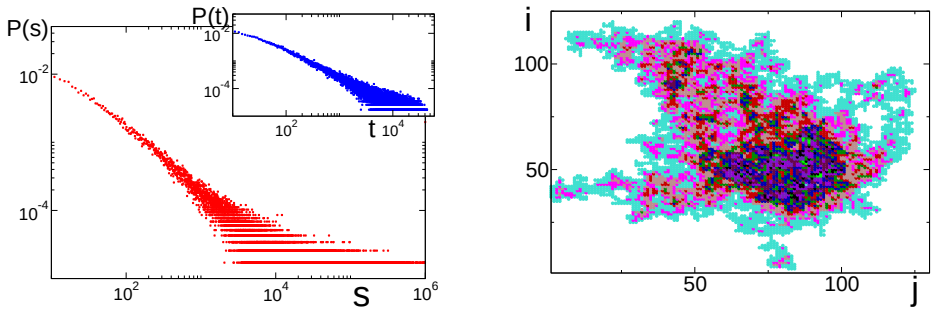

Figure 1.9: Left: Size and lifetime probability distributions in a $d = 1$ Manna sandpile with $L = 32768$; the exponents measured are in table 1.2. Right: Example of activity pattern in a 150x150 Manna sandpile; the bulk, much more heterogeneous than in the BTW case, contains holes of activity.

able. In the random neighbors ensemble ($d = \infty$) the rules for the Manna model are mostly identical to the BTW rules. Driving and dissipation rules remain unchanged, but in the toppling rule each neighbor does not receive necessarily the same amount of distributed energy. For this ensemble, this is an irrelevant detail concerning critical behavior, which is again described by a branching process. Therefore, both the BTW and the Manna model share the same mean-field behavior.

Albeit for many years it has been a controversial question, with these arguments (and many more which will be given all along this thesis) it can be concluded that the BTW model and the Manna model exhibit a different critical behavior for $d < d_c$. This is not the case for mean-field behavior, at $d \geq d_c$.

The Oslo Ricepile Model

So far, two theoretical models of sandpile has been introduced. The BTW model was not created to reproduce the behavior of real sandpiles. It was created to collect essential physics of the behavior of many real systems in the simplest model possible. It was not the intention of its authors to obtain a realistic model. Actually it is not. However, it is an interesting question whether real experiments reproduce the scale-free behavior present in theoretical models. As we will see in chapter 6, all granular experiments with rounded "sand" grains failed in their attempt of find avalanches of all sizes and durations fulfilling the finite size scaling ansatz, being *intertia* the main problem in all cases.

Inertia appears when a moving grain is accelerated by gravity, and therefore its velocity and kinetic energy increases as the avalanche ensues. This mechanism is not implemented in any of the sandpile models studied here (and actually it leads to a lack of criticality, see chapter 6). The only way to reduce inertia is by using strongly irregular shaped grains, which increases the number of collisions (and, in consequence, friction) and allows non-trivial packaging of grains (local variablity) in order to gain stability.

This is the underlying idea of the most celebrated experiment in SOC: the Oslo Ricepile Experiment [57]. As we will deeply explain in chapter 6, the key point was to introduce grains of elongated shape, which can be packaged in many different and non-trivial ways, keeping stuck easily. This reduces the inertial effects, and sharpen the critical behavior of avalanches into the pile. This was called "the ultimate sandpile experiment" by Bak [1], because it is the only granular experimental setup in which avalanches with scale-free size/lifetime distributions have been observed, and the finite size scaling ansatz is fulfilled.

Real experiments with sand grains were performed to check whether the BTW model was realistic or not. In an opposite way, a theoretical model was proposed to reproduce with simulations the already observed critical behavior of the real ricepile experiment. The above explained non-trivial packaging of rice grains entails *local variability*, which affects to the updating rules, changing as the avalanche evolve [58]. This idea inspired the so-called **Oslo ricepile model** [59].

Albeit it was defined with slopes and boundary driven in the original article, for homogeneity criteria we will use the height, isotropic, bulk driven version of the model[22]. In this model, the toppling rule is identical to the BTW one:

$$\begin{cases} z_i \to & z_i + \Delta_{i,i} \\ z_j \to & z_j + \Delta_{i,j}, \end{cases} \tag{1.17}$$

with the same definition of Δ made with Eq.(1.11). What is different in this model is the condition for a site to be unstable, given by $z > z_c^i$, where the threshold is stochastic and different for each site: z_c^i is now a quenched magnitude, updated only when site i topples, taking the values 1 or 2 with equal probability. Although it could seem that this sandpile is nearer the BTW than the Manna model because of the deterministic redistribution rule,

[22] See [37, 60] for a comparative study of both cases and chapter 3 to well-understand the differences.

Oslo model	τ	τ_t
$d = 1$	1.10(3)	1.16(3)
$d = 2$	1.26(3)	1.48(3)

Table 1.3: Critical exponents for probability distributions in the Oslo ricepile model. Own measurements for $d = 1, 2$

the fact is that the stochastic nature of the threshold makes the evolution into the avalanche also stochastic. With the threshold, a non-trivial noise is added to activity events (variablity, dynamically-varying rules) and, in this sense, this system and the Manna pile are described in a very similar way (see above). It is expected, then, that the critical behavior of the Manna model and the Oslo ricepile model coincide, giving as a result the same set of critical exponents. Actually, it is so, as can be seen by comparing the results on table 1.2 and table 1.3[23]. Also, in this pile the FSS ansatz is fulfilled.

In this way, the Manna and the Oslo model belong to the same **universality class**[24]. In fact, these models define a universality class known as the **Manna class**, characterized by the stochastic nature of the updating rules into the avalanches (not only of the driving rule, as usual in sandpiles). This allows to use one model or the other indistinctly to study a concrete problem, depending on how clean its critical behavior is displayed in each case.

As will be shown in subsequent chapters, the critical behavior of systems in this universality class is different from, for instance, the behavior of deterministic sandpiles as the BTW one. Also, the Manna class is very robust, in the sense that many changes in updating rules are irrelevant for the critical behavior if and only if they keep stochasticity in relaxation. For example, suppose that some small walls are introduced in the pile to close the pass towards some neighbors of each site, keeping the original updating rules; this is equivalent to a Manna model in which some bonds of the regular lattice are removed in the initial stage. This structural quenched disorder is not relevant and it does not alter the universal behavior of Manna[25]. Neither do so the continuous energy description of the Manna model[25]; nor a Manna model in which the energy given to each site, z, is a parameter of the system (fulfilling $z = z_c$)[25]; nor the Manna model in which the probability for a site to be activated when activity reaches it is a continuous increasing function

[23] Additional results will be given in chapters 2-4 to justify this statement.
[24] See appendix A.2
[25] Own measurements. Not shown. See also [61].

of its stored energy density[25]...

Sandpiles as the BTW model will be called, hereinafter, *deterministic sandpiles*, while piles in the Manna class, *stochastic sandpiles*.

1.5 Concluding Remarks

Power laws, reflection of complexity, are ubiquitous in Nature. Self-Organized Criticality (SOC) was born aimed to be an explanation for this ubiquity, and therefore with the aim of being a general theory of complexity.

Despite it is clear that it is not the general mechanism in which "How Nature works", it still attracts the attention of the scientific community. After more than 21 years under study SOC is still a controversial, interesting topic, full of details. Many of its most important fundamental aspects are not clarified yet, and there is not even an accepted definition of the term.

There is not an accepted set of conditions to be fulfilled for a system to be SOC; any proposed set is questioned. It is not even a general acceptance of what the order and the control parameter are. The only certainty is that SOC systems are, somehow, *naturally posed on criticality*.

In this chapter, the basic concepts related with SOC are introduced to settle notions that will be important to understand the body of the thesis. Apart from systems which use extremal dynamics, the basic ingredients for a system to exhibit SOC are:

- A slow-driving and boundary dissipation ($\kappa \to 0$ limit).
- A threshold in the dynamics.
- Metastability.
- Infinite separation of time scales.

All these ingredients are coupled, and they all are necessary conditions for SOC. On the other hand, conservation is a common feature of the paradigmatic examples of SOC models: sandpiles and ricepiles. In all these systems, critical exponents can be measured in correlations and other response functions, and universality classes can be defined.

According to the ideas introduced, a definition of SOC can be enunciated:

Self-Organized Criticality is a mechanism through which open systems achieve a self-organized statistical stationary state in which a nonequilibrium phase transition is undergone; by means of the existence of a slow-driving, threshold, time scale separation, metastability and boundary dissipation, the dynamics of the system leads it to a critical state in which scale invariance is present in all the observables.

This definition will be completed in chapter 5, after discerning whether conservation is a necessary or a sufficient condition for SOC.

Chapter 2

SOC as an Absorbing Phase Transition

The study of SOC can be divided, historically, in two stages: one, of research on general features of SOC by creating new models, focused on their properties and their analytical treatment; the second one, concerning the classification of models in universality classes and the quest for a continuous description for the dynamics of the models, a mesoscopic *field theory* representative of each universality class. The previous chapter dealt with the issues of the first described stage.

This chapter is devoted to look for a field theory to describe the essentials of the most generic universality class of all SOC systems: the universality class of stochastic sandpiles, or Manna universality class. In turn, a new ensemble for stochastic SOC sandpiles will be devised, with which the self-organized critical point can be treated as the critical point of a second-order phase transition. This characterization will allow to stablish two different but equivalent ensembles to describe the behavior of stochastic SOC systems, and to compare with the universality class of Directed Percolation (DP). In the end, the differences between the SOC ensemble and the new one established in this chapter will be highlighted, to discern the range of validity of each of them.

2.1 The Universality Class of Stochastic Sandpiles

In section 1.4, sandpiles were introduced, and their general characteristics explained. Also, the universality class of *stochastic sandpiles* was presented and put forward from the class of *deterministic sandpiles*, to which the Bak-Tang-Wiesenfeld (BTW) model belongs.

Ten years after the first paper about SOC [6], a classification of sandpiles into universality classes was still a controversial topic (see, for example, [61–63]). Whether the BTW [6] and Manna [54] models formed part of a same universality class was not clear yet. Even the tools employed to analyze the problem or the very existence of true scaling in BTW were under debate [63], which points out the non-triviality of the task. Some authors, for instance, proposed to distinguish between avalanches which reach the border (dissipative avalanches) [43] and internal avalanches, in order to observe a clean scaling with which better discern the universality class [64].

Measurements of critical exponents (see tables 1.1 and 1.2, for example), the study of the FSS ansatz [41], and the meagre number of articles with analytical results about the isotropic Manna model (for instance, [56, 65]) and isotropic Oslo model [59] (see [66] and references therein) corroborate a different behavior for stochastic and deterministic sandpiles at criticality. This will become more evident all along this chapter.

Relevant Ingredients of Stochastic Sandpiles

So far, many arguments have been presented to ultimately claim that the Manna model and the Oslo model belong to the same universality class, different from the BTW universality class. But in order to deeper understand the universality class of the stochastic sandpiles, it is indispensable to know what are the relevant ingredients which define this universality class.

To this end, the dynamic rules of both Manna and Oslo models are now compared. Apart from the common mechanism for the driving and the dissipation, there do not seem to be more common points in their rules: the threshold in Manna is fixed, but in Oslo is a random quenched variable; and the choice of neighbors in Manna is random, but in Oslo is deterministic. However, at a coarse-grained level, in which microscopic details are cast aside, there are two key common ingredients: **conservation and stochasticity**.

In both models, the presence of stochasticity in the relaxation rule, either by means of a quenched variable or at the annealed choice of the target site to which topple a grain, prevents the rule from being deterministic. This feature distinguishes these models from the BTW model. On the other hand, as in the usual definition of a sandpile, the dynamics is conservative, and the only present dissipation can be considered a finite-size effect.

As explained in the previous chapter, the existence of a threshold, together with conservation, allows the develop of a correlated **background** of grains at sites below threshold. The number of grains stored at a site defines the response of a site when receives a grain during an avalanche; therefore, the activation of a site depends on the value of its background. This leads to the existence of a coupling between the stable grains and activity.

Then, it can be concluded that, for a system to belong to the stochastic sandpile universality class, stochastic relaxation rules as well as a coupling between the activity and the conserved background of the system are necessary conditions. This statement defines the universality class of the Manna sandpile model, into which many more models can be included (see below).

This supports the claim that *the BTW model does not belong to the same class of the Manna model*. The form of the correlations of the background depends on the relaxation rules and, thus, at a coarse-grained level, the correlations of the background of a deterministic sandpile differ from the ones of a stochastic sandpile.

It would be desirable to confirm these claims with the analysis of a continuous mesoscopic equation in which the irrelevant microscopic details are not present, and its properties can be rigorously deduced. However, already at the microscopic level of the Manna model there are fundamental problems which make difficult any analytical calculation: the presence of two time scales, and the broken translational invariance (inhomogeneity) due to the restrictive dissipation only at boundaries.

2.2 Regularization of a Sandpile

The presence of the $\kappa \to 0$ condition, necessary to reach the SOC state, introduces two time scales for the system: one is the slow-driving time scale and, the other one, the relaxation time scale or lifetime of each avalanche.

The existence of two different time scales entails certain theoretical problems, like ambiguous definitions of time-correlation functions and other time-

related observables. Also, the driving event implies a general knowledge of the state of the system (because no driving is possible while activity remains into the lattice), and hence a certain degree of non-locality [67, 68].

In principle, to describe the overall behavior of the avalanche, both time scales are to be taken into account. But, as mentioned in the previous chapter, it is possible to use one only time scale if the slow-driving is replaced by a constant driving which acts with a rate $h \ll 1$. In this way, the slow-driving time scale disappears, and only the relaxation-time scale remains.

The other singular part of the dynamics, the dissipation at the boundaries, can be also overtaken by introducing a dissipation rate ϵ, acting at any part of the system. This dissipation mimics the effect of the open borders and, therefore, allows to close the boundaries[1], acquiring the system translational invariance.

With these changes, the dynamics of the sandpile occurs in a single well-defined time scale into an homogeneous (translationally invariant) spatial extent. In other words, its dynamics becomes **regularized** [67–71].

The constant rate h can be interpreted as an external field applied to the system; also, by defining the response function associated with the activity in the sandpile it is clear that, for a finite ϵ, a function of the inverse dissipation rate establishes the maximum correlation length on the system [67–70, 72, 73][2]. Thus, ϵ could be considered as the distance to the critical point of an ordinary phase transition (see Eq.(A.1.6)), i.e. the *control parameter*.

In this way, the values of the rates must be adjusted in order to recover the critical behavior. As the driving time scale is now given by $\sim 1/h$, if $h \to 0$ the rate of driving is so small that the additions of activity seeds are not performed during the course of an avalanche and, therefore, individual events can be univoquely defined. Boundary dissipation imposes a very specific dependence of ϵ on the system size, due to which the thermodynamic limit leads to $\epsilon \to 0$.

To ensure the existence of a stationary state, ϵ must be always larger than h. Therefore, the system reaches the critical stationary state at the limits $h, \epsilon \to 0$ and $h/\epsilon \to 0$. By taking into account the identification of h and ϵ rates with the time scales of the non-regularized system, the Grinstein parameter is equivalent to $\kappa = h/\epsilon$ (see Eq.(1.8)); hence, by taking the

[1] Actually, to minimize finite-size effects, periodic boundary conditions are used.

[2] This topic will be deeply discussed in chapter 5.

above mentioned limits, the $\kappa \to 0$ condition, necessary for the sandpile to be critical, is recovered.

This vanishing limit is naturally attained by systems which evolve by means of SOC avalanche dynamics (see the previous chapter), whose definition implicitly brings the necessary time-scale separation. Due to this, these systems are said to be *posed on criticality*, or that they are critical *in apparent absence of parameter tuning*. Moreover, the negligible limit for h and ϵ to reach criticality confers robustness to the critical point: a change $h \to kh$ and $\epsilon \to k\epsilon$, with k a constant real value, still keeps the system into the critical regime. This is not the case of systems whose critical point is localized at a non-vanishing value, where such change moves the system far apart from criticality. It makes SOC systems (even if regularized) more probable to be found in Nature than those undergoing an ordinary phase transition [9].

The Loss of Self-Organization

In the previous chapter, energy density $\overline{E}$ was defined as the dynamic control parameter of the sandpile models, which is attracted, due to the self-organized dynamics, to its critical value (and the system to criticality). When ϵ (or κ) is introduced, it arises as the new control parameter. The average energy still increases until the system achieves a stationary state, but the stationary value of the energy depends now on the selected fixed value for ϵ.

Actually, $\overline{E}$, h and ϵ are coupled due to the dynamics: is the limit $h, \epsilon, \kappa \to 0$ (equivalent to the slow-driving and boundary dissipation) which makes possible the self-regulation of the energy of the system and the rearrangement of the background to a critical configuration. Without driving ($h = 0$), $\overline{E} < \overline{E}_c$ and all avalanches are subcritical; without boundary dissipation ($\epsilon = 0$), $\overline{E} > \overline{E}_c$ and all avalanches are supercritical. This points out a dependence between the three parameters in the regularized system.

After the regularization of the dynamics, to achieve the critical regime it is necessary a specific limit for these three parameters. The regularization of the dynamics entails, thus, the necessity of a fine-tuning for criticality: the system is not self-organized anymore.

But as mentioned above, the regularization also permits to reach configurations a-priori forbidden for SOC systems: arbitrary off-critical states. In SOC sandpiles, any non-critical configuration is a transient of the dynamics (see the previous chapter), and only the barely subcritical configurations resulting from a critical avalanche are accessible. The absence of a tuning

control parameter prevents the system from reaching an arbitrary-far-from-equilibrium configuration. But the existence of a standard control parameter (ϵ) in the regularized sandpiles gets rid of this problem.

In summary, the regularization of the dynamics of stochastic sandpiles allows to well-define a unique time-scale, as well as to acquire spatial translational invariance, two essential features of the systems studied in the theory of ordinary phase transitions. Also, any point of the phase transition of these systems is now accessible; but, in turn, one characteristic feature of these models has been lost: the self-organization.

2.3 Fixed-Energy Sandpiles

The identification in sandpiles of an external field and a control parameter which takes into account the distance to the critical point was early proposed by Tang and Bak [74]. The definition of the distance to the critical point is useful to study off-critical properties of the system, like the dependence of the order parameter or the correlation length on such a distance[3].

With these observables, it would be possible to characterize the SOC state like an **ordinary nonequilibrium second-order phase transition**. But, according to the arguments of the previous section, this possibility is discarded in "non-regularized" (standard) SOC systems. In the case of the regularized ones, the coupling between $\overline{E}$, h and ϵ leads to the existence of a unique possible set of values for the parameters to achieve criticality (namely $h, \epsilon, \kappa \to 0$, and $\overline{E}$ dynamically raising up to $\overline{E}_c$). The coupling and the evolution of $\overline{E}$ make the description of the critical point, in some sense, pathologycal. But there exists a way to de-couple these parameters.

Consider a SOC system in the thermodynamic limit (where the effect of the borders can be not taken into account, and therefore $\epsilon = 0$) which keeps the same relaxation rules, but in which there is no driving ($h = 0$). For finite systems, the $\epsilon = 0$ condition can be mimicked by means of periodic boundary conditions. This defines a new ensemble for the SOC system.

In this new ensemble, the system is not SOC anymore, because none of the mechanisms responsible for self-organization is present; the density of energy is now strictly (both locally and globally) conserved, and therefore the initial level of energy does not change during its evolution. If the SOC counterpart

[3] See appendix A.1.2.

is a sandpile, these systems are called **fixed-energy sandpiles** (FES) [69,75] (see also [67] for an early approximation to the problem), but it is possible to bring any SOC model into a fixed-control-parameter ensemble.

In such ensemble, the identification of the relevant parameters is straightforward: activity density $\overline{\rho}$ is the order parameter, and energy density $\overline{E}$, the control parameter of the system, which must be fine-tuned to its critical value to reach criticality. It is now a static, independent parameter. Also, there is only one time-scale and translational invariance. The criticality of the system can be described now as **the critical point of an ordinary phase transition**.

Consider a SOC sandpile like, e.g. the Manna model. To bring it into the FES ensemble, a fixed $\overline{E}$ and periodic boundary conditions are considered, remaining the activation condition and the relaxation rules unchanged. As there is no driving, $\overline{E}$ is already distributed among the sites of the system at the initial state.

When the fixed energy $\overline{E}$ is small, there can be only a few active sites, the background is subcritical, and activity decays exponentially fast to zero. Once it is in such a state, the system remains frozen at one of the many possible subcritical background configurations. This activeless state is identical to the frozen configurations of the SOC counterpart. As, once reached, the system cannot scape from it by itself, it receives the name of **absorbing state**.

If, on the other hand, $\overline{E}$ is too large, the conservative dynamics of the sandpile makes activity diffuse but, due to the closed boundaries, it remains into the sandpile, reaching the system a stationary supercritical state.

For a specific value of energy, $\overline{E}_c$, in the thermodynamic limit, activity decays slowly to the absorbing value following a power law; the system is at the critical point of a nonequilibrium phase transition into absorbing states, or **absorbing phase transition**.

The critical point reached with the FES ensemble is not different from the critical point of the SOC ensemble. Apart from the mechanism to reach the critical value for the control parameter, the rest of the dynamics is identical. Therefore, for a large enough system size, the energy level necessary for correlations to span throughout the system must coincide in both ensembles. Hence, the critical value $\overline{E}_c$ in the FES ensemble must be identical, in the thermodynamic limit, to the stationary critical value of the SOC ensemble [11, 60, 76]. The two ensembles are just two equivalent mechanisms to reach **the same critical point**. Recalling the SOC sandpile mechanism to reach

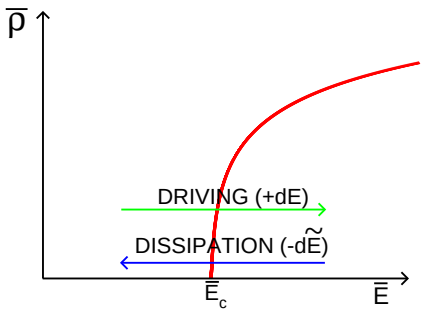

Figure 2.1: Phase diagram (activity versus energy densities) for the FES ensemble. The arrows represent the SOC driving (energy increasing $+dE$) and dissipation (energy decreasing $-d\tilde{E}$; see the previous chapter), which keep the system infinitesimally around *the* critical value of the density, $\overline{E}_c$. Due to this, the overcritical phase is not accessible for the SOC ensemble (unlike the FES ensemble, for which the whole phase space is avaliable).

the critical state (see section 1.2), the discussion about this equivalence is summarized in Fig.2.1

Moreover, as correlations are built up by means of the same internal rules, all the observables are expected to behave the same in the critical regime of each ensemble [76]. The phenomenology associated with them is so similar in their critical regime that it is possible to map the paradigmatic event of SOC (avalanches) into one of the possible experiments typical in absorbing state transitions: **spreading experiments** [77].

Definition of Observables

Dynamic Behavior

In the study of phase transitions into absorbing states it is usual to measure, *at the critical point*, observables related with the spreading of an initial seed of activity throughout an otherwise absorbing configuration. Each experiment stops by falling into another absorbing state or by reaching the borders, to avoid boundary effects. As activity spreads, the temporal evolution of the following observables can be measured [78]:

$$N(t) \sim t^{\eta}, \tag{2.1a}$$

$$P_s(t) \sim t^{-\delta}, \tag{2.1b}$$

$$N_s(t) \sim t^{\eta+\delta}, \tag{2.1c}$$

$$R^2(t) \sim t^{z_{spr}}, \tag{2.1d}$$

$N(t)$ is the average over many trials of the number of sites which have been declared active during the spreading experiment; $P_s(t)$ is the surviving probability of one experiment up to time t; $N_s(t)$ is the average *over surviving trials* of the number of active sites; and $R^2(t)$ is the average (as well over surviving experiments) of the mean-square distance to the seed of activity. Below the critical point, these observables decay exponentially fast to zero, and in a supercritical regime they converge to a stationary value. Therefore, they can be used as well to determine the position of the critical point.

It is straightforward to see why, before reaching the borders, avalanches and spreading experiments are the very same phenomenon: in both, an initial perturbation is introduced into an absorbing critical configuration, and some properties of its evolution are measured. Whereas the typical observables in SOC consider avalanches as a whole by measuring quantities like the total number of topplings, spreading experiment magnitudes take into account the internal relaxation processes of the spanning of the activity.

But, as both processes are equivalent, it must be possible to measure spreading observables into avalanches, and avalanche probability distributions in spreading experiments[4]. Moreover, there must exist relations between all these quantities. Such relations will be deduced now, following the steps of [79].

The size of an avalanche is the total number of sites which have been activated during the event; as an avalanche is the counterpart of a surviving experiment, and attending to the definition of $N_s(t)$ made above:

[4]Indeed, this will be the strategy to follow from now on to study the critical behavior of a system. See below.

$$s = \int_0^t N_s(t)dt \propto t^{1+\delta+\eta}, \tag{2.2}$$

where Eq.(2.1c) has been used. On the other hand, the probability to survive up to a time t is the accumulated probability to find an avalanche duration t. Therefore:

$$P_s(t) = \int_0^t P(t')dt' \propto t^{1-\tau_t}. \tag{2.3}$$

$P(t)$ coincides with the probability for an experiment to die at time t. Following the assumption that $P(s|t)$ (conditional probability to have a size s in an event which died at time t) is bell shaped with a maximum at a size s fulfilling Eq.(2.2) (which is numerically verified in [79]), it is possible to write it as:

$$\begin{aligned} P(s|t) &= s^{-1}F(s/t^{1+\eta+\delta}) \\ &= t^{-(1+\eta+\delta)}F(s/t^{1+\eta+\delta}), \end{aligned} \tag{2.4}$$

where F is a conveniently normalized scaling function. Then, it is possible to relate the probability to have an event size s with the probability to die at time t:

$$\begin{aligned} P(s) &= \int_0^t P(s|t')P(t')dt' \\ &= \int_0^t t'^{-(1+\eta+\delta)}F(s/t'^{1+\eta+\delta})t'^{-\delta-1}dt' \\ &= \int_0^t t'^{-(2+\eta+2\delta)}F(s/t'^{1+\eta+\delta})dt' \\ &= \int \left(\frac{s}{u}\right)^{\frac{-(2+\eta+2\delta)}{1+\eta+\delta}} F(u) \left(\frac{s}{u^{2+\eta+\delta}}\right)^{\frac{1}{1+\eta+\delta}} du \\ &= s^{\frac{-(1+\eta+2\delta)}{1+\eta+\delta}} \int u^{\frac{\delta}{1+\eta+\delta}} F(u)du, \end{aligned} \tag{2.5}$$

where the convolution integral stems from the fact that a size s can be the result of many events with different durations, and the change of variables $u = s/t'^{\,1+\eta+\delta}$ has been performed; the limits of the u-integrals have been

omitted for the sake of simplicity. From Eq.(2.3) and Eq.(2.5), it is possible to define the identities (also called *scaling relations*[5]):

$$\tau = \frac{1+\eta+2\delta}{1+\eta+\delta} \tag{2.6}$$

$$\tau_t = 1+\delta. \tag{2.7}$$

And with Eq.(1.4) and Eq.(1.7), and relation Eq.(2.2):

$$D_f = z(1+\eta+\delta) = \frac{2(1+\eta+\delta)}{z_{spr}} \tag{2.8}$$

or, equivalently:

$$(\tau-1)D_f = \frac{2(\tau_t-1)}{z_{spr}}. \tag{2.9}$$

With these relations (and also the ones obtained in [79]), the equivalence between avalanche events and spreading experiments is perfectly characterized. We can use any of the observables defined above as well as avalanche distributions for both processes, indistinctly.

The Initial Absorbing Configuration

Concerning the initial non-active configuration, in systems (like sandpiles) with many possible absorbing states the choice is not trivial. To perform the spreading experiment keeping the same critical behavior of the static critical point, it is essential to select a *natural* critical absorbing configuration [80]. Such a natural configuration is one generated by the own dynamics of the system, which ensures a properly correlated underlying background.

In an experiment starting from an homogeneously active state, as all sites are initially active, critical correlations develop throughout the system all along the experiment. However, in a spreading experiment there exists an activity front propagating through an absorbing medium; if such medium is not properly correlated, the spread of the front shows non-universality. Only

[5]See appendix A.1.2.

when the absorbing background is built from an homogeneous relaxation of activity at the critical value of the control parameter ($\overline{E} = \overline{E}_c$ in the case of sandpiles), the front spans in a universal critical way.

An absorbing configuration is, by definition, subcritical. Then, how can be obtained a natural *critical* configuration? There exist two different types of absorbing states: the ones obtained due to a low value of the control parameter ($\overline{E} < \overline{E}_c$), and absorbing configurations achieved for $\overline{E} \geq \overline{E}_c$ due to finite size effects because of strong fluctuations near (although above) the critical point. The number of frozen states grows exponentially with the system size; thus in the thermodynamic limit, there is an **infinite number of possible absorbing states**.

Thus, the only way to obtain an absorbing state with $\overline{E} = \overline{E}_c$, to be used in the spreading experiment, is due to a finite size effect. It is usual to obtain the initial state by allowing an homogeneously active initial state of a small system at the critical point to decay to a frozen state. With this procedure, critical correlations are generated as the system evolves, but the strong fluctuations make the activity dissappear, obtaining an absorbing state. By cloning it so many times as necessary to fill the original system size, the initial state is obtained [80].

This procedure is not necessary in the SOC ensemble. In there, where each avalanche is a new spreading experiment, the own SOC dynamics in the SOC stationary state builds such an absorbing configuration next to the critical point by means of the dissipation process, in which activity is dissipated, getting the system trapped into one critical absorbing state. This acts as the initial state for the next experiment, which starts when the next driving event is performed.

In absorbing phase transitions, it is also usual to measure the decay of the activity density $\overline{\rho}$ starting from an homogeneously active initial configuration. This observable follows a power law as a function of time at the critical point $\overline{E} = \overline{E}_c$:

$$\overline{\rho}(t) = t^{-\theta}. \tag{2.10}$$

Now, as long as $\overline{E} = \overline{E}_c$, the initial state is not important, because activity is present throughout all the system and correlations are steadily generated in it. Like spreading observables, deviations of $\overline{\rho}(t)$ from a power-law can be used to locate the critical point.

Static Behavior

One of the advantages of the FES ensemble is the possibility to measure steady-state quantities at any part of the phase space. As explained in appendix A.1.2, the effect of a finite size is to shift the critical point; therefore, the distance to the critical point $\Delta = \overline{E} - \overline{E}_c$ is a function of the size such that, if $\overline{E}$ takes the $L \to \infty$ critical value $\overline{E}(\infty) = \overline{E}_c$:

$$\Delta(L) = \overline{E} - \overline{E}_c(L) = \overline{E}_c(\infty) - \overline{E}_c(L) > 0 \tag{2.11}$$

approaching $\Delta(\infty) = 0$ in the thermodynamic limit. Thus, for $\overline{E} = \overline{E}_c$, correlations in a system small enough span so fast through the lattice that, in a finite time, they make the order parameter converge to a stationary value $\overline{\rho}_{st}$. This time is larger as the size increases, and the stationary value smaller, in order to recover the pure power-law behavior in the thermodynamic limit.

These saturation values are not arbitrary; for an over-critical state, these values depend on the distance to the critical point:

$$\overline{\rho}_{st} \sim \Delta^{\beta}. \tag{2.12}$$

As the relation between the distance to the critical point and the correlation length is given by (see appendix A.1.2):

$$\xi \sim \Delta^{-\nu_\perp}, \tag{2.13}$$

at the critical point, where the maximum correlation length is given by the finite system size:

$$\overline{\rho}_{st} \sim L^{-\beta/\nu_\perp}. \tag{2.14}$$

With similar arguments, and using Eq.(A.1.9), for saturation times:

$$t_{st} \sim L^{z}, \tag{2.15}$$

where z (defined in the previous chapter, see Eq.(1.7)) is related with the above defined z_{spr}:

$$z = \frac{2}{z_{spr}}. \tag{2.16}$$

2.4 Other systems with Absorbing States

In the previous section, stochastic SOC sandpiles have been brought into a fixed-energy ensemble, translationally invariant, in which an unambiguous identification of order and control parameters is possible; energy is an independent tuning parameter, not dynamic anymore. It allows, for instance to reach any point of the phase diagram.

In the FES ensemble, SOC is treated as a nonequilibrium second-order phase transition into an infinite number of absorbing states. Both ensembles describe in a different way the very same critical point, which is associated with the relaxation rules. Due to this, the formalism which is applied to absorbing phase transitions can be applied to the FES version of SOC systems.

The paradigm of systems with an absorbing phase transition are those belonging to the universality class of **Directed Percolation** (DP) [78, 81]. Janssen [82] and Grassberger [83] conjectured a quarter of century ago that *in the absence of other symmetries, the phase transition of a one-component model from an active phase to a single absorbing state belongs to the DP universality class*. The archetypical microscopic model of DP is the *contact process*, an infection model in which each active site of a d-dimensional hypercubic lattice infects (creates a particle, or activates) a neighboring site with probability p, or dies (annihilate itself) with probability $1 - p$ [78, 81]. At a mesoscopic level, the DP class is represented by the Langevin equation [84] of the Reggeon Field Theory (RFT):

$$\partial_t \rho(\vec{x}, t) = D\nabla^2 \rho(\vec{x}, t) + \mu\rho(\vec{x}, t) - \lambda\rho^2(\vec{x}, t) + \sigma\sqrt{\rho(\vec{x}, t)}\eta(\vec{x}, t) \qquad (2.17)$$

where ρ is a field which represents the activity density at a coarse-grained level[6], and D, μ, λ and σ are constants, representative of the probabilities for each microscopic event to occur. Spatial and temporal dependency will be omitted when not necessary.

The first term of the right hand side of the equation takes into account the diffusion of activity due to infection processes. The second and the third terms are representative of the creation and annihilation of activity. Concerning the noise, it is a short-range gaussian noise; its dependence on the square root of the activity field is due to the Poissonian distribution of the

[6] Therefore, only non-negative values are allowed.

number of microscopic creation and annihilation events, Gaussian distributed in the continuum limit, which makes the noise variance proportional to the mean rate of the process, namely the activity field ρ. This kind of noise (**multiplicative noise**) is associated with many stochastic creation and annihilation processes.

One essential feature of this equation is the fact that, when $\rho(\vec{x},t) = 0\ \forall\vec{x}$, the state remains frozen, i.e. falls into the **unique** absorbing configuration, from which it cannot scape by itself. The Renormalization Group (RG) procedures have succeeded in the calculation of the critical exponents for the RFT (see table 2.1 and table 2.2), which are known in any dimension.

DP with an Infinite Number of Absorbing States

The conjecture has been extended, and now is not limited to one-component systems nor to one single but infinitely many possible absorbing configurations. This is the case of the pair contact process (PCP) [85]. In this model, pairs of particles annihilate with a certain probability p, or create a new particle at a randomly chosen neighboring site with the complementary probability $1-p$. In this way, there is an effective diffusion of pairs, which are the active species, and isolated particles (which form the background) do not diffuse nor react.

An infinite number (in the thermodynamic limit) of absorbing configurations, in which only isolated particles are present, can be defined. By tuning p (which is the control parameter), it is possible to find a critical value p_c for which the system undergoes a phase transition, from an active state to one of these absorbing configurations, which belongs to DP universality class [80, 85–87].

The Lagevin equations associated with this model are [86]:

$$\begin{cases} \partial_t\rho = & D_\rho\nabla^2\rho + \mu_\rho\rho - \lambda_\rho\rho^2 - \omega_\rho\rho\phi + \sigma\sqrt{\rho}\eta(\vec{x},t) \\ \partial_t\phi = & D_\phi\nabla^2\rho + \mu_\phi\rho - \lambda_\phi\rho^2 - \omega_\phi\rho\phi, \end{cases} \tag{2.18}$$

where ρ and ϕ are coarse-grained descriptions of activity and background species, respectively, and D_ρ, μ_ρ, λ_ρ, ω_ρ, σ, D_ϕ, μ_ϕ, λ_ϕ, and ω_ϕ are constant coefficients. *Irrelevant terms*, in the sense of the RG approach[7], have been

[7] Terms which do not influence the long-distance nor long-time behavior near the transition.

dropped off. Also, the values $D_\phi = \lambda_\phi = 0$ can be chosen, because the associated terms are generated by RG iteration of the resulting equations. By doing so, the second equation can be integrated and ϕ replaced into the activity equation [87]:

$$\begin{aligned}\partial_t\rho = \; & D_\rho\nabla^2\rho + (\mu_\rho - \omega_\rho\mu_\phi/\omega_\phi)\rho - \lambda_\rho\rho^2 \\ & +\omega_\rho(\mu_\phi/\omega_\phi - \phi(\vec{x},0))\rho\; e^{-\omega_\phi\int_0^t \rho(\vec{x},t')dt'} + \sigma\sqrt{\rho}\eta(\vec{x},t).\end{aligned} \tag{2.19}$$

This equation is essentially the RFT equation, Eq.(2.17), with an extra coupling term to a non-conserving non-diffusing field (ϕ) by means of the exponential of a non-Markovian term. This non-Markovian term arises from the presence of a non-trivial background, which creates an effective memory in the dynamics due to its non-diffusive character. The coupling prevents Eqs.(2.18) from being treated with RG procedures, because the non-Markovian term introduces highly singular propagators which reflect the static nature of the background field in the absorbing state.

It is straightforward to see that, starting from an homogeneous active configuration, as $\overline{\rho}$ decays, $\overline{\phi}$ evolves to reach a stationary value given by an average density μ_ϕ/ω_ϕ. For the long time behavior of the stationary active states, or for spreading experiments starting from a natural absorbing state (i.e. with average initial density $\overline{\phi}(t=0) = \mu_\phi/\omega_\phi$), the exponential term vanishes, and the Langevin representation of DP is recovered. Therefore, both static and dynamic long-time behavior at criticality are DP-like. This is one illustrative application of the discussion about the initial state made in the previous section.

A Different Background

Consider the PCP set of Langevin equations, Eqs.(2.18), with periodic boundary conditions. In this system, the background is not only a product of activity transport (like in sandpiles), but it can be locally created and dissipated. The total number of particles is not conserved. In fact, the evolution of its density (or, equivalently, $\overline{\phi}$) is a function of the decay of $\overline{\rho}$. It is not possible, then, to reach the critical state by fixing p to any arbitrary value and tune the density of particles, because there exist only *one* critical value for p (p_c), and a value of $\overline{\phi}$ associated with it. Out of this value, the background reaches a stationary non-critical state which fosters sustained activity (supercritical regime), or in which the system falls exponentially fast into the absorbing state (subcritical regime).

The universality hypothesis made for DP depends on the presence of any other symmetry in the system. This means that it is possible to lose the DP behavior in a system with absorbing states by imposing extra relevant ingredients [88]. It is the case, for example, of a symmetry between different types of absorbing states [89]; but it also can be the case of the presence of an ingredient such as a conserved field.

In PCP, as in stochastic sandpiles, the non-diffusive background is coupled to the activity. However, the key difference which distinguishes DP class from the class of stochastic sandpiles can be deduced from the above discussion: **the conservation law**. As said in the beginning of the chapter, the correlations developed in the background depends on the relaxation rules. The conservative dynamics of sandpiles is essentially diffusive: is the diffusion of the activity the *only* mechanism through which rearrangements of the background are performed. This generates strong and long-termed correlations.

Contrarily, in PCP there is a mechanism which, regardless the shape of the neighboring background and depending solely on the chosen value for the parameters of the system, creates or destroys pairs and isolated particles as soon as activity reaches the site. Therefore, the background of PCP, a priori, is correlated in a very different way from the one of sandpiles. Thus, it could be said that, for stochastic sandpiles, different critical behavior from DP is expected.

For the moment, this claim can be only confirmed by performing numerical experiments on microscopic models intended to be in the Manna class, and comparing the results with a microscopic DP model as the contact process or the many-absorbing-state DP model (PCP).

2.5 The C-DP Universality Class

As pointed out above, the universality class of the stochastic sandpiles is characterized by a coupling between a non-diffusive *conserved* field and the order parameter of an absorbing phase transition into one of many absorbing states. As, in principle, conservation is the only relevant ingredient which makes this class different from DP, the class of stochastic sandpiles will be called from now on **Conserved Directed Percolation**, or **C-DP class**.

For the C-DP class, a conjecture can be also made [90]: *in the absence of additional symmetries, all the stochastic models with an infinite number of absorbing states in which the order parameter is coupled to a nondiffusive*

$d=1$	η	δ	τ	τ_t	z_{spr}
DP	0.31368(4)	0.15947(3)	1.108(1)	1.159(1)	1.26523(3)
Manna$_{SOC}$	0.31(5)	0.14(5)	1.10(5)	1.14(5)	1.31(5)
Manna$_{FES}$	0.350(30)	0.170(25)	1.11(3)	1.17(3)	1.44(4)
Oslo$_{SOC}$	0.37(3)	0.16(3)	1.10(3)	1.16(3)	1.39(3)
Oslo$_{FES}$	0.35(2)	0.17(2)	1.11(2)	1.17(2)	1.38(2)

Table 2.1: Critical exponents for DP (first row) and many C-DP systems in $d=1$. Own measurements, except DP [79] and Manna$_{FES}$ [92, 93]. The rest of measured exponents can be found in table C.1, in appendix C.

conserved field define a unique and per-se universality class called C-DP.

All the isotropic stochastic sandpiles obviously belong to this universality class; but also other models like the conserved lattice gas (CLG) [90] (which is a conserved version of the model already introduced in [31]), or the conserved threshold transfer process (CTTP), the conservative counterpart of the model introduced in [91][8]. It is possible to compare the critical behavior of the stochastic sandpiles defined in the previous chapter and DP by using tables 2.1 and 2.2, in which it is evident that all these piles belong to a unique class (C-DP universality class), and the DP behavior (first row of each table) can be excluded. For $d=1$, results of both the SOC and FES ensembles are exposed. The coincidence of the critical exponents, as well as the fulfillment of scaling relations Eq.(2.6) and Eq.(2.7), and the coincidence of the critical value of the control parameter shows the equivalence between SOC and FES ensembles: for Manna$_{FES}$, $E_c = 0.8917(5)$ and for Manna$_{SOC}$, $E_c = 0.8913(2)$; in Oslo$_{FES}$, by fixing $E_c = 1.5$ and using p as control parameter, $p_c = 0.73195(5)$, and in Oslo$_{SOC}$ with $p = p_c$, $E = 1.4990(5)$ ...The only differences stem from finite size effects and the systematical error when the critical point is measured *a la FES*.

Also, by using the FES ensemble, it is fairly obvious that deterministic sandpiles like the BTW one definitively do not belong to this class. Extensive simulations by using this ensemble reveal non-ergodic behavior, as well as strong finite-size effects and finite-size scaling violation [75], a staircase-shaped phase diagram in $d=2$ and short-period attractors [94]. Analytical results for $d=1$ also confirm many of these pathologies [95]. Actually, the presence of *toppling invariants* in the BTW model [44] introduces extra-

[8]Both CLG and CTTP can be considered to belong to this universality class, despite some pathological behavior for $d=1$.

$d = 2$	η	δ	τ	τ_t	z_{spr}
DP	0.230(1)	0.451(1)	1.268(1)	1.451(1)	1.13(1)
Manna	0.22(5)	0.48(5)	1.27(5)	1.48(5)	1.25(5)
Oslo	0.23(5)	0.48(5)	1.26(5)	1.48(5)	1.28(5)
CLG_{FES}	0.29(1)	0.49(1)	1.29(1)	1.49(1)	1.31(2)
CTTP_{FES}	0.30(3)	0.49(1)	1.28(1)	1.49(1)	1.30(1)

Table 2.2: Critical exponents for DP (first row; taken from [79]) and many C-DP systems in $d = 2$. Own measurements, except for DP, CLG and CTTP [90].

conservations different from the usual conservation of grains and, therefore, violates the conjecture of the C-DP class. This confirms that **the BTW pile does not belong to the same universality class of the Manna model**.

So far, numerical simulations confirm the conjecture made before for the C-DP class. However, still a mesoscopic description is required in order to state the claims of the conjecture using a Langevin equation (free of microscopic details which can mask with long-transient behavior the real critical scaling of a system) with which, hopfully, some analytical calculations can be done.

2.6 Reaction-Diffusion Models

For DP, it is possible to deduce rigorously the RFT equation (Eq.(2.17)) by means of coarse-graining a **reaction-diffusion** model which captures the essential features of the class (see below). This model can be summarized with the reactions [81]:

$$A \to 2A \qquad \text{with rate } \varsigma_1 \tag{2.20a}$$

$$2A \to A \qquad \text{with rate } \varsigma_2, \tag{2.20b}$$

along with an effective diffusion of activity due to the infectation process. The first reaction represents the infection or creation of activity, and the second, the healing or annihilation. As in the simple contact process, there is only one species: the active particles.

To represent the characteristics of the C-DP class, two different species are necessary: one which represents the diffusing activity of the dynamics (species A), and a non-diffusive background species (B)[9]. Then, a set of reactions which could represent in the most simple way the characteristic processes of the dynamics of a C-DP system are [96]:

$$A \to B \qquad \text{with rate } k_1 \tag{2.21a}$$
$$A + B \to 2A \qquad \text{with rate } k_2. \tag{2.21b}$$

With the first equation, an active particle is transformed into a background particle with a probability which depends on the rate k_1 (toppling). Through the second equation, a new active particle is generated with a rate k_2 from the convergence of an active and a background particle (activation). Also, a diffusion equation for activity must be added, in order to take into account the diffusive nature of this species:

$$A + \varnothing \to \varnothing + A \qquad \text{with rate } D_A, \tag{2.22}$$

This model, represented by means of the reaction-diffusion equations Eq.(2.21a)-Eq.(2.22), and introduced by Pastor-Satorras and Vespignani in [96], will be called here the **RD model** from now on.

Note that this model possesses a strictly-conservative dynamics. If there are n_A particles of species A and n_B particles of species B, the sum of both $N = n_A + n_B$ is not altered by any of these reactions. When $n_A = 0$, none of the reactions is possible and the system remains frozen in one of the many possible absorbing configurations, which differ in the distribution of the B particles throughout the system.

Thus, the RD model fulfills the conditions imposed by the C-DP conjecture, namely conservation, stochastic dynamics, multiple absorbing states and a coupling of activity with a non-diffusive background field[10]. As there are no more ingredients, the scaling of this system is expected to be very clean.

[9] These are abstract species, in the sense that there is not a one-to-one correspondence between these particles and grains.

[10] Diffusion in the background field, $D_B \neq 0$, influences dramatically the critical behavior of this model (see [97] and references therein for analytical approach, and [98] for numerical results).

The Critical Behavior of the RD Model

To check this claim, numerical simulations must be performed. Consider the two species A and B interplaying by means of reactions Eq.(2.21a)-Eq.(2.22) at a $d = 1$ array of size L whose sites, labeled with the index i, store a number n_{A_i} of active particles and n_{B_i} background particles. In this system, the total number of each species is:

$$n_A = \sum_{i=1}^{L} n_{A_i} \qquad n_B = \sum_{i=1}^{L} n_{B_i} \qquad (2.23)$$

$$N = n_A + n_B.$$

Periodic boundary conditions are used. The initial state can be generated by randomly distributing a number n_A^0 and n_B^0 of particles among the sites of the lattice, fulfilling $N = n_A^0 + n_B^0$; in this way, the occupation numbers n_{A_i} and n_{B_i} of the system follow a Poissonian distribution [96]. As there is activity on the system, reactions must be performed. Without loss of generality, the following order is selected:

1. Diffusion: At each site of the system, each active particle A moves to a randomly chosen site with probability D.
2. Reaction Eq.(2.21a): Each active particle A of the system is transformed into a background one with a probability r_1.
3. Reaction Eq.(2.21b): Each background particle B is turned into an active one with probability $1 - (1 - r_2)^{n_{A_i}}$.

Probabilities D, r_1 and r_2 are increasing functions of rates D_A, k_1 and k_2, respectively. The probability for reaction Eq.(2.21b) can be easily deduced: if $(1 - r_2)$ is the probability for an A particle of a site i to *not* react with a B particle at this site, $(1 - r_2)^{n_{A_i}}$ is the probability for a B particle to react with none of the A particles on site i; thus, $1 - (1 - r_2)^{n_{A_i}}$ is the probability for a B particle to react with, *at least*, one of the A particles of the site.

By tuning one of the possible parameters of the dynamics, the critical point can be found. By fixing $\overline{E} = N/L = 1$, $D = 1$, and $r_2 = 0.5$, and using r_1 as control parameter, the critical point is found at $r_{1c} = 0.17155(3)$. It is possible also to perform spreading experiments, in which a natural initial configuration of B particles is perturbed with an initial seed of activity (i.e.

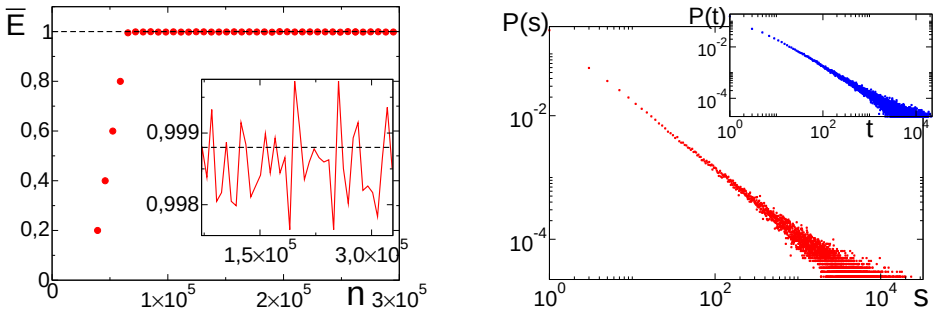

Figure 2.2: Left: Evolution of the density of particles $\overline{E}$ as a function of the number of driving events, n, in $d = 1$ RD model with $r_1 = 0.17155$, $r_2 = 0.5$, $D = 1$, and size $L = 32768$. For $n \geq 30000$, the stationary critical state is reached, and $\overline{E}$ fluctuates around the critical value $\overline{E}_c = 0.9988(5)$ (inset). Right: Avalanche size and lifetime (inset) distributions.

RD model	η	δ	τ	τ_t	z_{spr}
$d = 1$	0.34(2)	0.16(2)	1.11(3)	1.16(3)	1.34(2)
$d = 2$	0.27(5)	0.49(5)	1.29(5)	1.49(5)	1.24(5)

Table 2.3: Critical exponents for the spreading observables and the probability distributions in RD model. Own measurements.

one A particle). Of course, by using open boundaries and slow-driving, the SOC counterpart for this system can be simulated [99], in which critical avalanches are developed when the number of particles reaches the stationary critical state ($\overline{E}_c = 0.9988(5)$, if $r_1 = 0.17155$, $r_2 = 0.5$; see Fig.2.2).

For both ensembles, the measured exponents can be found in table 2.3. Due to the coincidence, within error bars, with the C-DP exponents (see above), the RD model is representative of the C-DP class.

Once it is well-stated that the RD model is a good representative of the C-DP class, it is time to exploit its major advantage: the possibility to map microscopic reaction-diffusion equations into mesoscopic continuous equations.

2.7 A Continuous Description for Stochastic Sandpiles

A new simple model with the same ingredients of the C-DP universality class has been devised to naturally connect microscopic and mesoscopic levels of description. In order to obtain a mesoscopic representative for the C-DP universality class, Doi-Peliti and Fock-space formalism [100–107] techniques will be applied to the RD model in the FES ensemble.

Let $P(\alpha, \beta; t)$ be the probability distribution for the system to be in the configuration $\alpha = \left\{n_{A_1}, n_{A_2}, ..., n_{A_{L^d}}\right\}$ and $\beta = \left\{n_{B_1}, n_{B_2}, ..., n_{B_{L^d}}\right\}$ at time t. Then, the evolution equation for the probability distribution (i.e. the **master equation**) can be written as:

$$\begin{aligned} \partial_t P(\alpha, \beta; t) = & \sum_{(\alpha', \beta')} w((\alpha', \beta') \to (\alpha, \beta)) P(\alpha', \beta'; t) \\ & - \sum_{(\alpha, \beta)} w((\alpha, \beta) \to (\alpha', \beta')) P(\alpha, \beta; t), \end{aligned} \tag{2.24}$$

where the first term represents the probability inflow to state (α, β), and the second term, the outflow from it to a generic state (α', β'), with $w((\alpha', \beta') \to (\alpha, \beta))$ the rate of the transition from (α', β') state to (α, β), and $w((\alpha, \beta) \to (\alpha', \beta'))$ the opposite one.

As mentioned in appendix B, by taking into account each concrete example, the master equation can be written as:

$$\partial_t |\Psi(t)\rangle = -\hat{H} |\Psi(t)\rangle. \tag{2.25}$$

In this case, the operator $\hat{H}$ can be expressed as the sum of the contribution of each single site and each single process:

$$\hat{H} = \sum_i \left[\hat{H}_i^{Eq.(2.21a)} + \hat{H}_i^{Eq.(2.21b)} + \hat{H}_i^{Eq.(2.22)} \right] \tag{2.26}$$

This permits to calculate separately each of the parts of the $\hat{H}$ operator for each site, and consider in the last steps the joint contribution[11]. Equations

[11] Except, of course, for the diffusion, in which two sites (the origin and the target) are involved.

Eq.(2.25)-Eq.(2.26) remain justified when each contribution is calculated.

Now, each reaction will be studied separately, applied to a single site, by using the concepts introduced in appendix B; the index of the site will be omitted when not necessary.

a) Reaction $A \xrightarrow{k_1} B$

For the reaction Eq.(2.21a), the transition rates are:

$$\begin{aligned} w((m',n') \to (m,n)) = &\quad k_1 \binom{m'}{1} \delta_{(m',n'),(m+1,n-1)} \\ w((m,n) \to (m',n')) = &\quad k_1 \binom{m}{1} \delta_{(m',n'),(m-1,n+1)}, \end{aligned} \tag{2.27}$$

because only active particles react, and only states with one more or one less active particle are accessible from (m,n). By doing so, the master equation for this reaction takes the form:

$$\partial_t P(m,n;t) = k_1(m+1)P(m+1,n-1;t) - k_1 m P(m,n;t). \tag{2.28}$$

Multiplying by the $|m,n\rangle$ state all terms of the above equation and summing over all the possible states:

$$\begin{aligned} \partial_t \sum_{(m,n)} P(m,n;t)|m,n\rangle = &\quad k_1 \sum_{(m,n)} (m+1)P(m+1,n-1;t)|m,n\rangle \\ &- k_1 \sum_{(m,n)} m P(m,n;t)|m,n\rangle, \end{aligned} \tag{2.29}$$

where it is easy to see that, using creation and annihilation operators $(\hat{a}, \hat{a}^\dagger)$ and $(\hat{b}, \hat{b}^\dagger)$ (see appendix B) in the standard way for each species:

$$\begin{aligned} (m+1)|m,n\rangle = &\quad \hat{b}^\dagger \hat{a}|m+1,n-1\rangle \\ m|m,n\rangle = &\quad \hat{a}^\dagger \hat{a}|m,n\rangle. \end{aligned} \tag{2.30}$$

By performing a change of variables in the first addend on the right hand side (r.h.s):

$$\begin{aligned}\partial_t \sum_{(m,n)} P(m,n;t)|m,n\rangle = \; & k_1 \hat{b}^\dagger \hat{a} \sum_{(m,n)} P(m,n;t)|m,n\rangle \\ & -k_1 \hat{a}^\dagger \hat{a} \sum_{(m,n)} P(m,n;t)|m,n\rangle\end{aligned} \tag{2.31}$$

and, by applying Eq.(B.1.12), the master equation for the reaction $A \xrightarrow{k_1} B$ at site i becomes:

$$\partial_t |\psi(t)\rangle = k_1(\hat{b}^\dagger - \hat{a}^\dagger)\hat{a}|\psi(t)\rangle \tag{2.32}$$

and, therefore:

$$\hat{H}_i^{Eq.(2.21a)} = k_1(\hat{a}^\dagger - \hat{b}^\dagger)\hat{a}. \tag{2.33}$$

b) Reaction $A + B \xrightarrow{k_2} 2A$

For the reaction Eq.(2.21b), the transition rates are given by:

$$\begin{aligned} w((m',n') \to (m,n)) = \; & k_2 \binom{m'}{1}\binom{n'}{1}\delta_{(m',n'),(m-1,n+1)} \\ w((m,n) \to (m',n')) = \; & k_2 \binom{m}{1}\binom{n}{1}\delta_{(m',n'),(m+1,n-1)}. \end{aligned} \tag{2.34}$$

Again, only states differing in one particle are accessible from (m,n). Replacing these terms on the master equation for the process:

$$\begin{aligned}\partial_t P(m,n;t) = \; & k_2(m-1)(n+1)P(m-1,n+1;t) \\ & -k_2 m\, nP(m,n;t).\end{aligned} \tag{2.35}$$

Now, the state $|m,n\rangle$ is introduced, along with the sum over all the possible states:

$$\begin{aligned}\partial_t \sum_{(m,n)} P(m,n;t)|m,n\rangle = \; & k_2 \sum_{(m,n)} (m-1)(n+1)P(m-1,n+1;t)|m,n\rangle \\ & -k_2 \sum_{(m,n)} m\, nP(m,n;t)|m,n\rangle.\end{aligned} \tag{2.36}$$

Using creation and annihilation operators for each species:

$$\begin{aligned}(m-1)(n+1)|m,n\rangle = \; & \hat{a}^{\dagger 2}\hat{a}\hat{b}|m-1,n+1\rangle \\ m\, n|m,n\rangle = \; & \hat{a}^{\dagger}\hat{a}\hat{b}^{\dagger}\hat{b}|m,n\rangle,\end{aligned} \tag{2.37}$$

and, by performing a change of variables in the first term of r.h.s. of Eq.(2.36):

$$\begin{aligned}\partial_t \sum_{(m,n)} P(m,n;t)|m,n\rangle = \; & k_2\hat{a}^{\dagger 2}\hat{a}\hat{b} \sum_{(m,n)} P(m,n;t)|m,n\rangle \\ & -k_2\hat{a}^{\dagger}\hat{a}\hat{b}^{\dagger}\hat{b} \sum_{(m,n)} P(m,n;t)|m,n\rangle.\end{aligned} \tag{2.38}$$

Therefore, applying Eq.(B.1.12), the i-th site master equation for the reaction $A + B \xrightarrow{k_2} 2A$ is:

$$\partial_t|\psi(t)\rangle = k_2(\hat{a}^{\dagger} - \hat{b}^{\dagger})\hat{a}^{\dagger}\hat{a}\hat{b}|\psi(t)\rangle \tag{2.39}$$

and, the $\hat{H}_i$ operator for this site is:

$$\hat{H}_i^{Eq.(2.21b)} = k_2(\hat{b}^{\dagger} - \hat{a}^{\dagger})\hat{a}^{\dagger}\hat{a}\hat{b}. \tag{2.40}$$

c) Diffusion of A Particles

For the master equation of the diffusion, we need to consider two adjacent sites; suppose that, in a diffusive step, one active particle jumps from site i to a nearest neighbor j of i. Therefore, there are two independent contributions to each probability flow: the diffusive motion started at i (one active particle lost) and the diffusive motion ended at i (one active particle arriving). The

state depends now on the number m_i of A particles at i and m_j at j. The transition rates are now:

$$\begin{aligned} w((m_i', m_j') \to (m_i, m_j)) = \; & D_A \binom{m_i'}{1} \delta_{(m_i', m_j'),(m_i+1, m_j-1)} \\ & + D_A \binom{m_j'}{1} \delta_{(m_i', m_j'),(m_i-1, m_j+1)} \\ w((m_i, m_j) \to (m_i', m_j')) = \; & D_A \binom{m_i}{1} \delta_{(m_i', m_j'),(m_i-1, m_j+1)} \\ & + D_A \binom{m_j}{1} \delta_{(m_i', m_j'),(m_i+1, m_j-1)}. \end{aligned} \tag{2.41}$$

Once again, only states differing one particle are accessible from (m_i, m_j). The master equation for the process is:

$$\begin{aligned} \partial_t P(m, n; t) = \; & D_A(m_i + 1)P(m_i + 1, m_j - 1; t) \\ & + D_A(m_j + 1)P(m_i - 1, m_j + 1; t) \\ & - D_A m_i P(m_i, m_j; t) - D_A m_j P(m_i, m_j; t). \end{aligned} \tag{2.42}$$

Now, introducing the state $|m_i, m_j\rangle$, independent of the number of B particles and summing over all the possible states:

$$\begin{aligned} \partial_t \sum_{(m_i, m_j)} P(m_i, m_j; t)|m_i, m_j\rangle = \; & D_A \sum_{(m_i, m_j)} [(m_i + 1)P(m_i + 1, m_j - 1; t) \\ & + (m_j + 1)P(m_i - 1, m_j + 1; t)]|m_i, m_j\rangle \\ & - D_A \sum_{(m_i, m_j)} [m_i P(m_i, m_j; t) \\ & + m_j P(m_i, m_j; t)]|m_i, m_j\rangle, \end{aligned} \tag{2.43}$$

where:

$$\begin{aligned}(m_i+1)|m_i,m_j\rangle &= \hat{a}_j^\dagger\hat{a}_i|m_i+1,m_j-1\rangle\\ (m_j+1)|m_i,m_j\rangle &= \hat{a}_i^\dagger\hat{a}_j|m_i-1,m_j+1\rangle\\ m_i|m_i,m_j\rangle &= \hat{a}_i^\dagger\hat{a}_i|m_i,m_j\rangle\\ m_j|m_i,m_j\rangle &= \hat{a}_j^\dagger\hat{a}_j|m_i,m_j\rangle\end{aligned} \tag{2.44}$$

and, with a change of variables in the first two terms of Eq.(2.43), one obtains:

$$\begin{aligned}\partial_t\sum_{(m_i,m_j)}P(m_i,m_j;t)|m_i,m_j\rangle = \; & D_A(\hat{a}_j^\dagger\hat{a}_i+\hat{a}_i^\dagger\hat{a}_j)\sum_{(m_i,m_j)}P(m_i,m_j;t)|m_i,m_j\rangle\\ & -D_A(\hat{a}_i^\dagger\hat{a}_i+\hat{a}_j^\dagger\hat{a}_j)\sum_{(m_i,m_j)}P(m_i,m_j;t)|m_i,m_j\rangle\end{aligned} \tag{2.45}$$

which, with Eq.(B.1.12), is transformed into:

$$\partial_t|\psi(t)\rangle = D_A(\hat{a}_i^\dagger-\hat{a}_j^\dagger)(\hat{a}_j-\hat{a}_i)|\psi(t)\rangle \tag{2.46}$$

and the $\hat{H}_i$ operator for this site is:

$$\hat{H}_i^{Eq.(2.22)} = D_A(\hat{a}_j^\dagger-\hat{a}_i^\dagger)(\hat{a}_j-\hat{a}_i) = -D_A\nabla\hat{a}^\dagger\nabla\hat{a}. \tag{2.47}$$

Overall Process

Now that the contribution of each reaction to $\hat{H}$ operator has been obtained, it can be written explicitely for the whole system:

$$\hat{H} = \sum_i\left[-D_A\nabla\hat{a}_i^\dagger\nabla\hat{a}_i + k_1(\hat{a}_i^\dagger-\hat{b}_i^\dagger)\hat{a}_i + k_2(\hat{b}_i^\dagger-\hat{a}_i^\dagger)\hat{a}_i^\dagger\hat{a}_i\hat{b}_i\right]. \tag{2.48}$$

The next step is to use this Hamiltonian into the generating function of the process (see appendix B). To this end, it is necessary to perform a coarse-graining of the operators. This coarse-grained form is:

$$\begin{array}{ll} \hat{a} \to \varphi(\vec{x},t), & \hat{b} \to \phi(\vec{x},t), \\ \hat{a}^\dagger \to \bar{\varphi}(\vec{x},t), & \hat{b}^\dagger \to \bar{\phi}(\vec{x},t). \end{array} \tag{2.49}$$

where the overlined fields are called **response fields**. From now on, spatial and time dependence of fields will be omitted when not necessary. Using these fields, the generating function of the overall process is given by Eq.(B.1.37), where the associated action is (see appendix B):

$$\begin{aligned} S(\varphi,\bar{\varphi},\phi,\bar{\phi}) = & \int d^dx \int dt \left[i\bar{\varphi}\partial_t\varphi + i\bar{\phi}\partial_t\phi\tilde{H} \right] \\ - & \int d^dx \left[(1+i\bar{\varphi}_0)n_A^0 + (1+i\bar{\phi}_0)n_B^0 \right] \end{aligned} \tag{2.50}$$

and:

$$\begin{aligned} \tilde{H} = & \ H(\varphi, 1+i\bar{\varphi}, \phi, 1+i\bar{\phi}) \\ = & \left[-D_A i\nabla\bar{\varphi}\nabla\varphi + k_1(i\bar{\varphi}-\bar{\phi})\varphi + k_2(i\bar{\phi}-i\bar{\varphi})(i\bar{\varphi}\varphi\phi + \varphi\phi) \right]. \end{aligned} \tag{2.51}$$

Next, the new fields [97]:

$$\begin{array}{ll} \rho(\vec{x},t) = \varphi; & E(\vec{x},t) = \varphi + \phi - \bar{n}\Theta(t); \\ \bar{\rho}(\vec{x},t) = \bar{\varphi} - \bar{\phi}; & \bar{E}(\vec{x},t) = \bar{\phi}; \end{array} \tag{2.52}$$

are defined, where $\bar{n}$ represents the density of total number of particles[12] and, after introducing them into the generating function, rearranging and grouping terms:

$$\begin{aligned} \hat{H} = & \ i\bar{\rho}\left[k_1\rho + k_2\rho^2 - k_2\rho E + \bar{n}\rho\Theta(t) \right] \\ & -D_A i\nabla\bar{\rho}\nabla\rho - D_A i\nabla\bar{E}\nabla\rho + k_2\rho\bar{n}\Theta(t)\bar{\rho}^2 \\ & -k_2\rho^2\bar{\rho}^2 + k_2\bar{\rho}^2\rho E - k_2(\rho^2 - E - \rho\bar{n}\Theta(t))\bar{\rho}\bar{E} \end{aligned} \tag{2.53}$$

Power counting techniques provide a preliminary intuition of which terms are irrelevant; by performing this analysis, the last three terms on Eq.(2.53)

[12]The step function $\Theta(t)$ ensures that this extra term is well-defined into the integrals.

can be neglected [97]. Dropping these terms from the previous result and by introducing it into the new action of the whole process:

$$\begin{aligned} S(\rho,\bar{\rho},E,\bar{E}) = & \int d^dxdt[i\bar{\rho}(\partial_t - D_\rho\nabla^2)\rho + \mu\rho(i\bar{\rho}) + \lambda\rho^2(i\bar{\rho}) - \omega(i\bar{\rho})\rho E \\ & + i\bar{E}(\partial_t - D_E\nabla^2\rho) + \bar{\sigma}\rho\bar{\rho}^2] \end{aligned} \tag{2.54}$$

where the integration by parts of the gradients has been performed in order to write them as the Laplacian of the activity. Also, initial-state factors have been omitted, and coarse-grained coefficients (D_ρ, μ, λ, ω, D_E and $\bar{\sigma}$) have been defined; they are un-specified functions of the original reaction rates. Thus, the generating function takes the form:

$$Z = \int \mathcal{D}\varphi\mathcal{D}\bar{\varphi}\mathcal{D}\phi\mathcal{D}\bar{\phi}e^{-S(\rho,\bar{\rho},E,\bar{E})}. \tag{2.55}$$

If it is considered apart from the rest of terms of the generating function, the quadratic term in $\bar{\rho}$ can be linearized by using that:

$$\begin{aligned} e^{-\int d^dxdt\bar{\sigma}\rho\bar{\rho}^2} &= \prod_{(\vec{x},t)} e^{-\bar{\sigma}\rho\bar{\rho}^2} \\ &= \int \mathcal{D}\zeta P(\zeta)e^{-\int d^dxdt(i\bar{\rho})\zeta}, \end{aligned} \tag{2.56}$$

where $P(\zeta)$ is the distribution function of the stochastic variable ζ; this new variable is a Gaussian-distributed noise with correlations:

$$\langle\zeta(\vec{x},t)\zeta(\vec{x}',t)\rangle = 2\bar{\sigma}\rho\delta(\vec{x}'-\vec{x})\delta(t'-t) \tag{2.57}$$

Equivalently, it can be written from now on as:

$$\zeta(\vec{x},t) = \sigma\sqrt{\rho}\eta(\vec{x},t), \tag{2.58}$$

where:

$$\langle\eta(\vec{x},t)\eta(\vec{x}',t)\rangle = \delta(\vec{x}'-\vec{x})\delta(t'-t), \tag{2.59}$$

and $\sigma = \sqrt{2\bar{\sigma}}$. With this, the action S is now a linear function in $\bar{\rho}$ and $\bar{E}$:

$$\begin{aligned} S(\rho,\bar{\rho},E,\bar{E}) = & \int d^dxdt[i\bar{\rho}(\partial_t - D_\rho\nabla^2)\rho + \mu\rho(i\bar{\rho}) + \lambda\rho^2(i\bar{\rho}) - \omega(i\bar{\rho})\rho E \\ & + i\bar{E}(\partial_t - D_E\nabla^2\rho) - i\sigma\sqrt{\rho}\eta\bar{\rho}] = \\ = & \int d^dxdt\left[i\bar{\rho}(\partial_t\rho - F(\rho,E)) + i\bar{E}(\partial_t E - G(\rho,E))\right] \end{aligned} \tag{2.60}$$

where, defining:

$$\begin{aligned} F(\rho,E) = & -D_\rho\nabla^2\rho + \mu\rho + \lambda\rho^2 - \omega\rho E - \sigma\sqrt{\rho}\eta \\ G(\rho,E) = & -D_E\nabla^2\rho, \end{aligned} \tag{2.61}$$

the generating function can be written as:

$$Z = \int \mathcal{D}\eta\mathcal{D}\rho\mathcal{D}\bar{\rho}\mathcal{D}E\mathcal{D}\bar{E}P(\eta)e^{-i\int d^dxdt\bar{\rho}(\partial_t\rho - F(\rho,E))}e^{-i\int d^dxdt\bar{E}(\partial_t E - G(\rho,E))}. \tag{2.62}$$

Now, the path integral over these *response fields* can be performed using the path integral representation of the delta function:

$$\int \mathcal{D}\bar{\phi}e^{-i\int d^dxdt\bar{\phi}(\phi - F(\phi))} = \prod_{(\vec{x},t)} \delta\left(\phi - F(\phi)\right). \tag{2.63}$$

With this last step, two delta functions appear in the generating function:

$$\delta\left(\partial_t\rho - D_\rho\nabla^2\rho + \mu\rho + \lambda\rho^2 - \omega\rho E - \sigma\sqrt{\rho}\eta(\vec{x},t)\right) \tag{2.64}$$

and:

$$\delta\left(\partial_t E - D_E\nabla^2\rho\right) \tag{2.65}$$

These delta functions impose restrictions for the evolution of ρ and E fields:

$$\begin{cases} \partial_t\rho = & D_\rho\nabla^2\rho + \mu\rho - \lambda\rho^2 + \omega\rho E + \sigma\sqrt{\rho}\eta(\vec{x},t) \\ \partial_t E = & D_E\nabla^2\rho, \end{cases} \tag{2.66}$$

where the convention $\mu \to -\mu$ has been used. These are, thus, the Langevin equations of the whole process.

The fields $\rho(\vec{x},t)$ and $E(\vec{x},t)$ are coarse-grained counterparts of the density of A particles and the total density of particles, respectively. Note that, therefore, **the E field contains both activity and background densities**.

This set of Langevin equations were first deduced from the set of reactions of the RD model in [96], but the same expression was also reached in other articles by only using symmetry assumptions (see [67,69,75], and [68,70] for mean-field equations).

The first term of the activity equation represents the diffusion of particles involved in activity processes (like spreading experiments). The second term is due to the creation of activity, but limited (third term) by a maximum level which cannot be exceeded[13]. The last term is the stochastic part of Eqs.(2.66), and its form stems, as in RFT (Eq.(2.17)), from the fact that the number of creations and annihilations of A particles is Poissonian distributed. Also, for $\rho(\vec{x},t) = 0 \quad \forall\ \vec{x}$, the dynamics remains frozen, trapped into an absorbing state. All these features are identical to the DP class continuous equation. The key new ingredient is the presence of a *conserved non-diffusing background field*: $E(\vec{x},t)$.

Concerning the parts related with this field, the coupling term (fourth term of the first equation) comes from the fact that creation of activity is fostered by the presence of a high density of the background field, which is conserved (second equation). If the equation for the energy is integrated, the equation of the activity takes the form:

$$\partial_t \rho = D_\rho \nabla^2 \rho + \mu_{eff}\rho - \lambda\rho^2 + \omega\rho \int_0^t D_E \nabla^2 \rho(\vec{x},t')dt' + \sigma\sqrt{\rho}\eta(\vec{x},t) \quad (2.67)$$

where $\mu_{eff} = \mu + E(\vec{x},0)$. There are three important points to discuss here:

i) The first one is that any evolution of the system is linked to activity; in sandpiles, for instance, every change in the initial configuration is due to the spread of an avalanche. Therefore, when no activity is present in

[13] In fermionic theories, to avoid density to exceed unity; in bosonic descriptions like this, to bind activity and prevent divergencies.

the system ($\rho = 0$ for all sites), it remains frozen and the configuration, stable.

ii) It is important to note that the integral, as in the PCP case (see Eq.(2.19)) entails a non-Markovian term into the activity equation which takes into account the history of the site up to time t. It is a memory effect, product of the non-diffusive character of the passive particles (or, in original SOC models, of the presence of a non-trivial threshold for activity): after a spreading experiment (or an avalanche), a non-trivial configuration of B particles remains as a reflect of the former activity. Therefore, when a new perturbation is introduced into the lattice, the spreading of it over the system depends on the background configuration, and then on the history of the system. It is also a balance mechanism, because when a region has been more active than the average, $\nabla^2\rho < 0$ there, and creation of activity is hindered; and on the opposite situation, when a zone is below the average level of activity, $\nabla^2\rho > 0$ and creation is fostered.

iii) The last important point is the term $E(\vec{x}, 0)$ on μ_{eff}; it is a quenched disorder, and it could influence the critical behavior of the system. Nonetheless, the non-Markovian balance mechanism and the presence of large events in the stationary state allow the system to be dominated by more recent changes, and therefore to easily forget initial configurations.

The set of microscopic reactions of the RD model defines the local relaxation rules and, therefore, after the coarsening process through which the two species are transformed into coarse-grained fields, the final set of equation is a **mesoscopic** representation of the universality class. As the RD model captures the basic ingredients of the C-DP class, **Eqs.(2.66) are the continuous representation for the class of stochastic sandpiles**, and all the features of the C-DP class are reflected in these equations.

Now, all irrelevant microscopic details are cast out, remaining the basic symmetries defining the universality class. In this way, a more rigorous comparison between the C-DP and DP classes can be done; in the end, this is a comparison of their mesoscopic equations. For obvious reasons, for the DP class the PCP mesoscopic representation will be used.

Comparison of non-Markovian terms

By comparing the Langevin equations for DP with many absorbing states (Eqs.(2.18)) and for C-DP (Eqs.(2.66)), the only difference can be found at the equation for the background field. However, the form of this equation is essential for the C-DP class to be different from DP.

Albeit in both systems activity is coupled to a non-diffusive background by means of a non-Markovian term, in the PCP Langevin equation this background field can be created or removed, while in C-DP is conserved. Due to this, in the latter no mass term (terms linear in the order parameter) is present for the evolution of the energy.

Considering the single-equation forms for both sets of equations, the exponentially decaying coupling of PCP (Eq.(2.19)) or the integrated Laplacian coupling in C-DP (Eq.(2.67)) are the result of the presence or absence, respectively, of a mass contribution to the background field equation. By comparing both non-Markovian terms, it is obvious that the memory effect of the former equation vanishes at much shorter times than the one in the latter. Therefore, its influence into the critical behavior is weaker.

It can be understood with the following heuristic argument. Consider the PCP model at its critical point; in it, changes in background are not only due to activity diffusion, but also of direct creation and dissipation of passive particles; this contributes to get rid of the history of the system. On the contrary, in a critical FES system conservation implies solely a rearrangement of background, which remains strongly correlated due to redistributions.

To summarize, it could be argued that the memory effect introduced by the coupling to a conserved field is more relevant than nonconservative coupling, and then it can influence more strongly the critical behavior of the system.

A RG calculation would provide rigorous theoretical arguments, more than the heuristic presented above, to discern the influence of the non-Markovian term. But is precisely the presence of the latter what prevents from a complete RG treatment of Eqs.(2.66) (or Eq.(2.67)), because it introduces, as commented for Eq.(2.18), highly singular propagators which reflect the static nature of background field in the absorbing state[14].

[14] Although the case of a diffusive conserved background (i.e. $D_B \neq 0$ for B particles of the original RD model) was already studied both theoretically [97] and numerically [98], the limit $D_B \to 0$ is not analytic; any non-vanishing diffusion in this field non-trivially influences the universality class [96].

$d=1$	η	δ	τ	τ_t	z_{spr}
DP	0.31368(4)	0.15947(3)	1.108(1)	1.159(1)	1.26523(3)
C-DP	0.41(5)	0.17(5)	1.11(5)	1.17(5)	1.40(5)

Table 2.4: Critical exponents for DP (upper row [79]) and C-DP (lower row) Langevin equations -see text- in $d=1$. Own measurements.

$d=2$	η	δ	τ	τ_t	z_{spr}
DP	0.230(1)	0.451(1)	1.268(1)	1.451(1)	1.13
C-DP	0.22(5)	0.58(5)	1.32(5)	1.58(5)	1.26(5)

Table 2.5: Critical exponents for DP (upper row [79]) and C-DP (lower row) Langevin equations -see text- in $d=2$. Own measurements but $\beta/\nu_\perp$ and θ, taken from [112].

Renormalization calculations with different proposed mesoscopic descriptions of sandpiles (either deterministic or stochastic), in which only one coarse-grained field is used (resembling the first phenomenological equations deduced for the BTW sandpile -see, for instance, [10]), can be also found in the literature [108–110]. Unfortunately, none of these works have succeeded in obtaining the set of exponents measured for the BTW and C-DP classes.

Within this scenario, the only way to check the influence of the extra symmetry introduced with conservation is by direct numerical integration of the equations. By using the integration method of [111], and measuring all the observables defined above in both equations (see Fig.2.3 for some observables measured for Eq.(2.66)), the complete set of critical exponent of tables 2.4 and 2.5 can be used to this end.

Although the exponents for both classes are very similar, the difference is large enough to ensure a different critical behavior. Therefore, Eq.(2.66), representative of C-DP, describes the behavior of a universality class, different from DP, characterized by a diffusing order parameter whose dynamics is coupled to a non-diffusive conserved field. In this way, the conjecture about the universality class made above is confirmed by means of the numerical integration of its continuous equation[15].

[15] In a more rigorous way than by using microscopic models.

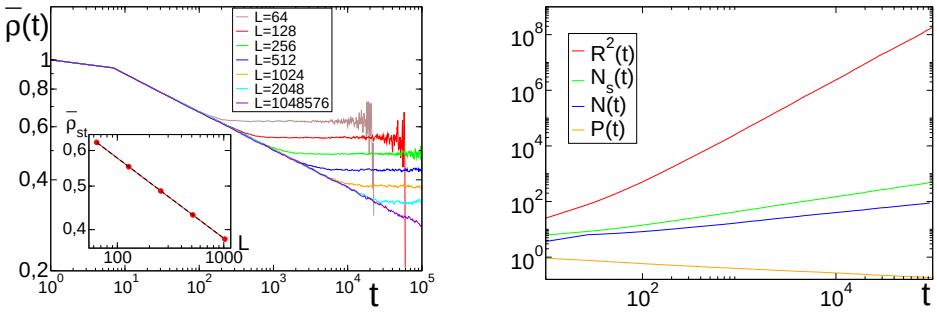

Figure 2.3: Left: Finite size effect in the decay of $\overline{\rho}(t)$ of Eqs.(2.66) at the critical point; the stationary value $\overline{\rho}_{st}$ is smaller as the system size increases: from top to bottom, $L = 64, 128, 256, ..., 2048, 1048576$. Inset: Stationary value versus size L; from this plot, the exponent $\beta/\nu_\perp$ is measured (see table C.1). Right: Spreading experiment measurements.

The C-DP Langevin Equation in the SOC Ensemble

As long as a SOC counterpart of all models into the C-DP class exists, it is possible also to integrate this equation by using the SOC ensemble. Consider Eq.(2.66) with open (Dirichlet) boundary conditions:

$$\begin{cases} \rho(0,t) = 0 & \forall\, t \\ E(0,t) = 0 & \forall\, t \end{cases} \tag{2.68}$$

where the site $\vec{x} = 0$ represents to any neighbor of the border sites out of the system. Thus, the dynamics of the SOC integration goes as follows: consider a d-dimensional hypercubic lattice with empty initial condition ($\rho(\vec{x}, 0) = 0, E(\vec{x}, 0) = 0$) for all positions of the system. An initial seed of activity $\delta\rho$ is introduced at position $\vec{x}$, and therefore $(\rho, E) \to (\rho + \delta\rho, E + \delta\rho)$ for this site. In this way, an avalanche starts and "updating rules", Eqs.(2.66), are applied until no more activity is present in the system; then, the avalanche has finished. The lifetime of the avalanche is the time interval between the initial perturbation time, t_0, and the time at which the system falls into a frozen state, t_f. The size of the avalanche is given by the number of active sites for which $\rho \neq 0$ at any time or, equivalently, by the accumulated activity during this time interval:

$$s = \int_{t_0}^{t_f} dt \int d^d x \rho(\vec{x}, t) \tag{2.69}$$

How is the SOC state reached? In the initial stages of the evolution, driv-

ing events create small avalanches. There are small bumps of activity, so that $\nabla^2\rho < 0$ in these sites and the bump tends to be dispersed through the neighborhood; in its advance, activity can be created and removed, but steadily is transformed into background. Therefore, the main contribution of small events is to build up the background and, with initial seeds, to increase the energy density ($d\overline{E}/dn > 0$, where n is the number of driving events). When $\overline{E}$ has grown enough, large events are possible which rearrange completely the initial configuration of the background; but, also, the conservation of energy represented by the Laplacian makes large activity bumps travel towards the boundaries to be dissipated. Hence, these events can reach the border, and in consequence energy can be lost ($d\overline{E}/dn < 0$). Thus, $\overline{E}$ evolves towards a stationary value $\overline{E}_c$ for which avalanches of all sizes are possible and correlations span throughout the system.

Avalanches leave behind a non-trivial spatially correlated configuration, which will be the initial state of the next avalanche. In this stationary critical state, the background is also critical, in the sense that its configuration allows the next initial seed to spread over the whole system (identically as discussed with the FES ensemble [80]). This is one of the important background features, represented by the memory (non-Markovian) term. Also it is so its balance effect: due to the conservative Laplacian term in the evolution of the energy field, activity bumps are redistributed among the neighboring positions and transformed into background, or travel until being dissipated at boundaries; this behavior does not depend on the set of values chosen for the coefficients of equations. Therefore, *the coupling with the locally conserved non-diffusing field is the responsible for the achievement of the SOC stationary state.*

The set of measured avalanche and spreading critical exponents are identical, within error bars, to the ones which can be found in table 2.4 and 2.5[16], as expected.

Concerning the mean-field behavior of Eqs.(2.66) (and, therefore, of the C-DP class), power counting analyses reveal that the upper critical dimension is $d_c = 4$ (see [72, 113, 114] for a discrepant point of view); above this dimension, pure mean-field behavior is expected. As spatial correlations are negligible in this approximation, the non-Markovian term has no influence, and mean-field DP behavior [78, 81] is expected. Both numerical and early

[16]Where the equations have been integrated by using the techniques introduced in [111]. All the numerical integrations of the Langevin equations appearing in this thesis have been performed using this method, due to the multiplicative shape of the noise; thus, this comment will be omitted hereinafter.

mean-field approaches to SOC models [68–71, 96, 115–117] confirm the value of the critical dimension and the DP value for critical exponents [93], which stems from the fact that the propagation of activity in both DP and C-DP mean-field systems are essentially a branching process (see the previous chapter) [46, 52].

It is also possible to recover the mean-field behavior with C-DP systems by using the random neighbor ensemble [118], or using a network with small-world feature instead of a regular lattice [119]. For a non-diffusing background, the structure of the network does not change the phase diagram of the system (see [120] for a study of both $D_B = 0$ and $D_B \neq 0$ cases).

2.8 Concluding Remarks

Isotropic stochastic sandpiles define a universality class, to which Manna and Oslo models belong. However, SOC dynamics possesses two infinitely separated time scales and open boundaries, which is an inconvenient for analytical calculations to be performed or continuous descriptions to be well-defined. This, which is intrinsically defined in the dynamics, prevents the system from translational invariance, hinders a correct definition of a unique time-scale for the overall process and impedes the study of many interesting off-critical observables.

One step further of a "regularization" process, a fixed-energy (FES) ensemble can be defined in which the system keeps its local dynamics, but driving and dissipation disappear. This entails many changes:

- The dynamics is not SOC anymore; the critical regime must be achieved by fine-tuning a parameter.
- Due to closed and periodic boundary conditions, the system is now homogeneous (translationally invariant).
- Order and control parameters can be straightforwardly identified: they are activity density and energy density, respectively (although in the presence of a set of possible parameters, any of them can be chosen as tuning parameter, as in the Oslo ricepile model).
- Energy is now locally and globally strictly conserved. It is a free parameter, not coupled to any of the others, and can be adjusted to visit any region of the phase space.

FES systems share the same critical exponents than their SOC counterparts; moreover, they share the very same value for the critical point in the thermodynamic limit. This shows that driving and dissipation are important to self-organize the SOC system to its critical point, but they do not influence the critical behavior, which is completely identical in the FES ensemble.

In this ensemble, the system undergoes an ordinary nonequilibrium phase transition into infinitely many absorbing states. This allows, with the help of the well-known statistical physics of this kind of systems, to identify the basic ingredients and symmetries of the universality class.

Thus, it has been conjectured that in the absence of additional symmetries, systems with an order parameter coupled with a conserved non-diffusive field undergoing a phase transition into infinitely many absorbing states define this universality class, coined as the C-DP class, whose main difference with DP is the conservative character of the coupled field.

It is possible to find the most simple model capturing the essential ingredients of these models in the reaction-diffusion (RD) model defined by Eq.(2.21a)-Eq.(2.22).

These microscopic equations can be translated into mesoscopic equations; using Doi-Peliti techniques, the continuous counterpart of RD model is deduced to be Eqs.(2.66). Therefore, these equations can be considered the mesoscopic description of the C-DP class.

Once the C-DP Langevin equations are obtained, the similarities and differences with DP universality class are identified by a simple comparison of terms. In both classes many different absorbing states can be found, and the fluctuations of the activity field are identical. The main difference stems from the conservative character of the background field of the C-DP class, which is linearly coupled with the activity field. This conserved background is able to generate long-termed memory effects essentially different from the non-Markovian effects in the DP class. However, this difference steadily vanishes as the dimension increases, and for $d \geq 4$, the mean-field behavior of both classes coincide.

Chapter 3

Discriminating DP and C-DP Universality Classes

In the previous chapter, the Conserved Directed Percolation (C-DP) universality class was defined. This is the class to which all systems undergoing nonequilibrium phase transitions into infinitely many absorbing states with an order parameter coupled to a non-diffusing conserved field belong.

Into the C-DP class can be found the isotropic stochastic sandpiles, as for instance the Manna pile or the Oslo ricepile model (see chapter 1). There exists also a mesoscopic description of the universality class, given by the set of Langevin equations Eqs.(2.66) (see chapter 2).

As already pointed out in chapter 2, this universality class presents similarities with the Directed Percolation (DP) class, the archetypical class of phase transitions into absorbing states. Indeed, also in DP models with infinitely number of absorbing states (as the PCP model), there is a coupling between a non-diffusing background field and the activity field.

Although there exists a key difference which defines the class of C-DP (the *conserved* character of its passive field), the resemblance of the scale-free behavior of their observables (i.e. of their associated critical exponents) makes very difficult and computationally-expensive to discriminate between C-DP and DP critical behavior in those systems where a complicated dynamics blurs their real critical behavior.

In this chapter, the reaction of these two classes to the presence of certain additional ingredients which can induce a very different critical behavior (i.e. different critical exponents) for both universality classes will be studied.

First, a preferred direction will be introduced at both microscopic and mesoscopic levels for the C-DP class, and the resultant behavior will be compared with the one of the DP class. Next, the relevancy of the presence of a surface (with two different realizations: absorbing and reflecting wall) in systems of the two classes will be studied. The different response of C-DP and DP systems to these perturbations will allow to stablish some criteria to be applied for the easy-discrimination of the universality class in controversial examples of sandpiles. After that, a phenomenological overview of the effects of both types of perturbations on the background of such systems will be made. In the end, anisotropy and walls will be applied to examples of stochastic sandpiles claimed to be into the DP universality class.

3.1 Anisotropy in Systems with Absorbing States

When a *preferred direction* is introduced in the dynamics of d-dimensional systems, it is created an effective flow of activity in such direction which, in the case of a total biased diffusion (**directness**), can be identified with the "time" coordinate of a $d-1$ dimensional system. This fact can simplify considerably the analysis of these systems.

Moreover, the presence of anisotropy can lead to a relevant change in the critical behavior of the system and, therefore, of the associated critical exponents.

In this section, it will be studied how the presence of (total or partially) biased dynamics affects to systems into C-DP or DP classes, considering both microscopic and mesoscopic levels of description, and using the above mentioned simplification in order to obtain some analytical results from these systems.

Anisotropy in the C-DP class

As explained in chapter 2, in systems of the C-DP class there exists a conserved background field coupled to activity. Then, a biased diffusion of the activity field entails a biased diffusion of the energy field, which can affect in

a non-trivial way to the critical behavior of such systems[1]. Next, this effect will be analyzed.

Microscopic Systems

Consider the Abelian sandpile model (ASM) [34]; as seen in previous chapters, although many analytical results are avaliable, this system is not yet completely solved, in spite of the deterministic character of its simple dynamic rules. There are no exact results for its critical exponents.

However, its directed (totally anisotropic dynamics) counterpart, the directed ASM or **Dhar-Ramaswamy (DR) model**, can be exactly solved [123].

The Dhar-Ramaswamy Model

Consider a $d = 1$ ASM sandpile. As explained in chapter 1, the dynamics of this model is deterministic: a grain is dropped into randomly chosen sites of the pile and, thus, their height z_i is increased. When, at one site i, a threshold z_c is overcome, the site becomes unstable and topples part of its energy (concretely, two grains) to its neighbors. This can involve more activations which lead to an avalanche event. When no more sites are active, a driving grain is again introduced into the system.

In the directed case, only one grain is toppled, and it is given to the neighbor at the direction defined by the total anisotropy. Then, if site i relaxes, $z_i \to z_i - 1$ and, at the neighbor situated at its, e.g. right $z_{i+1} \to z_{i+1} + 1$.

After a transient regime, the driving and avalanche events drive the system to a stationary state in which only the trivial configuration in which $z_i = 1$ at all sites is possible. Any grain introduced by the driving starts a biased walk to the border, where is dissipated. The number of temporal steps of the lifetime of each avalanche depends only on the site at which the grain is initially introduced. Then, as in the $d = 1$ ASM, *this one-dimensional anisotropic deterministic model is trivial*.

Due to this, Dhar and Ramaswamy centered their attention only in the cases with $d \geq 2$ [123]. Consider a $d = 2$ square lattice. Let (i, j) be the

[1]Early works about how anisotropy affects the universality or even the SOC character of conserved systems can be found in [10, 53, 121, 122].

coordinates of an active site into a square lattice; in the DR model, the ASM relaxation rules (Eq.(1.10) and Eq.(1.11)) are changed to:

$$\begin{cases} z_{i,j} \rightarrow & z_{i,j} - 2 \\ z_{i+1,j} \rightarrow & z_{i+1,j} + 1 \\ z_{i,j+1} \rightarrow & z_{i,j+1} + 1. \end{cases} \tag{3.1}$$

In this model, d particles instead of $2d$ are redistributed. Also, the selected neighbors to which these grains are toppled changes. With this choice of neighbors, the preferred direction is given by $(1, 1)$; it is possible to obtain the same asymmetry by selecting the downwards direction in a square lattice rotated 45° in this direction. The initial driving seed is located always at the uppermost row of the system.

Total anisotropy does not break the Abelian character of the rules; this fact allows to choose an order of toppling in which the active sites of each row topple at once, and rows are selected from top to bottom. In this way, the identification of downwards direction with "time" (see above) is possible, and avalanche exponents can be exactly obtained by analytical calculations [123, 124].

But it is also possible to obtain them by noticing that this simple model can be mapped into an unbiased *random walk* problem. Observe the left part of Fig.3.1; in it, a typical $d = 2$ activity pattern obtained with rules Eq.(3.1) is depicted. The cluster is compact with fractal boundaries, as usual for the ASM in this dimension. But in this case, one of the directions is "time"[2] and, therefore, the boundaries can be seen as the path of two $d = 1$-dimensional annihilating random walkers (the green lines in Fig.3.1): they start at the same "time" (position of the initial seed in the preferred direction), and their walks finish when they meet again (the last active site).

These two walkers are equivalent in turn to a $d = 1$ random walker with an absorbing boundary (see right part of Fig.3.1); therefore:

- The "duration" of the avalanche (total number of rows of active sites in the preferred direction) can be mapped into the *first return time* of the walker [A4], which follows a power law with a well-known exponent ($\tau_t = 3/2$) [125].

[2]Downwards direction, in the case of the rotated lattice, or south-east direction in the usual square lattice.

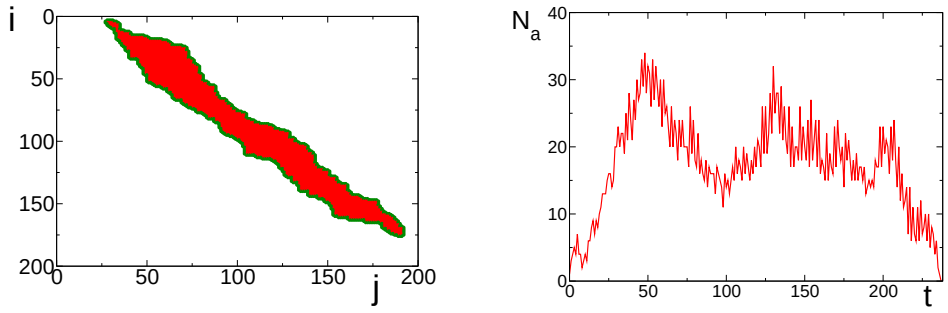

Figure 3.1: Left: Activity cluster for the DR model; the boundaries (green) of the compact cluster (red) perform a random walk which is annihilated when both collide, i.e. in the end of the avalanche event. Right: The single random walk of the number of active sites N_a per "time" t (distance of the activity front to the origin of the avalanche in the anisotropic direction).

- The number of active sites which make the cluster grow is constant in "time" (only the two boundary sites per row: the random walkers), and therefore $\eta = 0$.

- The number of topplings is equivalent to the area below the random walk; therefore, $s \sim r^{3/2}$, that is, $D_f = 3/2 = \tau_t$. [3]

Together with these exponents, there exists an exponent which is common to any dimension of any system with biased diffusion: $z = 1$ (or, equivalently, $z_{spr} = 2$ -see Eq.(2.16)). Consider this DR model, in which there is a totally anisotropic flow in one direction. It is possible to define a privileged system of coordinates respect to which the spatial coordinates of the system are not affected by the anisotropy. To this end, the system of reference must move in the preferred direction with the same effective velocity imposed by the anisotropic flow of grains (this is equivalent to a Galilean transformation, $x \to x + vt$, $t \to t$). Therefore, in this system of coordinates, space and time are proportional ($x \sim t$) and, as z is defined by the relation between space and time (see Eq.(A.1.10)), the dynamic exponent takes the value $z = 1$. This pure diffusive motion can be defined in any totally anisotropic system, regardless the dimension, reason why this exponent is said to be **superuniversal**.

[3] The coincidence between D_f and τ_t is product of the identification between the temporal and linear-spatial extent of the cluster in this direction.

Thus, by using the scaling relations of the previous chapter, the rest of exponents can be obtained.

Note that the cluster (see Fig.3.1) is identical to the ones formed in *compact DP*, corresponding to the Domany-Kinzel cellular automaton with infection probabilities $x = 0$, $y = 1/2$ and $z = 1$ (using the original notation), which is also exactly solvable and the exponents are identical to the exposed ones [126].

The same set of exponents is valid for **deterministic** sandpiles with any degree of anisotropy, not only for directed models [123, 124], although the explained mapping is not possible. The upper critical dimension for this model is $d_c = 3$ [123], that is, one less than the isotropic case. It is not surprising, because the identification of one spatial direction with time leads to an effective **dimensional reduction** regarding with the isotropic case. For $d > d_c$, the spatial structures and correlations are not a relevant factor anymore and, except z, the rest of the isotropic mean-field exponents are recovered.

Abelian Stochastic Directed Models

It is possible to devise similar Abelian models including stochasticity in its dynamical rules (in order to obtain the stochastic counterpart of the deterministic DR model), that will be called here **Abelian stochastic directed models** (Ab-SDM). Again, it is essential the Abelian character of the dynamics in order to make exact deductions of exponents.

One of the first examples is the "model A" defined by Maslov and Zhang in [127]. In this work, the authors introduced an anisotropic (directed) variation of the Zaitsev model [19] in order to obtain a set of dynamical rules very similar to the ones of the stochastic sandpiles.

In this system, defined in $d = 1$, each active site topples a random quantity Δf (an increment of "force") such that the site becomes stable, to its neighbor in the defined preferred direction. Therefore, Δf performs a random walk if such a direction is identified with "time". Thus, the identification of avalanches with a first return process for a $d = 1$ random walker becomes straightforward, where the size of the event is given by the area under the walk. Therefore, the exponents $\tau_t = 3/2$, $\eta = 0$, $D_f = 3/2$ and $z = 1$ are recovered (see above).

Then, the set of exponents of this $d = 1$ directed stochastic sandpile are

identical to the already seen in the case of $d = 2$ DR model. But this does not mean that the DR model and this Ab-SDM belong to the same universality class; their behavior in the same dimension is completely different (for instance, $d = 1$ DR model is trivial, in contrast with this model). There exists only a punctual coincidence between the $d = 2$ DR model and this $d = 1$ Ab-SDM due to the special shape of the avalanches and the choice of "time" in each case.

Although more stochastic anisotropic models have been defined (the model in [128], for instance, is a generalization of the previous example), there exist also Abelian anisotropic/directed variations of the well known Manna sandpile [129–132] or Oslo ricepile model [133–135]. For many of them, continuous equations for the evolution of z_i, reflecting the special circumstances of the model, have been devised.

Actually, one of these continuous representations, obtained by Kloster et al. in [131][4], is especially useful to easy-understand the overall phenomenology of these Ab-SDM.

Consider a rotated two-dimensional lattice similar to the one defined for the DR model (see above). In this new model, the preferred (downwards) direction is labeled as $x_\parallel$, and the DR model relaxation rules, Eq.(3.1), are modified by simply choosing each neighbor randomly between the two possibilities in the $x_\parallel$ direction ($(i+1, j)$ or $(i, j+1)$, with the DR model notation).

In this way, the model is transformed into a directed variation of the Manna model in which an active site topples a fixed amount of energy (2 grains in $d = 2$) instead of all its grains. As commented in the previous chapter, when the number of toppling grains is fixed, the Manna model becomes Abelian. Then, it is possible to choose an order for topplings in which each active site relaxes as many times as necessary to become stable. With this order, the $x_\parallel$ direction can be identified with "time" [131].

Let $S(x_\parallel)$ be the number of topplings of row $x_\parallel$; therefore, the total number of grains transferred from this "time" to the next one is $2S(x_\parallel)$. At this layer, the difference between the number of incoming and outgoing grains is 0 if the number of incoming particles is *even* because, regardless which sites receive grains (and due to the 2-grain toppling rule and the relaxation until the site is deactivated), $2k$ new grains at a site implies k relaxations. But a site receiving $2k + 1$ particles can topple k times (if it was empty before

[4] A slightly different approach of the same model, performed by Paczuski and Bassler, can be found in [132].

receiving energy) or $k+1$ times (if it stored 1 grain).

Therefore, $2S(x_\parallel)$ performs an unbiased *random walk* whose fluctuations (i.e. the length of the step) are given by a noise which depends on the number of active sites $N_a(x_\parallel)$ at each layer. Thus, the following continuous equation can be proposed [131]:

$$\partial_{x_\parallel} S(x_\parallel) = \frac{1}{2}\sqrt{N_a(x_\parallel)}\hat{\eta}(x_\parallel), \tag{3.2}$$

where $\hat{\eta}$ is a Gaussian white noise. Assuming $S(x_\parallel) \sim x_\parallel^{\alpha_s}$ and $N_a(x_\parallel) \sim x_\parallel^{\alpha_a}$:

$$N_a(x_\parallel) \sim S(x_\parallel)^{\alpha_a/\alpha_s}. \tag{3.3}$$

Bringing Eq.(3.3) into Eq.(3.2) and solving:

$$\alpha_s = (1+\alpha_a)/2, \qquad \tau_\parallel = 1+\alpha_s. \tag{3.4}$$

Thus, as the total number of topplings is:

$$s = \int S(x_\parallel)dx_\parallel \sim x_\parallel^{1+\alpha_s} \tag{3.5}$$

and, as $s \sim x_\parallel^{D_f/z}$ (see Eq.(1.4) and Eq.(1.7)):

$$1+\alpha_s = \frac{D_f}{z} = 1+\eta+\delta, \tag{3.6}$$

where Eq.(2.8) has been used. Thus, we can identify $\alpha_s = \eta+\delta$; but (recalling that $x_\parallel$ is "time" in this example) $\tau_\parallel = \tau_t$ and, using Eq.(3.4) and Eq.(2.7):

$$\alpha_s = \delta, \qquad \eta = 0. \tag{3.7}$$

As said above, in any directed Abelian model it is possible to identify the preferred direction with time, remaining the number of active sites constant in each of these temporal steps. Thus, in any directed model, $\eta = 0$, and can be said that also η is a *superuniversal exponent*. Moreover, using $\eta = 0$ and $z_{spr} = 2$ (i.e. $z = 1$), with Eq.(3.6) and these superuniversal values, $D_f = z(1+\eta+\delta) = 1+\delta = \tau_t$ (see above) and the identification $D_f = \tau_t$ is now justified.

Ab-SDM	η	δ	τ	τ_t	z_{spr}
$d = 1$	0	1/2	4/3	3/2	2
$d = 2$	0	3/4	10/7	7/4	2

Table 3.1: Exact values of some critical exponents for anisotropic stochastic sandpiles in $d = 1, 2$.

For the $d = 2$ square lattice under discussion, $N_a \sim x_{\parallel}^{1/2}$ ($\alpha_a = 1/2$) [131]; with the scaling relations seen here and in the previous chapter, and the superuniversal exponents $z_{spr} = 2$ and $\eta = 0$, the rest of exponents can be obtained: $\delta = 3/4$, $\tau = 10/7$, and $\tau_t = D_f = 7/4$. They are gathered also in table 3.1.

For $d = 1$, the only spatial dimension avaliable is identified with time, and therefore the "time rows" are 0-dimensional manifolds. Thus, there can be only an active site per row and, therefore, $N_a(x_{\parallel}) = 1$, i.e. $\alpha_a = 0$; this leads to $\delta = 1/2$, $\tau_t = 3/2 = D_f$, $\tau = 4/3$, and the rest of the values of the previous $d = 1$ Ab-SDM are recovered.

The A-C-DP Universality Class

The results obtained with the previous examples of Ab-SDM can be extended to *any degree of anisotropy* [129–131, 133]. In [132] for the directed Abelian Manna model, and in [134] for the directed Abelian Oslo model, the same exponents are obtained with strictly analytical arguments. For both models, as well as for any Ab-SDM, the upper critical dimension is, again, $d_c = 3$, due to the dimensional reduction (see above), and isotropic mean-field results are recovered (with the exception of the superuniversal exponents, which remain valid also for $d > d_c$). But, as shown by Hugues and Paczuski [136], these exponents can be also found for *non-Abelian* versions of the above mentioned models.

As the critical behavior of all these anisotropic stochastic piles coincide, regardless the degree of anisotropy or the Abelian character, the set of exponents of table 3.1 represents the critical behavior of the C-DP stochastic sandpiles with any degree of anisotropy present in the dynamics. As the critical behavior is completely different to that of the isotropic C-DP, it can be said that this set of exponents defines a new universality class, **anisotropic C-DP (A-C-DP) class**, resulting from the presence of anisotropy in C-DP systems.

The fact that non-Abelian stochastic anisotropic models are as well embraced by this universality class is quite important, because one of the fundamental features of an Ab-SDM is the decorrelated essence of its configurations. This decorrelated background permits the random walkers to jump with independent individual steps, which is essential for the validity to the deductions made above to obtain the continuous descriptions and the critical exponents of stochastic systems.

But if the Abelianity condition can be relaxed, the decorrelation condition for the background can also be so. As it is argued in [135, 137], whereas the width of the avalanche size probability distribution is upperly bounded, the random walks converge to be uncorrelated for sizes large enough (at least for $d = 1$). In this way, the critical exponents of table 3.1 remain valid even for correlated backgrounds.

Concerning the DR model, note that Eq.(3.2) is also valid for the $d = 2$ DR model. There, the number of active sites per row is constant (as in the $d = 1$ stochastic model of the previous section), so that $\alpha_a = 0$ and the reported exponents for the $d = 2$ DR model are recovered. This explains the numerical coincidence of the $d = 2$ DR model and $d = 1$ A-C-DP, even when they form part of different universality classes.

Mesoscopic Level

At a mesoscopic level, it is possible to introduce a preferred direction by simply adding a **drift term** to the Langevin equation.

A term $v\nabla\rho$ can be added to both the C-DP Langevin equations, Eqs.(2.66), to take into account a biased diffusion of energy because of a biased activity spreading:

$$\begin{cases} \partial_t\rho = & D_\rho\nabla^2\rho + \mu\rho - \lambda\rho^2 + \omega\rho E + v\nabla\rho + \sigma\sqrt{\rho}\eta(\vec{x},t) \\ \partial_t E = & D_E\nabla^2\rho + v\nabla\rho, \end{cases} \tag{3.8}$$

where v is the **drift strength**. There are many ways with which study the relevancy of this term. One way is by performing a power counting analysis. Another method is by performing a Galilean transformation for space-time variables (i.e. $x \to x + vt$, $t \to t$, see above), establishing a new system of coordinates which is moving with the velocity v imposed by the drift. If this change of variables reabsorbs the drift term, this will mean that, by only

$d=1$	η	δ	τ	τ_t	z_{spr}
A-C-DP	0.02(3)	0.45(3)	1.31(3)	1.48(3)	1.98(3)
DP	0.33(3)	0.14(3)	1.07(4)	1.14(4)	2.00(3)

Table 3.2: Critical exponents for $d = 1$ A-C-DP (upper row) and A-DP=DP (lower row), obtained by integrating Eq.(3.8) and Eq.(3.9), respectively (see text). Own measurements.

$d=2$	η	δ	τ	τ_t	z_{spr}
A-C-DP	0.03(5)	0.80(5)	1.43(5)	1.75(5)	2.02(5)
DP	0.230(1)	0.451(1)	1.268(1)	1.451(1)	2.00(1)

Table 3.3: Critical exponents for A-C-DP (upper row), obtained by integrating Eq.(3.8), and A-DP=DP (lower row, taken from [79]), in $d = 2$.

redefining the spatial coordinates, the critical behavior of the isotropic case is recovered, i.e. anisotropy is not a relevant ingredient for the system[5].

However, when the energy equation is integrated and E is replaced into the equation for the activity (see chapter 2), the Laplacian coupling term prevents this drift from being reabsorbed. Thus, anisotropy is expected to be relevant for this universality class. This justifies why anisotropic C-DP systems belong, as stated above, to a different universality class (the A-C-DP class).

As said in the previous chapter, Renormalization Group (RG) calculations are prohibitively difficult to be performed in Eqs.(2.66). This is also the case of Eqs.(3.8). Thus, the only way in which the critical exponents of table 3.1 can be confirmed to represent to the A-C-DP class is, so far, by direct numerical integration of these equations.

The measured critical exponents are illustrated in the first row of table 3.2 and table 3.3. As can be seen, the critical exponents coincide within error bars with those of table 3.1, and are significatively different from the exponents of the C-DP class (see table C.1). This confirms that the microscopic models studied above belong to the A-C-DP universality class, which is the result of the flowing of the C-DP critical point to a new fixed point when any degree of anisotropy is introduced (i.e. any value of $v \neq 0$ is chosen).

[5]In such cases, the system is said to possess "Galilean invariance".

Anisotropy in the DP class

When the same drift term above mentioned is introduced into the RFT equation, Eq.(2.17), representative of DP universality class:

$$\partial_t \rho = D\nabla^2 \rho + \mu\rho - \lambda\rho^2 + v\nabla\rho + \sigma\sqrt{\rho}\eta(\vec{x}, t), \tag{3.9}$$

a Galilean transformation is able to reabsorb this drift term. This means that, in this new system of reference (see above), the drift has no effect. Therefore, anisotropy is *not* a relevant perturbation for the DP RG fixed point, i.e. anisotropic DP (A-DP) is still DP, because the DP universality class is invariant under Galilean transformations[6].

By considering not only the single absorbing state Eq.(3.9), but also the many absorbing states model PCP (Eqs.(2.18)) with the same drift term $v\nabla\rho$ introduced into both equations (see above), a quantitative comparison between A-DP and A-C-DP can be done by simply integrating the equations. This permits to study the possible different behavior, and how it is reflected in differences in critical exponents.

The results of such integrations for $d = 1$ are gathered in the lower row of table 3.2. The results confirm that A-DP is still the DP universality class (i.e. A-DP=DP). Thus, there is a very different response of the two classes, DP and C-DP, in the presence of anisotropy.

In summary, in this section the universality class of anisotropic stochastic sandpiles, A-C-DP, has been defined and characterized. Its critical exponents, indeed, are different from those of the isotropic case (C-DP). On the other hand, the presence of anisotropy is irrelevant for the DP class, which means that its critical exponents are not affected by this new ingredient. The different response of both classes is translated into a large increase in the difference between the critical exponents, which can be useful in order to distinguish between both universality classes.

[6]It can, as in the C-DP case, be checked by means of a power counting.

3.2 Surfaces in Systems with Absorbing States

The presence of a surface can dramatically affect the critical behavior of equilibrium systems [138,139]. In the case of nonequilibrium systems, similar effects can be observed.

DP in the Presence of a Wall

Consider, for instance, the case of the *contact process* [81], a DP microscopic system with probability p for the creation of particles at one of the empty neighbors of an existing particle, and $1-p$ for self-annihilation.

When a wall is present into an otherwise infinite system, translational invariance is broken. If now a different probability $\tilde{p}$ is defined for sites next to the surface, a competition between surface and bulk dynamics appears. Thus, a critical point $\tilde{p}_c$, different from the bulk one (p_c), can be defined for the sites next to the wall.

Defining $\Delta = p_c - p$ for the bulk and $\Delta_s = \tilde{p}_c - \tilde{p}$ for the surface, it is possible to control the distance to their respective critical points independently. With this possibility, many different phase transitions can be identified in the mean-field phase diagram (see Fig.3.2) [140]:

- An *ordinary transition* (O), if the bulk is critical but the surface is in its subcritical regime.
- An *extraordinary transition* (E), when the bulk is critical but the surface is supercritical.
- A *special transition* (Sp), in which both parts of the system are critical.
- A *surface transition* (S), when both parts of the system are supercritical.

Surface transitions occur when, due to the highly active bulk, the surface must take an otherwise supercritical $\tilde{p} > \tilde{p}_c$ to become critical. By tuning the bulk control parameter to its critical value, the extraordinary transition is achieved and, taking the critical value of surface probability, the special transition is reached. The ordinary transition is the phase transition which the system suffers when the surface is "free" (open).

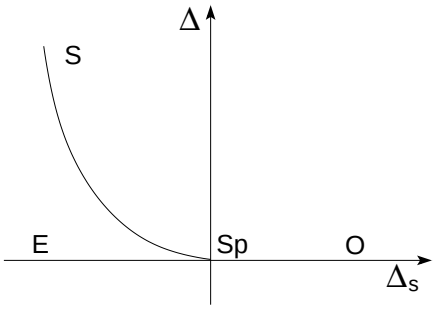

Figure 3.2: Phase diagram of DP with a wall, where the surface phase transitions are depicted (see text).

Of course, any of these transitions can be not present under certain circumstances; for example, in $d = 1$, the surface is zero-dimensional and cannot become critical; therefore, only ordinary or extraordinary transitions would be possible in this case.

We will be focused on surface effects on $d = 1$ DP systems where the site which forms the 0-dimensional wall is treated as a bulk site (i.e. $\tilde{p} = p$). As local fluctuations always kill any activity in $d = 0$, the 0-dimensional surface remains subcritical in $d = 1$ DP. Thus, there is a competition between the subcritical behavior of the surface and the behavior of the bulk: when the bulk is subcritical, any particle created next to the wall is eventually lost into the bulk, where activity decays exponentially; the effect of the boundary decays exponentally fast. But when the bulk is critical, its correlations diverge and so does the effect of the boundary. Thus, *the only possible phase transition in these $d = 1$ systems is achieved at the bulk critical point*, and the boundary is controlled by bulk correlations.

Boundary Conditions Associated with the Surfaces

It is possible to define different types of surfaces; here, only **reflecting** and **absorbing boundaries** will be considered [141].

In the case of a *reflecting surface*, the sites into the wall reflect the state of the sites into the system. In other words, each site $i' = -i$ into the wall is identical to the site i of the original system. In a mesoscopic description like the RFT, Eq.(2.17), this can be expressed by using Neumann boundary conditions. For instance, for a $d = 1$ semi-infinite system, this is equivalent to:

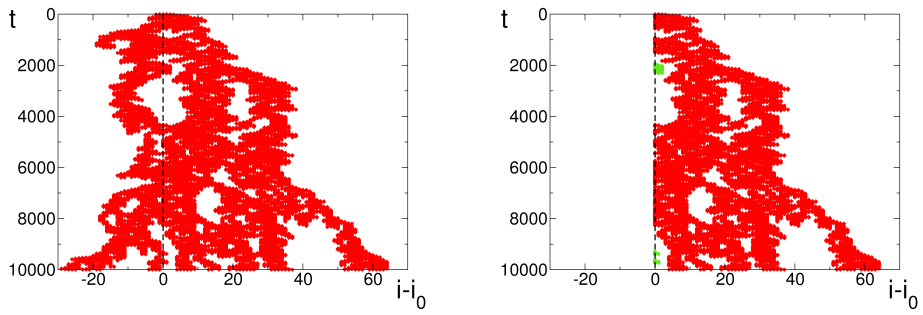

Figure 3.3: Activity cluster for a one-dimensional DP system. In the left part, an infinite system; in the right part, a semi-infinite cluster with a wall next to the initial seed of activity (site i_0). The green sites in the right part represent lost feedback due to the presence of the wall.

$$\rho(-1,t) = \quad \rho(1,t) \quad \forall t, \tag{3.10}$$

where a reflecting wall is placed just at $x = 0$.

In the case of an *absorbing surface*, all the sites into the wall are in an absorbing state. This condition is easily represented by Dirichlet boundary conditions, which in $d = 1$ can be written as:

$$\rho(-1,t) = \quad 0 \quad \forall t \tag{3.11}$$

For DP, the effect of both boundaries coincides: they prevent an activity feedback which would exist if there was no surface [142]. This fact can be observed in Fig.3.3, where a typical DP spreading cluster is depicted. In the left part, the surface-free system; in the right part, a cluster obtained with the same dynamics but taking into account an absorbing wall placed next to the initial seed, perpendicular to the spatial direction of the system. The lack of feedback causes some branches, which otherwise would be reactivated, to die.

This lack of activity affects the surviving probability: the presence of the (absorbing or reflecting) surface and the corresponding absence of feedback makes the number of surviving experiments decrease, as well as their lifetime. In this way, the value of the associated critical exponents changes.

However, bulk observables remain unaffected. The reason is that the cluster of surviving sites is a subset of the surface-free cluster and, effectively, they are not affected by the presence of the wall, i.e. a bulk dynamics is

well defined into the system, despite the possible boundary correlations. In fact, the correlations at the border are governed by bulk correlation exponents (see above) [139–141]. Moreover, even the critical point value for the control parameter remains unchanged while the rest of exponents, surviving-probability-dependent, take different values. The critical exponents associated with $d = 1$ DP systems are gathered in the upper half of table 3.4 (see also appendix C.2.1).

With the arguments above exposed, it can be said that the effect of both absorbing and reflecting surfaces on a DP system is identical, and defines a change of exponents which **does not alter the universality class** (because the critical point and the associated bulk exponents remain the same), but which involves an **extra phenomenology** that here will be referred to as **surface DP (S-DP)**.

For $d > 1$, the phenomenology is even richer: not only the effect of the $d-1$ hypersurface has to be taken into account, but also the effect of the sites where these hypersurfaces cross. For $d = 2$, for instance, it is also relevant the behavior of the system when the initial seed is placed where two borders cross (an *edge*), being the response of the system different from the surface case, and with dependence on the angle between crossed walls [143, 144].

C-DP in the Presence of a Wall

In C-DP, the control parameter is the average energy in the system. This quantity changes for each site at each time, although its average is strictly conserved (FES ensemble) or remains with small fluctuations around its critical value (SOC ensemble). Therefore, it is not possible to define a different control parameter for the surface in a way in which the dynamics does not suffer relevant changes. In the C-DP class, then, it does not make sense to talk about surface transitions like the ones depicted in Fig.3.2; this does *not* mean that the presence of a wall has no effect for this class. Quite the opposite.

Absorbing Surfaces

For the C-DP universality class, *absorbing walls* have been already used in this thesis. In the SOC ensemble, the d-dimensional C-DP models are posed between $2d$ absorbing surfaces, to allow energy and activity to be dissipated in a proper way regardless the driving seed position. Therefore, when the

seed is placed next to the absorbing boundary, the effect of the wall is to destroy the activity growing from such seed[7].

Like in the DP universality class, it is expected that surviving-probability-related exponents change because, as activity dies faster in the presence of such absorbing surfaces, the lifetime of the spreading processes (avalanches) must be shorter. Therefore, the critical behavior changes, and so do the exponents above mentioned (see table 3.4). There is, thus, a new rich phenomenology arising from C-DP in the presence of an absorbing wall next to the initial seed, which will be here referred to as **C-DP$_{\mathbf{abs}}$**.

This phenomenology has been already noticed for some sandpiles where the seed of the slow driving is localized, by definition, next to one of the (open) boundaries. This is the case of, for instance, the original definition of the Oslo model [59], in which avalanche exponents different from the C-DP ones (but identical to the C-DP$_{abs}$ ones) are measured, because the initial rice grain is placed next to an absorbing boundary. When, in these systems, the driving seed is changed to be randomly chosen between all sites, the C-DP exponents are recovered [60, 144, 145].

Reflecting Surfaces

For *reflecting boundaries*, conservation and the threshold character of the activity make the effect of these surfaces very different from the DP case.

Consider, for instance, a microscopic sandpile with one closed boundary next to which the initial driving grain is introduced. At this level of description, Neumann boundary conditions Eq.(3.10) are modelled by imposing site $x = -1$ to be active if site $x = 1$ is so. In this way, every grain toppled from $x = 1$ to its surface neighbor is given back again into the system due to the immediate toppling of $x = -1$.

With such boundary conditions, it is not surprising the accumulation of energy observed next to the reflecting wall[8]. What is more stunning is that *all the measured critical exponents correspond to the exponents of the bulk C-DP behavior.*

The phenomenology of surfaces is very rich [146], and examples in which

[7] Obviously, the FES ensemble does not make sense when an absorbing wall, which means a sink for energy, is present.

[8] This phenomenology can be, indeed, observed for both SOC and FES ensembles.

a reflecting boundary keeps unchanged the critical behavior are not difficult to find [147]. But this case is very different, due to the identification of the background and the control parameter.

One possible explanation for the observed phenomenology could be a *compensation effect*: the observed structure of the background means that, close to the reflecting boundary, there is a zone of the system with an energy density always above the average. These sites must be under threshold in stationary configurations, because this is a mandatory condition for an avalanche to finish. But in this zone (which, in addition, is the part where the initial seed of activity is introduced), due to its energy density, it is expected for this site to generate many overcritical avalanches, which compensate the lack of feedback due to the presence of a wall (which would lead to a subcritical avalanche).

Another argument could be one similar to that of the DP case used to explain the identical behavior of DP in the presence of both surfaces, i.e. *the existence of a flow of energy*: with a reflecting wall at the border, the grains that would be lost in the case of an absorbing boundary bounce in the wall and return to the pile. Activity is momentary lost, but recovered as energy stored next to the boundary. Due to the threshold, the presence of the reflecting boundary permits to keep next to the wall the grains which would pass "through it", which in a C-DP system is equivalent to an increase of activity creation probability. This *potential activity* balances on average the lost feedback, and surviving probability is, in the end, not affected by the presence of such a surface. In an effective way, there is still a flow through the wall (similar to the case in which there is no wall at this site). Thus, the same critical behavior of C-DP must be expected.

Although there is not a demonstration of any of these arguments, the fact is that the numerical simulations of both microscopic and mesoscopic systems lead to the same conclusion: while the phenomenology associated with the background of a C-DP system in the presence of a reflecting wall (i.e. C-DP$_{ref}$) is different, the critical behavior of the observables are identical to that of the C-DP class.

Two Different Behaviors for Two Different Types of Surfaces

To summarize the results of the last sections, it can be said that the presence of a wall affects in very different way to C-DP systems. While the behavior of the observables in the case of the reflecting wall remains as in the bulk-

$d=1$	η	δ	τ	τ_t	z_{spr}
DP	0.313(1)	0.159(1)	1.108(1)	1.159(1)	1.265(1)
DP_{ref}	0.045(2)	0.426(2)	1.28(3)	1.426(2)	1.257(2)
DP_{abs}	0.046(2)	0.425(2)	1.25(3)	1.425(2)	1.275(2)
C-DP	0.35(2)	0.17(2)	1.11(2)	1.17(2)	1.40(2)
C-DP_{ref}	0.35(3)	0.16(3)	1.11(3)	1.15(3)	1.42(3)
C-DP_{abs}	$-0.33(2)$	0.85(2)	1.56(2)	1.81(2)	1.42(2)

Table 3.4: Critical exponents for $d=1$ DP and C-DP without and with a surface next to the initial seed position. DP exponents measured both with numerical integration of Eqs.(2.17) and PCP microscopic simulations, but also confirmed with [141]. The results for C-DP have been obtained both with numerical integration of Eqs.(2.66) and by using the microscopic Oslo model. System size: $L=32768$.

driven case (i.e. all the exponents coincide with those measured in bulk-driven experiments), the presence of an absorbing wall next to the driving seed leads to the measurement of very different critical exponents.

These results are summarized in the lower half of table 3.4, where numerical integrations of the $d=1$ Langevin equations Eqs.(2.66) with the corresponding boundary conditions (Eq.(3.10) or Eq.(3.11)), as well as microscopic representative models, have been used[9].

In summary, the presence of a wall next to the initial seed of activity affects in a very different way to DP and C-DP systems. For DP, the two studied types of surface lead to the same phenomenology (S-DP), with a surviving-related exponents very different from those of the DP class, but identical bulk exponents. In the case of C-DP, in contrast, a reflecting wall does not alter the critical exponents, while an absorbing wall leads to, again, the same bulk exponents but a lower surviving probability.

[9]Note that extra boundary conditions for the background field are not necessary, because it is a non-diffusing field, and no spatial derivative of the field appears in the equations.

3.3 A Recipe for Discrimination

It is not unusual that, due to the complicated dynamic rules of some microscopic models, the real scaling of the system arises after long transient periods only when very large system sizes are used.

This is not the case of the representative continuous equations seen in the previous chapters because, at this mesoscopic level, all microscopic irrelevant details are not present and only the essential symmetries of the universality class remain. Thus, a long and clean scaling region can be observed.

In chapter 2 it was stated that the DP and C-DP classes are, conceptually, very different, due to the consequences of the existence of a conservation law in the latter. However, there exist only small *numerical* differences between the critical exponents of these classes (see table 2.4 and table 2.5, or appendix C).

Thus, it is not strange for systems belonging to C-DP with complicated relaxation rules to be classified into a wrong universality class when a transient behavior is mistaken as the asymptotic one. Then, it is necessary to have a discrimination criterium with which discern to which universality class the real critical behavior of the system belongs, beyond transients and crossovers, and without using very large systems nor prohibitive computational times.

Using some critical exponents, *bulk-driven isotropic* DP and C-DP classes can be distinguished (for instance, η) if the critical point is accurately localized (for the FES ensemble) or the system is large enough (SOC ensemble). But for other exponents like τ, the difference is approximately of 0.2% ($\tau_{\text{C-DP}}$ is 1.002 times τ_{DP}); even with the best and fastest computer would be very difficult to discriminate the universality class, because the intrinsic systematic error of the standard computer simulation already embraces both values.

As can be seen in table 3.1, table 3.2 and table 3.3, the exponents in the presence of an anisotropic direction or surfaces next to the initial seed are very different in the DP case from the C-DP case. For instance, the difference in the τ exponent for anisotropic systems increases up to 16.7%, and using absorbing (reflecting) walls, up to 16.8% (13.8%)[10]. This fact is reflected in plots, where obviously the larger the difference, the easier to discriminate the universality class.

[10] An extreme case is the η exponent: together with the different sign, $\eta_{\text{C-DP}_{abs}}$ is 7.14 times $\eta_{\text{DP}_{abs}}$.

The response of DP and C-DP when a preferred direction or a surface is introduced next to the seed of activity of an avalanche (equivalently, spreading experiment, see chapter 2) gives a quantitative criterium to discriminate between the two classes. A method to distinguish between DP and C-DP can be given by the following steps:

1.- Measure the critical exponents of the isotropic, bulk-driven (or surface-free) system.

2.- Introduce a **reflecting wall** at one boundary, and define the site next to it as the site for the driving events or initial seed of avalanche propagations. If the exponents change, the system belongs to the DP class. In contrast, if it does not alter its critical behavior, the system belongs to the C-DP class.

3.- Introduce an **absorbing wall** at one boundary of the original model, and define the site next to it as the site for the driving events or initial seed of avalanche propagations. If the exponents change with respect to the ones measured at the first step, and coincide with the ones measured in the previous step, the system belongs to the DP class. In contrast, if they are different from those of any of the above described points, the system belongs to the C-DP class.

4.- Define a preferred direction (**anisotropy**) for the dynamics of the original model. If the measured critical exponents do not vary, the system belongs to the DP class. On the contrary, if they change to the exact values of a random walker, it belongs to the C-DP class.

Although usually the first and one of the rest of steps are enough to easy-discriminate the class, to perform the rest of the steps is (as it will be shown in the examples of section 3.5) a useful check for consistency which allows to purge mistakes of transients for the real asymptotic behavior.

3.4 The Effect of the Perturbations on the Background Field

When the above described perturbations are present in the systems, a structured nonhomogeneous background arises.

This can be an inconvenient because many observables describing the critical behavior of a system need from a translational invariance in most of the system[11].

Therefore, it is very important that an homogeneous bulk can be defined in the stationary background landscape of the systems, even in the presence of the mentioned perturbations. Thus, *if any structure is formed, its contribution must be negligible in the thermodynamic limit.* Next, the effect on the background of the presence of anisotropy and surfaces is studied.

The Effect of Anisotropy

For the DP class, anisotropy has no effect on the behavior of the system, and therefore it does not affect the background field. However, it is usual to find a non-homogeneous structure in the background of non-Abelian sandpiles when strong anisotropy is present in the relaxation rules. This structure is a product of the biased flow of energy in the preferred direction.

This structure is more pronounced as the degree of anisotropy increases, and it can be more sharply observed in systems in which the driving event is performed always over the same site.

For both, fixed and randomly chosen seeds, the threshold nature of the dynamics, which establishes a maximum value for the height of a site, allows to define an homogenous bulk part in systems which are large enough. Moreover, the finite size effects are more pronounced in anisotropic systems due to the fast diffusion of the energy in the preferred direction.

Therefore, it is essential for a reliable analysis of anisotropic systems to use large system sizes. In [133, 148], for instance, a crossover size L_x depending of the degree of anisotropy is defined. Only for systems with size $L > L_x$, the effect of the anisotropy can be reliably measured. For $L << L_x$, the isotropic behavior dominates. This crossover size is inversely proportional to the degree of anisotropy[12]

The fact that *any* degree of anisotropy leads to the same critical behavior could be interpreted as a support for the existence of a bulk part into the

[11] This is the reason why, for stationary-state-related magnitudes, the spatial average (density) can be taken as representative of the system.

[12] Therefore, for no anisotropy, L_x diverges and there is no crossover, but only isotropic behavior.

anisotropic structured background for large enough systems. If it was not so, the measured critical exponents would depend on the degree of anisotropy, as it is expected for the structure of the background.

A perfect example of the importance of the presence of a bulk is the case of the two $d = 1$ models of [136]. In there, a non-Abelian version of the Ab-SDM systems defined in section 3.1 in which the number of toppled grains coincide with the total number of grains stored by the active site[13] is considered. Two variants are studied:

- In the first example, the rule only involves the nearest neighbor of the active site. As a result, the background is not structured (that is, there is a constant density of particles with regard to the only spatial dimension), and the exponents measured are in perfect agreement with the ones depicted in table 3.1.
- However, for the second case, the next nearest neighbors are also considered. Thus, the anisotropic effect is more pronounced. However, for the same system sizes, a structured background with no bulk is reported, and the measured exponents take intermediate values between the C-DP and the A-C-DP critical exponents.

This leads to the conclusion that **only when an homogenous background can be defined, the measured critical exponents are reliable**, and it is possible only for *large enough system sizes*.

The Effect of Surfaces

The presence of a surface next to the seed of activity breaks the translational invariance of systems even in the thermodynamic limit; it is natural to wonder whether there are more effects which can affect to the otherwise homogeneous structure of the system.

Surfaces on the DP Universality Class

In the DP systems where a background can be defined, for instance in the PCP model, the effect of the boundary is barely reflected in the background field, as it is clearly shown in Fig.3.4.

[13] That is, the directed version of the original Manna model.

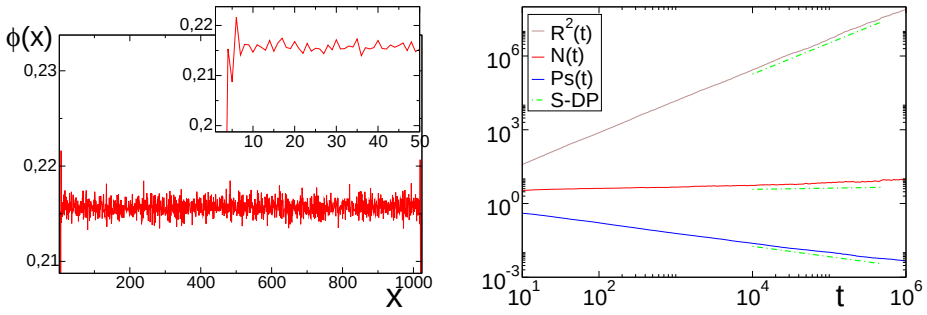

Figure 3.4: Left: Stationary background landscape of the $d = 1$ PCP Langevin equations, Eqs.(2.18) with absorbing boundary conditions, for a system size $L = 1024$, and averaging over many different trials. There is no relevant effect nor defined structure, as can be observed in the inset of the figure, where an enlarged part next to the leftmost boundary is depicted. Right: Spreading observables measured for the model of the landscape on the left; the exponents of the associated power laws are indistinguishable from the ones of S-DP.

There, a stationary background landscape of a $d = 1$ DP system is depicted. In these experiments, the initial seed of activity is placed next to one absorbing boundary, and the boundary condition is modelled using Eq.(3.11). The observed landscape is the averaged final absorbing configuration of spreading experiments performed by numerical integration of the PCP equations, Eqs.(2.18).

The effect of such surfaces has little reflection in the homogeneous structure of the background field, whereas the critical exponents (see right panel of Fig.3.4) are identical to the ones of the third row of table 3.4. The same results are obtained by using reflecting boundary conditions, Eq.(3.10), or the microscopic PCP model with any of the both types of surfaces placed next to the initial seed (not shown).

The nonconservative nature of the dynamic rules is the responsible for this behavior. The value of the background at each site does not depend only on the diffusion of activity, but there exist more relevant terms in the evolution equation (see Eqs.(2.18)) which create or eliminate background according to the (fixed) critical parameters of the equation.

In this way, each site makes the background be recovered up to the level imposed by the set of parameters of the theory, with little influence of the neighbors which are into the surfaces. Then, although the lack of a feedback next to the wall prevents the activity from spreading as fast as in the bulk, the background field has not a relevant structure, regardless the type of surface.

Surfaces on the C-DP Universality Class

In the C-DP class, the effect on the background is very different [149]. When both absorbing or reflecting boundary conditions are present in a C-DP system, the background next to the surface is non-trivially structured. Therefore, the question of whether an homogenous background zone, i.e. a bulk, can be defined in the system arises. This is not a futile question, because of the consequences of its answer:

- In the SOC ensemble, the system is surrounded by absorbing surfaces which provide energy dissipation, essential to reach the stationary critical state. As said above, the measurements made are supposed to be reliable because they are assumed to be representative of the behavior of the whole system. Therefore, any site-dependent effect in the observables is considered to be negligible. On the contrary, if no bulk can be defined, most of the results of SOC would seem a mirage, because all the measured exponents would be influenced by the structure generated by the presence of the wall.
- The equivalence of the SOC and FES ensembles (see the previous chapter) would not be valid. For this equivalence to be rigorous, in the thermodynamic limit the energy of the SOC system must reach its critical value and the critical bulk must coincide with the infinite-size FES-bulk at its critical point. To this end, the effect of the boundaries must be negligible.

The structure of the background in C-DP is the result of the conservative dynamics of these systems. The amount of energy at each site, E_i, depends only on the diffusive motion of activity; therefore, as a surface of the types defined above tends to dissipate (absorbing wall) or accumulate (reflecting wall) background, they make the zone close to the surfaces be under or above (respectively) the average energy of the bulk.

In fact, as said above, the effect of surfaces on the background is not trivial. For both absorbing and reflecting surfaces, a power law decay to the bulk average value of the background density for a certain size L ($E_{bulk}(L)$) can be observed[14].

[14]However, while in the absorbing case the structure is just the result of the boundary condition, the reflecting landscape is formed only when fluctuations are present on the system (i.e. the landscape is flat in the mean-field regime); it is a *noise-induced* effect [149].

For $d = 1$, and calling x the distance from the surface:

$$|E_{bulk}(L) - E(x)| \sim x^{-\alpha_w} \mathcal{G}\left(x/x_{\xi_w}\right), \tag{3.12}$$

where the exponent is $\alpha_w = 0.80(5)$ in both cases, x_{ξ_w} is the correlation length associated with the boundary effect, and $\mathcal{G}(y)$ is a scaling function.

The α_w exponent coincides with the inverse of the spatial correlation length exponent, $\nu_\perp$, in the thermodynamic limit. The reason is that, in this limit, $E_{bulk}(L \to \infty) = E_c$, and therefore $|E_{bulk}(L) - E(x)|$ can be considered a distance to the critical point, Δ. As its scaling with spatial coordinates is given by the relation (see Eq.(A.1.6)):

$$|\Delta| \sim x^{-1/\nu_\perp}, \tag{3.13}$$

and the correlations next to the surface are governed by bulk correlation exponents, an agreement between the inverse of $\nu_\perp$ and α_w is expected. Indeed, the inverse of $\nu_\perp$ is $1/\nu_\perp = 0.75(5)$ (see table C.1), and therefore both exponents, within error bars, coincide.

Thus, the degree of influence of the boundaries can be studied by using the relation Eq.(3.12) [149]. The dependence of the cutoff x_{ξ_w} of the scaling relation can be shown to be $x_{\xi_w} \sim L$, with which Eq.(3.12) is transformed into:

$$|E_{bulk}(L) - E(x)| \sim x^{-\alpha_w} \mathcal{G}\left(x/L\right). \tag{3.14}$$

This last expression can be checked with a simple representation of the scaling function $\mathcal{G}$. To this end, $|E_{bulk}(L) - E(x)|x^{\alpha_w}$ must be plotted versus x/L, in order to recover the scaling function. This is done in the left part of Fig.3.5, where the exponent $\alpha_w = 0.80(5)$ and the SOC Oslo ricepile have been used. The plot is a straight line up to $x \sim 0.35$ when a logarithmic vertical axis is used, which shows the exponential shape of the scaling function up to $x/L \sim 0.35$, and a faster decay onwards.

The cutoff fraction of 0.35 is, however, a large value, which into the context of two absorbing boundaries (present in $d = 1$ SOC systems) leads to approximately only a 30% of the system belonging to the bulk. Nonetheless, the power-law in Eq.(3.14) allows to write:

$$|E_{bulk}(L) - E(x)| \sim L^{-\alpha_w} \mathcal{H}\left(x/L\right), \tag{3.15}$$

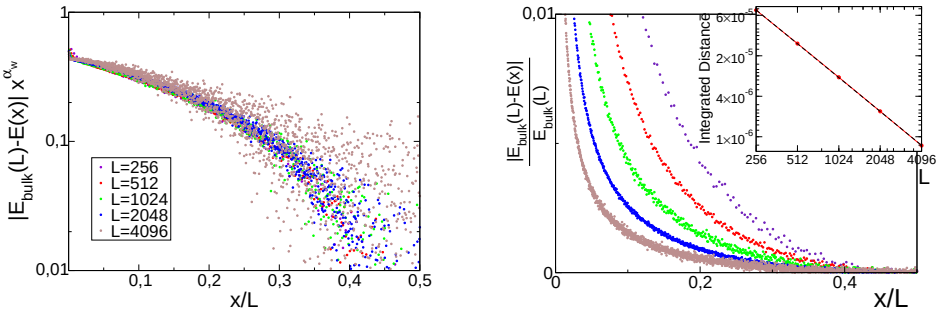

Figure 3.5: Left: Collapsed background fields, $|E_{bulk}(L) - E(x)|x^{\alpha_W}$ as a function of x/L for the boundary driven SOC Oslo model with absorbing walls, and for different system sizes. Using $\alpha_W = 0.80(5)$, all curves collapse into a unique one (see text). Right: Weighted distance to the bulk energy; inset: integral of $|E_{bulk}(L) - E(x)|$, normalized by the system size, as a function of L.

where $\mathcal{H}(x/L) = (x/L)^{-\alpha_w}\mathcal{G}\,(x/L)$.

In the right part of Fig.3.5, the relative distance to the bulk density is depicted. It can be observed how the fraction of sites with a relative distance below a 1% of the bulk energy is lower as system size increases. In the inset, the relation Eq.(3.15) is checked by using its normalized spatial integral. This behavior leads to the conclusion that **the larger the system, the smaller the fraction of sites with a relevant distance to the critical point** (i.e. a relevant difference between its background level and the bulk energy). Thus, in the thermodynamic limit, the distance to the critical point of *all* sites of the system is negligible.

A Self-Organized Cutoff

An heuristic reasoning can be given to support this statement. Consider an homogeneous $d = 1$ C-DP system of size L with periodic boundary conditions. Suppose that a slow driving is switched on and an absorbing wall is placed next to the seed of activity.

As said above, the effect of the surface is controlled by bulk correlations, and therefore the effect of the boundary depends on the distance of the bulk to its critical average value. Thus, for finite L, the effect of the borders has a finite cutoff, and cannot span throughout the system.

When $L \to \infty$, the bulk is closer and closer the critical value, and correlations can spread further and further. Then, the effect of the border penetrates

more and more into the bulk; but as the bulk dissappears, the distance to the critical point increases, appearing a shorter correlation length. This allows the bulk to be regenerated by means of the slow driving, in order to recover its critical value, and the explained cycle starts again. This is straightforwardly extended to any SOC system, regardless the kind of surface.

With this heuristic argument, it could be said that, for any system size, a certain fraction of sites with an homogenous structure can be always defined. As seen above, this fraction increases with the system size and, for large enough systems, the percentage of sites with a relevant distance of its energy to the bulk energy is negligible. In conclusion, **the influence of the surface vanishes as the system size increases**.

To summarize: in the DP class the presence of surfaces does not change the homogeneous structure of the background in a relevant way. In contrast, in SOC C-DP systems, conservation makes the surfaces influence the background field and form a non-trivial structure. However, the self-organized character of these systems prevents correlations from expanding their effect (negligible as the system size increases) up to an arbitrary site into the bulk, which can be safely defined. Moreover, this bulk is identical to the one of the FES ensemble for large enough system sizes.

The Anisotropic Bulk and the Surface Bulk in C-DP

As seen above, a structure is associated to all the types of perturbations discussed for C-DP, although a bulk part can be also defined. However, this homogenous part of the system behaves in a very different way for each perturbation.

In systems with surfaces, the microscopic rules remain unchanged respect to the surface-free model. Thus, the bulk and its critical behavior remain unchanged for both types of boundary conditions. However, the bulk of the anisotropic case is subject to the anisotropic rules, and therefore its behavior is completely different from the critical behavior of the isotropic bulk (see above).

It is also remarkable that, while in isotropic models the number of toppling events per added particle (or, equivalently, the mean number of jumps that a sand grain has to perform to fall out of the pile) is [34, 53, 74, 144, 148]:

$$\langle s \rangle \sim L^2, \tag{3.16}$$

in directed models and isotropic boundary driven systems, the number of steps for each grain to reach the border is reduced to [46, 53, 124, 144]:

$$\langle s \rangle \sim L. \tag{3.17}$$

By using Eq.(1.4) and the scaling of the first moment of the distribution [40]:

$$\langle s \rangle \sim \int_1^{s_c} sP(s,L)ds \sim s^{2-\tau} \sim L^{D_f(2-\tau)}, \tag{3.18}$$

it is possible to obtain τ by simply measuring the fractal dimension (and viceversa). These relations can be checked by using the corresponding values for D_f (see appendix C.1)[15]:

$$\begin{array}{lllll} \textit{Isotropic bulk} & \longrightarrow \langle s \rangle \sim L^2, & D_f = 2.18(2) & \longrightarrow & \tau \sim 1.08 \\ \textit{Anisotropic bulk} & \longrightarrow \langle s \rangle \sim L, & D_f = 1.45(5) & \longrightarrow & \tau \sim 1.31 \\ \textit{Absorbing boundary} & \longrightarrow \langle s \rangle \sim L, & D_f = 2.14(2) & \longrightarrow & \tau \sim 1.53 \end{array} \tag{3.19}$$

In perfect agreement with the measured avalanche exponents τ.

In summary, when a bulk in anisotropic systems exists, it is qualitatively different from the isotropic one, whereas this is not the case for systems driven from different boundaries (at least in $d = 1$).

3.5 Two Controversial Examples

The discrimination method defined in section 3.3 can become a fundamental tool in the task of the classification of SOC models into universality classes.

In the previous chapter, it was conjectured that all stochastic models with many absorbing configurations and an order parameter whose dynamics is coupled to a non-diffusive conserved field belong to C-DP universality class.

[15] Note that, as the fractal dimension is a bulk property, a different behavior of the bulk must be reflected in this exponent.

However, there are two examples which, despite of fulfilling the conditions of the conjeture, are still believed to be examples of DP sandpile models. The above described discrimination methods will be used now to distinguish which universality class these systems belong to.

3.5.1 The Isotropic Sticky-Grain Sandpile

When the relaxation rules of a sandpile are defined, it is usual to fix a finite threshold, common to (BTW sandpile [6], Manna model [54]...) or randomly chosen for (Oslo model [59]) all sites, which prevents the stored grains at a site from growing unbounded. The toppling probability of a site i can be thought to behave as a step function, which makes the site topple with probability 1 when the height of the site is above z_c, and with probability 0 when it is below the threshold.

In [150], Tadić and Dhar studied a variant of the d-dimensional DR model [123]. The relaxation rules, Eqs.(3.1), are complemented with a stochastic add-on: even when the condition $z_i > z_c = d$ is fulfilled, *the toppling of the active site is only possible with a certain probability* p, fixed for all active sites. In a subsequent work [151], Mohanty and Dhar extended the study of this model by introducing a bulk dissipation probability ϵ. Also, an isotropic version of this last model (equivalent thus to the ASM -see chapter 1- with bulk dissipation) was analyzed. Is in this last isotropic version on which this section is focused.

Consider a two-dimensional lattice with open boundaries at whose sites a threshold z_c for heights is defined. A grain is introduced into the sandpile at randomly chosen sites until, for a given site i, the threshold is overcome. Thus, with probability p the site relaxes *four* of its grains to its nearest neighbors, while with probability $1-p$ it remains stable until receiving more activity. As usual in the dynamics of a sandpile, the relaxation of a site gives raise to an avalanche, which can involve more activations. The driving event is repeated when no more active sites remain in the pile. By means of driving and dissipation, the pile reaches its stationary state.

The new relaxation rule can be written as:

$$\begin{cases} z_i \rightarrow & z_i + \Delta_{i,i} \\ z_j \rightarrow & z_j + \Delta_{i,j} \quad \forall j \end{cases} \tag{3.20}$$

where:

$$\Delta_{i,j} = \left\{ \begin{array}{ll} -4 & \text{for } i = j \\ 1 & \text{for } j \text{ n.n. of } i \\ 0 & \text{elsewhere} \end{array} \right\} \quad \begin{array}{c} \text{with probability} \\ p(1-\epsilon), \end{array} \tag{3.21}$$

that is, the usual ASM toppling rules;

$$\Delta_{i,j} = \left\{ \begin{array}{ll} -4 & \text{for } i = j \\ 0 & \text{elsewhere} \end{array} \right\} \quad \begin{array}{c} \text{with probability} \\ p\epsilon, \end{array} \tag{3.22}$$

which means that all toppled grains are dissipated before reaching the neighboring sites, and not only at boundaries; and

$$\Delta_{i,j} = \ 0 \qquad \forall (i,j) \qquad \begin{array}{c} \text{with probability} \\ (1-p) \end{array} \tag{3.23}$$

which entails that the grains remain *stuck* in the site instead of being redistributed. Due to this last rule, this sandpile will be called here the **isotropic sticky-grain (SG) model**.

Three different regimes can be distinguished [151, 152]:

- When $p = 1$ and $\epsilon = 0$, the results of the ASM are recovered.
- For $p < p^*$, grain columns of arbitrary height are possible, and no stationary state can be defined unless $\epsilon \neq 0$.
- For $p > p^*$, only for $\epsilon = 0$ a true critical stationary state can be defined.

The point p^* was argued to be the critical point of Directed Site Percolation, and $p < p^*$, to entail a subcritical regime [151, 152]. Indeed, although the dynamics is conserved (to achieve the only possible true stationary state) and stochastic (due to the probabilistic character of the toppling rule), Tadić et al. [150], Mohanty et al. [151] and Vázquez et al. [152, 153] claimed that the critical exponents of this system are related with the ones of the DP universality class. Moreover, in [151] the authors claimed (based in their results) that, in general, *all sandpile models* belong to DP universality class. The C-DP models would be unstable under perturbations which, in the end, bring them to the DP RG fixed point.

It was also argued [152, 153] that, for high enough energy density, all sites are above threshold, and the probability p is the only parameter with which

control their relaxation. In consequence, the dynamics of this sandpile defines a process which can be exactly translated into a DP one.

Mesoscopic Description of the Model

In [151], the following Langevin equation is proposed:

$$\begin{cases} \partial_t \rho = & D_\rho \nabla^2 \rho + \mu\rho - \lambda\rho^2 + \omega\rho\Theta(E - \rho - E_c) + \sigma\sqrt{\rho}\eta(\vec{x}, t) \\ \partial_t E = & D_E \nabla^2 \rho, \end{cases} \tag{3.24}$$

where ρ is the activity field, E is the energy field, η is a Gaussian white noise, E_c is the coarse-grained counterpart of z_c, and $\Theta(x)$ is the Heaviside step function, defined as:

$$\Theta(x) = \begin{cases} 0 & \text{if} \quad x \leq 0 \\ \\ 1 & \text{if} \quad x > 0. \end{cases} \tag{3.25}$$

The proposed set of equations is, basically, the C-DP set of Langevin equations, Eqs.(2.66), but with a step function which represents explicitely the threshold character of the dynamics: only at sites where the threshold is overcome, the coupling between the activity and the background field is considered. These equations, thus, are not only applicable to this model, but to a generic sandpile model.

According to the arguments of Mohanty and Dhar, the highly non-linear step function prevents these equations from showing C-DP critical behavior. The real behavior of a model represented by Eqs.(3.24) would flow from C-DP to the DP RG fixed point. This leads to their conclusion, above exposed, that the universality class of a generic sandpile is the DP class.

Thus, the probabilistic toppling rule associated to the dynamics of both the directed and the isotropic versions of this sandpile leads, as claimed in [150–153] to a DP critical behavior, instead of the A-C-DP or the C-DP (respectively) critical behavior that would be expected due to the stochastic nature of the rules. In the next section, the results of these works will be deeply analyzed.

The SG Model Revisited

Preliminary Discussions

The first point to take into account is the bulk dissipation defined in [151]. As will be argued in chapter 5, bulk dissipation in SOC systems does not alter their universality class, but destroys criticality. Therefore, the stationary state with $p < p^*$, $\epsilon \neq 0$ is to be subcritical. Indeed, Mohanty and Dhar already noted that, only for $p > p^*$ and $\epsilon = 0$, a true stationary state can be defined (the "SOC regime", as they called it).

As mentioned above, it is claimed in [152,153] that a high level of energy leads to the irrelevancy of the threshold, which means that the dynamics is only driven by the parameter p. However, such high columns are only achieved by values $p < p^*$, which as argued by the own authors is a subcritical non-stationary state. Thus, the only interesting case to discuss would be the regime $p > p^*$, $\epsilon = 0$.

Concerning the identification of p^* with the critical point of Site-DP, it can be argued the irrelevancy of this exact value for the universal behavior of the system. Consider a variation of the rules in which the site does not relax $2d$ grains but all the grains stored at it. This variation is trivial, in the sense that it does not entail a change in the critical behavior of a sandpile[16]. With this change, it is obvious that arbitrary high columns cannot be formed at any value of p, and therefore it is possible to define with the rules described above a SOC stationary state for any chosen value $p \neq 0$, provided $\epsilon = 0$. The fluctuations around the stationary value of the energy (or, equivalently, the mean height of the system) are higher as p is decreased.

In summary, the initial arguments which support the classification of this model into the DP class are not, in our opinion, conclusive. This leaves this claim only sustained by the Langevin Equation and the numerical simulations performed for the SG sandpile cellular automata summarized with the rules Eq.(3.20)-Eq.(3.23). On these two aspects of the problem is the discussion centered hereinafter.

[16]Indeed, this change is the used to define the Abelian version of the Manna model.

The SG Langevin Equation

As an intermediate point between theoretics and simulations, the set of Langevin equations Eqs.(3.24) is now analyzed. Consider the equations proposed for this SG sandpile model. Except by the coupling term, the set of equations is identical to the one defined for C-DP (Eqs.(2.66)).

The coupling in Eqs.(3.24) possesses a Heaviside step function $\Theta(E-\rho-E_c)$ which, using the definition Eq.(3.25), would lead to a coupling term given by:

$$\Theta(E-\rho-E_c) = \begin{cases} 0 & \text{if} \quad E-\rho \leq E_c \\ \\ 1 & \text{if} \quad E-\rho > E_c, \end{cases} \tag{3.26}$$

and the set of equations would be identical to the DP Langevin equation (Eq.(2.17)) at under-threshold sites, and a slightly trivially modified DP equation at sites above threshold. Moreover, the background field would be now a decoupled non-interacting field, irrelevant for the critical behavior for the system.

However, the step function is seldom used in mesoscopic equations because its microscopic character makes it flow, in the RG sense, to a modified shape in a coarse-grained description:

$$\Theta(x) \sim \tanh(x) \sim x + \ldots \tag{3.27}$$

In such a case, the threshold term would flow to:

$$\omega\rho\Theta(E-\rho-E_c) \rightarrow \omega\rho E - \omega\rho^2 - \omega\rho E_c \tag{3.28}$$

and, therefore, a slightly modified C-DP set of Langevin equations would be recovered at any site of the system. The modification is given by a different coefficient for the saturation term, $\hat{\lambda} = \lambda + \omega$, and a new mass term given by $\hat{\mu} = \mu + \omega E_c$ [154].

To observe the coarse-grained behavior of the coupling term, a numerical integration of Eq.(3.24) can be performed, and the effective mass coefficient which can be defined directly in Eq.(3.24):

$$\mu_{eff}(\vec{x},t) = \mu + \omega\ \Theta(E(\vec{x},t) - \rho(\vec{x},t) - E_c), \tag{3.29}$$

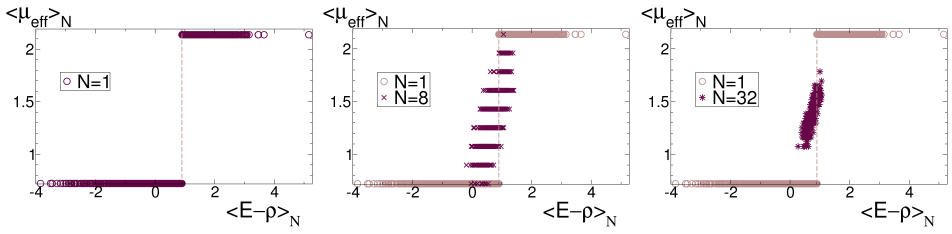

Figure 3.6: Effective mass, as defined by Eq.(3.29), as a function of the field difference averaged in Kadanoff blocks of size N, for $\mu = 0.72313$ (active phase). The vertical line corresponds to the threshold value $E_c = 0.9$. Observe that the larger the block size, the smoother the dependence of the effective-mass on the coarse-grained field difference.

measured in order to check that it flows to the mesoscopic behavior defined with Eq.(3.28).

The first step to follow is the determination of the critical point for a selected set of parameters. For $d = 1$, and using the parameters $E(x, t = 0) = 1\ \forall x$, $\lambda = \sigma^2 = 1$, $E_c = 0.9$, $D_\rho = D_E = 0.33$, $\omega^2 = 2$, and $dt = 0.2$, the critical point is localized at $\mu_c = 0.72308(5)$.

To reach a stationary state for the system, a supercritical value for $\mu > \mu_c$ must be taken. By using $\mu = 0.72313$, now a numerical Renormalization procedure is made by using Kadanoff blocks of length N. Thus, the block-averaged quantity $\langle \mu_{eff} \rangle_N$ is measured.

When this effective mass is depicted as a function of $\langle E - \rho \rangle_N$, the result can be observed in Fig.3.6. As can be seen, for a block as large as a site, a step-like form for the mass (with the jump at E_c) is observed. But the larger the size of the block, the more the effective mass looks like the linear curve predicted by Eq.(3.28)-Eq.(3.29), and for blocks of size $N = 32$ sites, a sharp linear dependence of the mass on E and ρ arises. In this way, the step function behaves as predicted in Eq.(3.28), and therefore the critical behavior of C-DP universality class is to be expected.

Indeed, using the parameters above mentioned at the critical point $\mu = \mu_c$, the critical exponents measured by the numerical integration of Eqs.(3.24) are in perfect agreement with the C-DP critical exponents. They are gathered in the first row of table 3.5. Therefore, it is shown with both theoretical and numerical arguments that Eqs.(3.24), devised to represent to the sticky-grain sandpile, belongs to the C-DP universality class.

Microscopic Simulations

Despite the strong indication obtained in the previous section, it can be argued that the proposed set of Langevin equations is not really a representative of the microscopic sandpile model and, therefore, the C-DP critical behavior observed is not the real critical behavior of the model.

Moreover, the critical exponents measured in [151–153] can be argued to be not conclusive because, maybe due to transients and crossover effects, the error bar of the measurements embraces the possibility of both universality classes or, in many cases, even the measured results incline for the C-DP side [153]. Due to this, a careful study of the microscopic model, in which the steps defined in section 3.3 are applied, is now performed in order to clarify which class this model belongs to.

1.- Isotropic Bulk-Driven (Surface-Free) Model [154]:

To analyze the isotropic SG model, two different versions can be defined: the one described by rules Eq.(3.20)-Eq.(3.22), and another one in which each neighbor is randomly chosen between the nearest sites (which, in the $p = 1$ limit, becomes identical to the well-known Manna model).

In both cases, the original isotropic SG model and the random SG model (RSG) are simulated in the *FES ensemble*, with the energy density fixed to $E = 2$, and the probability p used as control parameter. The position of the critical point is obtained by looking for a straight line in a log-log plot of observables like the activity density. It can be done because of the scale-free character of both its dynamic (Eq.(2.10)) and static (Eq.(2.14)) behavior near the critical point. These power-law functions can be observed in the left part of Fig.3.7, where the original SG model has been used.

As can be seen, a clean power law is observed for the largest size of the left plot, and for the *finite-size scaling* behavior of the system at the considered value, which can be considered a good estimate of the critical point. Thus, the critical points are estimated to be $p_c = 0.76750(3)$ for the SG model, and $p_c = 0.84937(2)$ for the RSG model [154].

These critical points are confirmed by SOC experiments where these probabilities are used. In this way, the dynamics attracts the energy density up to reach a stationary value around $E_c = 2$, confirming the validity of the estimate made with the FES ensemble.

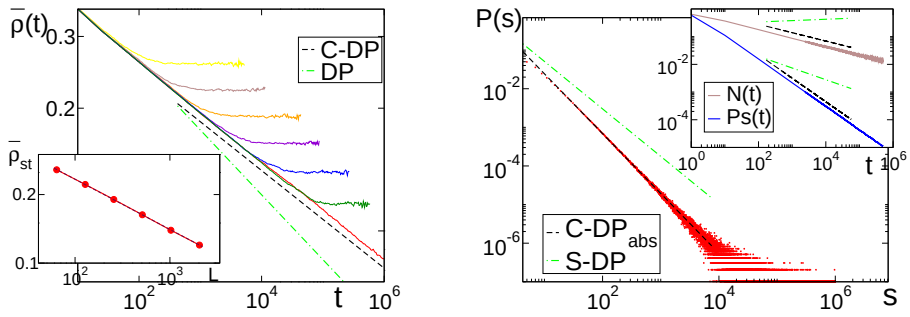

Figure 3.7: Left: Power law decay of activity density for the original SG model by using different system sizes; from top to bottom, $L = 64, 128, 256, \ldots, 262144$. Inset: Finite size scaling of the stationary values depicted in the main plot; from this graph, the exponent $\beta/\nu_\perp = 0.22(1)$ is measured. Right: Avalanche size distribution (main plot) and spreading observables (inset) in experiments driven from an absorbing boundary in the SG model, with a system of size $L = 32768$.

$d = 1$	η	δ	τ	τ_t	z_{spr}	θ
Eq.(3.24)	0.34(2)	0.18(2)	1.11(3)	1.18(3)	1.38(2)	0.14(2)
SG model	0.35(2)	0.17(2)	1.11(3)	1.17(3)	1.35(2)	0.12(2)
SG_{ref}	0.33(3)	0.16(3)	1.12(3)	1.16(3)	1.37(3)	–
SG_{abs}	−0.31(2)	0.85(2)	1.56(2)	1.85(2)	1.37(2)	–
A-SG	−0.04(5)	0.47(5)	1.33(5)	1.47(5)	1.89(5)	–

Table 3.5: Set of critical exponents for the sticky-grain model. All coincide, within error bars, with their C-DP counterparts, excluding the DP class.

Spreading exponents also can be measured, as well as avalanche exponents (see chapter 2), for both ensembles. The resulting measurements are gathered in the second row of table 3.5, where only the results of the original SG model are shown because RSG exponents result indistinguishable from the SG ones. By comparing with the C-DP value for these exponents, it is possible now to conclude that almost all of the measurements agree with this universality class, excluding in this way the DP behavior; $d = 2$ simulations, as well as high energy density trials (not shown) have been performed, confirming this conclusion.

2.- Isotropic Model with a Reflecting Wall [155]:

By placing a surface next to an initial seed of activity, surface experiments can be performed [155]. As said above, to simulate a reflecting wall introduced

into a microscopic system, the boundary condition consists in considering the sites into the surface as a reflect of the ones into the system, and therefore each grain which topples towards the wall is given back again to the system.

By using this kind of border next to the origin of the experiment, the critical exponents for both variations of SG model can be observed in table 3.5. The critical exponents measured for the SG model and the RSG model with a reflecting wall are identical, into error bars, to the bulk-driven case. Moreover, the critical exponents are very different from the DP_{ref} (S-DP) ones (see table 3.4).

Then, it is possible to confirm the tentative of classification performed above: the SG model belongs to the C-DP class. Nonetheless, this statement can be reinforced if the absorbing-wall step of the discrimination method is also performed.

3.- Isotropic Model with an Absorbing Wall [155]:

As explained above, when an absorbing wall is used the FES ensemble makes not sense anymore; therefore, only the SOC ensemble is to be used.

By placing the initial driving of each avalanche next to one of the open boundaries, the measured critical exponents are in table 3.5. Again, the critical behavior of the system is very different from DP_{abs} (S-DP) critical behavior (see the right part of Fig.3.7), and coincides with C-DP_{abs} behavior[17].

4.- Anisotropic Bulk-Driven (Surface-Free) Model:

In the $d = 1$ RSG model, it is possible to introduce an anisotropic direction by choosing a different probability for each side of the active site when it topples. For the original SG model, the only way to do it is by introducing total anisotropy, directness, in order to select deterministically always one of its neighbors.

When anisotropy is introduced, as explained above (see section 3.4), a large enough system must be used in order to avoid finite size effects. For systems up to $L = 262144$, the measured exponents for $d = 1$ are in the last row of

[17] See [156] for a discrepant opinion.

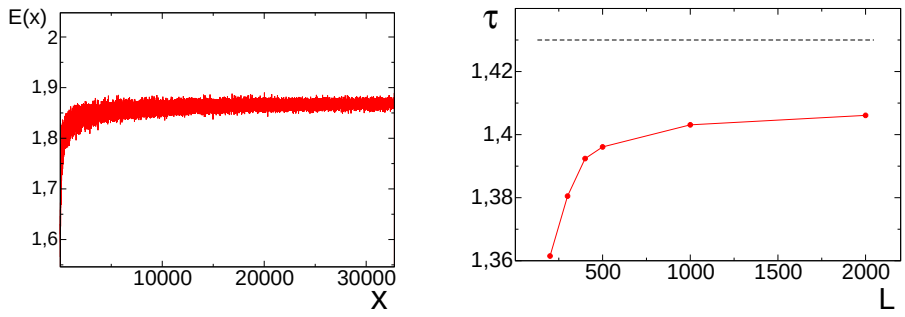

Figure 3.8: Left: Averaged landscape of the stationary background in a $d = 1$ anisotropic SG model of size $L = 32768$; although a structure can be observed next to the initial seed of activity (fixed at site $i = 1$), a well-defined bulk is present in most of the system. Right: Measured avalanche size exponent τ for many different sizes in the $d = 2$ directed SG model; the exponent increases with L, revealing the finite size influence on the measured exponent.

table 3.5. As can be observed, they are very different from the exponents of the isotropic case, which in principle rejects the possibility of Galilean invariance, i.e. of DP critical behavior. Moreover, when compared with the A-C-DP exponents of table 3.1 or table 3.2, it can be observed that they coincide within error bars.

Thus, the clean scaling of the observables and the sharp bulk part of the background landscape (see left part of Fig.3.8) allow to state that the anisotropic SG model belongs to A-C-DP and, therefore, the SG model is into the C-DP universality class.

It is a remarkable point that in its original definition [150, 151, 157] the model is, in fact, totally anisotropic. Indeed, for the $p = 1$ case, the results of the $d = 2$ DR model are obtained. However, for $p \neq 1$, the measured exponents in [150, 157] are not the ones of A-C-DP class, but seem to remain between DP and A-C-DP ones.

If the exponents took DP values, this would be an argument to support the claims of the authors, because the system would remain in the same class even when anisotropy is introduced, a feature which characterizes DP (see section 3.1). However, together with the intermediate value of the exponents, there are two facts which point to a *finite size effect* direction: the first one is the small sizes used to analyze the models (up to 200x200). The other one, the fact that the avalanche exponent change "from $\tau = 1.108$ to $\tau = 1.321$" when the pile is boundary driven.

As explained in section 3.4, there is a crossover size which depends on the

strength of anisotropy; below this size and for light anisotropy, isotropic results are recovered. As anisotropy is increased, a larger system size is necessary to observe the anisotropic true critical behavior. For the directed SG model [150,151,157], there is total anisotropy, and therefore large system sizes are necessary. Indeed, the measurements reported in the last row of table 3.5 correspond to a degree of anisotropy such that the homogeneous part of the landscape depicted in Fig.3.8 (left) can be observed. If there is no such an appreciable bulk, the measured critical exponents correspond to transient values.

On the other hand, when a directed model is boundary driven and the anisotropic flow moves away perpendicularly to the selected border, this surface has no effect on the critical behavior. All initial seeds have to travel, for example in $d = 1$, through the entire system to reach the only avaliable border: the opposite one. Therefore, with this kind of driving, the "effective size" of the system is larger than in the randomly-driven case. This effect is less marked in higher dimensions, but also the heuristic argument can be applied.

In this way, for the boundary driven experiments of the $d = 2$ system in [150], the results are less affected by finite-size effects, an thus more reliable. By using these results ($\tau = 1.313(12)$; $\tau_t = 1.460(14)$), the possibility to belong to DP ($\tau = 1.268$; $\tau_t = 1.450$, [79]) is under suspect. The values of the exponents make one recall the previously explained behavior: a crossover between isotropic ($\tau = 1.27(5)$; $\tau_t = 1.48(5)$, for the Manna model -see chapter 1) and A-C-DP ($\tau = 10/7 = 1.43$; $\tau_t = 7/4 = 1.75$) behavior.

This claim can be confirmed with a simple plot of the measured avalanche exponents versus the corresponding size for the very same directed model defined in [150], where these exponents are presented. In the right part of Fig.3.8, the best fit of the avalanche size distribution of each size is plotted. There is a marked dependence on the system size, with a convergence to the A-C-DP universality class in the limit of very large sizes. This close the loop and confirms that the SG model, with all its versions, behaves like a C-DP system in the presence of anisotropy, and therefore can be classified into this universality class.

In summary, a probabilistic version of the ASM, the sticky-grain (SG) model, originally claimed to belong to DP class, has been studied. By using the different response of both DP and C-DP classes to the presence of the perturbations explained in previous sections, and following the discrim-

ination method proposed in section 3.3, **DP universality class has been definitely excluded** as representative of the critical behavior of this model, which in fact belongs to C-DP class.

3.5.2 The Reshuffling Sandpile

In a typical sandpile, as explained in the previous chapter, the diffusion of the energy is linked to the diffusion of activity, because grains only flow when an avalanche is in course. This defines a very specific mechanism for the motion of the background field represented at a coarse-grained level by a Laplacian term $\nabla^2\rho$.

In [158], Maslov and Zhang devised a model in which the diffusion occurs by means of a stronger mechanism, which they called *reshuffling*. This new mechanism characterizes this model, that will be called here the **Maslov-Zhang (MZ) reshuffling sandpile model**.

In this model, the energy is continuous. Consider a d-dimensional hypercubic lattice. Each driving event introduces a small continuous quantity δE (instead of a discrete grain) at the central site of the lattice, which is declared active. The energy of this site i, *together with the energy of its neighbors*, is redistributed between the sites of the neighborhood (including i) (**reshuffling**). With a probability given by the stored energy of each visited site, it is declared active[18]. When no more active sites remain into the system, the avalanche stops and another driving event is performed. In this way, with the balance of driving events and boundary dissipation, the stationary state is reached.

The mentioned microscopic rules of the MZ model can be summarized as follows:

i) Driving: A small amount of energy, $\delta E \leq 1$, is added to the central site, which is declared active, and an avalanche starts.

ii) Relaxation: The energy of an active site and its neighborhood is locally redistributed ("reshuffled") among these sites:

$$E_i = \frac{r_i}{\sum_{j=1}^{2d+1} r_j} \sum_{j=1}^{2d+1} E_j, \tag{3.30}$$

[18]Thus, every site with $E_i \geq 1$ is an active site by definition.

where $r_i \in [0,1]$ are uniformly distributed random variables, and the sums are performed over the site i and its $2d$ nearest neighbors.

iii) Activation: Each of the sites involved in the reshuffling is declared active with a probability given by its own energy. If $E \geq 1$, the site is declared active with certainty.

Relaxation rule *ii*) is called by the authors "neutral" rule, because all the sites involved in the redistribution receive, on average, the same amount of energy. But also a "charitable" rule can be defined, in which the active site keeps a quantity lesser than the amount of their neighbors ($r_i < r_j$, $\forall j$ in the neighborhood of i)[19]; and a "greedy" rule, in which the opposite case happens.

In [158], only the "neutral" model was studied. In this work, the numerical results led to classify this model into the DP universality class for $d = 2$ whereas, for $d = 1$, an anomalous non-universal behavior was observed. As argued by the authors, in a sandpile model, the background field fosters the creation of activity at a site when more activity arrives, and the neighborhood is highly correlated; but in DP systems, the creation of a new active site depends on a fixed probability, equal for all the system. Thus, by means of the reshuffling rule, which is probabilistic but background dependent, a strong diffusive motion of activity which, a priori, prevents the background to be correlated is generated.

In a subsequent article, the study of the FES counterpart of the model leads to similar conclusions [75]. Indeed, the atypical redistribution of energy can result to be a relevant change for the C-DP dynamics of the sandpiles. By using the discrimination method proposed above, it is possible to classify this model into its real universality class.

The MZ Model Revisited

As a previous step in the analysis of the MZ model, the Langevin equation associated with the new mechanism for the diffusion of the energy is considered.

[19] For $r_i = 0$ and r_j constant and equal for all j, this model is identical to the Zhang model [47], which was shown to belong to the C-DP class when r_j are random numbers [49].

Mesoscopic Description

In the MZ model, the basic ingredients satisfying its dynamic rules are the continuous character of energy, the deterministic choice of neighbors, the reshuffling rule and the probabilistic activation as a function of the stored energy of a site. Apart from the reshuffling rule, the rest of ingredients are trivial modifications of rules which can be found in other C-DP examples (see chapter 1 and chapter 2).

With this novel feature, not only the energy of an active site but also the one of its neighborhood is redistributed. This microscopic rule leads to an extra term when a coarse-grained description is considered. Thus, Eqs.(2.66), representative of stochastic sandpiles, must be modified in order to gather all the ingredients of the model in the same mesoscopic description. A subsequent analysis of the resulting equation determines whether the modifications are relevant (i.e. able to modify the C-DP fixed point), or irrelevant for the set of equations and, therefore, C-DP behavior is the real critical behavior of the model [159].

a) Phenomenological Deduction

As described by Maslov and Zhang [158], the effect of the reshuffling relaxation rule is to generate a strong flow of the energy of the system. Thus, the modifications for the C-DP Langevin equation must be focused on this aspect.

In the C-DP equation, Eqs.(2.66), the diffusion of the background stems from the diffusion the activity field ρ represented by means of the Laplacian term in the evolution of the energy field E; therefore, a current $j(\vec{x}, t)$ can be defined:

$$j = -D_E \nabla \rho, \tag{3.31}$$

and the evolution of the energy is written in terms of this current as:

$$\partial_t E = -\nabla \cdot j = -D_E \nabla^2 \rho. \tag{3.32}$$

In the case of the MZ model, although an associated activity is still necessary for the diffusion of the energy (it is still necessary for the site to be in the

neighborhood of an active site), the redistributed energy belongs not only to the active site, and therefore a simple Laplacian term for its activity does not describe this scenario. The current, thus, cannot depend only on the activity field, but also on the energy field:

$$j = -\widetilde{D_E}(\rho)\nabla E, \tag{3.33}$$

where $\widetilde{D_E}(\rho)$ is an activity dependent functional, required in order to conserve the absorbing state character of the transition and diffusion of energy only in the presence of activity.

Without loss of generality, it can be considered that this dependence is linear. On the other hand, the evolution of the activity field is not expected to change significatively with regards to the usual C-DP system. In this way, the Langevin equations for this model can be written as:

$$\begin{cases} \partial_t \rho = & D_\rho \nabla^2 \rho + \mu\rho - \lambda\rho^2 - v\nabla\rho + \omega\rho E + \sigma\sqrt{\rho}\eta(\vec{x},t) \\ \partial_t E = & D_E \nabla \cdot [\rho \nabla E] \end{cases} \tag{3.34}$$

b) Deduction from the Microscopic Dynamics

It is possible also to deduce the energy equation by using a simple mapping of the microscopic rules to a coarse-grained description. To this end, a version of the MZ model with parallel updating is considered.

In this version, it is assumed that each site uses a fraction $1/(2d+1)$ of its energy in each reshuffling event. It is also assumed that each site receives, on average, the same fraction of energy from all its neighbors $(1/(2d+1))$. In this way, and at a mean-field level, the energy at next time of a site i can be described by the equation:

$$E_{i,t+1} = \frac{1}{(2d+1)} E_{i,t} \sum_{j=1}^{2d+1} [1 - \Theta(\rho_{j,t})] + \frac{1}{(2d+1)} \sum_{j=1}^{2d+1} \Theta(\rho_{j,t}) \sum_{k=1}^{2d+1} \frac{E_{k,t}}{(2d+1)}, \tag{3.35}$$

where j runs over the nearest neighbors of i, and k over the nearest neighbors of j; Θ is the Heaviside step function, defined above (Eq.(3.25)).

The first part of the r.h.s. of Eq.(3.35) represents the amount of energy which is kept by the system, unused during reshuffling events. This term considers that any of the sites of the neighborhood, including the site i, can remain non-active. The second term takes into account the reshufflings in which the site is involved.

As said in section 3.5.1, the step function has a microscopic origin and, therefore, at a coarse-grained description, it can be replaced by its argument (see above). In this way, the equation becomes:

$$E_{i,t+1} = \frac{1}{(2d+1)} E_{i,t} \sum_{j=1}^{2d+1} [1-\rho_{j,t}] + \frac{1}{(2d+1)} \sum_{j=1}^{2d+1} \rho_{j,t} \frac{\sum_{k=1}^{2d+1} E_{k,t}}{(2d+1)}. \tag{3.36}$$

Now, Eq.(3.36) is split into two parts, in order to simplify each of them. The time dependence will be omitted when not necessary. By defining the discrete d-dimensional Laplacian,$\nabla^2 E_i = \sum_{j=1}^{2d}(E_j - E_i)$, the first part of the r.h.s. of Eq.(3.36) can be written as:

$$\begin{aligned}
\frac{1}{(2d+1)} E_i \sum_{j=1}^{2d+1} [1-\rho_j] &= E_i - \frac{1}{(2d+1)} E_i \sum_{j=1}^{2d+1} \rho_j \\
&= E_i - \frac{1}{(2d+1)} E_i \left[\rho_i + \sum_{j=1}^{2d} \rho_j \right] \\
&= E_i - \frac{1}{(2d+1)} E_i \left[(2d+1)\rho_i + \sum_{j=1}^{2d} \rho_j - 2d\rho_i \right] \\
&= E_i - E_i\rho_i - \frac{1}{(2d+1)} E_i \left[\sum_{j=1}^{2d} (\rho_j - \rho_i) \right] = \\
&= E_i - E_i\rho_i - \frac{1}{(2d+1)} E_i \nabla^2 \rho_i,
\end{aligned} \tag{3.37}$$

and the second one:

$$\begin{aligned}\frac{1}{(2d+1)^2}\sum_{j=1}^{2d+1}\rho_j\sum_{k=1}^{2d+1}E_k = & \frac{1}{(2d+1)^2}\sum_{j=1}^{2d+1}\rho_j\left[E_j+\sum_{k=1}^{2d}E_k\right] = \\ = & \frac{1}{(2d+1)^2}\sum_{j=1}^{2d+1}\rho_j\left[(2d+1)E_j+\sum_{k=1}^{2d}(E_k-E_j)\right] = \\ = & \frac{1}{(2d+1)}\sum_{j=1}^{2d+1}E_j\rho_j+\frac{1}{(2d+1)^2}\sum_{j=1}^{2d+1}\rho_j\nabla^2E_j = \end{aligned}$$

$$= \frac{1}{(2d+1)}\left[E_i\rho_i+\sum_{j=1}^{2d}E_j\rho_j\right] + \frac{1}{(2d+1)^2}\left[\rho_i\nabla^2E_i+\sum_{j=1}^{2d}\rho_j\nabla^2E_j\right] =$$

$$= \frac{1}{(2d+1)}\left[(2d+1)E_i\rho_i+\sum_{j=1}^{2d}(E_j\rho_j-E_i\rho_i)\right]$$

$$+\frac{1}{(2d+1)^2}\left[(2d+1)\rho_i\nabla^2E_i+\sum_{j=1}^{2d}\left(\rho_j\nabla^2E_j-\rho_i\nabla^2E_i\right)\right]$$

$$= E_i\rho_i+\frac{1}{(2d+1)}\nabla^2\left(E_i\rho_i\right)+\frac{1}{(2d+1)}\rho_i\nabla^2E_i+\frac{1}{(2d+1)^2}\nabla^2\left(\rho_i\nabla^2E_i\right). \tag{3.38}$$

By gathering both results:

$$\begin{aligned}E_{i,t+1} = & E_i-\frac{1}{(2d+1)}E_{i,t}\nabla^2\rho_{i,t}+\frac{1}{(2d+1)}\nabla^2\left(E_{i,t}\rho_{i,t}\right)+\frac{1}{(2d+1)}\rho_{i,t}\nabla^2E_{i,t} \\ + & \frac{1}{(2d+1)^2}\nabla^2\left(\rho_{i,t}\nabla^2E_{i,t}\right),\end{aligned} \tag{3.39}$$

and using that:

$$\begin{aligned}\nabla^2\left[\rho_iE_i\right] = & \nabla\left[\nabla\left(\rho_iE_i\right)\right] = \nabla\left[\rho_i\nabla E_i+E_i\nabla\rho_i\right] = \\ = & \rho_i\nabla^2E_i+E_i\nabla^2\rho_i+2\nabla\rho_i\nabla E_i\end{aligned} \tag{3.40}$$

and reorganizing terms, the expression for the energy of the site i at the next step of the dynamics can be obtained:

$$E_{i,t+1} = E_{i,t} + \frac{2}{(2d+1)}\nabla\left(\rho_{i,t}\nabla E_{i,t}\right) + \frac{1}{(2d+1)^2}\nabla^2\left(\rho_{i,t}\nabla^2 E_{i,t}\right). \quad (3.41)$$

Using the definition of the discrete temporal derivative, the final expression for the energy is, in the end:

$$\partial_t E_i = \frac{2}{(2d+1)}\nabla\left(\rho_{i,t}\nabla E_{i,t}\right) + \frac{1}{(2d+1)^2}\nabla^2\left(\rho_{i,t}\nabla^2 E_{i,t}\right). \quad (3.42)$$

The second term of this last equation is irrelevant from a RG standpoint, because it involves higher spatial derivatives and, therefore, it can be neglected. Thus, by defining $D_E = 2/(2d+1)$, the set of equations Eqs.(3.34) is recovered.

To bring the deduced equation for the energy of Eqs.(3.34) out of the mean-field trivial approach to a non-trivial fluctuating regime, conserved noise terms could be added. However, this kind of noise is irrelevant in comparison with the deterministic term. In this way, Eqs.(3.34) can be considered the final mesoscopic description of the evolution of MZ model in any dimension d.

These equations must be studied by using the RG approach for a complete understanding of them and a calculation of the associated critical exponents. Unfortunately, likewise the C-DP set of Langevin equations (Eqs.(2.66)), singular propagators arise (see the previous chapter). It is not possible even an orientative naïve power counting. There are not even heuristic theoretical arguments like the exposed for the continuous representative of the previous model, Eq.(3.24). Therefore, we do not have theoretical arguments to clarify whether is DP or C-DP the universality class of this model.

Thus, in order to answer the question about the universality class to which this model belongs, the steps described in section 3.3 will be followed in the next section by means of MonteCarlo simulations of the defined microscopic model and the direct numerical integration of the proposed equations, Eqs.(3.34) [159].

Microscopic Simulations

To simulate the microscopic version of the MZ model, without loss of generality, the original rules are here changed to consider the position of the initial seed randomly chosen, instead of fixed. Also, the seed position is considered an ordinary site, in the sense that it is declared active with the probability marked by the background at this site. These little variations do not affect the universality class, and permit to treat all the sites of the lattice in an identical way at every time step.

The discussion now considered is focused on the conflictive one-dimensional case (see above), but the $d = 2$ simulations performed are in perfect agreement with the conclusions of the following $d = 1$ study of the system.

1.- Isotropic Bulk-Driven (Surface-Free) Model [159]:

For the isotropic version of the MZ model, and using systems up to $L = 32768$, the critical density in the FES ensemble is estimated to be $E_c = 0.4928(2)$ by using the same procedure described for the case of the SG model (see above). No anomalous scaling nor non-universality is observed, apart from very long transients and strong finite size effects, product of the "fast"-diffusive character of the dynamics.

Concerning the SOC ensemble, the stationary value for the energy (achieved by means of the rules defined above and the slow-driving and boundary dissipation of energy) coincides with the critical value of the energy reported for the FES ensemble. As in there, strong finite-size effects can be observed.

The measured exponents can be found in the first row of table 3.6. Except by z_{spr} and θ, the rest of measurements embrace the possibility of any of both universality classes; however, the exceptions favor to the C-DP universality class.

$d=1$	η	δ	τ	τ_t	z_{spr}	θ
MZ	0.32(5)	0.20(5)	1.13(5)	1.20(5)	1.40(5)	0.13(1)
MZ_{ref}	0.37(5)	0.15(5)	1.09(5)	1.14(5)	1.30(5)	–
MZ_{abs}	−0.36(5)	0.84(5)	1.57(5)	1.84(5)	1.25(5)	–
A-MZ	−0.02(3)	0.51(3)	1.35(5)	1.48(5)	1.98(3)	–

Table 3.6: Critical exponents for DP, C-DP, and MZ model for $d=1$. DP values taken from [79].

2.- Isotropic Model with a Reflecting Boundary [159]:

For the MZ model, the implementation of the reflecting boundary condition is more subtle than in other sandpiles. If site $i=-1$, into the wall, is used for the reshuffling considering it the reflect of site $i=1$, energy conservation is broken. Therefore, an alternative method must be used. Considering $i=2$ the only neighbor of the driving site $i=1$, the energy rebound at the surface is also mimicked, without breaking conservation.

For a probability distribution to show a clean scaling, hundreds of thousands of data must be collected. The presence of a reflecting wall can produce very long avalanches, which need of large computational effort. Due to this, to measure avalanche observables, only systems up to $L=4096$ have been used. On the other hand, a clean scale-free spreading observable can be obtained with many few trials or avalanches. Then, to perform experiments in which only spreading observables are considered, systems up to $L=32768$ have been used.

The critical exponents associated to the measured observables are gathered in the second row of table 3.6. After a long transient, spreading experiment curves reach the true asymptotic regime, whose exponents are identical within error bars to the C-DP exponents, and clearly different from the DP_{ref} ones (S-DP; first row of table 3.6). By considering the results of the two last sections, the possibility of the DP critical behavior can be rejected and, indeed, a classification into the C-DP class can be already done.

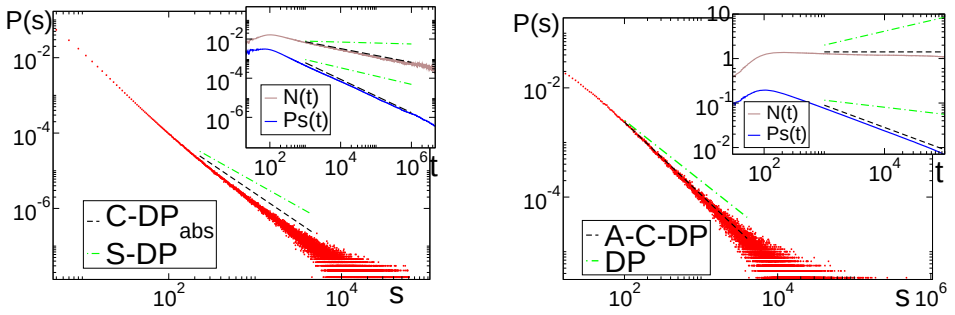

Figure 3.9: Left: Observables measured placing the activity seed next to an absorbing wall for the MZ model ($L = 32768$). Note the long transient for the avalanche size distribution. Right: Avalanche and spreading observables for an anisotropic MZ model ($L = 262144$).

3.- Isotropic Model with an Absorbing Boundary [159]:

Next, absorbing surface experiments are performed. Now, the reflecting wall is replaced by an absorbing wall, and the only possible ensemble is SOC.

The system is similar to the original MZ SOC model, but with the driving site localized next to one of the boundaries. For this experiment, the results can be observed in the left part of Fig.3.9 and the third row of table 3.6. Despite the long transient observed in avalanche-related distributions, the scaling for the rest of measured observables is clean and largely different from DP_{abs} behavior, which makes very easy to state the equivalence of the behavior of the MZ_{abs} model and C-DP_{abs} and, therefore, to classify the MZ model into the C-DP universality class.

4.- Anisotropic Bulk-Driven (Surface-Free) Model [159]:

Although it is already clear which the universality class of this model is, more numeric benchmarks can be performed to ensure the certainty of these conclusions.

There are many ways in which anisotropy can be introduced in the system. As strong anisotropy needs of large systems to avoid finite-size effects (see section 3.4), here only partial anisotropy is used. It is implemented by allowing the site in one preferred direction to receive more energy than the rest during the reshuffling.

$d=1$	η	δ	τ	τ_t	z_{spr}	θ
Eq.(3.34)	0.28(5)	0.21(5)	1.14(5)	1.21(5)	1.25(5)	0.14(2)
Eq.(3.34)$_{ref}$	0.36(5)	0.18(5)	1.12(5)	1.18(5)	1.29(5)	0.11(5)
Eq.(3.34)$_{abs}$	−0.39(5)	0.85(5)	1.58(5)	1.85(5)	1.22(5)	0.15(5)
A-Eq.(3.34)	−0.01(2)	0.50(2)	1.39(5)	1.64(5)	1.98(2)	0.51(2)

Table 3.7: Critical exponents for Eq.(3.34), with a reflecting or an absorbing wall, or with an anisotropic term added.

Consider the one-dimensional lattice, and i, an active site; if the chosen direction is, for instance, rightwards, we fix the random number r_{i+1} to its maximum possible value, $r_{i+1} = 1$. This ensures that the fraction of the neighborhood-total-energy that this site receives is larger than any of the other fractions. This generates a biased diffusion of the energy, a rightwards flow, which constitutes the desired anisotropy of the system. Other choices of anisotropy, including directness (total anisotropy), do not affect the final conclusions.

The results of the anisotropic experiments are conclusive. The obtained results present even a cleaner scaling regime than surface exponents (see right part of Fig.3.9), and the measured exponents are identical to the A-C-DP class (see table 3.6); therefore it can be said that **the MZ model belongs to the C-DP class**. Results in $d = 2$ confirm this statement [159].

The MZ Langevin Equation

For the MZ continuous Langevin equation, Eqs.(3.34), one-dimensional numerical integrations have been also performed. For reflecting wall experiments, the boundary conditions Eq.(3.10) are to be used, whereas for absorbing wall experiments, Eq.(3.11) are the appropriate choice. To introduce a certain degree of anisotropy, an extra $v\nabla\rho$ term can be introduced into each of Eqs.(3.34) (see section 3.1).

The results of all these simulations are gathered in table 3.7. These critical exponents are identical to the ones measured for the discrete MZ model, which confirms that Eqs.(3.34) **are the mesoscopic description of the microscopic model**. And they also support the conclusions obtained above with the MonteCarlo simulations: the MZ model is into the C-DP universality class.

In summary, the MZ sandpile model has been analyzed by using the dis-

crimination method described in section 3.3. Also, a mesoscopic description has been proposed which considers the different energy diffusion process characteristic of this model. The proposed equations have been integrated into the above explained approach. For all the mentioned experiments, the same conclusion arises: the MZ model belongs to the C-DP universality class.

This result is to be expected also for the "charitable" version of the model[20]. In this way, the universality class of C-DP is enlarged, embracing also types of energy relaxation different from the usual redistribution rules.

3.6 Concluding Remarks

For the models of a universality class with the simplest dynamics, wide scaling regions, clean of anomalous effects, can be observed. However, for systems with complicated dynamic rules, the scaling region can be plagued of long transients which can blur the real critical behavior of the model.

This is also applicable to C-DP systems. Indeed, although this class is conceptually very different from the DP class, the numerical closeness of the critical exponents makes that, sometimes, transient DP-like behavior is mistakenly considered as the true asymptotic behavior of the system.

The response of DP and C-DP classes to certain perturbations is largely different, and this fact can be used to easy-discriminate between these two classes.

For DP, the presence of a preferred direction does not alter its critical behavior. On the other hand, in DP, a wall is a relevant perturbation. Due to the coincidence of the behavior in the presence of any of the two surfaces (absorbing and reflecting) presented here, it can be used a generic name, *surface DP*, for the phenomenology originated when a surface is present in an otherwise DP system.

On the contrary, a C-DP system behaves in a different way:

- Reflecting walls are not a relevant perturbation in this class: when such a surface is placed next to the initial seed of activity of spreading experiments (avalanches), the measured exponents coincide with their corresponding bulk counterparts (i.e. C-DP$_{ref}$=C-DP).

[20]But not for the "greedy" one, which presents an anomalous "anti-diffusion" of energy.

- Absorbing walls affect the corresponding surface critical behavior. In particular, the surviving probability of avalanches and spreading experiments performed nearby an absorbing boundary is largely affected, and so they are the exponents which depend on this probability (non-bulk exponents).

- Spatial anisotropy is a relevant ingredient. The corresponding critical behavior of the A-C-DP class is described by the set of Eqs.(2.66) with an extra term $v\nabla\rho$, Eqs.(3.8), and its exponents are known exactly in any dimension.

By using the different responses of both universality classes to these perturbations, a discrimination method can be defined; this method can be used in cases in which the complicated relaxation rules of a stochastic sandpile introduce long transients or finite-size effects.

Here, two controversial sandpile models, claimed to belong to DP, have been studied. By analysing the change in their asymptotic behavior when both surface experiments are performed or a preferred direction is defined, it is concluded that both models belong to the C-DP universality class. In the case of the second model, the result is more remarkable, because of the underlying singular diffusion of energy associated with its dynamic rules; this expands the universality class to embrace different types of diffusion mechanisms for energy, remaining all of them associated with a source of activity.

In this way, the conjecture of universality exposed in the previous chapter has no exceptions, and the methods presented here arise as perfect tools for the analysis of any other conflictive example of conserved stochastic SOC models fulfilling the conditions presented in the conjecture.

Chapter 4

SOC as a Pinning-Depinning Transition

In chapter 2, the similarities between SOC and systems with absorbing states were pointed out, stating that isotropic stochastic sandpiles are systems that undergo a second-order phase transition to one of many possible absorbing states, with a conserved background field coupled to the order parameter of the transition.

This identification was possible after introducing a new ensemble, completely equivalent to the SOC one, in which the boundaries of the system are closed and the driving, interrumpted: the ensemble of fixed-energy sandpiles (FES).

Whereas in the SOC ensemble the dynamics drives the energy to reach its critical value, in the FES ensemble energy is the control parameter, and must be fine tuned to this same critical value in order to achieve the phase transition. Thus, the subcritical and supercritical regimes, which are not accessible by using the SOC ensemble, can be reached in FES, and the associated observables and critical exponents can be measured.

Although Directed Percolation (DP) is the paradigmatic universality class of systems with absorbing states, in chapter 2 it was shown that the conservation of the background field of sandpiles is a relevant ingredient, and the critical behavior of this kind of systems *does not* belong to DP. Indeed, when stochasticity is present in the relaxation rules of the pile, its critical behavior can be classified into a new universality class, called Conserved Directed Percolation (C-DP) class. The differences between both classes were pointed out and, in chapter 3, a method to easy-discriminate the universality class of systems suffering long transient regimes was defined.

In this chapter, it will be shown how the FES (and, consequently, SOC) critical point is intimately related to another problem in Statistical Physics: the depinning transition of elastic interfaces in disordered media. This transition, whose importance stems in its applications in Material Science and other disciplines, is undergone when an external force is applied to this type of manifolds.

First, these interfaces and the mentioned phase transition will be introduced by means of the mesoscopic representative of elastic manifolds in random media: the quenched Edwards-Wilkinson equation. After that, their common features with FES systems will be pointed out, in order to build a conceptual bridge linking both universality classes. This link will be reinforced by measuring, not only the typical exponents of interfaces, but also the usual absorbing phase transition observables, for such manifolds, and by translating one system of each class into one representative of the other class. In the end, the origin of this equivalent behavior of both interfaces and stochastic sandpiles will be explained, and universal functions intimately related with the physics of both kinds of systems will be measured.

4.1 Elastic Manifolds in Random Media

Consider an Ising magnet below the Curie temperature (see appendix A.1.2). At low temperatures, its dynamics is mainly controlled by the motion of domain walls separating regions of spins with opposite sign. In pure systems, when T is lowered to $T = 0$, the interface between both phases is completely flat; the manifold is not rough. But in real, imperfect systems, where impurities are present, something very different occurs: the disorder deforms, even at $T = 0$, the interface which separates the above-mentioned phases, becoming rough to accommodate to new energy minima. This is one example of **elastic manifold** moving in a disordered medium, as is the case of crack or dislocation propagation, vortices in superconductors... [160].

Different types of this disorder can be defined depending on how it appears in the medium. Here, only two are introduced: **random field** (RF) and **random bond** (RB) disorder. RF disorder is present when some spins (in the example of the domain walls) are coupled to an external random field, and the phases energetically differentiated due to this field. RB disorder is related to defects (missing spins or random interaction between them, for instance) in the system.

Such inhomogeneous media hinder the interface motion at the so-called **pin-**

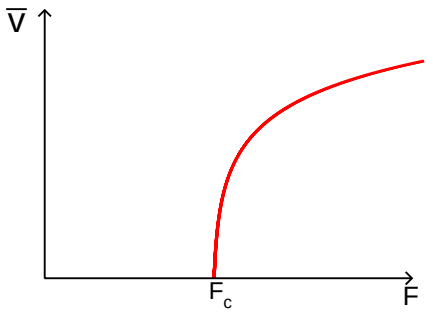

Figure 4.1: Phase diagram for depinning transitions; the mean velocity $\overline{v}$ is the order parameter which changes its value when the critical value of the force F (control parameter) is reached.

ning centers, which are minima of the disorder potential. There is a competition between *i)* the energetically favorable choice of remaining stuck at such positions, which makes the interface rougher, and *ii)* the surface tension force of the interface, which tends to flatten it. When an **external force** F is applied, two different regimes are to be distinguished: for large enough values of the force, all pinning positions are overcome and the interface moves **depinned**, with a non-vanishing mean velocity $\overline{v}$, reaching the *only* stationary state possible. When the force is small enough, some pinning centers are overtaken, but the interface can be anchored by many others; therefore, the system remains **pinned** ($v = 0$ for all sites) in one of the many possible trapping configurations. The energy of these configurations is very close to that of the ground state ($T = 0$ in pure systems), but their configuration space is very different.

In this way, for the suitable value of F, F_c, the interface undergoes a **depinning phase transition**, in which velocity $\overline{v}$ changes from a vanishing value (pinned phase) to a finite value (depinned phase), arising this magnitude, therefore, as the order parameter of the transition (see Fig.4.1).

Let $H(\vec{x}, t)$ be the height of the interface (its position in the growing direction) at time t and $\vec{x}$ its position in the spatial d-dimensional sub-space of the substrate. The system is defined, thus, in a $d+1$ space (position+height), in which periodic boundary conditions for the substrate can be chosen. Then, the motion of the elastic manifold in disordered media can be represented in a simple mesoscopic way by the equation:

$$\partial_t H(\vec{x}, t) = D_H \nabla^2 H(\vec{x}, t) + F + \eta(\vec{x}, H(\vec{x}, t)) \ , \tag{4.1}$$

which is the so-called **quenched Edwards-Wilkinson equation** [160,161]. The first term in the right-hand side of the equation represents the elastic recovering force, being D_H the surface tension coefficient (i.e. its strength or the stiffness of the manifold); the second term is the external force; and the last term is a **quenched noise** which takes into account the effect of the disorder of the medium (pinning centers). The mean value of this noise is chosen to be, without loss of generality, $\langle \eta(\vec{x},t)\rangle = 0$, where $\langle . \rangle$ means average over many different initial configurations of the disorder[1], and its correlations are given by:

$$\langle \eta(\vec{x},H)\eta(\vec{x}',H')\rangle = \delta^d(\vec{x}-\vec{x}')\Delta(H-H') \ , \tag{4.2}$$

where $\Delta(u)$ is a decaying function with a finite maximum length. In this way, the noise is short correlated in space and, as it will be shown below, short correlated in H. At a coarse-grained level, after performing a Renormalization procedure (see chapter 2 and chapter 3), the form of the correlations is identical in depinning transitions for both RF and RB disorders [162], and therefore it is so the observed critical behavior for both different potentials.

Eq.(4.1) describes the motion of a linear[2] interface. This is the reason why the universality class represented by this equation is called qEW or **linear interface model** (LIM) class.

Analysis of the qEW Equation

To determine the exponents which characterize the critical behavior of Eq.(4.1), it is possible to use the so-called **Functional Renormalization Group** (FRG) approach, whose application to the qEW equation [162–164] has been carried out up to 2-loop order of the calculation [165].

On the other hand, to obtain numerical results, a numerical integration of Eq.(4.1) can be performed directly, or by using an equivalent cellular automaton [164, 166].

a) Direct Numerical Integration

When the equation is directly integrated, the space of the substrate needs to

[1] If $\langle \eta(\vec{x},t)\rangle = C \neq 0$, an effective force $\tilde{F} = F + C$ can be defined, in order to recover a zero-mean noise.

[2] Note the absence of non-linearities in the equation.

be discretized whereas the height of the interface remains continuous. Also, an approximation for the noise is needed: to preserve its above mentioned features, for integer values of H the noise is randomly selected into $[-1, 1]$ and, for real values, it is obtained by linear interpolation of the former random numbers. Periodic boundary conditions are used.

Consider the case of $d = 1$; the discretized Eq.(4.1) is [164]:

$$H_i(t+dt) = H_i(t) + dt\,[H_{i+1}(t) + H_{i-1}(t) - 2H_i(t) + F] + g\sqrt{dt}\eta_i(H_i), \quad (4.3)$$

where g is a constant to control the strength of the noise and D_H has been fixed to one. An interface moving backwards at a site has no physical meaning in this context, and therefore negative values of $v = \partial_t H$ are forbidden.

The critical point is located by monitoring the average number of sites at which the interface advances, which is an order parameter equivalent to the velocity itself: when $F < F_c$, the only stationary value for both order parameters is zero, and for $F > F_c$, both quantities achieve a stationary state. If the noise strength is fixed to $g = 3\sqrt{dt}$ and the time mesh to $dt = 0.1$, the critical point is $F_c = 1.41605(5)$. Before defining the observables to be measured, the second way to integrate the equation will be introduced.

b) Integration by Using a Cellular Automaton

It is also possible to use a cellular automaton, the Leschhorn cellular automaton [166], which is in the same universality class of Eq.(4.1). It allows to save computational time when measuring the critical exponents associated with this equation.

In this automaton, the parameter F is fixed to zero, and the rest of variables are discrete. The noise of a site i can take only two different integer values: $\eta_i(H_i) = +1$ with probability p, and $\eta_i(H_i) = -1$ with probability $1 - p$; therefore, when its velocity:

$$v_i = H_{i+1} + H_{i-1} - 2H_i + g\eta_i(H_i)\ , \quad (4.4)$$

is positive, the height of the site is increased by an integer step:

$$\begin{cases} H_i(t+1) = & H_i(t) + 1 & \text{if } v_i > 0 \\ H_i(t+1) = & H_i(t) & \text{if } v_i \leq 0. \end{cases} \quad (4.5)$$

The parameter g is, without loss of generality, fixed to one. The effective driving force is represented by the average value of the noise, $2p-1$, and therefore p can be selected as the control parameter. With these choices, the critical point is located at $p_c = 0.8008(1)$.

Typical Interface Observables

For interfaces, the usual set of observables to measure is composed by the interface width (or **roughness**), defined as:

$$W^2(L,t) = \overline{\left(H_i(t) - \overline{H_i(t)}\right)^2}\ , \tag{4.6}$$

where the overline means, as in previous chapters, spatial average, and averages over many independent runs of the experiment are also necessary. This magnitude, which measures the fluctuations of the interface, increases in time with the power law [167]:

$$W^2(L,t) \sim t^{\beta_W} \mathcal{F}_1(L^z/t). \tag{4.7}$$

where β_W is the so-called *growth exponent*, and z the dynamic exponent (see chapter 2). The observable of Eq.(4.7) changes its behavior when a certain saturation time t_x is reached; the stationary value of the width, from such a time on, scales with the system size:

$$W^2(L,t) \sim L^{\alpha} \mathcal{F}_2(L^z/t), \tag{4.8}$$

where α is the *roughness exponent*. These two equations represent the so-called *Family-Vicsek scaling* of the interface [167]. If $\alpha > 1$, it is said that the manifold is a **superrough interface**, due to the fast increase of its width with the size. Using the relation between space and time (Eq.(A.1.10)), and Eq.(4.7)-Eq.(4.8):

$$\beta_W = \frac{\alpha}{z}. \tag{4.9}$$

In some types of interfaces, it is possible that the scaling given by Eq.(4.8) changes when a local range of sites is considered. For this *local width*, another exponent α_{loc} is defined. When $\alpha_{loc} \neq \alpha$, it is said that the interface exhibits

LIM	α	α_{loc}	β	κ_W	z
$d=1$	1.25(1)	0.96(3)	0.86(3)	0.17(3)	1.39(3)
$d=2$	0.75(2)	–	0.48(1)	0^+	1.56(6)

Table 4.1: Critical exponents for the LIM class, obtained by numerical simulations of the cellular automaton or taken from [164] (see also [170, 171])

anomalous roughening, i.e. different scaling for local and global fluctuations of the interface [168, 169].

The last observable to be considered is the average of the square of the slopes in the interface:

$$(\nabla H)^2 \sim t^{2\kappa_W}, \tag{4.10}$$

which can be easily related to the above-defined exponents by using simple scaling relations [169]:

$$\alpha - \alpha_{loc} = z\kappa_W. \tag{4.11}$$

Therefore, the value of the κ_W exponent is an indicative of the anomalous character of the interface: $\kappa_W \neq 0$ means that the interface shows anomalous roughening.

For the LIM class, the values of these exponents can be found in table 4.1. As illustrated in this table, the LIM interfaces in $d = 1$ are superrough and exhibit anomalous roughening. However, for $d = 2$, the behavior of the interface changes, following standard roughening ($\alpha < 1$ and $\kappa_W \approx 0$).

The upper critical dimension can be obtained by means of standard naïve power counting arguments; noting that the dimension of the elastic force is given by $d - 2$ and the dimension of the noise, by $d/2$, the noise is relevant when $d/2 > d - 2$, that is, when $d < 4 = d_c$.

It is also possible to use the arguments of Larkin [164, 172]. Consider a $(d+1)$-dimensional interface with a substrate of size L. The **Larkin length** is defined as the space scale at which the elastic energy of the manifold and the pinning force balance.

This scale, L_c, depends algebraically on the parameter $\varepsilon = 4 - d$ in a way that, for $d > 4$ and weak disorder, the elastic force can always flatten the interface and no pinning is possible. Then, for $d > d_c$, $F_c = 0$, and the

depinning transition is only recovered for stronger disorders. However, for $d < d_c$ and at scales $L > L_c$, the elastic force does not suffice to balance pinning forces, being necessary an external field. In this case, a non-trivial F_c as well as multiple pinning configurations exist.

4.2 Equivalence Between LIM and C-DP Universality Classes

Already in very early works on SOC, a relation between LIM interfaces and sandpiles is pointed out [18, 74, 173], but also in works concerning qEW interfaces [174]. This would mean that behavior of a LIM system above and below its critical point could be related with the behavior of systems with many absorbing states like the ones into the DP or C-DP classes. In this section, this relation will be investigated.

Consider a $(d+1)$-dimensional LIM manifold, described by Eq.(4.1). For $F < F_c$, the quenched noise of Eq.(4.1) is responsible for the existence of many possible pinning states. If the external force is fixed, the state remains frozen, with a total absence of activity. These states are **absorbing states**. For $F > F_c$, a stationary active state with a certain $\overline{v} \neq 0$ is reached[3].

Thus, there exists a phase transition between an active and a frozen phase just when the external force F, is fixed to its critical value F_c. *The depinning transition can be identified with an absorbing state phase transition.*

To continue with this identification, a **spreading experiment** can be also defined for elastic interfaces. For a fixed $F = F_c$, by increasing "by hand" the height of a site i, this negligible perturbation of order $\sim L^{-1}$ can create an active site with $v_i \neq 0$ into the manifold. This activation can trigger many more and, in this way, the initial perturbation can be spreaded. Due to the identification between a non-vanishing velocity and activity, a site i with $v_i \neq 0$ can be considered active, and all the observables of the spreading experiments (Eq.(2.1a)-Eq.(2.1d)), and the avalanche related ones (Eq.(1.5) and Eq.(1.6)) (see chapter 2) can be measured[4]. The values of the associated

[3]Moreover, for $F \gg F_c$ (or for $T \neq 0$), the motion is dominated by the external force; in an effective way, $H = v \cdot t + \tilde{\eta}(\vec{x}, t)$, and the usual *Edwards-Wilkinson* equation [175], identical to Eq.(4.1) but with an annealed (instead of quenched) noise, is recovered [164].

[4]The identification $v \leftrightarrow \rho$ allows to measure also observables like the decay to the absorbing state (Eq.(2.10)) or the finite size scaling (Eq.(2.14)).

LIM	η	δ	τ	τ_t	z_{spr}	θ
$d = 1$	0.39(3)	0.18(3)	1.11(3)	1.18(3)	1.39(3)	0.12(2)

Table 4.2: Spreading and avalanche exponents for the LIM class, obtained by numerical simulations of the Leschhorn cellular automaton; they coincide, within error bars, with their C-DP counterparts (see table C.1).

exponents for $d = 1$ can be found in table 4.2.

The determined exponents are compatible with both C-DP and DP classes, which was expected due to the identification with absorbing-state systems made above. However, in LIM systems it is possible to find two *conserved quantities*: the external force, which is fixed, and the elastic force, which is conserved by definition in these closed systems. At each site, the sum of both magnitudes, $\phi(\vec{x}, t) = \nabla^2 H(\vec{x}, t) + F$, acts as an effective driving force [176]. This competes with the random pinning force, which leads the manifold to the absorbing state. Therefore, the **background field** $\phi(\vec{x}, t)$ controls the probability for each site of the interface to advance (i.e. to be active). As there is a critical force for the system, there is also a critical mean value for ϕ, $\overline{\phi}_c$, for which the phase transition is undergone.

Therefore, the universality class of the depinning phase transition is to be related with C-DP better than with the non-conservative DP class. This can be stated by observing the critical exponents of table 4.2, but also with the response of LIM systems to perturbations like anisotropy [133] and (absorbing) boundary driving [177], identical to the response of C-DP systems.

A priori, both LIM and C-DP classes share the same critical behavior (i.e. they are the same universality class). Nonetheless, it would be desirable to reinforce these conclusions by means of some analytical background, with which the equivalence is settled in a more rigorous way.

4.2.1 LIM Sandpiles and C-DP Interfaces

If both LIM and C-DP classes are indeed the same universality class but described with different languages, it should be possible to translate a typical model representing one of these languages into a typical system of the other one. The resultant systems belong to the same universality class of their original models, but the change permits to treat them with other language, in order to compare classes.

In this section, the two directions of the path connecting LIM and C-DP are explored[5]. In turn, it permits to identify the usual interface observables in a C-DP system, in order to close the loop of the comparison of critical exponents.

Due to the similarities between the two kinds of models, the possibility to map one type into the other arises naturally. In [174], an early sketch of a mapping is done in order to improve the numerical results of the numerical integration of a LIM interface, i.e. a sandpile is "built" from an interface. As we will see, the opposite direction is more frequently found in the literature.

From LIM to C-DP

First, starting from a LIM interface, a C-DP system will be obtained. Concretely, the set of C-DP Langevin equations, Eqs.(2.66), will be derived starting from a discrete LIM model. Here, the steps of the deduction of Alava and Muñoz [176] will be followed.

Consider the Leschhorn cellular automaton, described in section 4.1. In it, the qEW equation is discretized (see Eq.(4.3)); also the noise is discrete, taking the value $\eta(\vec{x}, H) = +1$ ($\eta(\vec{x}, H) = 1$) with probability p ($1 - p$). If periodic boundary conditions are used, either the average driving force, $F = 2p - 1$, or p can be considered the control parameter of the system. The advance of the interface is conditioned to the sign of its velocity $v_i = H_{i+1} + H_{i-1} - 2H_i + \eta_i(H_i)$:

$$H_i(t + 1) = H_i(t) + \Theta[v_i], \tag{4.12}$$

where Θ is the Heaviside function (see Eq.(3.25)). By tuning p to its critical value $p_c = 0.8008(1)$, the depinning transition is undergone.

The height of the discrete interface described by Eq.(4.12) is built by adding to H_i one unit each time the velocity of the site takes a positive value, i.e. each time the site remains active. At a microscopic level of description, the height at a time t is the accumulated activations of the site up to this time. By using coarse-grained fields, the activity of a site can be written, in a mesoscopic translation of Eq.(4.12), as:

[5]Due to the marked differences between certain parts of their mesoscopic equations as, for instance, the noise, a rigorous direct change of variables between both equations seems not to be a reasonable option.

$$\rho(\vec{x},t) = v(\vec{x},t) = \partial_t H(\vec{x},t). \tag{4.13}$$

This identification stems from the fact that, when the velocity is zero (negative velocities are forbidden -see above), the interface does not move at this position, which is non-active; and for positive values of $v(\vec{x},t)$, the site is active and the manifold advances.

The *background field* has already been defined as the sum of the elastic force and the external force:

$$\phi(\vec{x},t) = \nabla^2 H(\vec{x},t) + F. \tag{4.14}$$

Therefore, by using Eq.(4.13) and Eq.(4.14), the temporal evolution of this field can be written as:

$$\begin{aligned} \partial_t \phi(\vec{x},t) = &\ \nabla^2 \partial_t H(\vec{x},t) + 0 \\ = &\ \nabla^2 \rho(\vec{x},t). \end{aligned} \tag{4.15}$$

Concerning the dynamic equation of the *activity field* ρ, it must contain a *coupling term* with the background field ϕ (which can be considered an *effective force*) because it fosters the creation of activity. Moreover, the interface at a site, in the absence of such force, remains always pinned. The lowest order contribution (i.e. the linear one) of the possible couplings is taken; the rest of them are irrelevant for long time behavior in the thermodynamic limit.

The equation must also contain a term $\mu\rho(\vec{x},t)$, which takes into account possible variations of activity as the manifold advances; and a saturation quadratic term $-\lambda\rho^2(\vec{x},t)$, to prevent the interface from growing unbounded. The usual Laplacian term $\nabla^2\rho(\vec{x},t)$ must be also included, in order to describe the tendency of the neighbors of a site to follow its motion in such a diffusive system.

The last step is to add a noise. In the qEW equation, the noise is quenched; this means that it only changes when the height of the site varies. In other words, the noise changes only when the velocity at this site is non-zero, i.e. when the site is active. On the other hand, an annealed multiplicative noise in activity (that is, a noise whose amplitude is proportional to the activity field) is only different from zero when $\rho \neq 0$. Therefore, if the site is active, both types of noises change at each time. And while the site is not active, the activity field is zero and the values of the annealed noise during this time

are statistically irrelevant. In conclusion, for both $\rho = 0$ and $\rho \neq 0$ states for a site, an annealed multiplicative noise can be used instead of the quenched noise in order to mimic the behavior of the interface. Moreover, the activity creation and destruction at a microscopic level can be considered Poissonian, and therefore in a coarse-grained description the noise is Gaussian, with a mean value which depends on the mean rate of creation ρ. Thus, the noise term can be written as $\sqrt{\rho(\vec{x},t)}\eta(\vec{x},t)$[6].

With all these ingredients, the final equation for the evolution of the activity field is given by:

$$\partial_t \rho(\vec{x},t) = \nabla^2 \rho(\vec{x},t) + \mu\rho(\vec{x},t) - \lambda\rho^2(\vec{x},t) + \rho(\vec{x},t)\phi(\vec{x},t) + \sqrt{\rho(\vec{x},t)}\eta(\vec{x},t), \tag{4.16}$$

and including general constants and omitting the spatial and temporal dependence in the coarse-grained fields, the final set of equations is:

$$\begin{cases} \partial_t \rho = & D_\rho \nabla^2 \rho + \mu\rho - \lambda\rho^2 + \omega\rho\phi + \sigma\sqrt{\rho}\eta(\vec{x},t) \\ \partial_t \phi = & D_\phi \nabla^2 \rho, \end{cases} \tag{4.17}$$

which is the set of Langevin equations of the C-DP class.

Then, starting from a discrete model of LIM interface, and by a simple identification (in its coarse-grained dynamics) of the fields which are used in C-DP systems, the mesoscopic description of the class of the stochastic sandpiles has been obtained in a justified way. This leads to the conclusion that, when the microscopic details of the concrete LIM model are cast out by the coarsening procedure and the mesoscopic behavior arises, LIM and C-DP systems are described by the same set of coarse-grained equations, i.e. both *are* the same universality class.

From C-DP to LIM

To complete the journey from LIM to C-DP and back, a stochastic sandpile model will be used here to obtain the mesoscopic Langevin equation which describes linear interfaces in random media, Eq.(4.1).

[6]There exist also techniques in the literature which are devised precisely to map a quenched noise into an annealed one. The Run-Time Statistics [178], applied to many different fields like DP systems or growth models, permits to transform a quenched noise in a long memory term into the evolution of activity.

Many works about the rough surface of a growing sandpile and its interfacial properties can be found in the SOC literature [11,75,92,145,176,177,179, 180, ...]; even the surface exponents of a sandpile (Oslo model) have been measured in a $d = 2$ real experiment [181]. All these works share the same procedure to reach the qEW equation starting from a sandpile model. With it, either the deterministic BTW sandpile or stochastic models like Manna, RD or Oslo models, can be obtained. Here, the steps of [75, 176] will be followed. The Abelian version of the Manna model[7] and the FES ensemble will be used, but the generalization to other sandpiles is straightforward.

Let i be a site of a d-dimensional Manna sandpile, and t the label for the steps of the spreading of activity. The simple balance condition between the energy inflow $I_i(t)$ and outflow $O_i(t)$ at a site i (given by the conservation law) allows to deduce the equation for the evolution of the height at this site.

The height is, according with Eq.(4.13), the accumulated activity of a site; from this equation, integrating over time:

$$H(\vec{x}, t) = \int_0^t \rho(\vec{x}, t')dt', \tag{4.18}$$

or, for discrete models:

$$H_i(t) = \sum_{k=0}^{t} \Theta(\rho_i(k)). \tag{4.19}$$

Therefore, the number of times a site topples is given by its height. Thus, the inflow of a site i can be defined as:

$$I_i(t) = \tilde{\zeta}_i(t), \tag{4.20}$$

where $\tilde{\zeta}$ is an accumulated noise which takes into account the random number of grains that the site receives at time t, i.e. the number of grains that its $2d$ neighbors have toppled to this site:

$$\tilde{\zeta}_i(t) = \sum_j \sum_{k=0}^{H_j(t)} \zeta_{i,j}(k). \tag{4.21}$$

[7] As commented in previous chapters, the only variation in its dynamic rules is the number of toppled grains, fixed to 2.

j sweeps over the nearest neighbors of i, and $\zeta_{i,j}(k)$ is a random number given by:

$$\zeta_{i,j}(k) = \begin{cases} 0 & \text{with probability} \quad (1-1/(2d))^2 \\ 1 & \text{with probability} \quad (1-1/(2d))/d \\ 2 & \text{with probability} \quad (1/(2d))^2. \end{cases} \tag{4.22}$$

This noise has a non-zero mean equal to $1/d$ and variance $(1-1/2d)/d$; the noise can be shifted ($\zeta_{i,j}(k) \to \zeta_{i,j}(k) - 1/d$) in order to have a zero-mean noise and, consequently:

$$I_i(t) = \frac{1}{d}\sum_j H_j(t) + \sum_j \sum_{k=0}^{H_j(t)} \left(\zeta_{i,j}(k) - 1/d\right). \tag{4.23}$$

Then, the number of grains received for the site at time t depends on the random contribution of neighboring sites, in which it is taken into account the number of times these sites have toppled up to time t ($H_j(t)$).

Concerning the outflow, it is, by definition, only two grains per toppling of site i, that is:

$$O_i(t) = 2H_i(t), \tag{4.24}$$

and, therefore, the number of grains of a site at time t is given by:

$$\begin{aligned} z_i(t) = &\quad z_i(0) + I_i(t) - O_i(t) \\ = &\quad z_i(0) + \frac{1}{d}\sum_j H_j(t) + \sum_j \sum_{k=0}^{H_j(t)} \left(\zeta_{i,j}(k) - 1/d\right) - 2H_i(t) \\ = &\quad z_i(0) + \frac{1}{d}\nabla^2 H_i(t) + \tilde{\zeta}_i(t) \end{aligned} \tag{4.25}$$

where the same name $\tilde{\zeta}_i$ has been used for the accumulated shifted noise.

In a sandpile, active sites are those for which $z_i(t) > z_c$; therefore, the definition of the velocity of this discrete sandpile interface is $v_i = z_i(t) - z_c$. In a last step, as only sites for which $v_i > 0$ are updated, and pinned sites can be depinned only by means the arrival of neighboring activity, $\tilde{\zeta}_i$ can be considered as a quenched noise (see above), and then:

$$v_i(t) = z_i(0) - z_c + \frac{1}{d}\nabla^2 H_i(t) + \tilde{\zeta}_i(H_i), \tag{4.26}$$

and the evolution of the interface is given by:

$$H_i(t+1) = H_i(t) + \Theta[v_i(t)], \tag{4.27}$$

where, again, backward motion for the interface is forbidden. This final equation is similar to the qEW equation, Eq. (4.1). However, the correlations of the noise terms are very important in order to define the physics of the system. Here, two different quenched-noise terms are present.

The first quenched noise is the *columnar noise* introduced by the initial condition, $z_i(0)$. As said in chapter 2, in SOC systems the initial-condition dependence is easily removed by avalanches; the initial configuration could be responsible, at most, for a transient regime. For this system, arguments of relevancy (in the RG sense) must be considered [176]. Compared with the quenched noise, the columnar noise is irrelevant in high enough dimensions ($d > d_c$). However, for low dimensions, the time necessary to get rid of the non-trivial initial condition represented by the columnar noise can be divergently large. Thus, the contribution of this noise cannot be, a priori, eliminated.

On the other hand, the correlations of the second noise $\tilde{\zeta}_i(H_i)$ are unknown and, in principle, not trivial. It takes into account not only the random diffusion of the particles, but also the threshold character of the dynamics.

Therefore, for both noises, there are no reliable arguments to state whether the above obtained interface belongs to the LIM class.

Numerical Simulations of the C-DP Interface

In order to decide whether the sandpile interface described with equations Eq.(4.26) and Eq.(4.27) belongs to the LIM class, numerical simulations must be performed, and the typical exponents of both absorbing states and interface models must be measured. Scaling relations between avalanche and interface exponents, as for instance the ones deduced in [182], can be used as consistency check, and allow to state that the interface observed is the result of the underlying avalanche dynamics [181].

In table 4.3, some of the results of the numerical simulation of a $d = 1$ Manna model simulated in the FES ensemble can be observed. The interface

Manna Interface	δ	θ	β	κ_W	z
$d=1$	0.16(3)	0.13(2)	0.89(2)	0.43(1)	1.42(2)

Table 4.3: Selected set of critical exponents for the interface built with a $d=1$ Manna sandpile by using Eq.(4.26) and Eq.(4.27). Note the high value of the κ_W exponent (see text).

exponents have been measured by using the definition Eq.(4.19), which gives rise to the evolution equations Eq.(4.26) and Eq.(4.27).

As can be seen, all the exponents coincide with the LIM class ones (see table 4.1 and table 4.2). Moreover, by comparing with the interface exponents of a DP manifold built by means of the same definition of H [183], the possibility of a DP scaling is absolutely discarded. Then, the arguments given in the first part of the section about the identification of LIM and C-DP classes would be confirmed.

However, the value of the local-slope exponent κ_W for this Manna interface is much larger than the LIM exponent (see table 4.1). It is necessary, then, to clarify the role of this exponent into the universality class before to conclude the equivalence of both universality classes.

The Local Slope of the Sandpile Interface

By comparing the landscapes of a LIM interface and the sandpile interface, the differences which lead to this discrepancy in the κ_W exponent arise. In Fig.4.2, a $d=1$ LIM interface (up) is compared with the interface of a $d=1$ FES Manna sandpile; while the shape of the former is smooth, in the latter the local fluctuations are large, which is the reason why the κ_W exponent takes that large value. However, the new interface exhibits, as LIM interfaces, superroughness $\alpha > 1$ and anomalous roughening $\kappa \neq 0$ in $d=1$.

In [171], it is argued that the large value of this exponent stems from the divergence of the noise $\tilde{\zeta}_i(H_i)$ in the limit $t \to \infty$ because, after all, is the sum, over time, of random variables. On the contrary, the LIM quenched noise remains bounded. Therefore, this fact would make essentially different LIM and C-DP, and their critical exponents would be "coincidentally close".

However, many arguments, different from the numerical coincidence of exponents, have been presented all along this chapter to justify the identification of both classes. Then, if LIM and C-DP classes coincide, the observable

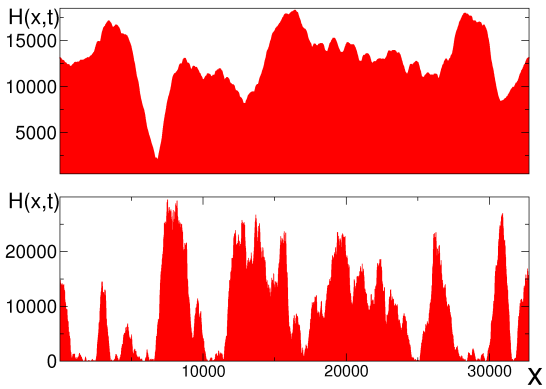

Figure 4.2: Interface landscape of two $d = 1$ LIM (up) and FES Manna (down) models, using a size $L = 32768$.

represented by the κ_W exponent should be irrelevant for the determination of the universality class. To confirm this last statement, the two different values measured for the κ_W will be searched for the same universality class.

Two κ_W Values for C-DP

To this end, the definition of the height of the interface must be changed. Pruessner, in [184], used another approach to obtain the qEW equation from a stochastic pile (the Oslo ricepile[8]). Thus, if the height is now defined as the number of grains received by the site[9], the relation between this new interface $\tilde{H}$ and the used in the previous section is:

$$\tilde{H}_i(t) = \sum_j H_j(t), \tag{4.28}$$

where j are the nearest neighbors of the site i. By using this definition of a smoother interface with the Oslo ricepile model, the LIM value for the local-slope exponent, $\kappa_W = 0.18(2)$, can be measured [185]. As the dynamics of the model remains as the ones defined in chapter 1, this model is still in

[8]Recall that, in this pile, the stochasticity is in the random choice of the threshold of each site, and not in the redistribution of toppling grains, equally scattered between the neighbors.

[9]A more intuitive definition than the usual one, because it identifies the height of a site with its number of accumulated grains.

the C-DP universality class. Thus, together with the results of table 4.3, measured for the Manna sandpile interface, it can be said that both the large value and the small value of the κ_W exponent can be measured in C-DP systems.

The origin of the two possible values of κ_W can be clarified by using simple scaling arguments. Due to the former definition of the height, Eq.(4.18), and the scaling dimension of time and activity (see Eq.(2.10)), the scaling dimension of H is $[H] \sim t^{1-\theta}$; therefore, as κ_W is the exponent of decay of the local slope (see Eq.(4.10)), and it scales as $[\nabla H] \sim [L]^{-1}[H] \sim t^{-1/z}t^{1-\theta}$, in the end:

$$\kappa_W = 1 - \theta - \frac{1}{z}. \tag{4.29}$$

For $d = 1$, and using the C-DP values $\theta \approx 0.13$ and $z \approx 1.42$ (see table C.1), $\kappa_W \approx 0.17$, which coincides with the value measured for LIM. This will be called the *smooth scaling* value of the κ_W exponent hereinafter. However, if the neighboring sites are assumed to be uncorrelated, the scaling of the slope changes to $[\nabla H] \sim \sqrt{H} \sim t^{(1-\theta)/2}$, and therefore:

$$2\kappa'_W = 1 - \theta, \tag{4.30}$$

that, by using C-DP values, is $\kappa'_W \approx 0.44$. This will be called the *heavy scaling* value of the κ_W exponent. This heavy scaling arises from the $\tilde{\zeta}_i$ noise because it is the sum of random variables and, if sites are considered uncorrelated, due to the Central Limit Theorem, its amplitude behaves like the square root of the average of $\sum_j H(j)$, where j sweeps over the nearest neighbors of the site under consideration, i; or, in other words, the amplitude of the fluctuations behaves like the square root of H.

For stochastic sandpiles in which this noise can be "smoothed" (for example with the definition of the interface in [184]), the κ_W exponent takes its smooth value. Recalling that the threshold and the random diffusion of grains are the source of the noise, a good model in which such a smooth interface can be measured is one with a deterministic choice of neighbors and toppling grains, but with stochasticity in a different part of the dynamics. In this way, systems like the Oslo ricepile or the sticky-grain (SG) model are good candidates, while in systems like the Manna model or the random relaxation version of the SG model, the heavy scaling value of the local-slope exponent is expected [185]. The fluctuations associated with each defined

interface are, then, the responsible for the different measured values of the κ_W exponent.

To confirm this, the integration of the C-DP equations (Eqs.(2.66)) with periodic boundary conditions is performed, measuring two different interfaces: one attending to the usual definition at a coarse-grained level, $H(\vec{x},t) = \int \rho(t')dt'$, and the other which advances a unit step each time the site is active, $H^\dagger(\vec{x},t) = \int \Theta(\rho(t'))dt'$. In this way, whereas the local slopes of H scale in a smooth way ($\kappa_W = 0.19(2)$), the slopes of $H^\dagger$ posses the heavy scaling ($\kappa'_W = 0.43(2)$). Therefore, in the same system, two different values for the slope exponent are measured by using two different definitions of the height.

As it is well stated that all these models belong to the C-DP class, only one conclusion is possible: the value of the κ_W exponent depends on the definition of the observable with which it is measured, and therefore it is not relevant in the determination of the universal critical behavior of the system. Also, the fact that the global roughness exponent α and the dynamic exponent z remain unchanged means that α_{loc} changes when the definition of the interface is changed (see Eq.(4.11)), and therefore **local properties are not to be considered in the classification of a system into a universality class**. Thus, the claim of [171] is completely cast out.

Two κ_W Values for LIM

If LIM manifolds belong to the same class of the stochastic sandpile interfaces, and κ_W depends only on the definition of the observable, it should be possible to measure both types of scaling values for the same LIM model, as it is done above with C-DP equation [185].

To this end, the Leschhorn cellular automaton is used. Apart from the usual definition of the interface H (Eq.(4.19)), another interface is defined in order to recover the heavy scaling value for the slope exponent. The new height, $H^\dagger$, corresponds to an interface which changes when H changes, but that is increased, randomly, just one time or $K+1$ times the own increase of H interface; in a simpler way:

$$\partial_t H^\dagger(\vec{x},t) = \partial t H(\vec{x},t) + \zeta(\vec{x},H), \tag{4.31}$$

where the noise is[10]:

$$\zeta(\vec{x}, H^\dagger) = \begin{cases} 0 & \text{with probability} \quad p \\ K & \text{with probability} \quad 1-p. \end{cases} \tag{4.32}$$

Therefore, for any time t:

$$H^\dagger(\vec{x}, t) = H(\vec{x}, t) + \tilde{\zeta}(\vec{x}, H^\dagger), \tag{4.33}$$

and $\tilde{\zeta}$ is the accumulated noise resulting from adding a discrete random quantity each time. With these definitions, the dynamic equation for this new interface is:

$$\partial_t H^\dagger(\vec{x}, t) = [\nabla^2(H^\dagger(\vec{x}, t) - \tilde{\zeta}(\vec{x}, H^\dagger)) + \eta(\vec{x}, H^\dagger)]\ [1 + \zeta(\vec{x}, H^\dagger)]. \tag{4.34}$$

In this equation, derivatives of the noise as $\nabla^2\tilde{\zeta}$ are irrelevant (in the RG sense), and also $\zeta(\vec{x}, H^\dagger)$ when added to 1. In this way, the same set of critical exponents are expected for both H and $H^\dagger$ interfaces. However, the strong fluctuations in the new noise $\tilde{\zeta}$ change the behavior of the slope.

Observe the left and right panels of Fig.4.3; in the left part, the interfaces originated with H and $H^\dagger$ interfaces are depicted. At a coarse-grained level, both interfaces are indistinguishable if the value of the vertical axis is ignored. But when a small zone of the interface is enlarged, the differences arise. The interface $H^\dagger$ is much more *locally* rough than H. This behavior is translated into the measurement of local observables (see right part of Fig.4.3) like the average value of the slope at each site (Eq.(4.10)), but not in other observables like the temporal decay of the number of active sites. Therefore, *global critical exponents coincide, while local exponents are very different.*

With this last result, it is shown that two different values for local exponents are also possible in LIM interfaces, depending only on the definition of the observable with which they are measured. This confirms the irrelevancy of this kind of measurements in order to classify a system into the universality class.

[10] As H and $H^\dagger$ are updated simultaneously, the dependence of the noise on H is as well a dependence in $H^\dagger$.

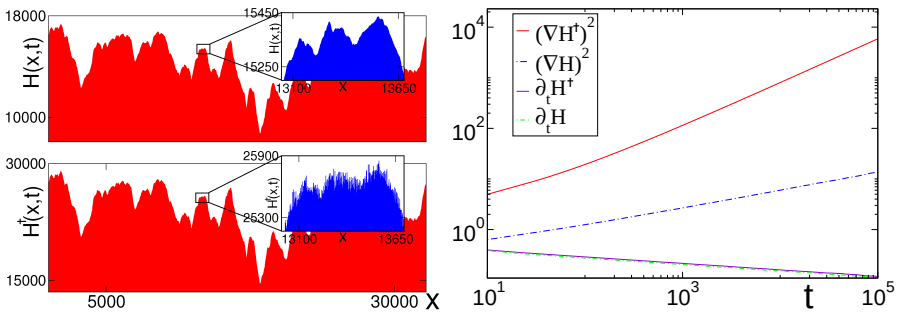

Figure 4.3: Left: Interfaces grown by using the usual H (up) and the new $H^\dagger$ (down) definitions; the latter is, locally, much more fluctuating interface than the former. Right: Time behavior of a local ($(\nabla H)^2$, $(\nabla H^\dagger)^2$) and global ($\partial_t H$, $\partial_t H^\dagger$) observables for both interfaces.

4.2.2 Self-Organized Critical LIM

In the beginning of section 4.2, it has been pointed out that the different pinned configurations of a LIM interface are absorbing states.

When one of these absorbing states is slowly perturbed with a little increase of F, the absorbing state changes (i.e. it is a **metastable** state): the force can release some sites, changing the previous configuration. This rearrangement of sites can be small, or can involve many sites, giving rise to a large **avalanche**. The approaching to the critical point from below (i.e. from the absorbing phase) is made, thus, by means of rapid reorganizations, instantaneous as compared with the time scale of the perturbation.

Due to the existence of avalanches, it is natural to wonder whether it is possible to define a SOC counterpart of conserved LIM systems. Once the equivalence between the C-DP and LIM magnitudes is done, this is a straightforward task.

Consider a one-dimensional substrate following the qEW growth equation (Eq.(4.1)) with open boundary conditions (H fixed to zero at the outer sides of the system) in which the external force can be applied independently to each site, in a way that $F \to F(\vec{x})$ [182]. Let $H(\vec{x},t)$ and $F(\vec{x})$ be initially set to zero. If the force is increased a small quantity δF at a randomly selected site, the balance of elastic, external and pinning forces, given by Eq.(4.1), determines whether the interface advances or remains stable at this site. When the increase of the force triggers its motion, the interface can drag

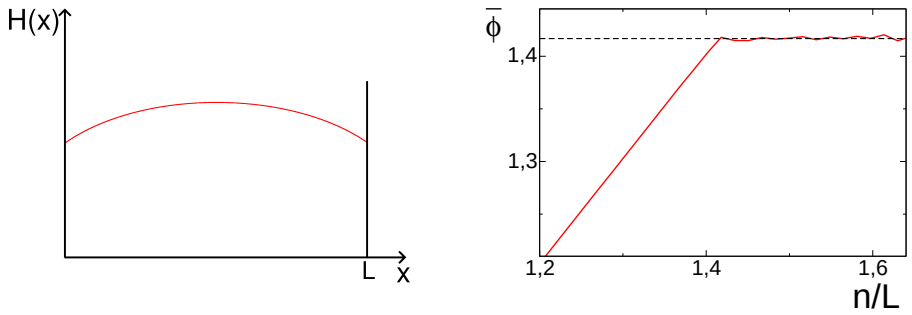

Figure 4.4: Left: The parabolic shape of a one-dimensional self-organized LIM manifold. Right: Evolution of $\overline{\phi} = \overline{\nabla^2 H} + \overline{F(\vec{x})}$ versus the number of driving events n of the qEW equation with SOC dynamics, using $D_H = 1$, $g = 3\sqrt{dt}$, and $dt = 0.1$; the driving force increases until the same critical value of the conserved system (see text), $\overline{\phi}_c = 1.41605$, is reached.

with it the advance at many more sites, and thus an avalanche can ensue[11].

How does this system reach the SOC stationary state? The external force on the system increases with steps δF; when the mean force $F = \overline{F(\vec{x})}$ is small, so it is the effective driving force (or density of background) $\overline{\phi} = \overline{\nabla^2 H} + \overline{F(\vec{x})}$, only at a few sites $v = \partial_t H(\vec{x}, t) > 0$ (see Eq.(4.1)), and the interface soon falls into an absorbing configuration. As F increases, the interface advances at more and more sites, and the avalanches span throughout the system. When the boundaries are reached, the $H = 0$ condition in there makes the average value of the Laplacian be non-zero, acquiring the manifold a parabolic shape. It is precisely the formation of this paraboloid what allows a balance between the pinning forces and the increasing $\overline{\phi}$, which reaches a stationary state (see Fig.4.4). To achieve such a state, avalanches of all sizes and all durations must exist. It is the SOC stationary state.

In fact, the value of the effective driving force when the described SOC dynamics is used for the qEW equation, Eq.(4.1), coincides with the critical value of the control parameter $\overline{\phi}_c = F_c = 1.41605$ in the integration of the closed-boundary equation explained in section 4.1 (see right panel of Fig.4.4). The measured critical exponents also coincide, in spite of the fact that the driving force F is transformed in this ensemble into a columnar noise (see above).

There exists as well a *regularized* (see chapter 2) version of this SOC LIM

[11] This slow-driving mechanism for interfaces is indirectly mentioned in [174] for the expansion of Eq.(4.1) around its mean-field theory.

system [11]. If the fixed force F of Eq.(4.1) is replaced by a force derived from a parabolic potential (i.e. each element of the interface is attached to a spring with elastic constant k), the velocity explicitely enters the equation, which is to be written now as:

$$\partial_t H(\vec{x},t) = D_H \nabla^2 H(\vec{x},t) + k\left(vt - H(\vec{x},t)\right) + \eta(\vec{x}, H(\vec{x},t)) \ . \qquad (4.35)$$

By taking closed boundaries and the limit $\delta F, k, v \to 0$, the system evolves quasistatically until achieving the critical stationary state for the total driving force. This is equivalent to the limit $h, \epsilon, \kappa \to 0$ studied in chapter 2 for C-DP to reach the time-scale separation necessary for the critical behavior.

Thus, different equivalent ensembles can be defined to measure the critical exponents of the qEW equation; for all of them, the same critical point is reached and, in it, the same universal critical behavior of LIM (which ultimately is the critical behavior of the C-DP class) arises.

There also an extremal version of these systems. Extremal growth models, as the Sneppen model [18], inspire a variant which can be called *extremal LIM*, in which the external force is again $F = F(\vec{x})$, and the boundaries are closed. The site with the smallest external force is chosen, and its height (and, consequently, the one of its neighbors) is updated according to Eq.(4.1). Eventually, a stationary state is reached where the force fluctuates around its critical value.

In summary, in this section many different arguments have been presented in order to show that LIM and C-DP are just to different languages with which phase transitions into frozen states are described. In LIM systems, there exists a *conserved background field* which acts as control parameter, coupled with the dynamics of the order parameter (either activity or velocity). Therefore, LIM systems fulfill the conditions of the conjecture made in chapter 2 for the C-DP universality class.

Moreover, it is possible *i)* to measure the same interface, spreading and avalanche exponents in both types of systems, *ii)* to map the dynamics of interfaces into the dynamics of stochastic sandpiles and vice-versa, and *iii)* to use the SOC and the FES ensembles for both cases. Once the relevant observables have been identified, it can be said that LIM and C-DP are, indeed, the very same universality class, but described in a different way.

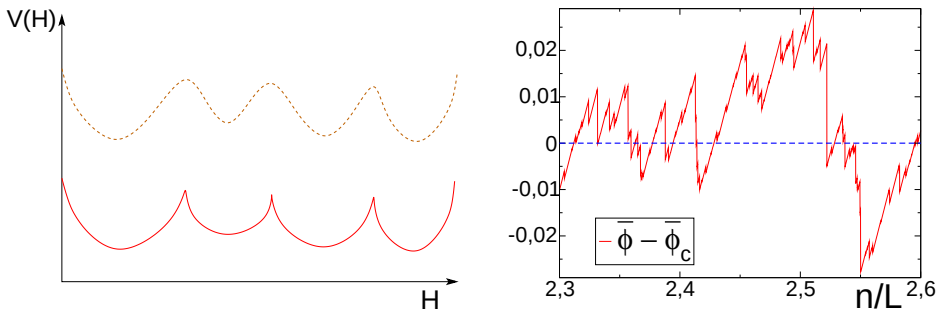

Figure 4.5: Left: Sketch of a microscopic random pinning potential (up) and its renormalized form (down); the smooth frontiers between the parabolic wells change to sharp peaks in the Renormalization process. For interfaces described by Eq.(4.1), due to the $v \geq 0$ rule, the potential is *semi-parabolic*. Right: Detail of the evolution of the driving force of the qEW equation ($\overline{\phi}$) with SOC dynamics, in the stationary regime, with a ratcheted shape due to the singular points of the potential. The critical value, $\overline{\phi}_c$, has been subtracted.

4.3 The Singular Correlation Function

In previous sections, it has been shown that the subcritical (pinned) stationary states of a linear interface in a random medium are indeed absorbing configurations, and the approaching of such manifolds to the critical point from below can be understood as a series of jumps between configurations closer and closer to criticality, by means of avalanche processes.

But, why does the evolution of the interface occur in such a way? Why does the manifold not change smoothly from one configuration to another one? The answer to these questions is deeply rooted in the physics associated with the quenched noise and, ultimately, in its correlations.

The "shocking" character of the approaching to the critical point has its origin in the shape of the coarse-grained (i.e. *renormalized*) random pinning potential. Consider a metastable subcritical configuration for the manifold. This corresponds to a local minimum of the pinning potential. An increase of the external force is translated into an increase in the energy of the interface, which eventually can be pulled to another metastable state, i.e. to overcome the barrier between minima and fall into another local minimum of the potential.

If the shape of the potential is such that the separation barrier is smooth, the transition from one configuration to another one is to be smooth. This is the case of the *microscopic* pinning potential. However, in the observed coarse-

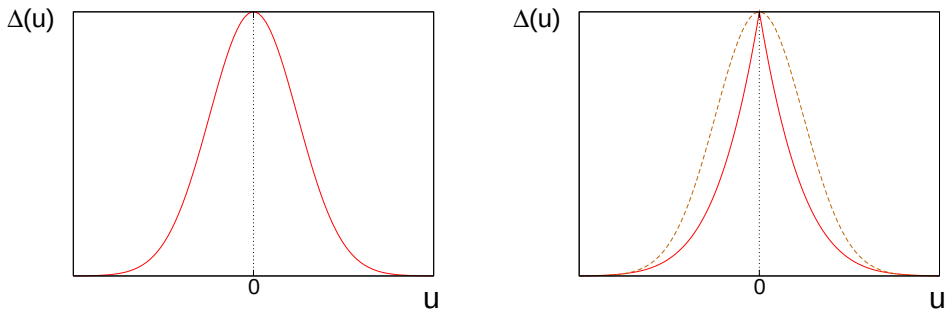

Figure 4.6: Left: Sketch of the smooth shape of the correlator $\Delta(u)$ before the Renormalization procedure. Right: Sketch of the renormalized correlator, for which $\Delta'(0^-) = -\Delta'(0^+)$.

grained potential of LIM systems, there is an abrupt change between minima. The random pinning potential exhibits singular peaks at the frontiers of minima (see left panel of Fig.4.5). Such a singular pinning potential gives rise to a discontinuous pinning force[12], and therefore the driving force necessary to balance it also shows steps. These "jumps" are translated into avalanches into the interface evolution when the barrier is overcome and, in the end, can be observed in the evolution of the total driving force. This last statement can be very easily observed if the SOC ensemble is used for Eq.(4.1) (see right part of Fig.4.5).

For the discontinuous quenched noise which represents the pinning potential, the singular shape of the latter is reflected in the pinning force-force correlations, Eq.(4.2) and, concretely in the shape of the height correlator $\Delta(u)$ [162, 164, 186]. When this microscopic correlator is renormalized in order to obtain its mesoscopic form, it flows to a renormalized fixed point function in which its initial smooth shape is transformed into a singular **cusp** or singularity at the origin, because the Renormalization procedure "moves" the inflection points to $u = 0$ (see Fig.4.6).

This cusp is not an artifact, but the evidence of the singular coarse-grained pinning potential, responsible for the observed dynamics of LIM systems; a physical property essential to well-understand the physics of disordered systems. It is the responsible not only for the existence of many different metastable states for LIM interfaces, but also for the avalanche behavior which allows to jump from one configuration to other, as well as for the existence of a non-trivial critical point.

[12] In the RB case, for instance, the force is the derivative of the random potential.

As mentioned above, the application of FRG to Eq.(4.1) has been carried out up to 1-loop order [162–164], and recently extended to 2-loops [165]. The authors of this last work, Le Doussal and Wiese (LDW), also have devised a procedure to measure the renormalized correlator in many different situations for interfaces following the qEW equation [187–189].

Measuring the Cusp

The LDW method allows to measure the observed mesoscopic fixed point function arising from the Renormalization of the microscopic (pinning) force-force (or, equivalently, noise-noise) correlator $\Delta(u)$ of the qEW equation.

Consider a $(d+1)$-dimensional interface of size L whose dynamics is described by the qEW equation, Eq.(4.1), with periodic boundary conditions. It is possible to control its evolution if it is posed into a quadratic potential whose center w and curvature m^2 can be tuned at will. With this procedure, very similar to the one followed in section 4.2.2 for the regularization of the SOC dynamics of the qEW equation, the external force F is replaced by an elastic force, and Eq.(4.1) is written now [187–189] as:

$$\partial_t H(\vec{x},t) = D_H \nabla^2 H(\vec{x},t) + m^2 \left(w - H(\vec{x},t)\right) + \eta(\vec{x}, H(\vec{x},t)) \ , \qquad (4.36)$$

where the correlations of the noise are given by:

$$\langle \eta(\vec{x},H)\eta(\vec{x}',H')\rangle = \delta^d(\vec{x}-\vec{x}')\Delta_{m=0}(H-H') \ , \qquad (4.37)$$

Initially, $w = w_0$, and the system is in a stable configuration, i.e. a local minimum of the pinning potential. As in the regularized SOC dynamics of the equation, if w is increased quasistatically the energy of the manifold increases until, at a certain value of w, the energy is large enough to overcome the barrier separating minima. Thus, the system "jumps" to another metastable pinned state by means of an avalanche process whose duration is negligible as compared with the time scale of the increase of w. In this way, after a transient, the average driving force, i.e. the mean value of $m^2\left(w - H(\vec{x},t)\right) + \nabla^2 H$ in each absorbing configuration, $m^2\left(w - \overline{H}(w)\right)$, reaches a stationary value.

In such steady state, the fluctuations of this force are, in the limit $m^2 \to 0$, related to the FRG functions [188] by means of [189]:

$$
\begin{aligned}
& m^2 \left\langle w - \overline{H}(w) \right\rangle = F_c(m) \\
& m^4 L^d \left\langle \left(w - \overline{H}(w)\right) \left(w' - \overline{H}(w')\right) \right\rangle_c = \Delta_m(w - w') \\
& m^6 L^{2d} \left\langle \left(w' - \overline{H}(w') - \left(w - \overline{H}(w)\right)\right)^3 \right\rangle_c = S_m(w' - w),
\end{aligned}
\tag{4.38}
$$

where the subscript c means *connected* averages (see Eq.(A.1.2)-Eq.(A.1.3)) over many different trials of the experiment (or different intervals of w, due to the finite-length decay of $\Delta(u)$ function). $S_m(u)$ is related with the first derivative of the correlator; to the lowest order [188]:

$$
S_m(w) = \frac{12}{m^2} \Delta'_m(w) \left(\Delta_m(0) - \Delta_m(w)\right). \tag{4.39}
$$

The usual way to represent these measurements is by means of their parameter-free forms, which get rid of any non-universal feature and permit to compare these observables for different systems. It is possible to define the functions:

$$
\begin{aligned}
& Y\left(u/u_\xi\right) = \frac{\Delta_m(u)}{\Delta_m(0)} \\
& Q\left(\Delta_m(w)/\Delta_m(0)\right) = \frac{\int_0^w S_m(w')dw'}{\int_0^\infty S_m(w')dw'},
\end{aligned}
\tag{4.40}
$$

where u_ξ is fixed in such a way that $\int_0^\infty dz Y(z) = 1$. By using the described procedure with $m^2 = 0.001$, the resulting functions are plotted in Fig.4.7.

As it can be deduced, the LDW procedure to measure the cusp of the correlation function is very similar to the way in which the regularized-SOC or the own SOC ensemble for the qEW equation (section 4.1) have been devised. In fact, the value of the average driving force at the stationary state, reached with the LDW procedure, coincides with its SOC stationary value. At this point, a question arises: are the fluctuations of the LDW driving force equivalent to the fluctuations of the SOC driving force, $\overline{\phi} = \overline{\nabla^2 H(\vec{x}, t) + F(\vec{x})}$, defined in the previous section?

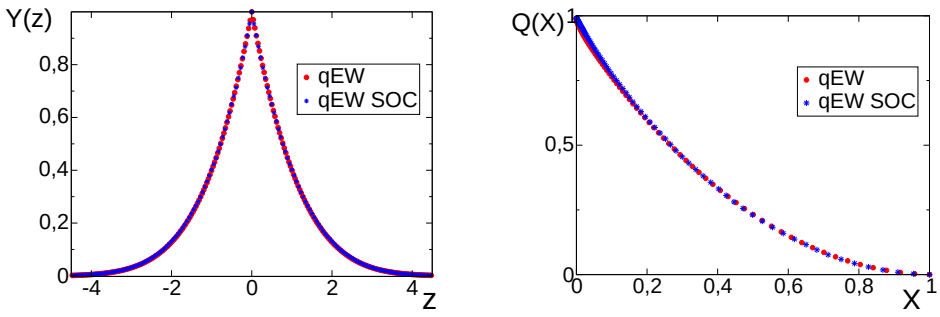

Figure 4.7: Left: $Y(z)$ function ($z = u/u_\xi$) of a $d = 1$ system of size $L = 1024$, measured with LDW and SOC procedures to integrate qEW equation. Right: $Q(X)$, with $X = \Delta(w)/\Delta(0)$, measured by means the same procedures.

To answer this question, the same universal functions must be measured in the stationary regime of the Eq.(4.1) with SOC dynamics [190]. In the SOC ensemble, the borders are open, and the driving is controlled by means of δF. The value of the minima cannot be chosen as in the LDW procedure, and a quantity m^2 cannot be defined. The quasistatically driving regime is obtained here by taking $\delta F \to 0$.

The result of such measurements is depicted in Fig.4.7. As can be observed, the curves obtained with both procedures are indistinguishable, which points out the equivalence, not only between both procedures to integrate the equation, but also between the fluctuations of the driving forces (whose quasistatical increase is a key common feature). The one devised by LDW is a new equivalent ensemble with which the same critical point and, therefore, the same universal features of qEW are reached.

Cusps in C-DP

In section 4.2, it has been argued that both the LIM class, represented by Eq.(4.1), and the C-DP class, describe the same critical point. The singular shape of the $\Delta(u)$ correlator is responsible for the existence of a non-trivial critical point, many metastable states and, in the end, the avalanche-like behavior of LIM systems, being all these features shared by the C-DP class. Therefore, to state the equivalence of the two classes, an ultimate benchmark is the measurement of the universal functions $Y(z)$ and $Q(X)$ in a C-DP system [190].

Such measurements can be done by using both LDW and SOC ensem-

bles. For both experiments, the integration of the $d = 1$ C-DP Langevin equation, Eqs.(2.66), is used. Due to the one-to-one equivalence between the background fields of both LIM ($\overline{\phi}$) and C-DP systems ($\overline{E}$) (see section 4.2), the observable to be measured is the correlations of the energy density of the system at its stationary state.

i) SOC ensemble: Consider Eqs.(2.66) with open boundary conditions and an initial state in which $\rho = 0$ and $E = 0$ for all sites. A small quantity of activity (and, therefore, of energy) $\delta\rho$ is added at a randomly chosen site, triggering an avalanche during which no more initial seeds are introduced into the system. For a certain number of driving events, the avalanches are small; it is the transient regime. When the stationary state is reached, the initial activity is able to span throughout the system, and $\overline{E}$ fluctuates around its critical value $\overline{E}_c$. The fluctuations of $\overline{E}$ are then measured to obtain the universal functions $Y(z)$ and $Q(X)$ defined above; for small values of $\delta\rho$, these functions are related with the FRG functions commented above.

ii) LDW ensemble: For this ensemble, periodic boundary conditions are used. Here, an elastic pulling force $-m^2\rho$ is added to the background equation of Eqs.(2.66). Note that when the integrated form of the equations, Eq.(2.67), is considered, this term turns into $E_0 - m^2 \int \rho dt'$, that can be written as $m^2(w-H)$ due to the correspondence above described between ρ and $v = \partial_t H$ (see Eq.(4.13)). Thus, the usual shape for the pulling force is recovered into the activity equation. Starting from the absorbing state associated with an initial w_0, w is increased in order to "jump" between different metastable states. In this way, the mean value of the energy (in which the contribution of the new pulling force is taken into account) reaches a stationary state in which it fluctuates around the same critical value of the SOC ensemble. The fluctuations of such field are measured to calculate $Y(z)$ and $Q(X)$ functions which, in the limit $m^2 \to 0$, represent the FRG functions described above.

For both experiments, the set of chosen parameters is $\mu = 0.86452$, $\lambda = \omega^2 = 1$, $\sigma^2 = 2$, $D_\rho = D_E = 0.25$, and $dt = 0.1$ [13] and, for the chosen size $L = 1024$, the stationary energy density reaches $E_c = 0.9968(5)$ in both cases. Their results are summarized in Fig.4.8.

In this figure, it is also depicted the measurement, by using the SOC ensemble, of the Y and Q functions associated with the fluctuations of the

[13] In the FES integration of this equation, if μ is used as control parameter and the energy is fixed to $E(x,t) = 1 \ \forall(x,t)$, the critical point is at $\mu_c = 0.86452(5)$; therefore, in the SOC integration with μ fixed to μ_c, a stationary value with average energy $E_c = 1$ is expected.

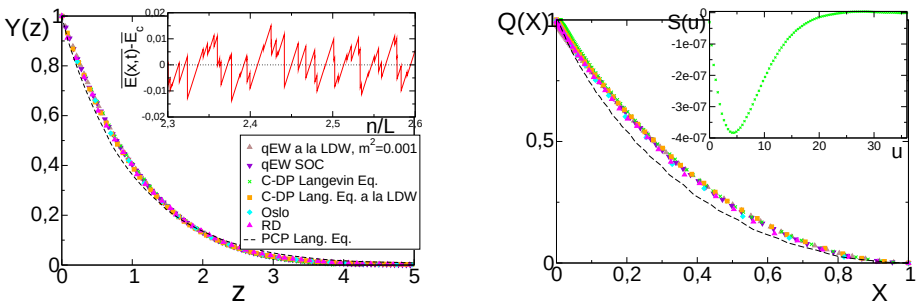

Figure 4.8: Left: $Y(z)$ function for many $d = 1$ C-DP systems of size $L = 1024$; inset: sawtooth landscape of the fluctuating background field in the stationary state for the C-DP Langevin equations (Eqs.(2.66)). Right: $Q(X)$ measured for the same systems (see the legend in the left part); inset: $S(u)$ function. Also, the same functions measured in a DP system with many absorbing states (PCP) are depicted (see text).

stationary energy density of two stochastic sandpiles studied in previous sections (the Oslo ricepile model and the C-DP reaction-diffusion (RD) model). Although each of these systems reaches a different stationary state, the spectacular collapse of these universal functions leads to the conclusion that all of them (qEW equation, C-DP Langevin equation, Oslo ricepile and RD model) share the same universal features, i.e. form part of the same universality class (LIM/C-DP class). A similar collapse is achieved for $d = 2$ simulations of the same models (not shown).

To supplement this last statement, the same simulation procedure used with Eqs.(2.66) and Eq.(4.1) is applied to the equation of a DP system with many different absorbing states (PCP), Eqs.(2.18).

Although PCP cannot be SOC in the strict sense of the term, it is possible to reach a critical stationary state if slow-driving (using either LDW or SOC ensembles) is applied *after a previous fine-tuning of the parameters of the equation to their critical values*. By doing so, the resulting curve is plotted with dashed lines in Fig.4.8.

The functions $Y(z)$ and $Q(X)$ for DP also show a cusp at the origin; for the former, the difference between DP and LIM/C-DP curves is small, but appreciable, while for the latter it is much more pronounced. In this way, the differences between both classes are stated by measuring a fundamental physical quantity, not only by a mere comparison of exponents.

The same measurements can also be performed for the $d = 2$ BTW deterministic sandpile (see section 1.4). By following the steps described for the SOC ensemble, used for the measurements in Oslo and RD models, a very different

(but also singular at the origin) $Y(z)$ and $Q(X)$ functions are obtained (not shown), which confirms that stochastic and deterministic sandpiles do not belong to the same universality class.

4.4 Concluding Remarks

Elastic manifolds in disordered media, represented by the quenched Edwards-Wilkinson (qEW) equation, are systems in which a continuous phase transition into one of the many possible absorbing states is undergone for the critical value of an external force applied to it. The existence of such states, as well as the avalanche-like approaching to the critical point, suggests the possibility of relating these manifolds to the already studied sandpile models.

The existence of a conserved background field coupled to the dynamics of the activity field, responsible for the motion of the interface, permits the identification of these linear interface models (LIM) with C-DP universality class systems. The equivalence between their observables and associated exponents, as well as the possibility of describing LIM dynamics by means of the SOC ensemble, confirms the claim.

A mapping between systems of the two classes can be performed; while the path to show that a discrete LIM system can be described at a mesoscopic level by the set of Langevin equations of C-DP is not problematic, the other way round is more subtle to justify.

The translation of the discrete rules of a stochastic sandpile results into a heavy fluctuating interface; once it is confirmed that these strong fluctuations affect only locally but no globally to the system, and that local observables are irrelevant for the determination of the critical (universal) behavior of a system, all the relevant critical exponents can be said to be identical for both LIM sandpile and sandpile interfaces. These exponents also coincide with the measured for LIM and C-DP classes. Therefore, no dangling end remains in the problem.

On the other hand, this equivalence can be shown by using more physical arguments. The avalanche-like character of the approaching to the critical point of LIM manifolds stems from the correlations of the pinning potential, whose renormalized function is related with the correlations of the average driving force. Here, two different methods to measure such correlations have been studied, and their results compared with the fluctuations of the driving force of sandpiles (the energy density). The collapse of all the measured

functions in LIM and C-DP systems allows to state that, in the end, LIM and C-DP classes share the same underlying physics, but described in a very different way.

In summary, both LIM and C-DP are different languages which describe the behavior of the same critical point. Along with the FES ensemble, studied in previous chapters, this allows to treat conserved stochastic SOC systems from many different points of view, and to be benefitted from the studies of many different sub-branches of Statistical Physics. It permits to use, for instance, the results of Functional Renormalization Group in the study of FES or stochastic SOC sandpiles (as it is done in this chapter), to complete their analytical characterization.

Chapter 5

Non-Conservation in SOC

In chapter 1, a list of essential ingredients for SOC was presented. Among them, local conservation was argued to be a *sufficient* condition for the existence of scale invariance.

The role of conservation has been a controversial topic from the very moment of the introduction of the concept of SOC. Many works supported the idea of conservation as a *necessary* and *sufficient* condition which a system must fulfill in order to exhibit SOC. However, the most "realistic" realizations of SOC are, by definition, non-conserved. This is the case of earthquakes or forest fires, for instance.

Is local conservation necessary for SOC? Or, in other words: Can a non-conservative system be SOC? If not, is such a constraint, as conservation is, realistic?, i.e. is it possible to find strictly conserved systems in real life? These are very important questions which define the range of applicability of SOC. The answer to them could eventually restrict SOC to be a theoretical concept instead of a candidate to explain much of the scale-free behavior observed in Nature.

This chapter is devoted to understanding which is exactly the role of conservation in SOC systems. First, a rate for the violation of local conservation will be introduced in one of the models studied in the previous chapters. After that, the phenomenology observed in the previous example will be put into an analytical context by means of a simple and solvable mean-field model of SOC. By using a mesoscopic equation representative of a SOC model, the role of dissipation in a conservative Langevin equation will be investigated. In this way, all the possible levels of description of the problem are embraced. Then, the two best known non-conservative models claimed to be SOC will

be studied, and variations of non-conservative models intended to balance the lack of conservation will be introduced. In the end, a way to relax the strongly restrictive constraint of conservation will be presented.

5.1 Dissipation in Sandpiles

Already in some seminal articles [10,122,191], the importance of conservation in different sandpile models was pointed out. Conservation would be not only a sufficient, but also a *necessary* condition for a system to exhibit SOC.

In chapter 1, the sufficient character of conservation was already stated. If conservation is a necessary condition for criticality, the violation of it must entail the breaking of the features observed in the critical regime of the system. Now, the consequences of the lack of conservation will be studied in a well known example of SOC model: the Oslo ricepile (see chapter 1 for details). Obviously, only the SOC ensemble will be used, as a fixed-energy ensemble (see chapter 2) makes no sense when the conservation of energy is studied.

The Oslo Ricepile with Bulk-Dissipative Dynamics

Consider a $d = 1$ empty lattice of size L with open boundaries; the slow-driving of a grain of rice into the sites of the pile makes its energy z_i (number of rice grains) increase. When the stored energy of a site overcomes a certain threshold z_i^c, the site becomes unstable and redistributes its energy among its nearest neighbors. This can activate more sites and, thus, the avalanche ensues.

The original redistribution rules (see [59] and section 1.4) in $d = 1$ are modified in this dissipative version by the rules:

$$\begin{cases} z_i \to z_i - 2 & \\ z_{j\pm1} \to z_{j\pm1} + 1 & \text{with probability} \quad 1-\epsilon \\ z_{j\pm1} \to z_{j\pm1} & \text{with probability} \quad \epsilon. \end{cases} \tag{5.1}$$

Therefore, there is a probability ϵ for each grain to "evaporate" from the surface of the pile (bulk dissipation). With these locally-dissipative rules, the ricepile evolves to a self-organized stationary state in which the usual observables defined in chapter 2 can be measured.

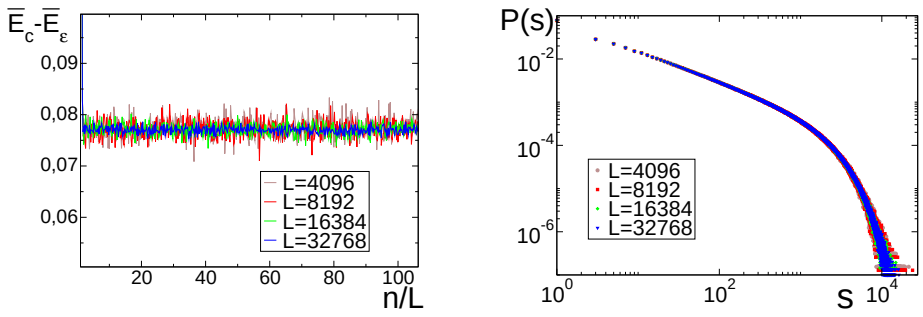

Figure 5.1: Left: Evolution of the distance of the stored energy density $\overline{E}_\epsilon$ to the critical value of the conservative system $\overline{E}_c$, versus the normalized number of driving events n/L for $\epsilon = 0.001$ and sizes from $L = 4096$ to $L = 32768$. Right: Avalanche size distribution for different system sizes. In both panels, the observed behavior does *not* depend on the finite size of the system.

Observe Fig.5.1. As it is shown in the left panel, the system reaches a stationary state. In a strictly conserved system ($\epsilon = 0$ case), this value depends on the system size (see chapter 1) and, in the thermodynamic limit ($L \to \infty$) it achieves the true critical value ($\overline{E}_c = 1.5$ in this case). However, in the dissipative case ($\epsilon \neq 0$), the stationary value of the energy *does not* depend on the size nor coincide with the value of its locally-conserved conterpart (the distance to $\overline{E}_c$ coincides for any size). Moreover, it is *smaller* than this value. Therefore, the stationary value is affected by **bulk dissipation**, which moves the system from the true critical value beyond finite-size effects.

Dissipation also affects the rest of observables of the system. In the right panel of Fig.5.1, a very illustrative example is depicted. As explained in chapter 1, for the $\epsilon = 0$ case the probability distributions characterizing the avalanches of the SOC stationary state show a *cutoff*, a characteristic length which is a consequence of the finite size of the system: as, close to the critical point, correlations diverge, a finite size represents the maximum length possible for correlations; this frustrates the scale-invariant behavior of the observables as of a certain value which depends on the system size (see Eq.(1.4)). However, when bulk dissipation is present, for large enough system sizes a cutoff which depends on such dissipation can be observed. This is the case of the size probability distribution shown on the right part of Fig.5.1, where the cutoff size s_ξ remains unaltered when the system size increases: **the finite-size scaling (FSS) is broken**[1]. A similar effect can be reported

[1]For ϵ small enough, the characteristic length (the dissipation-induced cutoff) can be larger than the system size, and the FSS still holds up to sizes comparable with this length.

for the rest of observables. This phenomenology has been previously reported in the literature for, e.g. the Abelian sandpile model (ASM) [192,193] or the case studied here (the Oslo ricepile model) [194].

This behavior for avalanches can be easily understood by means of the same heuristic arguments used in chapter 1 to justify the importance of conservation [9]. When there is local conservation, the only way in which the energy introduced into the pile can be dissipated is by means of the diffusive motion of grains, during avalanches, from their position to the border of the system. Due to this, arbitrarily large avalanches are possible, providing the scale-free shape for the avalanche size/lifetime distribution. However, when local dissipation is present, it is not necessary to reach the boundaries in order to balance the energy input; it is only necessary to develop avalanches large enough to ensure a proper dissipation of the initial input. Thus, the maximum size for the avalanches (i.e. the cutoff of the avalanche probability distributions) does depend solely on the degree of bulk dissipation, ϵ.

In light of these results, it can be concluded that when local conservation is violated, the system self-organizes to a state whose distance to the critical point depends on the degree of dissipation. Therefore, to recover criticality, the limit $\epsilon = 0$ is necessary. This was already pointed out in chapter 2, where a regularization of a sandpile model in which a rate of dissipation ϵ was introduced needed of a fine-tuning of this parameter to $\epsilon \to 0$ in order to recover the SOC behavior.

It can be argued that this conclusion makes SOC very restrictive and, in any case, the consequence of a "tuning" in which conservation is provided. But as we already justified in chapter 1, the mechanisms to achieve the SOC state can be found ubiquitously in Nature; as states the Noether Theorem, any conservation law is just the consequence of the existence of a symmetry in the system [195], and real systems are plagued of them. For instance, energy conservation implies a *temporal translational invariance*; when the conservation is broken with bulk dissipation, the symmetry also ceases, i.e. a characteristic (finite) time scale appears (for example, the finite cutoff for the lifetime distribution).

In the next section, these concepts will be put in a more rigorous context by means of a simple mean-field model analytically tractable.

5.2 The Self-Organized Branching Process

In chapter 1, it was mentioned that the avalanches in sandpiles with $d \geq d_c$ (i.e. the mean-field regime) can be seen as a **branching process**, but no further details were given. In this section, a self-organized model which follows the dynamics of a branching process is presented, and the effect of bulk dissipation on its dynamics, studied.

A branching process is a Markovian process in which an individual, called *ancestor*, creates a fixed number k of *descendants* with probability $p(k)$. The average number of descendants created per ancestor is the so-called **branching ratio**, $\sigma = \sum_k kp(k)$: for $\sigma > 1$, the process continues indefinitely; if $\sigma < 1$, it stops after a short number of new generations of descendants. When the branching ratio is exactly $\sigma = 1$, the process becomes critical [52], in the sense that it presents scale-free behavior.

Here, a branching process in which only two descendants can be created will be considered. With probability p, one site creates two new individuals or, with probability $1-p$, the banching process does not generate new sites from this ancestor. Therefore, $\sigma = 2p$, and there exists a critical value, $p_c = 1/2$, for which the branching process propagates in a marginal way.

From the Manna Model to a Self-Organized Branching Process

To study the equivalence between a high dimensional stochastic sandpile and a branching process, the system introduced in [196] by Zapperi et al. will be studied.

Consider a Manna sandpile model (see [54] and section 1.4). In any d, the threshold is fixed to $z_c = 2$, and an active site redistributes all its stored grains (a number which changes each time). Here, the frequently used version in which the number of toppling grains is fixed to 2 for any d is considered (see previous chapters). Once the number of distributed grains is fixed, the order in which the active sites relax becomes irrelevant and, the redistribution rules, Abelian. In this way, when the threshold is overcome ($z_i \geq z_c$), the site relaxes ($z_i \to z_i - 2$) and the height of two neighbors is increased by 1 unit, regardless of the dimensionality of the underlying lattice.

For $d \to \infty$ and these relaxation rules, due to the high number of neighbors of a site the activity never visits twice the same position, and correlations between sites can be neglected. Therefore, an avalanche with the Abelian rules above summarized can be translated into as a branching process [196]:

if a grain of a toppling event is dropped into a site with $z_i = 1$, the grain generates a new active site; in the case in which $z_i = 0$, no new active site is created and the avalanche does not propagate by means of this grain. Then, the propagation of an avalanche in a $d \to \infty$ Manna model is a branching process in which the branching probability is given by $p = P(z = 1)$ (i.e. the probability to find a site with $z = 1$)[2].

Now, to complete the mapping, open boundaries are necessary in order to balance the energy input of the driving process. A **generation** is defined as the set of sites created at the same time. By considering all the possible sites (either created or not) of the branching process, after m generations there are $L = 2^{m+1} - 1$ individuals (see left part of Fig.5.2). By fixing a maximum number of generations m (i.e. a maximum size for the avalanche), the effect of the borders of a spatially extended model is imitated. For the active sites of the m-th generation, each toppled grain is lost. In this way, the size of the system is given now by L (see above).

This allows to complete the translation between the high dimensional Manna model and the branching process: when no active sites are present in the system, a new grain is randomly added until a drop on a $z_i = 1$ site occurs (initial seed of the branching); avalanches proceed following the Manna relaxation rules defined above (which coincide with the branching process); energy can be dissipated at the boundaries, defined now as the sites of the last possible generation m (last branching sites).

By means of this dynamics, which defines the so-called **self-organized branching process** (SOBP) [196], a stationary value for the energy and, therefore, for the branching probability $p = P(z = 1)$, is achieved. The dynamic rules for this model can be summarized as follows:

- Driving: A random site i is selected.
- Avalanche: With probability p, the site creates two new active individuals, for which the condition of branching will be also checked. This process is iterated until no more branchings succeed. Each site at which the relaxation condition is checked is considered part of the avalanche.
- Dissipation: When the m-th generation branches, the new individuals are coinsidered to be out of the system.

[2]This equivalence was already pointed out in many articles (see [46], for instance), but in none of them a self-organized process was defined before the work under discussion [196].

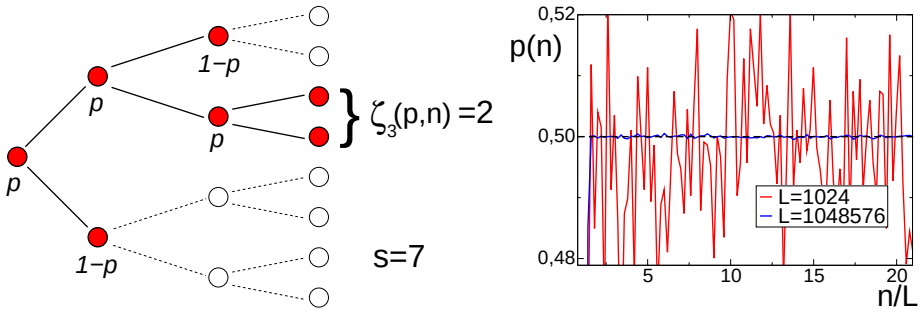

Figure 5.2: Left: Sketch of the propagation of an avalanche in a SOBP system of size $L = 2^{3+1} - 1 = 15$; this avalanche has size $s = 7$ (red spots), and has reached the border. The last possible generation ($m = 3$) has created two sites out of the system, i.e. $\zeta_3(p, n) = 2$. Adapted from [196]. Right: Evolution of the branching probability $p(n)$ versus the normalized number of driving events n/L for two different sizes; the fixed point is $p^* = 1/2$ in both cases, but the larger the system, the smaller the fluctuations.

- Updating of p: as the branching probability p is related with the total energy into the system (see above), it increases due to the external driving and decreases due to the number of branchings not performed because of the finite size of the lattice.

Next, the specific updating rule for the branching probability will be deduced.

Criticality in the SOBP

With these rules, a self-organized process is defined, but it is necessary to know whether it is critical, i.e. if the stationary value to which p tends coincides with the critical p_c (see above). Following the steps of Zapperi et al. [196], it is possible to determine it by using a simple balance equation for the energy.

If $\zeta_m(p, n)$ is the number of grains dissipated at the last possible generation m of the avalanche started after the n-th driving event (see left part of Fig.5.2), and $Z(n)$ is the total number of grains into the system at this *driving time*, the balance of energy which allows to reach a stationary state results in:

$$Z(n+1) = Z(n) + 1 - \zeta_m(p, n). \tag{5.2}$$

In any stable configuration of the stationary state, the total number of grains

is given by the sum of the energy of the sites with $z = 1$. At empty sites, $P(z = 1) = 0$. Therefore, $P(z = 1) = p$ (see above) can be used to calculate the total number of grains:

$$Z(n) = LP(z = 1) = Lp, \tag{5.3}$$

and the balance equation of the Manna model is translated into an equation for the probability of the equivalent branching process:

$$p(n + 1) = p(n) + \frac{1 - \zeta_m(p, n)}{L}. \tag{5.4}$$

As the average number of dissipated grains is given by $\langle \zeta_m(p, n) \rangle = (2p)^m$ [52], for each avalanche it can be written $\zeta_m(p, n) = (2p)^m + \eta(p, n)$, where $\eta(p, n)$ is a Gaussian white noise. Plugging this result into Eq.(5.4), and taking the continuum limit for n:

$$\frac{dp}{dn} = \frac{1 - (2p)^m}{L} + \frac{\eta(p, n)}{L}, \tag{5.5}$$

for which the fixed point of the deterministic part is trivially given by $p^* = 1/2 = p_c$. Therefore, in the thermodynamic limit (in which the effect of fluctuations can be neglected [196]), the dynamics of the system attracts p to its critical value (see right part of Fig.5.2). *This simple SOBP is a SOC system.*

Also, in [196] some analytical results for the SOBP model are deduced. Hereinafter, only large (but finite) system sizes will be considered (i.e. $m \gg 1$). In this limit, the fluctuations of p around the critical value in the stationary state can be neglected and, therefore, the distribution of p, $\varphi(p)$, can be approximated by a delta function $\varphi(p) = \delta(p - p_c)$ (see right part of Fig.5.2). This distribution is useful to calculate the avalanche size distribution $P(s)$:

$$P(s) = \int_0^1 \varphi(p) P_m(s, p) dp, \tag{5.6}$$

and the distribution $P(t)$ of avalanche lifetime t (or number of generations m):

$$P(t) = \int_0^1 \varphi(p) \left(\tilde{P}_{m+1}(\zeta = 0, p) - \tilde{P}_m(\zeta = 0, p) \right) dp. \tag{5.7}$$

The function $P_m(s,p)$ ($\tilde{P}_m(\zeta,p)$) is the generic probability distribution for avalanches of size s (ζ grains dissipated) after m generations, given by a fixed probability p. Using the integer character of s and ζ, the corresponding generating functions can be defined as:

$$f_m(x,p) = \sum_s x^s P_m(s,p) \tag{5.8}$$

and:

$$g_m(x,p) = \sum_\zeta x^\zeta \tilde{P}_m(\zeta,p). \tag{5.9}$$

By taking into account the peculiarities of the branching process (due to its hierarchical nature, s can only take odd values and ζ only even values; the maximum number of topplings is $s_{max} = 2^{m+1} - 1$, and for dissipated grains, $\zeta_{max} = 2m \ldots$), it is possible to deduce the recursive formulas:

$$f_{m+1}(x,p) = x\left[(1-p) + p f_m^2(x,p)\right] \tag{5.10}$$

with $f_0(x,p) = x$, and:

$$g_{m+1}(x,p) = (1-p) + p g_m^2(x,p), \tag{5.11}$$

where $g_0(x,p) = x$. We focus now our attention on $f_m(x,p)$. As $m \gg 1$, $m+1 \sim m$, and Eq.(5.10) can be trivially solved; two solutions are found:

$$f(x,p) = \frac{1 \pm \sqrt{1 - 4x^2p(1-p)}}{2xp}. \tag{5.12}$$

Rejecting the solution with the + sign, performing a series expansion of $f(x,p)$ in powers of x, and comparing with Eq.(5.8), for $1 \ll s \lesssim m$ [196]:

$$P_m(s,p) = \sqrt{\frac{2(1-p)}{\pi p}} s^{-3/2} \exp\left(\frac{s \ln(4p(1-p)}{2}\right), \tag{5.13}$$

which can be rewritten as:

$$P_m(s,p) \sim s^{-3/2} e^{-s/s_\xi(p)}. \tag{5.14}$$

The cutoff function, $s_\xi(p) = -2/\ln[4p(1-p)]$, diverges for the critical value of $p = 1/2$. For small s the probability distribution can be easily obtained from Fig.5.2; for instance, if $s = 1$, then the first branching attempt failed and, therefore, $P_m(1,p) = 1-p$; if the size is $s = 3$, the first attempt created the two descendants, but the avalanche stopped after that (i.e. $P_m(3,p) = p(1-p)^2$), and so forth.

For $m \lesssim s \lesssim L$, the probability distribution takes also a similar form; by assuming that $P_m(s,p) \sim s^{-\tau}\mathcal{F}(s\Delta^\varsigma)$ (where $\mathcal{F}$ decays faster than a power law and $\Delta = p - p_c$), and taking the continuous definition of the generating function:

$$\begin{aligned} f_m(x,p) = & \int_0^\infty x^s P_m(s,p)ds = 1 + \int_0^\infty (x^s - 1)P_m(s,p)ds \\ \sim & \; 1 + \int_0^\infty (x^s - 1)s^{-\tau}\mathcal{F}(s\Delta^\varsigma)ds; \end{aligned} \tag{5.15}$$

by changing $x \to e^{-y\Delta^\varsigma}$, using that $e^{-z} \sim 1 - z + \ldots$, and integrating by parts $\tau - 1$ times, the final result can be expressed as:

$$f_m(x,p) \sim 1 - (y\Delta^\varsigma)^{\tau-1}\,\mathcal{G}\,(y)\,, \tag{5.16}$$

where $\mathcal{G}$ has an integral shape depending on y. If this last expression is introduced into Eq.(5.10) with the same changes of variables and expansions used in the integral above, after some algebra it is easy to obtain the expression:

$$\begin{aligned} (2p-1)\,(y\Delta^\varsigma)^{\tau-1}\,\mathcal{G}\,(y\Delta^\varsigma) &= p\,(y\Delta^\varsigma)^{2(\tau-1)}\,\mathcal{G}^2\,(y\Delta^\varsigma) - y\Delta^\varsigma; \\ 2\Delta\,(y\Delta^\varsigma)^{\tau-1}\,\mathcal{G}\,(y\Delta^\varsigma) &= \left(\Delta + \frac{1}{2}\right)(y\Delta^\varsigma)^{2(\tau-1)}\,\mathcal{G}^2\,(y\Delta^\varsigma) - y\Delta^\varsigma. \end{aligned} \tag{5.17}$$

Thus, close to the critical point ($\Delta \to 0$), all the leading-order terms in Δ must have the same exponent, in order to keep the validity of the equation; in this way, by comparing terms, it can be deduced that $\tau = 3/2$ and, therefore, in the regime $m \lesssim s \lesssim L$, it can be written that:

$$P_m(s,p) \sim s^{-3/2}\mathcal{F}\,(s\Delta^\varsigma)\,. \tag{5.18}$$

In [196], another path to reach the same τ exponent, as well as a justification for an exponential shape for $\mathcal{F}$, can be found. We assume this form hereinafter. In this way, for any value of s, next to the critical point:

$$P_m(s,p) \sim s^{-3/2} e^{-s/\tilde{s}_\xi(p)}, \tag{5.19}$$

where $\tilde{s}_\xi(p)$ is a cutoff function of p that diverges close to the critical point. With this expression, the probability distribution can be obtained by using Eq.(5.6) and the delta-shape for the distribution of p in the stationary state (see above):

$$P(s) \sim s^{-3/2} e^{-s/\tilde{s}_\xi(p)}, \tag{5.20}$$

and by following similar steps for the lifetime distribution:

$$P(t) \sim t^{-2} e^{-t/\tilde{t}_\xi(p)}. \tag{5.21}$$

The exponential function establishes a cutoff for each distribution diverging at the critical point $p = p_c$, which coincides with the attractive fixed point of the dynamics. Thus, the SOBP model behaves as a mean-field sandpile when its SOC stationary state is reached (see table C.1). The numerical simulations performed in [196] and also own measurements confirm these values.

The SOBP model with Dissipation

Up to now, no local dissipation has been taken into account in this analytically solvable model. In [197], the same authors of the SOBP use the same model to study rigorously the effect of the lack of conservation in the relaxation rules.

Consider the same relaxation rules of the SOBP (mean-field Manna) model described above at a finite system of size $L = 2^{m+1} - 1$. But now, when a site relaxes, there exists a probability ϵ for the two toppled grains to be dissipated. Therefore, the branching probability must be corrected because, for a site to create two descendants, two situations must occur simultaneously: *i)* the grains of the site are not dissipated and *ii)* its toppled grains are dropped into a site with $z = 1$. Then, a branching event takes place with probability:

$$q = p(1 - \epsilon). \tag{5.22}$$

The branching ratio is calculated from the branching probability and, also in this case, $\sigma = 1$ implies $q = q_c = 1/2$. Thus, the critical probability p to which the SOBP model with bulk dissipation (SOBP-D) must evolve in order to reach a critical state changes to:

$$p_c = \frac{1}{2(1 - \epsilon)}, \tag{5.23}$$

that is, the larger the dissipation, the larger the value of p necessary to reach criticality. Thus, only if the evolution equation for p converges to this new $p_c \geq q_c$, the system will remain critical for any degree of ϵ. Now, following the steps of [197], the evolution equation for the probability will be deduced.

Recall the arguments which led to Eq.(5.2): the total energy at the driving event $n + 1$ is the sum of the total energy at the n-th driving event ($Z(n)$), the new grain added, and the negative contribution of the grains lost at the boundaries ($\zeta_{B_m}(q, n)$), which depends on the branching probability q. But in this SOBP-D model, the evaporation of grains must be also taken into account, with a contribution $\zeta_{\epsilon_m}(q, n)$. Therefore, Eq.(5.2) becomes:

$$Z(n + 1) = Z(n) + 1 - \zeta_{B_m}(q, n) - \zeta_{\epsilon_m}(q, n). \tag{5.24}$$

As in the SOBP, the total energy can be calculated by taking into account only the probability to find $z = 1$ at a site ($Z(n) = LP(z = 1) = Lp$), and therefore:

$$p(n + 1) = p(n) + \frac{1 - \zeta_{B_m}(q, n) - \zeta_{\epsilon_m}(q, n)}{L}. \tag{5.25}$$

Concerning the dissipated-energy terms, they can be written as a mean value with size-dependent fluctuations. The mean number of boundary-dissipated grains is given by the branching probability, as in the SOBP model [52]:

$$\langle \zeta_{B_m}(q, n) \rangle = (2q)^m = (2p(1 - \epsilon))^m . \tag{5.26}$$

The mean number of bulk-dissipated grains is the product of the number of grains dissipated per toppling (2, limited by the relaxation rules), the average

number of sites where there is no branching ($\langle\varphi\rangle$), and the fraction of sites for which this lack of branching is solely due to evaporation; thus:

$$\langle\zeta_{\epsilon_m}(q,n)\rangle = 2\langle\varphi\rangle\frac{p\epsilon}{(1-p)+p\epsilon}. \tag{5.27}$$

If π_k is the number of active sites at generation k, the number of sites which do not branch at this generation is given by the difference between π_k and a half of the number of descendants at the next generation ($\pi_{k+1}/2$). Then, the number of no-branching sites considering the overall avalanche (φ) is the sum of the contribution of each generation up to the last one, m [197]:

$$\varphi = \sum_{k=0}^{m-1}\left(\pi_k - \frac{1}{2}\pi_{k+1}\right); \tag{5.28}$$

by noting that the size of the avalanche is given by the total number of sites at which the condition for relaxation is checked (active sites), $s = \sum_k \pi_k$, and:

$$\begin{cases} \displaystyle\sum_{k=0}^{m-1}\pi_k = \sum_{k=0}^{m}\pi_k - \pi_m = s - \pi_m \\ \displaystyle\sum_{k=0}^{m-1}\pi_{k+1} = \sum_{l=1}^{m}\pi_l = s - 1; \end{cases} \tag{5.29}$$

then:

$$\varphi = \frac{1 + s - 2\pi_m}{2}. \tag{5.30}$$

Now, the average of this quantity must be considered. Noting that the average number of active sites at an arbitrary generation k coincides with the number of toppled grains at that generation, whose mean value is written above:

$$\langle\pi_k\rangle = \langle\zeta_k\rangle = \left(2p(1-\epsilon)\right)^k; \tag{5.31}$$

therefore, using the definition of s:

$$\langle s\rangle = \sum_{k=0}^{m}\langle \pi_k\rangle = \sum_{k=0}^{m}\left(2p(1-\epsilon)\right)^k = \frac{1-\left(2p(1-\epsilon)\right)^{m+1}}{1-2p(1-\epsilon)}, \tag{5.32}$$

and plugging Eq.(5.31)-Eq.(5.32) into Eq.(5.30):

$$\langle \varphi\rangle = \frac{1}{2}\left[1+\frac{1-\left(2p(1-\epsilon)\right)^{m+1}}{1-2p(1-\epsilon)} - 2\left(2p(1-\epsilon)\right)^m\right]. \tag{5.33}$$

Using Eq.(5.27) and Eq.(5.33), the mean value of the contribution of the evaporated grains to Eq.(5.25) is given by:

$$\langle \zeta_{\epsilon_m}(q,n)\rangle = \left[1+\frac{1-\left(2p(1-\epsilon)\right)^{m+1}}{1-2p(1-\epsilon)} - 2\left(2p(1-\epsilon)\right)^m\right]\frac{p\epsilon}{(1-p)+p\epsilon}. \tag{5.34}$$

As said above, for these mean values (Eq.(5.26) and Eq.(5.34)), a noise which depends on the system size L must be added; the fluctuations of both dissipative processes are grouped into the noise $\eta(p,n)/L$.

In the end, using Eq.(5.26), Eq.(5.34), the above described noise, and taking the continuum limit for the variable n, the final form for the evolution of the probability p, Eq.(5.25), can be written as:

$$\begin{aligned}\frac{dp}{dn} = &\ \frac{1}{L} - \frac{2\left(2p(1-\epsilon)\right)^m}{L} \\ &- \frac{p\epsilon}{L\left[(1-p)+p\epsilon\right]}\left[1+\frac{1-\left(2p(1-\epsilon)\right)^{m+1}}{1-2p(1-\epsilon)} - 2\left(2p(1-\epsilon)\right)^m\right] \\ &+ \frac{\eta(p,n)}{L},\end{aligned} \tag{5.35}$$

where each contribution has been written separately for the sake of clarity.

By following the steps of [197], the evolution equation for p has been obtained. Now, it is time to check whether the system is critical or not. Recall that, in the presence of local dissipation, the critical value for the

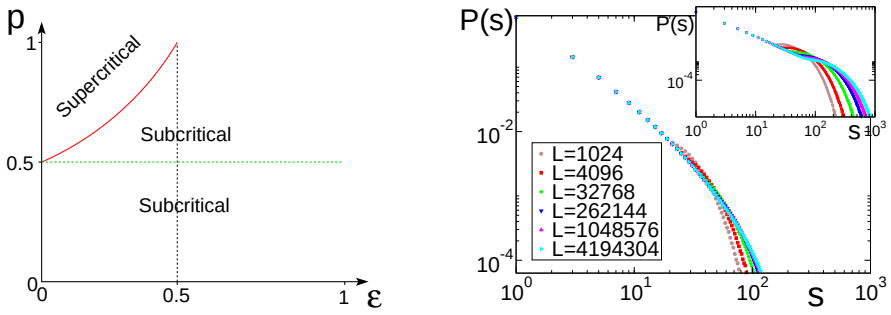

Figure 5.3: Left: Phase diagram for the SOBP-D and its conservative counterpart; the dissipation changes the critical line (red), which does not coincide with the one of the stationary state (green) anymore. Adapted from [197]. Right: Different behavior of the avalanche size distribution for the conservative (inset) and the non-conservative (main plot) case with $\epsilon = 0.2$; when bulk dissipation is present, the exponential cutoff does not depend on the system size for large enough sizes.

branching probability $q_c = 1/2$ makes the critical value for p increase up to a new $p_c > 1/2$ (see Eq.(5.23)). If the fixed point of Eq.(5.35), p^*, coincides with the new critical point, the bulk dissipation does not play a relevant role in the system, and conservation is not a necessary condition. However, the unique attractive fixed point for Eq.(5.35) is given by:

$$\frac{dp}{dn} = 0 \Longleftrightarrow p^* = 1/2, \tag{5.36}$$

regardless the value of ϵ. Therefore, the dynamics of the system drives p towards a stationary value smaller than the critical one. Thus, the branching ratio reaches a value $\sigma < 1$ in the stationary state, and the branching process can be propagated only a finite number of steps, i.e. the system reaches a **subcritical stationary state** [197]. The phase diagram for this SOBP-D model, and its comparison with the case $\epsilon = 0$, can be found in the left part of Fig.5.3.

To better understand the reason why the system is subcritical, the same analytical calculations performed for the SOBP model can be done here by using the new branching probability q instead of p. In this way, the final expression for the probability distributions is given by:

$$P(s) \sim s^{-3/2} e^{-s/s_\xi(q)}, \tag{5.37}$$

for the avalanche size distribution, and:

$$P(t) \sim t^{-2} e^{-t/t_\xi(q)}, \tag{5.38}$$

for the lifetime distribution. The main difference now is that the cutoff functions do not diverge for the fixed point value $q^* = p^*(1-\epsilon)$, but depend on the degree of bulk dissipation ϵ; for example, for the size distribution cutoff (see the previous section):

$$s_\xi(q^*) = \frac{-2}{\ln[4q^*(1-q^*)]} = \frac{-2}{\ln[1-\epsilon^2]} \sim \frac{2}{\epsilon^2}. \tag{5.39}$$

For the cutoff of the lifetime distribution, a similar power-law dependence on ϵ can be obtained. Therefore, an exponential cutoff effect is always present in the stationary state for any value of $\epsilon \neq 0$, and the system is subcritical. Only for the conservative limit $\epsilon \to 0$, the cutoff present on the observables diverges, and the critical features (for instance, the finite size scaling) are recovered.

This last situation is illustrated in the right part of Fig.5.3, where different system sizes are used for the strictly conserved case ($\epsilon = 0$), i.e. the original SOBP model, and for $\epsilon = 0.2$. As can be observed, in the original SOBP model (inset) the cutoff experimented by the distribution moves to larger values as the system size L is increased, disappearing in the thermodynamic limit. This corresponds to the usual finite-size effect already commented in chapter 1.

In the case of the SOBP-D model (main plot), the effect of the bulk dissipation establishes another cutoff which only depends on ϵ. For the smallest sizes, the finite-size cutoff is still smaller than the dissipation cutoff and, therefore, it is still appreciable a finite-size effect. However, for the largest sizes, the finite-size cutoff becomes larger than the dissipation cutoff, and the scale-free behavior is interrumpted at the same point for all these sizes. Therefore, in the dissipative case, correlations cannot diverge (i.e. remain finite), and the system is subcritical for any $\epsilon \neq 0$.

To summarize, by using an easy-to-understand and analytically tractable microscopic model (the SOBP model), the effects of local dissipation have been studied. When any non-vanishing degree of dissipation is present, the range of the correlations depends on it, and divergent critical correlation lengths cannot develop for a non-vanishing value of this parameter. All the observables show, for large enough systems, a cutoff which does not depend on the system size (that is, scale invariance is not recovered in the ther-

modynamic limit); any degree of bulk dissipation makes the system become **subcritical**. Thus, ϵ quantifies the distance of the system to the critical point (i.e. its acts as a *control parameter*) and the original SOC system is not self-organized anymore. Only when $\epsilon = 0$, criticality is recovered. In conclusion, **conservation is a necessary condition for SOC**.

5.3 Dissipation in a SOC Mesoscopic Theory

In the previous section, it has been shown, at a microscopic level of description, that any sandpile with broken local conservation is transformed into a standard non-equilibrium system with a control parameter (the degree of bulk dissipation), and only when it is set exactly to zero, criticality is recovered. At this level, it has been already rigorously proven for deterministic sandpiles [198, 199].

After the original article of Bak, Tang and Wiesenfeld (BTW) [6], many works were devoted to find a continuous equation for sandpiles. In this early stage of the history of SOC, its equivalence with absorbing states (see chapter 2) was not unveiled yet, and most of the equations (built from just symmetry principles) were devised to describe the evolution of the height of each site of the BTW pile. In such equations, a deterministic part takes into account the relaxation rules of the sandpile, and an extra noise term, the possible stochastic sources into the dynamics, as for instance the random choice of the original seed. Due to the diffusive character of the dynamics, the deterministic part of these equations use to contain only derivatives of the height, which entails a conservative dynamics. Depending on the noise term, the equation of motion could be strictly conservative or conservative with a non-conserved noise.

In [121], the conditions for a Langevin equation to describe a generic scale-invariant system were already pointed out. Broadly, when the equation describing the dynamics entails a conservative deterministic part and a conservative noise, scale invariance can be only achieved if there exists any degree of anisotropy in the dynamic rules. But when there appears in it a conservative deterministic part and a non-conserved noise with zero mean (which is the case of sandpiles), the Langevin equation describes SOC behavior.

In this section, the effect of bulk dissipation on this last generic mesoscopic example of SOC will be studied. The simplest mesoscopic equation for this generic-scale-invariant system is:

$$\partial_t \psi(\vec{x}, t) = D_\psi \nabla^2 \psi(\vec{x}, t) + \eta(\vec{x}, t). \tag{5.40}$$

The noise is defined by:

$$\begin{aligned} &\langle \eta(\vec{x}, t) \rangle = 0, \\ &\langle \eta(\vec{x}, t) \eta(\vec{x}', t') \rangle = \sigma^2 \delta^d(\vec{x} - \vec{x}') \delta(t - t'). \end{aligned} \tag{5.41}$$

The spatial and time dependence of the mesoscopic field ψ will be omitted when not necessary. More conservative terms can be added, but in comparison with the already present Laplacian, they are irrelevant from the point of view of Renormalization Group (RG) theory.

When bulk dissipation is introduced into the system described by Eq.(5.40), the equation must be modified by introducing a dissipation term like, for instance, the lowest order $-\epsilon\psi$:

$$\partial_t \psi = D_\psi \nabla^2 \psi - \epsilon \psi + \eta(\vec{x}, t). \tag{5.42}$$

If the Fourier transformation is defined by:

$$\mathcal{F}[\psi(\vec{x}, t)] = \int_{-\infty}^{\infty} \psi(\vec{x}, t) e^{-i\vec{k}\vec{x}} d^d k = \tilde{\psi}(\vec{k}, t), \tag{5.43}$$

by applying this transformation to both sides of Eq.(5.42) for both time and space variables:

$$(-i\omega)\tilde{\psi}(\vec{k}, \omega) = D_\psi (-ik)^2 \tilde{\psi}(\vec{k}, \omega) - \epsilon \tilde{\psi}(\vec{k}, \omega) + \tilde{\eta}(\vec{k}, \omega), \tag{5.44}$$

where the noise is now defined by:

$$\begin{aligned} &\langle \eta(\vec{k}, \omega) \rangle = 0, \\ &\langle \eta(\vec{k}, \omega) \eta(\vec{k}', \omega') \rangle = \sigma^2 \delta^d(\vec{k} - \vec{k}') \delta(\omega - \omega'). \end{aligned} \tag{5.45}$$

Therefore, leaving alone the $\tilde{\psi}$ field:

$$\tilde{\psi}(\vec{k},\omega) = \frac{\tilde{\eta}(\vec{k},\omega)}{D_\psi k^2 + \epsilon - i\omega}. \tag{5.46}$$

In the Fourier space, and using Eq.(5.45) and Eq.(5.46), the two-point correlation function is:

$$\tilde{C}(\vec{k},\omega) = \langle \tilde{\psi}(\vec{k},\omega)\tilde{\psi}(\vec{k}',\omega')\rangle = \frac{\sigma^2\delta^d(\vec{k}-\vec{k}')\delta(\omega-\omega')}{(D_\psi k^2 + \epsilon - i\omega)\,(D_\psi k'^{\,2} + \epsilon - i\omega')}. \tag{5.47}$$

Performing the inverse Fourier Transform in time:

$$C(\vec{k},t) = \frac{1}{2\pi}\int_{-\infty}^{\infty} \frac{\sigma^2 e^{i\omega t}}{(D_\psi k^2 + \epsilon - i\omega)\,(D_\psi k^2 + \epsilon + i\omega)} d\omega. \tag{5.48}$$

This integral possesses two poles of order one at the points $\omega_1 = i(\epsilon + D_\psi k^2)$ and $\omega_2 = -\omega_1$. By using the method of the residues, and taking the appropriate path of integration[3] [200], the correlation function can be written as:

$$C(\vec{k},t) = \frac{\sigma^2 e^{-(\epsilon + D_\psi k^2)t}}{2\,(D_\psi k^2 + \epsilon)}. \tag{5.49}$$

Performing, now, the inverse Fourier Transform in space:

$$\begin{aligned} C(\vec{x},t) = & \frac{1}{(2\pi)^d}\int_{-\infty}^{\infty} C(\vec{k},t) e^{i\vec{k}\vec{x}} d^d k \\ = & \frac{\sigma^2}{2(2\pi)^d}\int_{-\infty}^{\infty} \frac{e^{i\vec{k}\vec{x}} e^{-(\epsilon + D_\psi k^2)t}}{D_\psi k^2 + \epsilon} d^d k. \end{aligned} \tag{5.50}$$

Now, $\vec{k}$ is written in its generalized spherical coordinates (i.e. by considering $d-1$ angles and the modulus k). If the coordinates of $\vec{x}$ are taken as basis for $\vec{k}$, the integral takes the form [201]:

[3] Which, in this case, involves only one of the two poles; here, w_1 will be used without loss of generality.

$$C(\vec{x},t) = \frac{\sigma^2 k^{d-2}\pi^{\frac{d-2}{2}}}{(2\pi)^d\Gamma(1+d/2)}\int_{-\infty}^{\infty}dk\frac{e^{-(\epsilon+D_\psi k^2)t}}{D_\psi k^2+\epsilon}\int_0^\pi d\theta e^{ikx\cos\theta}\sin^{d-3}\theta. \tag{5.51}$$

By using expression 8.411.7 in [202]:

$$C(\vec{x},t) \sim \int_{-\infty}^{\infty}dk\frac{e^{-(\epsilon+D_\psi k^2)t}}{D_\psi k^2+\epsilon}x^{-\nu}k^{\nu+1}J_\nu(kx), \tag{5.52}$$

where $\nu = (d-3)/2$, J_ν is the first kind Bessel function of order ν, and the constants have been omitted for the sake of simplicity. Performing the change of variables $y = kx$ and, without loss of generality, fixing $D_\psi = 1$, after some algebra and using that, at leading order, $(y^2+1)^{-1} \sim 1$:

$$C(\vec{x},t) \sim e^{-\epsilon t}\int_{-\infty}^{\infty}dy y^{\nu+1}e^{-y^2t/x^2}J_\nu(y). \tag{5.53}$$

Solving the integral [202], the correlation function becomes:

$$C(\vec{x},t) \sim e^{-t/t_\xi(\epsilon)}e^{-\frac{x^2}{t}}, \tag{5.54}$$

where the cutoff function $t_\xi(\epsilon) \sim \epsilon^{-1}$ defines the time correlation length $\xi_t \sim \epsilon^{-1}$ and induces a spatial correlation length $\xi_x \sim \epsilon^{-2}$ (see the second exponential of Eq.(5.54)). Both correlation lengths depend solely on the degree of dissipation ϵ and, only when it is fine-tuned to zero, correlations diverge and the system becomes critical. The generic scale-invariance is lost.

In summary, a dissipative term $-\epsilon\psi$ in an otherwise "massless"[4] theory, introduces a characteristic length (inversely proportional to a certain power of ϵ) for the evolution of the ψ field and, therefore, only when the parameter of the new "mass" term (ϵ) is tuned to zero, the initial scale-free behavior of the system is recovered. Therefore, **conservation is a necessary and sufficient condition for SOC**.

[4]That is, with no linear term in the ψ field.

5.4 Nonconservative examples of SOC in Nature

In the previous sections, it has been stated that nonconservative local rules prevent a system from exhibiting SOC. Although, as it was argued before, conservation laws are abundant in Nature, there exist archetypical examples of systems which embraces the usual SOC characteristics in their dynamics despite of being clearly dissipative. This is the case of, for example, *earthquakes* and *forest fires*.

5.4.1 Earthquakes

Consider the outermost layer of the lithosphere of the planet. The crust is divided into the so-called *tectonic plates* which, roughly said, are floating on the liquid magma of the asthenosphere. The convective currents below them, originated due to gradients of temperature deep into the Earth, give rise to a slow motion of the plates.

The currents make the plates slowly move away or converge; when two plates converge, the points of contact constitute a zone with geological activity, where the friction between plates and the effect of the currents make them store energy in the form of stress. As the motion is slow, the rate of stored energy is small; the accumulation of tension can proceed during years until, suddenly, the plate releases the collected stress in the so-called **earthquakes**.

Consider the contact zone as a $d = 2$ lattice. The sites of the plates accumulate stress during long periods of time (years), until some sort of threshold is overcome into one of the sites (the *hypocenter*). Then, the energy is released, and rapidly travels in form of damped waves (the *seismic waves*) across the crust, reaching even its surface[5]. This relaxation event involves many sites of the system (all the sites reached by the seismic waves), which can in turn release part of their energy. This rapid chain reaction (it usually lasts no more than a minute) ends when all the surviving waves reach the surface, where the energy is eventually dissipated. The energy released during an earquake, quantified by means of its intensity I, obeys the scale-free Gutenberg-Ritcher law [2]:

[5]There exist another important point to be considered in an earthquake, the *epicenter*, which is the first site at the surface reached by the seismic waves.

$$P(I) \sim I^{-\gamma}, \tag{5.55}$$

represented by the exponent γ (see chapter 1 and Fig.1.1).

By using this basic characterization of an earthquake, some analogies with the SOC systems studied in the previous chapters can be done:

- The system is exposed to a slow driving process.
- There is one site, the hypocenter, at which an avalanche process is triggered.
- In this event, its accumulated tension is relaxed by redistributing energy among its neighbors, which can also become active and relax.
- The avalanche drives the released energy in form of waves towards the boundaries of the system, given by the surface of the Earth. There, the excess of energy of the system is dissipated.
- The duration of an avalanche is negligible in comparison with the scale of time of the driving process, that is, there is an infinite separation between perturbation and relaxation time scales.

This, together with the scale-free behavior of avalanches (see Eq.(5.55)), makes natural to think in earthquakes as a good example where SOC can be found into the real world. In fact, the easy identification of the SOC ingredients is the reason why this example was used in chapter 1 to introduce the basic notions of SOC. However, the damped propagation of the seismic waves breaks the local conservation of energy, a necessary condition (as stated in the previous sections) for a system to exhibit SOC.

Due to the "open" boundaries, the existence of avalanches, and the slow driving, it is reasonable to think that the crust of the Earth, after thousands of years of geological activity, has reached a stationary state in which the stored energy is balanced with the tension dissipated during earthquakes. The question to answer is whether this stationary state is critical or not, that is, if the power law observed for the intensity of the earquakes (Eq.(5.55)) is a result of a critical propagation of the earthquake.

Early Models of Earthquakes

Starting from the basic assumption of stationarity, many models were devised in the early years after the arising of the SOC concept. The first models were mere translations of the BTW sandpile model [6] to the language of earthquakes [203]; strictly conservative models which, in the end, were not realistic (i.e. did not reproduce the Gutenberg-Ritcher law, Eq.(5.55)).

In order to obtain more realistic results, the constraint of conservation was weaken. Although different models can be found in the literature (as, for instance, the one in [204]), the most notable models of earthquakes are based on the **stick-slip** spring-block model (or train model) introduced by Burridge and Knopoff in [205].

The Feder-Feder Model

The Feder-Feder nonconservative model [206], uses a system composed by a sandpaper and a carpet to model, by means of stick-slip processes, the motion of the tectonic plates on the Earth.

The sandpaper-carpet system serves as a intermediate between sandpile models and earthquake models; due to this, this experiment will be briefly explained. Consider a $d = 2$ sheet of sandpaper posed on a carpet. The motion of the sandpaper can be controlled by an elastic string. If a small amount of force is applied to the string in order to make the sandpaper move, the friction between the sandpaper and the loops forming the carpet[6] prevents the paper from moving. It keeps storing energy from the string (*stick* process) until the static friction is overcome, and a *slip* motion takes place, in which the accumulated energy is used to overtake the dynamic friction.

In [206], this motion is considered as a rough approximation to the motion of tectonic plates. A very refined setup is used in order to obtain experimental measurements of the energy released during the slip processes (the avalanches) of the sandpaper. Also, a $d = 2$ cellular automaton is devised to model this system. Calling $u_i \in \mathbb{Z}^+$ the displacement of the carpet fibers due to the (elastic or friction) forces between the carpet and the sandpaper at site i, the relaxation rules are given by:

[6] A "hairy" carpet is useless for this experiment [206].

$$\text{if} \quad u_i \geq U_{thr} \quad \begin{cases} u_i \rightarrow & 0 \\ u_j \rightarrow & u_j + 1 \quad \forall j \quad \text{n.n. of } i. \end{cases} \tag{5.56}$$

These rules are very similar to the rules of the BTW sandpile (see Eq.(1.10)-Eq.(1.11)) but, for $U_{thr} > 2d = 4$, a number of grains $U_{thr} - 2d$ is lost (dissipated) during the relaxation. This model (a nonconservative version of the early model introduced in [203]) is, thus, a nonconservative version of the BTW sandpile. The connection between sandpiles and stick-slip models becomes clear.

The Olami-Feder-Christensen Model

The variation devised by Olami, Feder and Christensen (OFC) [12], the **OFC model**, has also its origins in the Burridge-Knopoff spring-block model [205] but, as we will see, in the end it is reduced to simple rules similar to the above described for the Feder-Feder model.

Consider a two-dimensional fixed plate and blocks, labeled by pairs of integers (i, j), posed on it. The blocks are connected between them, and also with a moving plate, by means of perfect springs. The characteristic constant of the springs in the two directions of the plate are, without loss of generality, equal, but different from the constant of the springs connecting the blocks with the moving plate (see Fig.5.4).

By assuming a perfect elastic behavior of the springs, the dynamics of the system goes as follows: as the moving plate slithers, the elastic force of the springs is transferred to the (still) static blocks, which accumulate it; when, at any of these blocks, say the one labeled (i, j), the accumulated force $F_{i,j}$ overcomes a threshold F_{thr} (which represents the limit of the static friction with the fixed plate), a sliding occurs, and part of its energy is transmitted to its neighboring blocks by means of the springs, while the rest of the energy is lost in the dynamic friction with the static plate. This can trigger a chain reaction in which many more blocks are involved. An avalanche has started.

The cellular automaton is summarized in these basic rules:

- Initialization: All blocks are initialized with $F_{i,j}$ randomly distributed between 0 and F_{thr}.
- Driving: The site with the maximum force, $F_{i,j}^{max}$ is located, and the force of all sites is increased by a quantity $F_{thr} - F_{i,j}^{max}$ in order to create one active seed.

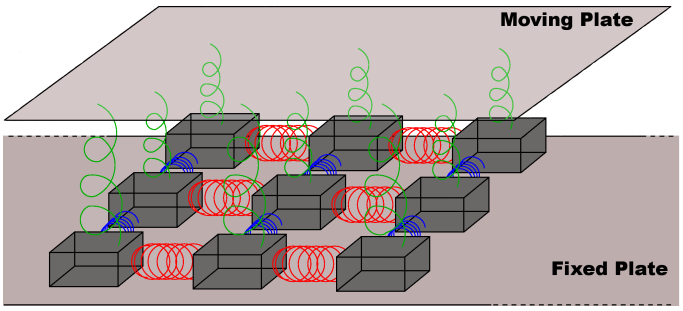

Figure 5.4: Sketch of a spring-block system as the one described in the text. The springs on the three main spatial directions have different colors. According to the definition of the OFC model, blue and red springs are identical.

- Avalanche: The relaxation rule of the original active seed and the rest of subsequent active sites, given by the following equation, is iterated until no more active sites remain in the system:

$$\begin{cases} F_{i,j} \rightarrow & 0 \\ F_{i',j'} \rightarrow & F_{i',j'} + \alpha_\epsilon F_{i,j} \quad \forall\ (i',j') \quad \text{n.n. of } (i,j). \end{cases} \tag{5.57}$$

- Boundary conditions: The force at sites out of the system are fixed to $F = 0$.

The degree of dissipation is given by α_ϵ; thus, in this $d = 2$ system, any $\alpha_\epsilon < 1/4$ defines a local violation of the energy conservation. These rules make the average force increase up to a certain stationary value, reported to be critical [12].

The Role of Conservation in the OFC Model

These rules are very similar to the relaxation rules used in sandpiles. Actually, the described rules define a nonconservative version of the Zhang sandpile model [47]. In [48], it is already pointed out for this continuous sandpile that any violation of local conservation entails a finite correlation time-scale which only diverges when the parameter of dissipation is fine-tuned to its zero value. In fact, the very same arguments used in the previous sections with the Oslo ricepile and the SOBP model with dissipation also hold for the modified sandpile which is the OFC model.

Even so, the question whether the OFC model is critical or not has generated a lot of controversy, due to the apparent critical behavior of the

model observed in computer simulations even for large amounts of dissipation ($\alpha_\epsilon \ll 1$).

Many works have been devoted to analyze this question. Early simulations of the original model [12,207–209] showed clean power laws in avalanche distributions and power spectra; the observables exhibited the finite-size scaling which can be expected from a critical model. This phenomenology was obtained even for small values of α_ϵ. However, the value of the measured exponents of these scale-free observables depends on the degree of dissipation, which is at least a sign of non-universality, unexpected in SOC as showed in the previous chapters.

Moreover, when periodic boundaries conditions are used, the scenario changes. As showed in [210, 211], and confirmed in subsequent works [212], in the stationary state the system enters a cycle of periodic configurations, which depends on the degree of dissipation (i.e. on the value of α_ϵ). These cycles are characterized by ordered configurations which lead to defined peaks in the avalanche size distribution. Only for values of α_ϵ close to conservation, the periodic behavior is prevented by strong fluctuations associated with the proximity to the critical point.

The differences between the original OFC model and its periodic version stem from the boundary conditions. Therefore, as pointed out in [210–212], it can be deduced that the origin of the apparent scaling reported in the OFC model is the **effect of the boundaries on the bulk**: when the system is slowly driven, the bulk starts to oscillate with a period $(1 - 4\alpha_\epsilon)$ which depends on the degree of dissipation; however, the sites at boundaries oscillate with a different period, because of the smaller number of neighbors avaliable.

As stated in [212], this originates an aperiodic disturbance which invades the bulk, steadily destroying the periodicity. In this way, a sort of marginal synchronization between the bulk and the boundaries is the responsible for the apparent scale-free behavior. The disturbance invasion distance depends on the number of driving events by means a power law, where the exponent is a function of the degree of dissipation. This explains the dependence of the avalanche distribution exponents on α_ϵ. As the exponent of the invasion distance is small, and decreases as α_ϵ increases, the formation of the synchronized configuration is slower for larger degrees of dissipation [212].

In conclusion, the apparent scale-free behavior of the OFC model stems from the existence of large boundary-controlled coherent domains in the bulk, which allow the development of apparently broadly-distributed avalanches. Due to the dependence on the degree of dissipation of the velocity with which

such domains are built, the observables are also affected by a dependence on α_ϵ.

Accepting this, the "scaling" behavior of the OFC model must disappear when the spatial structure becomes irrelevant, i.e. in the mean-field regime. An easy way to check this is by using the random-neighbor ensemble described in chapter 1, in which the neighborhood of a site is randomly chosen among all the sites of the lattice at each time. This ensemble allows to map the model directly into a branching process (see section 5.2).

Although the mapping and the analytical treatment of the resulting process has been attempted with different results (see, for instance, [213] for the OFC model, and [46, 214] for dissipative variants of the BTW and Zhang models, respectively), it is in [215] where the model is analytically solved and, in contrast to [213], without using open boundaries[7] or strong assumptions. In [215], Bröker and Grassberger calculate the energy distribution, as well as the branching ratio and the average avalanche size, among other quantities. The main conclusion is that, only in the limit $\epsilon \to 0$ (where ϵ is the degree of bulk dissipation), the branching ratio reaches its critical value $\sigma = 1$ and the average avalanche size diverges. That is, in the random-neighbor ensemble, the system is *not* self-organized. This supports the conclusion of the origin of the scaling in this model.

In light of the exposed results, it can be said that **the OFC model is not a SOC system**. The apparent scaling reported in the simulations of the model with open boundaries are due to the inhomogeneities represented by the open boundaries, which induce an interplay between synchronized and desynchronized configurations into the bulk. This interplay generates large coherent patches, but occasionally the synchronization is broken due to a strong driving [215]. In the end, apparent scale-free avalanches can be observed for even large degrees of local dissipation. When these inhomogeneities are not present, nor the spatial correlations of an underlying lattice, the scaling is recovered only for the limit of total conservation.

Extrapolating this result, it could be concluded that, therefore, *earthquakes are not SOC phenomena, or the models up to date lack of some ingredients to well describe them.* Nonetheless, the Gutenberg-Ritcher law illustrates an apparent critical behavior. As mentioned in chapter 1, the origin of such behavior cannot only resemble on critical behavior. However, the simi-

[7] Closed boundary conditions are crucial in this system in order to obtain reliable results, due to the above explained influence of the borders on the behavior of the observables.

larities between the phenomenology of an earthquake and SOC systems make one keep on thinking in the SOC character of this natural phenomenon. It is out of the scope of this thesis to answer the question of whether the scale-free behavior of real earthquakes is only the synergic effect of many factors acting at once, or the violation of conservation into the crust is low enough to prevent the observations up to date from measuring a clear cutoff not dependent on the size of the system (and the system is close to the SOC behavior).

5.4.2 Forest Fires

Forest fires have been historically considered, as well, a non-conservative example of SOC present in Nature. Indeed, there are many analogies between the dynamics of fires and the usual SOC systems:

- Triggering: A spark (for instance) sets on fire a tree.
- Avalanche: The fire propagates to each nearest neighbor tree of any burning one. The propagation stops when no more burning trees remain in the forest.

The effect of a fire on the poblation of trees allows to assume a stationary state for the number of trees. In fact, critical behavior (see, for instance, [17, 216, 217] and references therein) has been reported for real catalogs of fires. However, there is an *intrinsic lack of conservation* in the dynamics, where there is not a quantity for which conservation is broken. The question about its SOC character arises.

Early Models of Forest Fires

The first model of forest-fire (FFM1 hereinafter) was devised to show non-trivial scaling in a turbulent system out of equilibrium [13]. This model, subsequently modified in [218], is not a model in which a certain tunable degree of dissipation exists; the system is, by definition, non-conserved.

Consider a d-dimensional lattice with closed boundary conditions in whose sites (unitary areas of a forest, for instance) a certain number of trees, represented at site i by their density u_i, can grow. Trees at each site grow with a certain rate p, until a threshold is overcome. This originates a fire into the site, which propagates instantaneously to the neighbors. Thus, three situations can be found at a site: $u_i \geq 2$ (fire), $2 > u_i \geq 1$ (living trees), and

$1 > u_i \geq 0$ (ashes). Starting from a random initial distribution of densities, and by fixing a threshold $u_{thr} = 2$, the relaxation dynamics goes as follows:

- Driving: The value of the density at each site is increased by a quantity p.
- Avalanche: When the threshold is overcome at a site, say i, the trees at this site burn and, in consequence, its density is reduced ($u_i \to u_i - u_{thr}$). For any neighboring site, j, $u_j \to 2u_j$ if $u_j \geq 1$, and therefore more fires can be activated. This process is iterated until there are no more fires into the system.

For $p \to 0$, the avalanche process is supposed to be instantaneous in comparison with the perturbation time scale, and no new trees grow during the course of an avalanche. With these rules, the driving and the intrinsic nonconservative definition of the avalanche make the density of trees of the system reach a stationary state.

Early measurements of critical exponents in this *deterministic* model of forest-fire[8] pointed to a scale-free behavior [13,218]. However, in [219], Grassberger reported in $d = 2$ regular spiral patterns of smooth[9] fire fronts moving with a nearly constant velocity; the correlation length at long times was observed to scale as $1/p$, with the consequent power law behavior for $p \to 0$. But the quasi-deterministic behavior, the dependence on the initial conditions, and the fact that, for $d > 2$, periodic oscillations in the number of fires were found, led Grassberger to the conclusion that the model is "critical in a trivial way", not SOC in the strict sense of the word.

In [210], it was shown that the cause for the apparent scale-free behavior of the original system is its proximity to chaos. By slightly modifying the original model, even a chaotic regime can be found, in which the heavy fluctuations prevent the periodic oscillations but do not induce any power-law behavior. In this last regime, in fact, the susceptibility of the system *decreases* when p becomes low enough, instead of diverge.

Therefore, it was early stated that *this nonconservative and deterministic FFM1 is not a SOC system.*

[8] Note that no stochasticity is present in the above exposed rules.
[9] Fractal dimension close to the Euclidean dimension.

The Drossel-Schwabl Forest Fire Model

A few years later, a stochastic variant of the FFM1 was introduced. The rules were reinterpreted in a probabilistic way, and a new rate was introduced [14]:

- Driving: At an *empty* site, a tree grows with probability p. Then, the site becomes *occupied*.
- Initial spark: A tree not surrounded by any fire becomes a burning tree with probability f (due to a lightning strike, for instance). The site is called a *burning* site.
- Avalanche: A burning tree sets its neighbors on fire. The burning site becomes empty at the next time step.

With these rules, which define the **stochastic forest-fire model** (FFM2), the density of trees reaches a stationary state. The rules are similar to the ones of the FFM1, but the sparking probability f allows the smallest clusters (with size even smaller than $1/p$) to burn[10].

In the limit $f/p \to 0$, the time scale separation arises, and individual avalanches can be defined; indeed, the number of burnt trees during a fire diverges and, therefore, the system apparently becomes critical.

Actually, in this model there exists a **double separation of time scales**: for the system to become critical, it is not only necessary that avalanches proceed instantaneously in comparison with the slow-driving, but also the ignition of the initial trees must be slower than the driving ($f \ll p \ll (f/p)^{1/d}$ [14]). This fact is the essential feature which differences forest-fires and sandpiles, and what, a priori, makes the system critical even being its dynamical rules essentially nonconservative.

The first analytical results and mappings into a branching process suggested some similarities with standard percolation models [14,220,221]. There was a great controversy not only about the analytical but also about numerical results; as the analytical tractability of this forest fire is very limited, this controversy was mainly disputed by means of larger and larger numerical simulations (see, for instance, [222–226]). In this way the early reported integer values for exponents were corrected with non-trivial real values, which reinforced the claim of the nontrivial SOC essence of the FFM2.

[10]Such small burning clusters are not possible in FFM1 where, as said before, there exists a typical separation of size $1/p$ between fronts.

However, when large enough systems were simulated, some anomalies were reported; the most remarkable ones, the repulsive character of the fixed point ($f/p = 0$), the coexistence of largely-subcritical and supercritical clusters of trees, the existence of two length scales with different exponents into the system, the violation of the usual scaling ansatz of the distribution of fire (avalanche) sizes $P(s)$ (see Eq.(1.2)) and a pathological finite-size behavior [223, 225, 227, 228].

When massive simulations of extremely large systems very close to the critical regime are performed [229, 230], the apparent anomalies turn into a real lack of critical behavior. Although apparent scaling regimes appear, which cannot be discerned from a pure power law for smaller systems, these large scale simulations allow to distinguish a subsequent nonmonotonic regime in observables like the avalanche size distribution. Also, the presence of two different length scales (with different scaling) is confirmed.

Therefore, the divergence of the average number of burnt trees during a fire, which was the originally reported sign of criticality, is not enough to ensure the critical character of the stationary state, due to the existence of a second length scale. Together with the above mentioned nonmonotonic behavior of the observables, it leads to the conclusion that **the self-organized stationary state of this FFM2 is not critical**.

In conclusion, neither the earthquake models with broken conservation (as the OFC model) nor the nonconservative stochastic models of forest fires (as the FFM2) exhibit critical behavior. In the former, the local dissipation is the responsible, recovering authentic criticality in the limit of conservation. In the latter, it is still not clear the reason for such an anomalous behavior; in the next section, some ideas about the origin of the apparent critical behavior and also of these pathologies will be suggested.

5.5 Background Dynamics and Criticality

In the past sections, self-organized models with no local conservation have been studied. In some systems like the Oslo model or the SOBP model, the effect of a bulk dissipation is clearly distinguished from the real critical behavior. This is due to the fact that the level of conservation can be easily controlled, and the appropriate values for the size of the system and the degree of bulk dissipation can be fixed in order to observe the dissipation-induced cutoff in the observables.

In other cases, like in the FFM2, massive large simulations are necessary to discern the deviation from the scaling behavior and the rest of above mentioned anomalies. The intrinsic lack of conservation seems not to prevent the system from exhibiting a behavior *very close* to the critical one. Although this seems to contradict the assertions about the role of conservation in SOC systems, there is, as it is illustrated in what follows, a simple explanation for this behavior: the *repoblation mechanism* of the FFM2 (i.e. growth of trees with a certain small probability), that would be equivalent to a background dynamics in a typical SOC model like a sandpile.

5.5.1 A Second Driving Mechanism

The basic underlying idea of the repoblation mechanism is to compensate the energy dissipated during an avalanche. Consider the stationary state of a non-conserved sandpile like, for instance, the Oslo model with dissipation studied in the first section of this chapter. During an avalanche, many grains can be dissipated (depending on the rate of bulk dissipation, ϵ), and the background field remains with a subcritical average energy (see above).

Imagine that the number of grains dissipated at the bulk are stored into a reservoir. If these grains are reintroduced into the sandpile before the next driving event, the background field, a priori, recovers the same average energy level that it would have after an $\epsilon = 0$ avalanche. It is natural to think that, due to this, the system can compensate the effect of dissipation in order to exhibit true critical behavior again. By means of the two following examples, in which this idea is introduced in their dynamics, the validity of this assertion will be checked.

a) The SOBP-D Model Revisited

In [231], Juanico et al. introduce a background dynamics into the SOBP model with dissipation (SOBP-D; see section 5.2). Consider the sandpile rules of the original SOBP model. In analogy with networks of neurons, in [231] the following notation is used: the sites with $z = 2$ are called *excited*, the sites with $z = 1$, *quiescent*, and the sites with $z = 0$, *refractory*[11].

With probability α, an excited site transfers two grains to two different ran-

[11] In the literature of SOC, the nomenclature with three different types of sites (active, critical, and stable) is also common; see, for instance, [68].

dom neighbors among all the possible sites of the lattice; with probability β, only one grain is transferred to one neighbor; with probability $\epsilon = 1-\alpha-\beta$, the two grains are dissipated.

If p is the density of quiescent sites and $L = 2^{m+1}-1$ is the size of the system, the version of Eq.(5.35) with the small modifications above mentioned is [231]:

$$\frac{dp}{dn} = A(p;\alpha,\beta) + \frac{\eta(p,n)}{L}, \tag{5.58}$$

where:

$$\begin{aligned} A(p;\alpha,\beta) = \; & \frac{1}{L} - \frac{2\left(p(2\alpha+\beta)\right)^m}{L} \\ - \; & \frac{p\epsilon}{L\left[(1-p)+p\epsilon\right]}\left[1 + \frac{1-\left(p(2\alpha+\beta)\right)^{m+1}}{1-p(2\alpha+\beta)} - 2\left(p(2\alpha+\beta)\right)^m\right] \end{aligned} \tag{5.59}$$

and, as expected, Eq.(5.35) is recovered when $\beta = 0$.

In section 5.2, it has been already explained that the critical point of a branching process is given by a critical branching ratio (average number of descendants per ancestor), $\sigma = 1$. In the original SOBP-D model, only 2 or 0 descendants can be created, and therefore $\sigma = \sum_k kp(k) = 2p(1-\epsilon) = 1$ implies Eq.(5.23). Here, the branching ratio must take into account the possibility to create 2, 1 or 0 descendants; noting that, in the probabilities α and β, it is already implicit the failure of dissipation:

$$\sigma = \sum_k kp(k) = 2\alpha p + \beta p + 0 \quad \Longrightarrow \quad p_c = \frac{1}{2\alpha+\beta}. \tag{5.60}$$

Background Dynamics

A background dynamics is implemented in [231] by introducing a rate λ for a quiescent site to be turned into a refractory site, and a rate θ for the opposite transformation. This secondary driving process can be done, as in the "critical" limit of the FFM2, out of the course of avalanches, and no activity is created by means of these transformations. Thus, for an appropriate

balance of λ and θ rates, the background of the system can be regenerated. In this way, the **self-organized branching process with background dynamics** (SOBP-BD) is defined.

The creation of quiescent sites makes their density, $P(z = 1) = p$, increase an amount given by $(1 - p)\theta$, while their transformation into refractory sites makes it decrease in a quantity $-p\lambda$. Then, in the equation of evolution of p, the background dynamics is equivalent to the addition of a term $(1-p)\theta-p\lambda$ (which takes into account only driving times between two avalanches):

$$\frac{dp}{dn} = (1 - p)\theta - p\lambda + A(p; \alpha, \beta) + \frac{\eta(p, n)}{L}. \tag{5.61}$$

This new term, if alone, makes p increase to the value $p = \theta/(\theta+\lambda)$; therefore, if the background rates are adjusted to [231]:

$$\frac{\lambda}{\theta} = 2\alpha + \beta - 1 = \frac{1}{p_c} - 1, \tag{5.62}$$

the evolution of p possesses an attractive term which makes it tend to its critical value p_c.

Critical Behavior

To study whether the fixed value p^* of Eq.(5.61), in contrast to the case of Eq.(5.35), coincides with the critical point, the following function $R(p)$ is devised [231]. Its root is precisely the critical point p_c:

$$R(p) = \beta^2 p^2 - 4\alpha p\,[1 - (1 - \epsilon)p] - 2\beta p + 1. \tag{5.63}$$

On the other hand, the root of dp/dn, Eq.(5.61), as a function of p is its fixed point. In this way, by comparing the graph of $R(p)$ with the plot of dp/dn, it is possible to know how far the fixed point p^* is from the critical point p_c.

As can be seen in the left part of Fig.5.5, for $\beta = 0$ and sizes such that $m > 16$, the fixed point of the dynamics, Eq.(5.61), coincides with the critical point. This could lead to the conclusion that the SOBP-BD model reaches a SOC stationary state for finite sizes, *regardless the degree of dissipation.* Also, the same finite-size scaling and the critical exponents of the conserved SOBP can be measured for such sizes [231].

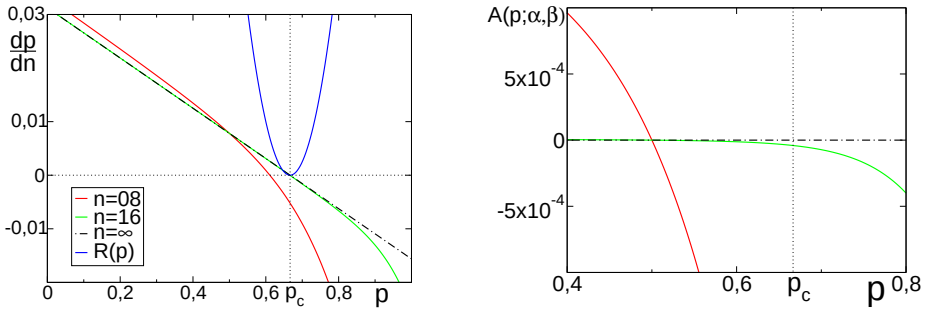

Figure 5.5: dp/dn and the function $R(p)$ (whose root is the critical point p_c, see text) for $\epsilon = 0.25$, $\beta = 0$, and $\eta = 0.03125$. Inset: Order of magnitude of $A(p;\alpha,\beta)$, which changes its sign at $p = p_2^* = 1/2$.

However, there are two important factors to take into account [232]:

i) The Critical Character of the SOBP-BD model: In Eq.(5.61), there are two main contributions:

- The term $(1-p)\theta - p\lambda$, which regenerates the background up to the value $p_1^* = \theta/(\theta+\lambda)$.
- The term $A(p;\alpha,\beta)$, whose fixed point for $\beta = 0$ was proven to be $p_2^* = 1/2$ for any value of ϵ (see section 5.2), which holds also for $\beta \neq 0$.

When the two contributions are represented versus p, the former reaches from below its fixed value $p_1^* = p_c$. Nevertheless, $A(p;\alpha,\beta)$ changes its sign, from positive to negative, at a value $p = p_2^* < p_c$ (see right panel in Fig.5.5).

Therefore, for values of the probability into the range $0 \leq p \leq p_2^*$, dp/dn increases towards its critical value from below with a positive contribution of both terms, with the fluctuations given by the noise term. However, for the range $p_2^* < p \leq p_c$, the contribution of $A(p;\alpha,\beta)$ is negative and prevents p from reaching its critical value[12]. Therefore, for significative values of $A(p;\alpha,\beta)$, it is not possible for the dynamics to drive p towards its critical value, but towards a stationary value $p^* < p_c$. In conclusion, the system **cannot be critical because of the presence of dissipation**. When $\epsilon = 0$, p does not need the background dynamics to reach its critical value, and the original SOBP is recovered.

[12]This is caused by the approaching from below of the term $(1-p)\theta - p\lambda$ to its fixed value.

In the SOBP-BD model, the reason why critical behavior is observed for a finite size regardless of dissipation is very simple: as m increases, the contribution of $A(p;\alpha,\beta)$ becomes smaller and smaller. In the right part of Fig.5.5, it is shown that, for the reported $m = 16$, the values of this term for $p < p_c$ are negligible in comparison with the secondary driving term.

ii) The Self-Organized Character of the Modifications: In the SOBP-BD, the value of the parameters λ and θ is essential in order to reach a stationary state with the appropriate value of the probability p. As it is established by Eq.(5.62), in this model there is an **explicit tuning** of these parameters to their critical values. The imposition of specific values for these parameters in order to reach the reported behavior turns this model into a standard non-equilibrium model, with a standard critical point given by Eq.(5.62) and large enough m.

To summarize, this modification of the SOBP model with dissipation, in which a background dynamics between avalanches makes the probability p increase in order to reach its critical value p_c, **is not a true SOC system**. Is not critical, because the dissipative dynamics prevents p from reaching the critical value; and is not self-organized, because a tuning is necessary to drive p towards a value close to criticality. Only for large enough system sizes, this value is *indistinguishable close* to p_c.

b) The OFC Model Revisited

As mentioned in section 5.4.1, in [215] Bröker and Grassberger exactly solved the OFC model in the random-neighbor ensemble. It was proven that it lacks of criticality due to the violation of local conservation. In [233], Pruessner and Jensen consider a slightly modified version of the random-neighbor OFC (RN-OFC) model in which a secondary driving process, by means of background dynamics, is used in order to compensate the dissipated energy. This analytically tractable model is the second example to be studied here.

Consider a square lattice whose L sites store a certain continuous amount of energy, z_i. Three species are defined: *stable* sites, which have energy $0 \leq z_i < 1 - \alpha_\epsilon$; *susceptible* sites, with energy $1 - \alpha_\epsilon \leq z_i < 1$; and *active* sites, with energy $z_i > 1$. As usual, the background field is formed by non-active sites (see chapter 2). Whereas the relaxation event remains like in the original RN-OFC model, the driving stage is split into two parts. The dynamics is the following [233]:

- Background Dynamics: In this stage, $(1/\theta)$ sites are chosen randomly

and, if they are stable sites, their energy is set to $1 - \alpha_\epsilon$. Otherwise, their energy remains untouched.

- Triggering: After the background dynamics, one site, say i, is randomly chosen and, only if it is susceptible, its energy is set to $z_i = 1$. In this way, an avalanche starts.

- Relaxation: Any active site relaxes completely its energy ($z_i \to 0$), and only a fraction α_ϵ of it is transmitted to its neighboring sites ($z_j \to z_j + \alpha_\epsilon z_i$, with $j \neq i$). The rest of the energy is dissipated. When no more active sites remain in the lattice, a new driving event is performed.

As it is defined in the random-neighbor ensemble, the neighbors of a site i are randomly chosen between all the sites of the square lattice, when necessary[13]. If the number of neighbors is fixed to m, the limit of conservation is established at $\alpha_\epsilon = 1/m$.

The parameter $(1/\theta)$ is related with the parameter introduced in [223] in an optimization of the simulations of the FFM2[14]. In the limit $(1/\theta) \to \infty$, the avalanches of the system are well-defined, with a duration negligible in comparison with the driving time scale.

The condition for stationarity is, as usual, a simple balance of energy: the dissipated energy must balance the increase resulting from the two driving stages. As:

- During a relaxation at the active site i, the total amount of energy dissipated is $(1 - m\alpha_\epsilon)z_i$; therefore, the average energy dissipated during an avalanche is $(1 - m\alpha_\epsilon)z_a\langle s\rangle$, where s represents the size of an avalanches and z_a, the average energy of an active site.

- In a triggering, the energy of the selected susceptible site, say i, is increased by an amount $1 - z_i$; therefore, on average, the increase of energy due to triggerings is $1 - z_s$, where z_s is the average energy of a susceptible site.

- In every background driving, the energy of a stable site, e.g. i, is increased an amount $(1 - \alpha_\epsilon - z_i)$; this is attempted $(1/\theta)$ times and, in

[13]Note that there is no boundaries in the system; the bulk dissipation is the only one of the dynamics.

[14]This new parameter depends on the inverse of the (f/p) parameter of the FFM2.

comparison with the triggering event, it is performed in a ratio $(\zeta_{st} : \zeta_s)$, where ζ_{st} (ζ_s) is the density of stable (susceptible) sites. Therefore, the average increase of energy due to this secondary driving is given by: $(1/\theta)(1 - \alpha_\epsilon - z_{st})(\zeta_{st}/\zeta_s)$, where z_{st} represents the average energy of a stable site.

Then, the balance equation ensuring stationarity is:

$$(1 - m\alpha_\epsilon)z_a\langle s\rangle = (1 - z_s) + (1/\theta)(1 - \alpha_\epsilon - z_{st})\frac{\zeta_{st}}{\zeta_s}. \tag{5.64}$$

It is straightforward deduced from this equation that, by assuming that both $\langle s\rangle/L$ and $(1/\theta)/L$ vanish in the thermodynamic limit [233], $\langle s\rangle$ diverges in one of these cases: *i)* total conservation (i.e. $\alpha_\epsilon = 1/m$) or *ii)* divergence of $(1/\theta)$ which, in fact, is the condition assumed in order to obtain the time scale separation appropriate for SOC. Therefore, a priori, the self-organized stationary state, reached in the limit $(1/\theta) \to \infty$, would be critical and the RN-OFC with background dynamics would be a SOC system.

By following a procedure similar to the used by Bröker and Grassberger in [215], Pruessner and Jensen calculate the essential energy distributions for the system. It is of special importance the distribution of energy of the active sites, $C(z)$, because of its relation with the branching probability. The support of this distribution is the interval $[1, 1/(1 - \alpha_\epsilon)]$. The lower value is, trivially, $z = 1$; for the upper value, the energy of the last active site of an infinite avalanche involving sites with energy $z = 1$ is to be considered: if double charges are neglected (which is possible for systems large enough, see section 5.2), its energy is given by $1 + \alpha_\epsilon(1 + \alpha_\epsilon(1 + \alpha_\epsilon(\ldots))) = 1/(1 - \alpha_\epsilon)$ [215, 233]. Thus, the branching ratio can be written as [233]:

$$\sigma = m\int_1^{1/(1-\alpha_\epsilon)} dz \int_1^{1/(1-\alpha_\epsilon)} dz' C(z')P(z - \alpha_\epsilon z'), \tag{5.65}$$

where $P(z)$ is the distribution of energies. This relation, Eq.(5.65), can be obtained when $C(z)$ is a δ-peaked function. Only in two limits, $C(z)$ converges to a δ function: in the trivial $\alpha_\epsilon \to 0$ limit, when the sites are isolated from the rest, and the only avalanches possible consist of one site; and the conservative limit $\alpha_\epsilon \to 1/m$, in which criticality and the power laws reported for all the here-studied mean-field SOC systems are recovered [233].

For any other degree of dissipation, the system is subcritical [232]. In fact, a similar dependence of σ and $\langle s\rangle$ on the parameter α_ϵ to the one reported

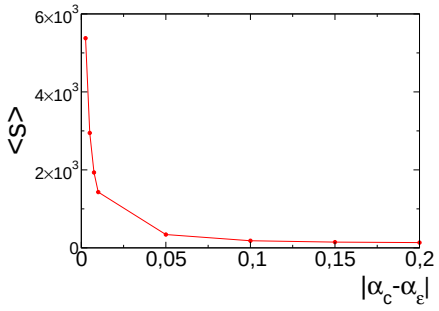

Figure 5.6: Divergence of the mean size of an avalanche for values of the parameter α_ϵ closer and closer to the conservative limit $\alpha_c = 1/m$ ($m = 4$, as in [233]).

for the RN-OFC model in [215], can be observed also in this system, as illustrated in Fig.5.6.

On the other hand, as these calculations are valid only in the thermodynamic limit, the parameter $(1/\theta)$ must be fine-tuned to a value which diverges slower than L, in order to achieve the stationary value. Again, a fine-tuning is necessary in order to ensure a stationary state for the energy, and criticality is recovered only in the conservation limit. In conclusion, **the RN-OFC model with background dynamics is not a SOC system**.

The Failure of Repoblation

At this point, it is natural to wonder why the repoblation mechanism is not able to make the system recover a critical behavior. As in sandpiles (see section 5.1), in the discussed systems the energy of the background acts as a dynamic control parameter, and its critical value is reached by using conservative dynamics (and only in the thermodynamic limit). The secondary driving (repoblation) mechanism should suffice in dissipative systems to make them recover the critical levels of energy, even if it implies a specific tuning of the repoblation parameter.

Recalling the concepts explained in chapter 2, the initial condition of an avalanche in the SOC stationary regime is a critical configuration of the background. It is critical not only due to the average value of the energy, but also because of its correlations, which are the result of the advance of the last avalanche (i.e. a long-term memory of the system). An arbitrary repoblation process can destroy these correlations, making the initial value not a critical one, regardless the average energy stored in it.

But this is not the only reason for the breaking of criticality. As stated in the first sections of this chapter, the bulk-dissipative dynamics by alone is subcritical. During the course of an avalanche, any local violation of conservation involves the appearance of a finite correlation length which prevents the observables measured during the spreading of activity from being critical. In this way, as the driving process affects only to the initial condition of the avalanches, regardless this initial configuration, a bulk-dissipative avalanche always develops finite correlation lengths. Moreover, in the course of the avalanche, the restored background becomes a subcritical one and, in the end of the event, there remains a subcritical configuration again.

All these phenomenology can be clearly observed in the already discussed avalanche-driven version of the pair contact process (PCP) model (see section 4.3). Consider the Langevin equations for the PCP model, Eqs.(2.18), in their simplified version:

$$\begin{cases} \partial_t \rho = & D_\rho \nabla^2 \rho + \mu_\rho \rho - \lambda_\rho \rho^2 - \omega_\rho \rho \phi + \sigma \sqrt{\rho} \eta(\vec{x}, t) \\ \partial_t \phi = & \mu_\phi \rho - \lambda_\phi \rho \phi, \end{cases} \tag{5.66}$$

where ρ represents the activity field, ϕ the background field, η is a Gaussian white noise and the rest of parameters are just constants. Due to the mass term $\mu_\phi \rho$, the background field is not conserved. Therefore, it can be created and removed at each site, and these processes are controlled by the fixed set of parameters.

By integrating the equation for ϕ and replacing it into the activity equation (see Eq.(2.19)), an effective parameter μ_{eff} (in which all the terms linear in ρ are considered) can be defined. In this parameter, both the field ϕ and μ_ρ appear. The parameter μ_ρ represents the distance to the critical point, i.e. the control parameter of this system. There is a stationary value for the background field ($\overline{\phi}$) associated with each value of μ_ρ; only when $\mu_\rho = \mu_c$, the background becomes critical ($\overline{\phi} = \overline{\phi}_c$), $\mu_{eff} = \mu_{eff_c}$, and the measured observables are scale free. Due to the fact that the control parameter is fixed during the dynamics, the system is not self-organized.

Suppose that the control parameter is tuned to a value $\mu_\rho < \mu_c$. In these local-dissipative dynamics represented by Eqs.(5.66), the average value of the background converges to a subcritical stationary value $\overline{\phi} = \overline{\phi}_{sub}$ and, therefore, μ_{eff} to $\mu_{eff_{sub}}$.

If repoblation processes are applied to this system in order to increase the average value of the ϕ field, the initial conditions for the spreading of activity (avalanche) are modified. Due to the increase of the background field, the

effective mass μ_{eff} can increase up to μ_{eff_c}. However, because of the chosen value for μ_ρ, during the course of the avalanche the dynamics makes the background field converge again to its associated value $\overline{\phi}_{sub}$ (and μ_{eff} to $\mu_{eff_{sub}}$). Thus, after a transient period, the behavior of the system becomes again subcritical.

The initial condition cannot influence the final state, as is usual in non-equilibrium non-chaotic systems. In this way, the effect of the repoblation in this avalanche dynamics for the PCP is just to make the background (or μ_{eff}) oscillate with very strong fluctuations with an average value determined by μ_ρ. In the case of $\mu_\rho < \mu_c$, the average background field $\overline{\phi}$ is always below its critical value, and the system is subcritical.

Due to these reasons, this kind of integration of the PCP equations, Eqs.(5.66), entails a previous fine tuning of μ_ρ to its critical value μ_c in order to measure critical observables. If $\mu_\rho < \mu_c$, as in the SOBP-BD and RN-OFC with background dynamics, although the repoblation brings the density of the background closer to its critical average value, the subcritical spreading of the avalanche (due to dissipation) eventually forgets the initial state and prevents the system from exhibiting true scale free behavior.

5.5.2 Conservation on Average

In light of these results, local conservation appears to be a rigid constraint which cannot be violated for the dynamics of a system in order to keep the SOC condition. However, this condition can be relaxed in a certain way.

Consider the Langevin equations for the C-DP class, Eqs.(2.66), in the SOC ensemble (see chapter 2). If a bulk dissipation term is introduced into the system, then:

$$\begin{cases} \partial_t \rho = & D_\rho \nabla^2 \rho + \mu\rho - \lambda\rho^2 + \omega\rho E + \sigma\sqrt{\rho}\eta(\vec{x},t) \\ \partial_t E = & -\epsilon\rho + D_E \nabla^2 \rho. \end{cases} \tag{5.67}$$

Using the arguments seen in the previous sections, it can be deduced that the self-organized stationary state reached by means of these equations is characterized by an average energy $\overline{E}_\epsilon$ below its critical value, $\overline{E}_c$, regardless the initial condition. The system is subcritical and, only for $\epsilon = 0$, the SOC behavior is recovered.

However, it is possible to consider this zero value as the mean value of a *stochastic rate for dissipation*, $\zeta_\epsilon(\vec{x},t)$, short range correlated, which can be

added to the equation. With this new term, the equation for the energy of the C-DP set of Langevin equations becomes:

$$\partial_t E = \zeta_\epsilon(\vec{x}, t) + D_E \nabla^2 \rho, \tag{5.68}$$

where:

$$\begin{aligned} &\langle \zeta_\epsilon(\vec{x}, t) \rangle = 0 \\ &\langle \zeta_\epsilon(\vec{x}, t) \zeta_\epsilon(\vec{x}', t') \rangle = \sigma_\epsilon^2 \delta^d(\vec{x} - \vec{x}') \delta(t - t'), \end{aligned} \tag{5.69}$$

that is, a simple Gaussian white noise. This noise mimics a microscopic compensation of the dissipation by means of the repoblation process *during the course of the avalanche* which results in a zero dissipation average value. Note that, if no new active site is created, the definition of individual avalanches is still preserved; the creation of spontaneous activity would entail, furthermore, the raising of an extra "mass" term into the evolution equation for activity which, as already checked in section 5.3, would lead to a characteristic length into the theory which only diverges by means of a fine-tuning [68].

If the noise term results to be irrelevant for the critical behavior, the SOC behavior is maintained while local conservation is only fulfilled **on average** [232]. This idea, which was already reported to work properly in microscopic sandpiles [234], can be checked, a priori, by means of a trivial power counting.

Consider the energy equation, Eq.(5.68), integrated and replaced into the equation for the activity field ρ. Thus, a new term with an accumulated noise appears into the action of the field ρ. By using the Central Limit Theorem [A4], the term with this integrated noise can be approximated with:

$$\omega\rho \int_{t_0}^{t} ds \zeta_\epsilon(\vec{x}, s) \sim \omega\rho \ \sigma_\epsilon \sqrt{t} \eta_\epsilon, \tag{5.70}$$

where η_ϵ is a Gaussian white noise. As seen in chapter 2 and appendix B, this noise is equivalent to a $\tilde{\rho}^2$ term; concretely:

$$\int d^d x \int dt \left(\omega^2 \sigma_\epsilon^2 t \rho^2 \tilde{\rho}^2 \right). \tag{5.71}$$

By defining $\nu_\epsilon = \omega^2 \sigma_\epsilon^2$, the possible relevancy of this constant indicates the

relevancy of the noise term. As Eq.(5.71) must represent a dimensionless term:

$$[L]^d[T][\nu_\epsilon][T][\rho\tilde{\rho}]^2 \sim 1. \tag{5.72}$$

From the contribution of the Laplacian term $D_\rho\nabla^2\rho$ and the time-derivative term $\partial_t\rho$, the scaling dimension of $\rho\tilde{\rho}$ is $[\rho\tilde{\rho}] \sim [L]^{-d}$ and $[T] \sim [L]^2$. Then:

$$[\nu_\epsilon] \sim [L]^{d-4} \sim [\Delta]^{4-d}, \tag{5.73}$$

where Δ represents the distance to the critical point. As $d_c = 4$, the noise is *marginal* and, with this kind of arguments, the relevancy of the noise cannot be managed. As RG calculations cannot be made (see chapter 2), only numerical simulations are a suitable tool in order to deduce the properties of the new added stochastic term.

To study the relevancy of the noise, numerical simulations of the Langevin equation using the SOC ensemble, but also with many different microscopic models as the Manna model, the Oslo model or the RD model (not shown) [232] have been carried out. In all the cases, the "conservative on average" behavior is indistinguishable from the conservative critical behavior, at least up to very large system sizes. This shows that it is possible to break the local conservation rule and keep a reasonable close-to-SOC behavior if and only if local conservation is fulfilled on average.

From a strict point of view, these systems are not really SOC, but the local on-average conservation allows to develop correlation lengths so large that the finite-size scaling is broken only for very large values of the system size L (so large as desired by controlling the amplitude of the fluctuations[15]). Maybe a model considering such a bulk-dissipation can explain the apparent scale-free behavior of phenomena like, for instance, earthquakes (and the astonishing scaling of the Gutenberg-Ritcher law, Eq.(5.55)), in Nature.

[15]Of course, for large values of the amplitude of the fluctuations, the noise becomes relevant and dominates over the Laplacian, which is the main term which participates in the self-organization.

5.6 Concluding Remarks

Conservation is a necessary and sufficient condition for the existence of SOC. In any SOC system in which local conservation is violated, finite correlations which depend solely on the degree of bulk-dissipation arise.

When such finite characteristic lengths appear, the degree of dissipation acts as the distance to the critical point, i.e. it becomes the control parameter of the dynamics.

Thus, a SOC system with bulk-dissipative dynamics reaches the critical stationary state only when this control parameter is fine-tuned to the conservation limit. Therefore, the system is not critical by means of self-organization.

For the archetypical models of real "SOC" systems like earthquakes and forest fires, it has been shown that no SOC behavior is possible due to their non-conservative dynamics.

In two different mean-field models, it has been shown that a repoblation trick (artificial increase of the average level of background) acting between avalanches makes the bulk-dissipative system strongly fluctuate around a subcritical steady state.

Only if the dissipation is exactly compensated during the avalanches, the obtained scaling behavior of the observables is indistinguishable from the true critical behavior, at least up to large system sizes.

Now, the initial definition of SOC made in the beginning of the thesis can be revisited:

Self-Organized Criticality is a mechanism through which open systems achieve a self-organized statistical stationary state in which a nonequilibrium phase transition **into absorbing states** *is undergone;* **due to local conservation**, *and by means of the existence of a slow-driving, threshold, time scale separation, metastability and boundary dissipation, the dynamics of the system leads it to a critical state in which scale invariance is present in all the observables.*

Chapter 6

Experimental Realizations of SOC

In previous chapters, some theoretical models which seek to capture by means of different microscopic rules the general features of SOC were studied. Starting from the simple deterministic Bak-Tang-Wiesenfeld (BTW) sandpile model, more complex behavior was found in the different stochastic versions discussed up to now.

Although the models studied so far were created in order to describe the phenomenology of a real system (i.e. they are not purely theoretical models, but applicable to real life), for none of them an experimental realization has been proposed (at least in detail) all along this thesis, nor the validity of their rules in order to produce SOC behavior in a real system has been checked thus far.

In this chapter, some experimental realizations of SOC will be studied. First, the early experimental setups devised to reproduce the SOC behavior of sandpile models will be briefly reviewed. In view of their lack of success in this challenge, and in order to get rid of the inconvenience of certain factors, the most relevant experimental granular pile will be described: the Oslo ricepile. Next, systems close to the behavior of sandpiles but whose "grains" are not affected by the mentioned factors will be considered, namely superconductors in the presence of a ramping magnetic field. In the end, it will be discussed the critical and SOC character of one of the most complex systems in Nature: neural networks.

6.1 Real Piles of Sand and Rice

In the quest for a theoretical model intended to reproduce certain features of a real system, a balance between simplicity in the rules and a realistic character for the model must be done, in order to obtain a simple (and theoretically tractable) but useful model.

Many simplifying assumptions make a system lose part of its applicability. For instance, even in the $p \to 0$ limit, the stochastic model of forest fires (FFM2) (see the previous chapter) has the possibility of an instantaneous creation of a tree at a site just after a fire has passed, which constitutes a very unrealistic scenario.

On the other hand, even when the theory is accepted to describe a real situation, like Directed Percolation (DP)[1], it is very difficult to find an experimental realization with which obtain a reliable measurement of its exponents. Although DP exponents were calculated decades ago by means of theoretical studies like the Renormalization Group (RG), it is only very recently that these exponents have been measured reliably and accurately enough [235].

As explained in previous chapters, the image of a sandpile was only a simple metaphor with which BTW intended to introduce in a simple way the concepts and features of SOC [1]. Thus, it can be expected for this model to be an oversimplification of real sandpiles, being many more ingredients necessary to reproduce their real behavior. Nonetheless, after the seminal work of BTW [6], many experimental groups looked for SOC in real piles.

6.1.1 Early Sandpile Experiments

The Chicago Group Experiment

In the first experiment with real sandpiles, carried out by the *Chicago Group* [236], three different experimental setups were used: a rotatory semicircular drum, an open box with sand added from the top, and a closed cylindrical drum. Instead of real sand, spherical glass beads and rough aluminum-oxide particles were used.

In the semicircular setup (see left part of Fig.6.1), an initial amount of

[1] This universality class describes the phenomenology around non-conserving absorbing states, which are ubiquitous in Nature.

particles partially filling the drum is introduced into it, and a controlled slow rotatory motion with a fixed angular velocity, started. Thus, the free surface of the pile can be tilted a certain angle at will. The behavior of the pile is characterized by means of the angle of the free surface of the pile with the horizontal (θ). If it is below a certain angle, called **angle of repose** θ_r, the pile remains as a solid (i.e. all the particles remain in their positions). When $\theta > \theta_r$, a few rearrangements take place (small avalanches); when $\theta > \theta_m > \theta_r$, avalanches spanning the whole system occur which reach the border of the drum. In such large avalanches, sand is lost at the rim, and these "grains" are measured by means of a parallel-plate capacitor, which can detect even a few "grains" falling. With the particle flow, the pile is able to dissipate at the boundary as much energy as necessary to recover a state with angle $\theta < \theta_r$.

Therefore, three different regimes can be distinguished for this pile:

i) For $\theta < \theta_r$, the particles remain at their position; no rearrangements are present (i.e. there is no activity).

ii) For $\theta_m > \theta > \theta_r$, small avalanches can take place when small variations in θ are considered. The system jumps between metastable states.

iii) For $\theta > \theta_m > \theta_r$, *any* increase in θ gives rise to avalanches as large as the system is. The pile, which behaves like a fluid, is unstable.

Therefore, the angle θ can be considered the control parameter of this experiment. With the deterministic dynamics of this experimental setup, no power laws were measured for the avalanche lifetime nor inter-avalanche-time probability distributions, and the exponent measured with the power spectra $S(f)$ (see Eq.(A.3.3)) does not coincide with the measured by BTW in their original model[2]. This system does not behave in a critical way[3]. Indeed, the system presented an oscillatory behavior, with peaks in the distributions corresponding to the largest avalanches with size of the order of the system. This means that the pile gets trapped in cycles of hysteresis connecting the

[2]Theoretical works supported that this difference stems from considering only the avalanches reaching the boundaries of the system. Indeed, the exponent predicted by simulations of the BTW sandpile considering only this kind of avalanches coincide with the measured in this experiment [237].

[3]The existence of $1/f$ noise does not imply criticality [16]; therefore, $S(f)$ is not a reliable observable to take into account in order to check the critical behavior of a system.

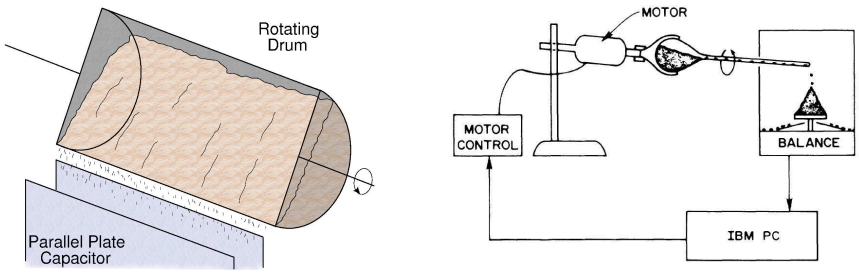

Figure 6.1: Left: Sketch of the semicircular rotatory drum of the *Chicago Group*. Right: Circular base experiment of the *IBM Group* (taken from [238]). Note that, in both cases, only avalanches reaching the border can be measured.

situations in which there is a total stability ($\theta < \theta_r$) and total instability ($\theta > \theta_m$) [236].

Critical behavior was not obtained for the open, rectangular box, with slowly added grains from the outside. And not even when mechanical vibrations were applied to both drums. When vibrations are present with zero angular velocity, their intensity acts as the control parameter, because vibrations are able to facilitate the transition from stable to unstable phase by controlling their intensity, regardless the value of θ provided $\theta > \theta_r$.

Even by using this procedure, aimed to break the hysteresis cycles, still non-critical behavior was observed. With these results, it was concluded that *real "sandpiles" are not SOC* [236].

The IBM Group Experiment

In a very different experiment, the *IBM Group* tried to check the results of the previous work by using an experimental setup more similar to the one described by BTW in their original article [238].

In this experiment, a funnel with a rotation controlled by a motor drops grains of sand or aluminum oxide particles one by one at a small zone above the center of a circular disk (see right panel of Fig.6.1). As the grains are added, the sandpile is built, acquiring a conical shape. When grains reach the border of the disk, they fall into a weighing pan connected to a computer. In this way, the addition of grains is controlled, and their boundary dissipation can be measured.

With this experimental setup, the pile, after a transient regime, achieves

a stationary state in which the total energy on the circular disk fluctuates around a fixed value. In this regime, the size distribution $P(s)$ and the power spectra $S(f)$ of the avalanches were measured. The new grains must be dropped when no one of these avalanches are in course.

One important point of this work is the *finite-size* study made in the experiment. As explained in previous chapters, the finite-size scaling (FSS) of the observables of a system is a sign of criticality. For the avalanche-related distributions, it is represented by the conditions Eq.(1.4)-Eq.(1.7). Thus, when $P(s)s^{\tau}$ versus s/L^{D_f} (where L is the system size) is represented, the resulting graph is a universal scaling function, and therefore a collapse of the plots for different sizes is expected.

In [238], many different sizes (diameter of the base) were used. For the smallest sizes, the usual stochastic-like fluctuating stationary state for the total amount of sand was measured, and power laws in both $P(s)$ and $S(f)$ were reported. In fact, the usual plot described above, with which the finite size ansatz is checked, showed a good collapse (i.e. critical behavior) for the smaller sizes. More exponents were also measured to reinforce the conclusions obtained from the FSS.

However, for larger sizes the periodic behavior observed in [236] was also noticed here. Although this behavior was tried to be controlled by means of variations in the experimental parameters (as, for instance, the height of the funnel, with which the initial kinetic energy of the pile can be controlled), the pathological relaxational oscillations exhibited by the system remained.

This behavior for a large size of the disk, preventing the system from being scale invariant, led the authors to conclude that *the presence of SOC in this experimental setup is only an effect of the finite size* of the bases, with a crossover size between the critical and the non-critical regime, whose dependence on the experimental parameters is not clear.

The Real Behavior of Real Sandpiles

As already explained, the results of this experiment indicated that the presence of power-law scaling for small avalanche sizes is just a finite-size effect [238]. In [239], it was pointed out that a certain minimum ratio 30 : 1 between the diameter of the grains (L_g) and the diameter of the base of the pile (L_p) is necessary in order to observe the oscillatory behavior. Indeed, this ratio grain/base, among others, was used in the IBM Group experiment, and the observed crossover separating stable from unstable behavior could

be the result of a change to smaller ratios.

In [240], a rotating-drum-like experiment, with a grain/container ratio larger than the 30 : 1 condition, is described. As in [236], an initial amount of "sand" (molecular sieve spheres) was introduced into the container, which can be rotated with a slow angular velocity tilting the free surface of the pile. Two different behaviors were also observed for angles $\theta < \theta_r$ and $\theta > \theta_m$.

The main difference with the previous experiments is the use of imaging techniques, which allows to measure the avalanche size of small events occurring also **into the bulk**, and not only the large ones reaching the borders. By means of these techniques, a power law behavior was reported in $P(s)$ for small sizes, and also for the dependence of the number of avalanches with the angle θ, taken here as the control parameter (with critical value θ_m). The important point of the conclusions of this experiment is that the scale-free behavior for small avalanches *did not disappear for larger system sizes*, i.e. the power law observed for small s is a characteristic of the avalanches, *not a finite-size effect*.

This is not an isolated case. In [241], an experimental setup similar to the one used by the IBM Group (see above) was used. This time, a systematic study of the effects of the ratio $L_g : L_p$ was performed. With no so large ratios as indicated in [239], a crossover between the fluctuating pattern of small systems and the oscillation pattern of large systems was found. Again, a scale-free $P(s)$ for small avalanches, obeying the FSS ansatz, and a scale-invariant power spectra, were observed. This power-law behavior remained also for large systems.

Moreover, the fraction of dissipated energy (E_{diss}/E_{tot}) in each avalanche was monitored as a function of the system size. As a result of these measurements, the explanation of the early discrepancies about the critical behavior of the sandpile experiments arises: for small system sizes, the fraction of energy carried away by small avalanches is large, because they are the only mechanism for the system to dissipate energy in order to gain stability. However, for large systems, the energy dissipated by means of these events is negligible as compared with the energy dissipated with large avalanches. Therefore, it is possible that an experimental setup prepared to detect the large avalanche sizes and durations cannot resolve such small avalanches.

The poor resolution for small events of the experiments which measured only large dissipative avalanches is the reason why the reported scale-free behavior, noticed in experiments performing a FSS study, was not observed in there.

However, the described behavior, even when scale invariance is reported for small avalanche sizes, is not the one expected for a SOC system. Moreover, in a subsequent reanalysis of the experiments, a stretched exponential behavior (for which a finite characteristic length can be defined) was reported for these real sandpiles [242]. Therefore, it can be concluded that **the real sandpiles are not SOC**.

The reason for the lack of SOC in these systems has been claimed to be **inertia** (see, for instance, [9, 16]). Unlike the ideal grains of the models, real grains have certain mass and, therefore an associated kinetic energy. As the grain advances into an avalanche event, it gains more and more inertia, which prevents it from interplaying and, therefore, from being halted by local interactions (the kinetic energy allows the grain to escape local friction forces). In this way, is inertia, and not the conservative local rules, what allows the avalanche to cover the large distances necessary to reach the borders in order to achieve a stationary state by means of the balance between driving and boundary-dissipated energy. This introduces a characteristic length which impedes the critical behavior of the system and induces the oscillatory behavior reported in experiments.

This conclusion was already checked in a sandpile model in [243], where a mechanism for grains to gain inertia is introduced. In this anisotropic model, similar to the ones studied in [53] (i.e. variations of the BTW sandpile model, see chapter 1), inertia is implemented by associating with each site a threshold which depends on the number of times the arriving grains have jumped until reaching this site. The more time the grain is in motion, the easier is that it jumps again when arrives to the next site. Large fluctuations and the break of criticality can be observed in this sandpile model.

Therefore, inertia is a drawback to observe SOC behavior in real sandpiles. In the next section, the influence of this factor will be studied by means the use of a slightly different type of grains.

6.1.2 The Oslo Ricepile Experiment

As round grains are largely affected by inertia, the simplest modification to carry out is to change the shape of these grains, in order to increase its kinetic friction and reduce inertial effects. In [57], the *Oslo Group* used three different types of **rice grains** instead:

- *Type A*, with an aspect ratio 3.8 (elongated) and a rough surface;

- *Type B*, with an aspect ratio 2 (rounded) and a smooth surface;
- *Type C*, with an aspect ratio 3.6 (elongated) and a smooth surface.

In this experimental setup, two vertical plates are placed in parallel separated by a gap of the order of magnitude of the size of a grain, with which a one-dimensional system is wanted to be imitated. Only one of the two extremal borders of this system is open. The grains (only one type of rice per experiment) are slowly added to the closed border. In this way, rice is stored into the pile; when the energy is large enough, some parts of the pile become unstable and avalanches are triggered. By means of these avalanches, some rice is able to reach the open border and can be dissipated in order to reach a stationary state in which energy input remains balanced with the dissipated energy. Imaging techniques were used in this experiment; for instance, the difference between the surface of the pile before and after an avalanche determines its size.

For grains of type A and C, a similar behavior was reported: the special shape of the elongated grains increases the number of possible stable configurations for the rice, which can get trapped more easily than the rounded rice of type B (see left part of Fig.6.2). Indeed, for the pile of elongated rice, it can be distinguished a coherent slow motion of many grains as a whole (in a solid-like motion), and the motion of rice grains which flow independently, both on the surface and even deep into the pile [59].

For elongated grains both, avalanches originated from the slide of grains on the top of the pile and from grains which make unstable the lower zones of the pile, were reported. Also, a power law behavior of the potential energy dissipated during an avalanche (i.e. its size) [57] and for the duration [59] was observed. The FSS of these observables was checked as well, for both spatial and temporal distributions, by using both types of rice grains, A and C.

However, for the rounded grains of type B, which roll instead of slide on the surface, the behavior is very different. The tendency to roll makes them gain kinetic energy, accumulating inertia which prevents local interactions from stopping the grains. Therefore, no FSS nor power laws were observed for this type of rice, but stretched-exponential-like behavior for the avalanche observables (behavior already noticed in real sandpile experiments affected by inertia, see above).

In light of these results, it was concluded that is the shape, rather than the surface properties, what determines the SOC behavior of the ricepile: the

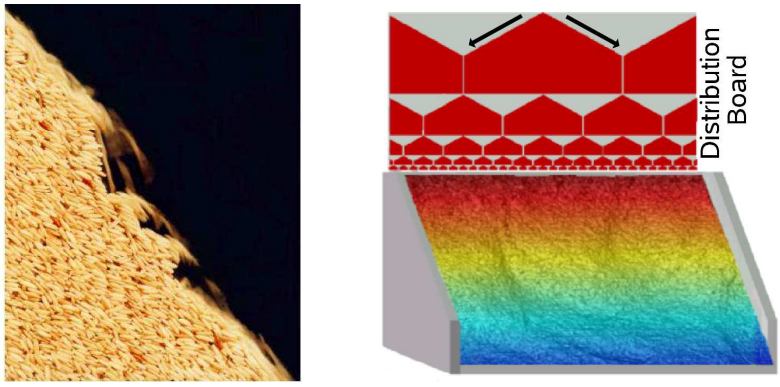

Figure 6.2: Left: Enlargement of a part of the $d = 1$ ricepile. Note that the elongated shape of the grain permits very different packaging possibilities. Taken from [59]. Right: Sketch of the experimental setup of the $d = 2$ ricepile. Taken from [181]

elongated grains are dominated by local interactions (as are the ideal grains of sandpile models) whereas, for rounded grains, inertia prevails (as happens with real sand grains). By using elongated grains, **the real ricepile can be considered a SOC system**.

As mentioned in chapter 1, in [58] was noted that a realistic model of sandpile must take into account the local variability of real systems: small differences in the shape and size of the grains, which are packed forming irregular landscapes, etc. This must be reflected by a local dynamic change of the relaxation rules, not identical and fixed for all the sites of the system.

Based on these concepts, the already studied Oslo ricepile model [59] was devised to reproduce the critical behavior observed in the above described experiment[4] by using quenched disorder for the thresholds of the system. Experimentally, quenched disorder in an otherwise ordered system has been reported to be an important factor in order to exhibit SOC behavior [244].

The $d = 2$ Ricepile Experiment

A two-dimensional version of the ricepile experiment was also performed by a different group. In [181], a $d = 2$ base with three closed boundaries (i.e. an

[4]Note that this is the only case of all the models studied in this thesis in which the theoretical model is created in order to imitate the successful critical behavior of an experiment.

open box with only one border open) was used to store *elongated* rice grains which were introduced using a distribution board (see right part of Fig.6.2).

This distribution board is devised to deliver one dropped grain to one of the 64 possible targets, uniformly distributed at the top of the pile, by means of random binary "choices" for the grain. Before the arrival of the grain at the top row of the pile, it is slowled down by means of a plastic sheet, in order to prevent the grain from acquiring a non-desired kinetic energy before entering the system. Thus, the pile grows, creating unstable zones where much energy is accumulated; in these zones, avalanches are triggered in order to dissipate the excess of activity at the only open boundary. In this way, the system reaches a stationary state due to the balance between energy inflow and outflow.

As in the original experiment of the Oslo Group, imaging techniques were used. As expected, these elongated grains allow local interactions to preveal over inertia, and scale-free behavior was reported for the measured observables.

Although in the $d = 1$ case the measured exponents did not coincide with the expected of its theoretical model (belonging to open-boundary-driven Conserved Directed Percolation, C-DP$_{abs}$, see [57, 59] and chapter 3), the improved resolution of this $d = 2$ experiment allowed to measure $\tau = 1.21(2)$ and $D_f = 1.99(2)$, which coincide with the values of the two-dimensional cellular automata (the bulk-driven Oslo model, see table 1.3 or table C.1).

Moreover, by using imaging techniques in which the distortion of a projected set of lines in the base colors allows to calculate the coordinates of the surface of the pile, the roughening exponents for this surface were measured. By using different methods, the roughening exponent α, the growth exponent β, and the dynamic exponent z, were obtained and the consistency of the results, checked. Also, by using scaling relations between roughening and avalanche exponents (see chapter 4), the measured exponents and the calculated ones coincide. This leads to the conclusion that *the roughening of the surface of the pile stems from the underlying avalanche dynamics*, as already was stated in chapter 4 for C-DP systems.

Thus, this $d = 2$ experiment confirms that, using Bak's own words, **the ricepile is the ultimate granular experiment in which SOC must be looked for** [1].

Experiments with granular systems can be also performed in the fixed-energy (FES) ensemble. Very recently [245], a sheared closed system of particles suspended in a liquid has been studied, and the critical exponents

for the experimental setup, as well as the $d = 1$ and $d = 2$ simulations of the proposed model, measured. Although the universality class is not clear yet, the basic ingredients of the system are compatible with the ones of the C-DP class.

In summary, it is very difficult to observe SOC behavior in a real granular pile; the presence of *inertia*, which breaks criticality, is a backward for this type of experiments. However, it is possible to avoid this lack of kinetic friction by using grains with a different shape: elongated grains. By eliminating inertia, the grains are dominated only by local rules, as happens in the theoretical models of SOC, and critical behavior is recovered. Moreover, for the more recent experiments of $d = 2$ ricepiles, the usual C-DP exponents have been measured.

It is possible to find real systems in which the SOC features of the piles are exhibited, but in which the "grains" are not affected by the undesired inertia. These systems will be introduced in the next section.

6.2 Superconductors in Ramping Magnetic Fields

The connection between SOC and magnetic systems has been already explored in this thesis. In chapter 4, the initial description of the elastic interfaces was made by using a domain wall into a ferromagnetic material with defects.

Related with this phenomenon is the *Barkhausen effect*, a noise produced by the dynamics of a ferromagnetic domain wall, characteristic of the burst-like behavior of such an elastic interface. The analogies are evident: the domain wall behaves like an interface externally driven, with avalanche dynamics, which reaches universal critical behavior when the limit of driving and "dissipation"(depolarizing field) are taken. *The universal mean-field exponents for the burst size and lifetime distributions have been measured in experiments* when the limit of negligible driving field and negligible depolarizing field are taken (see [246] for a review).

A few decades before the first article about SOC [6], the close relation between the phenomenology of different magnetic systems (**superconductors**) when posed into a magnetic field, and the phenomenology of grains of

sand when added to a sand hill, was pointed out [247]. This relation will be explored in the next section.

6.2.1 Superconducting Avalanches

Consider a conducting material; if it undergoes a phase transition when certain temperature T_c is reached from above, in which the electrons of the material join together in pairs called **Cooper pairs**, the material can be called a *superconductor*. Each of the Cooper pairs, as a whole, possesses an effective integer spin (unlike the half spin of the electrons separately), i.e. behaves as a *boson*. The coherent motion of these "bosonic" units provides a motion of the electrons without energy dissipation, a phenomenon which is called **superconduction**.

In the superconducting state, the material expels any magnetic field H from its bulk. However, even for $T < T_c$, there exists a critical value for the magnetic field above which the superconducting feature is destroyed. Thus, for **type-I superconductors**, above a certain H_c the material becomes a standard conductor. For **type-II superconductors**, the critical value for the standard conduction is H_{c_2}; however, for $H_{c_1} < H < H_{c_2}$ there exists a *mixed state* in which the external field H starts to penetrate into the bulk, but the system remains in its superconducting phase. The discussion will be focused on this mixed state of type-II superconductors hereinafter.

When the magnetic field exceeds the lower critical value H_{c_1}, **flux lines** are formed in the surface of the superconductor. These lines are standard-conducting-state cores surrounded by superconducting electrons which circulate around them with a nanometric radius. In this way, superconducting property starts to decrease at the border of the "orbit" of these electrons until it becomes zero at the center of such "orbit". The set of superconducting electrons circulating around a non-superconducting core is called a **vortex** (see left part of Fig.6.3). Each vortex carries a certain quantity of magnetic flux, given by $\Phi_0 = h/(2e)$, where h is Planck's constant and e is the charge of the electron; therefore the formation of such vortices allows the magnetic field to penetrate into the superconductor (see right part of Fig.6.3).

The interaction between vortices is mutually *repulsive*. Thus, when the superconductor is a perfect crystal, vortices tend to arrange by means of these forces into an hexagonal configuration. However, as pointed out in chapter 4, real materials possess defects. These inhomogeneities involve a non-conducting zone into the superconductor; as the minimum energy configu-

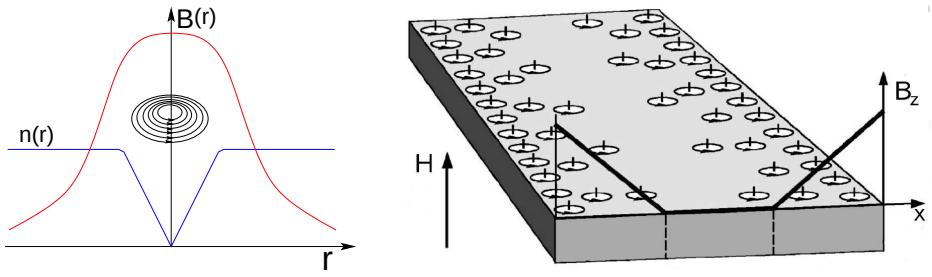

Figure 6.3: Left: Sketch of the vortices of a superconductor; the local magnetic field $B(r)$ (red line) as well as the density of superconducting electrons $n(r)$ (blue line) are depicted, as a function of the distance to the core of the vortex, r. Note that it reaches zero at the core of the vortex. Adapted from [16]. Right: Sketch of the formation of vortices in the surface of a superconductor when a external field H is applied. Adapted from [249].

ration is that in which the superconducting volume is maximized, vortices tend to be attracted by the defects, which act as *pinning centers*.

If the attractive force of the pinning center is larger than the repulsive force between flux lines, vortices can be piled up at the defects. The competition between the increasing density of vortices and the pinning forces results in the non-equilibrium critical state called the **Bean state** [248].

When a superconductor is in the Bean state, it can reach one of the many possible *metastable* states in which the magnetic and the pinning forces remain balanced. As the external field H is increased, more and more vortices accumulate at the inhomogeneities of the material; thus, when the total magnetic force at the defect overcomes the pinning force, vortices are released in a burst like event: a **vortex avalanche**, which rearranges the system in order to recover stability.

Analogies with SOC Systems

Once the Bean state and its phenomenology are defined, the analogies with sandpiles and SOC systems can be more easily understood. The behavior of a type-II superconductor in the Bean state can be interpreted:

i) As an interface: The phenomenology of the Bean state is very similar to the one described in the SOC dynamics of an interface (see section 4.2.2). The increasing external magnetic field H is like the slow-driving force, which can make the interface (the **penetrating front** of vortices

towards the bulk) leave the pinning centers to find another stable configuration. There exist also important differences, as for instance the dynamic character of the "base" of this interface: the vortices enter at the surface of the superconductor, and therefore the interface is not driven from above, but from its bottom. The "magnetic-pressure" character of the driving force is, thus, an important detail to take into account.

ii) As a vortex pile: This is the most accepted SOC image for superconductors. The presence of pinning centers allows to pile up vortices at these sites. The magnetic quanta Φ_0 associated with each vortex are the *grains* of this pile. The *height* at a site is given by the accumulated magnetic field B_z (see left part of Fig.6.4), with a *threshold* stated by the point of balance between pinning and magnetic forces. When this threshold is overcome, the vortices are redistributed and, while the magnetic field B_z decreases at the active site, increases at the new pinning sites where redistributed vortices get now trapped. This mimics the conservative relaxation rule of sandpiles. The approximate uniform distribution of the defects which can be achieved in the experiments facilitates the sandpile-like scenario. This is the image that will be used here from now on.

For both images, there exist two different time scales: the short time scale of the evolution of the vortex avalanches, during which vortices move with velocities orders of magnitude larger than when moving independently; and the large time scale of the ramping of the external magnetic field. Thus, in the Bean state, avalanches occur instantaneously in comparison with the driving time scale.

In this way, the equivalence with SOC will be completed if a scale-free behavior for avalanche-related observables can be noticed. Although many theoretical computational models have already reported such a behavior (see, for instance, [250]), there is an advantage in type-II superconductors which makes them the perfect realm where experimental realizations of SOC must be looked for: the **lack of inertia** of the vortices, stemming from the small mass and overdamped motion of such units.

On the other hand, it is necessary to pay some attention on the so-called **flux jumps**, which are thermically activated avalanches equivalent to the application of mechanical vibration in experimental sandpiles (see above). This type of avalanches are not originated by the dynamics of the system, but due to a rapid ramping of the field (i.e. a driving not slow enough)

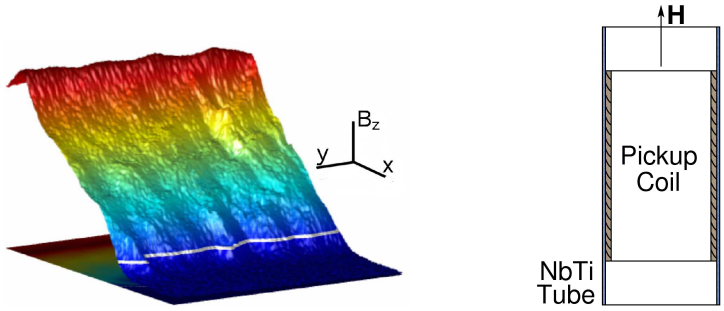

Figure 6.4: Left: Vortex density measured in a two-dimensional $YBa_2Cu_3O_{7-x}$ sample; taken from [260]. Right: Sketch of the experimental setup used in [251]. Adapted from [251].

in a superconductor with low thermal capacity and conductivity. In these avalanches, vortices are driven so fast that they dissipate energy in their motion, which increases the temperature of the sample. Due to its small thermal capacity, heat is accumulated; this produces a feedback effect in the system which tends to break the critical state. Therefore, the flux jumps are to be rejected in the discussion of the measurements in the vortex pile experiments.

6.2.2 Vortex Pile Experiments

Boundary Avalanches

The first experiment which found SOC behavior in a superconductor was described in [251]. The experimental setup is composed of a tubular superconductor (NbTi), in whose central space between the inner surfaces a copper *pickup coil* is placed (see right part of Fig.6.4). A ramping magnetic field is applied to the set, in order to produce the vortex avalanches.

As said above, each vortex possesses a quantum of flux field, Φ_0. As the field is increased in the experimental setup, more and more vortices are formed in the outer surface of the tube, penetrating into the bulk of the superconductor by means of the avalanche-like dynamics described in the previous section. Thus, the avalanches transport vortices until reaching the inner surfaces, where they enter the coil. The variation of the total flux inside the coil induces a voltage, $V = N\partial_t\Phi(t)$ (where N is the number of turns of the coil), electric pulses whose integral is proportional to the number of vortices leaving the pile. This was the only avaliable information in [251]

about the size of the avalanche ($s \propto \int V dt'$).

With this experimental setup, only a small fraction (3%) of the avalanches could be measured. However, in [251] it is argued that the most of the non-considered events are thermically activated avalanches, and therefore they are not important in the discussion of the results. In such a way, a power-law behavior was reported for the size probability distribution $P(s)$, with a non-universal exponent which varies depending on the central value of the ramping of the magnetic field. Also, a scale-free behavior was reported for the power spectra. As in sandpiles, overlapping avalanches were observed using large rates for the increasing of the external field H.

Despite the existence of non-universal behavior, this experiment can be considered the first experimental setup using superconductors in which the features of SOC were observed.

A discrepant point of view can be found in [252]. In there, a different method to measure, the *micro Hall probes*[5], was used with $YBa_2Cu_3O_{7-x}$ (YBCO) crystals. Still, only avalanches reaching the border were taken into account. The same hysteretic behavior was reported and sharply peaked avalanche distributions observed in the early sandpile experiments (see above).

Although in [252] this behavior was, in analogy with sandpiles, attributed to the inertia of the vortices, as said before this inertia is completely negligible for vortices even at such low temperatures ($< 1K$) [249]. Instead, the origin of such behavior is in the distribution of the disorder: as pointed out in [249, 253, 254], a broad distribution of low density pinning centers produces the same phenomenology reported in [252] whereas, when a high enough amount of quenched disorder is present, scale-free behavior is recovered.

Internal Avalanches

In [255], the first measurement of internal vortex avalanches was performed. In a thick Nb film, a matrix of Hall probes was used to measure local magnetizations. With this method, up to the 70% of increments in the magnetic field of the sample as small as $0.4\Phi_0$ could be resolved.

In an exhaustive sweep of a broad part of the field-temperature (H, T) space, very different behaviors were reported. For high enough temperatures, as

[5]Small sensors based on the Hall effect able today to resolve even individual vortices, but with the limitation of a small scanning area.

expected, the superconducting phase is destroyed and no avalanche-like behavior was observed. For very low temperatures and small external field, flux-jump-like (thermally activated avalanches, see above) with no critical behavior and huge catastrophic avalanches were reported.

But, for a wide part of the phase space, the increase of the field into the sample is staircase-shaped, with steps corresponding with rapid internal rearrangements into the superconductor; these avalanches were monitored, showing a wide distribution of sizes. Although the results are compatible with a power law, the falloff part of the plot does not correspond with a finite size scaling; guessing a stretched exponential shape (and therefore, a non-critical behavior for the system), in [255] the origin and meaning of such behavior remained as an open question.

The SOC Behavior of Vortex Avalanches

In [256, 257], the strongest indication of SOC behavior at superconducting materials was reported. Two-dimensional samples of $YBa_2Cu_3O_{7-x}$ and $NdGaO_3$ with uniformly distributed screw dislocations acting as pinning centers were used. Both were exposed to the influence of a slowly-increased external field H, which produces intermittent bursts into the samples.

With the high-resolution magneto-optic imaging techniques[6], the increases of the internal magnetic field ΔB_z are measured. These increases are produced by the motion and accumulation of vortices at the pinning centers (see above).

The measurements revealed a step like behavior of the response of the sample, into which stable periods are followed by sudden bursts of different sizes. The difference of the magnetic surfaces (see left part of Fig.6.5 for such a surface) gives an idea of the size of the avalanche:

$$s = \Delta\Phi = \frac{1}{2}\int |\Delta B_z(x,y)| dxdy. \tag{6.1}$$

With this definition, the avalanche size distribution measured exhibits a power law behavior with an exponent $\tau = 1.30(5)$. A direct measurement of the fractal dimension of the surface of the pile yielded the (very low) value

[6]Able to resolve not only individual vortices, but to use fields of view from a few centimeters to microns, and a time response of nanoseconds.

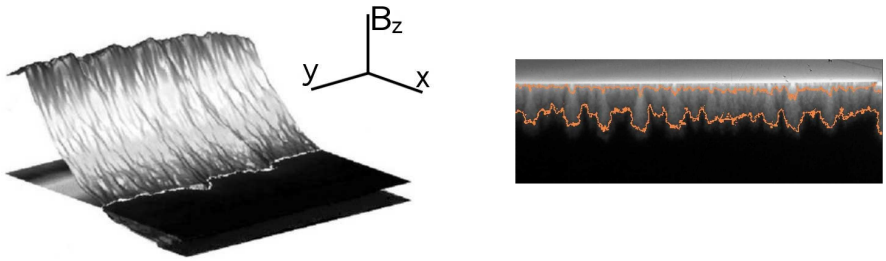

Figure 6.5: Left: Vortex density in a YBCO superconductor; both, magnetic rough surface and flux front, are depicted. Taken from [257]. Right: Flux penetration front (similar to the rough white line illustrated in the low part of the left panel) for a Nb film at two different levels of B_z (red lines); taken from [258].

$D_f = 1.92(5)$. Moreover, a *finite size scaling* study was performed.

If a system shows FSS, any part (of linear size e.g. L') of a larger system behaves like an independent system (of linear size L'). Due to this, the FSS study can be done assuming the FSS ansatz and performing the measurements by using different fields of view instead of systems of different sizes. If the universal curves of the ansatz collapse (see above), the system exhibits FSS and the assumption is justified. Using this method, in [256, 257] the exponents which produced the best collapse of the data for the different sizes of observation windows were $\tau = 1.29(2)$ and $D_f = 1.89(3)$, confirming the previous results.

Thus, for the superconductor systems studied in [256, 257], a state with self-organized metastable configurations was found. These systems changed from one of these configurations to another one by means of bursts or avalanches of all sizes whose distribution is scale free. Furthermore, the cutoff of this power law behavior depends in a non-trivial way on the system size. A priori, SOC was observed in these systems. The confirmation of this claim arrives with the study of the rough surface of the vortex pile.

Vortex Interfaces

As can be seen in Fig.6.5, as the vortices are accumulated at the pinning centers of a two-dimensional sample and the magnetic field increases, $B_z(x, y)$ forms a rough surface at the top layer at each position. In this case, this would be a $(d = 2) + 1$ interface, using the notation of chapter 4 (see left part of Fig.6.5).

Moreover, the flux penetrating front (the geometrical place of the deepest vortices into the bulk, regardless the value of the accumulated magnetic field in there) is also a rough manifold, a $(d = 1) + 1$ interface in this case (see right part of Fig.6.5). This front is the result of taking an horizontal cut at a certain value of B_z in the three-dimensional system.

In [258], the roughening properties of the penetrating front were studied in a sample of low-T_c Nb film. For this manifold, scale-free behavior was observed for the interface width (see Eq.(4.6)). Also, scale invariance for the local width, the height-height correlation function, and the power spectrum of the surface, was reported. Measurements of the Hausdorff dimension were as well performed. Together with the consistence of the measurements of the exponents by means of these different methods, two remarkable points were noticed:

- Non-universal values were measured for the different levels of B_z considered.
- There is no superroughening nor anomalous scaling (see chapter 4) in this interface.

This non-universal behavior is not observed when all the levels of the field are taken to build the $2 + 1$ interface above explained. In [259], a noise correction technique was devised with which more reliable measurements of the surface can be done. Indeed, when this technique was applied to a YBCO sample, a roughening exponent $\alpha = 0.75(6)$ and a growth exponent $\beta = 0.7(1)$ were reported, which represent a correction of a 188% and a 233% in the previously measured values, respectively (see [259] for further details).

Although the link with interfaces into quenched disordered media was already stated, only in a subsequent work [260], a correction in β allows to stablish a relation between the rough surface of the vortex pile and the $2 + 1$ interface built by using the quenched Edwards Wilkinson (qEW) equation (see chapter 4). With the new value of the growth exponent, $\beta = 0.57(6)$, the coincidence of exponents allows to classify this system into a universality class.

By comparing the set of interface critical exponents measured with the corresponding exponents of the qEW universality class (see table 4.1), in [257,260] it was claimed that the observed critical behavior of the sample under study (YBCO) *belongs to the qEW universality class*. Moreover, as the measured roughening exponents coincided with the values obtained by using scaling relations of avalanche exponents, it was stated that the surface was the result

of the underlying avalanche dynamics. Thus, by comparing the measured τ and D_f exponents with the ones illustrated in table 4.2, it is reasonable to think that the $2+1$ surface of the vortex pile belongs to the qEW (C-DP) universality class (see chapter 4).

However, the sources of experimental errors are numerous, and the prudence must refrain any attempt of classification into universality classes of these experimental systems; indeed, the actual controversy is focused on the more basic level of the existence of SOC behavior in such systems. Only if criticality is reliably stated by the experiments and universal behavior is observed, a classification into different classes will make any sense.

To summarize, when a type-II superconductor is exposed to a external slow-ramping magnetic field H, a metastable configuration of the created vortices (accumulated at the defects of the sample) is reached. This state, called the Bean state, is the result of the balance of the attractive (pinning) vortex-defect forces and the vortex-vortex repulsive forces. The slow increase of the field can originate avalanche events in which vortices are rearranged in order to achieve an energetically more favorable configuration.

The lack of inertia of vortices permits reliable experimental measurements of avalanche observables for this type of systems. By means of experimental techniques, the avalanches have been shown to be scale invariant, as well as the roughening observables associated with the "free surface" of this vortex pile. For the first time, SOC is cleanly observed in an experiment.

6.3 Existence of SOC in Neural Networks

Once reliable observations of SOC behavior have been made in real experiments (ricepiles and superconductors, see above), one question arises. Is it possible to observe SOC, as defined in the previous chapters, in more daily situations?

To answer this question, many possibilities can be considered because, as said all along this thesis, the features of SOC can be observed ubiquitously in Nature. But the results obtained in recent experiments, and the subsequent controversy generated, make **neural networks** be the perfect system with which this discussion about experimental realizations of SOC can be closed.

The brain is maybe one of the most complex systems in this world. The adaptation of each of its parts to the function that they carry out makes the brain be composed of many different sub-systems of neural networks, each of them with many different levels of organization, in which different operation mechanisms can be found.

In the case of these neural networks, it is not even clear whether they are critical, nor the implications of such behavior in the accomplishment of their functions.

However, recent experiments have claimed not only a critical behavior for neural networks, but the SOC character of such behavior. Is in these experiments in what this last section will be focused on.

6.3.1 Neuronal Avalanches

The brain is a system composed by billions of interacting units[7] called **neurons**. Each of these units can be roughly described as a central body (the *soma*) with many connections (*dendrites*) with other neurons or other cells, and a cable-like projection (the *axon*) which can extend up to tens of thousands of times the diameter of the soma in length to connect it with other neurons by means axon connections (see left panel of Fig.6.6). A set of connected neurons is called a **neural network**.

The connection between a neuron and another cell is called the **synapse**. Depending on the mechanism through which the information is transmitted between both cells, the synapse can be *electrical*, *chemical* or *immunological*. It will be more useful for the analogy with SOC to consider chemical synapses; in the case of such synapses, the dendrites consider only incoming information, while the axon connections transmit only the information output.

As commented in chapter 1, the usual image for the mechanism for a neuron to transmit information is the so-called **integration and fire** mechanism. In it, the neuron collects all the information inflow, which produces a *membrane potential* which is stored until a certain level is overcome; then, the neuron discharges this potential to the cells to which it is connected, remaining again under the firing level. This event can trigger more firings, and therefore the information can be transmitted to many different parts of the system.

[7] More than 10^{16} in the brain of children.

There are many techniques to measure the activity of the brain; maybe the best-known examples are the *electroencephalogram* (EEG) and the *magnetoencephalogram* (MEG), which are measurements of the electric and magnetic (respectively) output signal of a part of the brain. The *local-field potential* (LFP) measurements, instead, take into account the input signal (i.e. the synchronous activation) of the zone under study. Due to technical limitations, these techniques are able to measure the behavior of a (larger or smaller) group of neurons, but not of each of them individually.

Also, there are many different methods to use these techniques (on the surface of the cranium, directly applied to a zone of the brain...) and different ways in which the specimen to be studied can be obtained: the complete brain or one part of it conserved in a medium similar to the inner medium of the cranium (**in vivo** samples); or cultured set of connected neurons obtained from parts of a brain (**in vitro** samples). With in vitro samples, however, some relevant features of the intact system are lost.

As far as storage and information processing is concerned, the possibilities of one individual neuron are very limited. However, a set of neurons (i.e. a *neural network*) is able to perform very complex operations. This is an example of the emergent complexity of these systems. In the next experiment, the complexity of these networks is studied from the point of view of SOC.

The Measurement of Avalanches

In [261, 262], the relation between the brain and SOC was investigated. For this purpose, two different samples were used [261–263]:

- *Slices of rat cortex.* The brain of an anaesthetized rat is dissected and placed in a cold, oxygenated solution containing the salts and sugars of the cerebrospinal fluid. Then, it is divided into thin coronal sections (slices) large enough to allow oxygen and nutrients to diffuse into the tissue, and waste products to be eliminated. These slices can be kept alive for up to 12 hours after the dissection of the brain.

- *Organotypic cultures.* Slices prepared as described above are bathed into a culture medium with hormones and blood serum, which allows to keep alive the sample for even weeks.

For both, in vivo and in vitro samples, the zone of the somatosensory cortex was considered for measurements. LFPs of this zone were collected

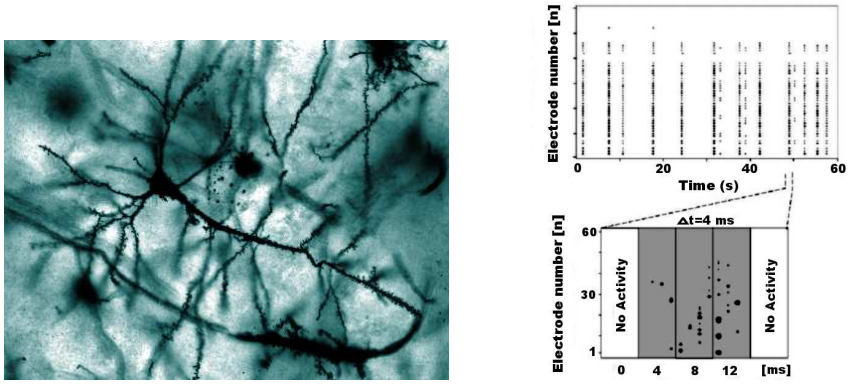

Figure 6.6: Left: Photography of a real neuron (pyramidal neuron in the hippocampus of an epileptic patient; 40 times magnification) where its parts, described in the text, are depicted. Right: Definition of a neuronal avalanche (lower panel); note that a lack of resolution (upper panel) make them go unnoticed. Taken from [261].

by means of square 8x8 electrode arrays without the corners (60 electrodes separated by a distance of 200 μm)[8]. In this way, each electrode represents a group of neurons placed around its position; thus, the results of this experiment can be posed on a *mesoscopic* level of observation.

In both types of samples, activity is not induced, but spontaneously generated due to the feeding medium in which they are immersed. When measurements of the activity of the neurons are performed, it is usual to find spatio-temporal activation patterns like the ones depicted in the upper panel of the right part of Fig.6.6. In it, the trivial pattern of the signal at the electrodes suggests that all neurons are firing in a synchronized way. Indeed, these patterns were also measured for both types of samples in [261, 262]. However, in these same experiments, temporal resolution was increased, and more complex patterns arose (see lower panel of the right part of Fig.6.6).

The new observed patterns suggest a consecutive, more than synchronized, activation of neurons, similar to a chain reaction. The set of activation events occurring between two periods of repose was in [261, 262] defined as a **neuronal avalanche**. A new way for the transmission of information in a neural network was, thus, reported. It is a natural question whether these avalanches can be related with SOC behavior.

[8]For further details of the experimental setup, see [261, 262].

Analogies with SOC Systems

The integration-and-fire mechanism of individual neurons described above (see section 6.3.1) exhibits the following characteristics [263]:

i) An accumulation period for a site during which it collects the incoming information in the form of membrane potential. Throughout this period, the site remains inactive.

ii) The existence of a threshold for the accumulated potential. Once it is overcome, the site turns into an active unit.

iii) A separation of time scales. The time between the spontaneous activation of a site (i.e. the triggering of avalanches) is of the order of tens of seconds, while the burst-propagation of activity lasts only a few milliseconds.

This mechanism, which better represents the behavior of neurons of an in vitro sample connected by chemical synapses, resembles the already studied behavior of the sites of a sandpile.

In [261–263] it was claimed that, by means of the described mechanisms, the studied neural networks were able to evolve towards a regime in which spontaneous activity allows the system to jump from one metastable state to another by means of bursts which rearrange the potential distribution of the network. In this sense, the system is self-organized. Measurements of avalanche observables were performed in order to confirm or reject a critical behavior for this system.

The SOC Behavior of Neuronal Avalanches

The relevant measured observables associated with neuronal avalanches were their size s (number of electrodes in which a signal is collected during an avalanche) and lifetime, and the duration of the repose period (inter-event interval, IEI).

A refractory period of 20 msec was considered to avoid the overlapping of events. Also, a convenient temporal binning of the data is necessary, to avoid the grouping of LFPs belonging to different avalanches. Once the binning was adjusted to be the average IEI, a universal critical behavior was observed for the probability distributions [261].

For both $P(s)$ and $P(t)$, a power-law shape with mean-field critical exponents ($\tau = 3/2$, $\tau_t = 2$) was reported. This value for the exponents is not surprising, because it is natural to find in such networks connections between neurons separated a long distance; with such connections the definition of local and global is blurred (as in small-world networks [264]), which confers the system a mean-field character.

Moreover, although a specific study of the FSS of the avalanche observables of these samples was not performed, the cutoff of the probability distributions presented a clear dependence with the maximum number of electrodes considered during the experiments; the larger the system, the higher the value of the cutoff.

Recalling that a mean-field avalanche in a sandpile can be translated into a branching process (see section 5.2), a study of the branching ratio was performed. This ratio, σ, was defined as the fraction of active electrodes in a time bin per each active electrode of the previous time bin. It was found that the value of σ measured for avalanches started from one single electrode was $\sigma = 1.04(19)$, in good agreement with the critical value $\sigma_c = 1$ of a critical branching process (see chapter 5).

In light of these evidences, more clearly exhibited for the in vitro sample (as expected, see above), the SOC character of neuronal avalanches was claimed [261, 262]. That is, it was claimed that *neural networks (or at least neural networks of certain parts of the brain) exhibit SOC behavior.*

This conclusion is robust over pharmacological variations in the medium made in the experiment, aimed to study the reaction of the network in the presence of substances which increase or decrease the excitability of the network [261]. In the presence of such extra-ingredients, the exponent of the power laws does not change, as expected, but the scale-free behavior is destroyed, indicating that the optimal excitability for the system is represented by the power-law with the mean-field exponent ($\tau = 3/2$).

The consequences of the reported critical behavior can be [261, 263]:

- A divergence in the average avalanche size, inherent of the power-law behavior of $P(s)$, implies an efficient transmission of information, due to the possibility for the information to reach any part of the system.

- A critical branching ratio implies a self-sustained activity, which as well improves the transmission of information. But also that the network is at the edge of stability, and does not suffer pathological runaways

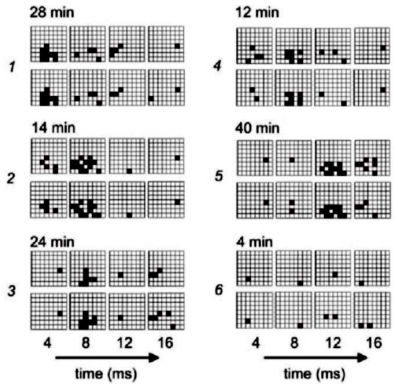

Figure 6.7: Example of recurrence patterns of avalanches; the difference in real time between the compared patterns is depicted above each pair. Taken from [262].

of activity (typical of, for instance, epileptic attacks) even under small perturbations.

Together with these important characteristics, one unexpected feature was also reported [262]: *the existence of recurrent avalanche patterns.*

By using different observables characterizing the correlation between the consecutive steps of two avalanches, in [262] it was possible to detect, in in vitro samples as the ones described above, the emergence of many different stable spatio-temporal patterns which could appear recurrently even after many hours (see Fig.6.7).

The characteristics of such patterns indicate the presence of a long-term stability and diversity necessary for the storage of information in these networks. In their critical regime, described above, the number of the patterns is maximized; the SOC state would be, therefore, a state for the most optimal performance of the neuronal network.

In conclusion, the experiments performed in [261, 262] led the authors to conclude that it is possible to find a self-organized optimal transmission and storage of information in the studied cortex neural networks; this self-sustained behavior can be the result of SOC activity avalanches taking place in the network, which also yield stable recurrent patterns.

An important discrepant result was obtained in [265], where similar measurements of cortical LFPs were made using the parietal cortex of a cat. None of the claims of [261, 262] were observed for this *in vivo* sample. Not only the observed behavior was not critical, but it was not possible even a

clear observation of avalanches[9].

As said before, in vivo samples exhibit less clearly the features of SOC; this could explain the lack of critical behavior observed. Also, as pointed out in [265], the absence of criticality could stem from the fundamental differences between the specific parts of the cortex considered (for instance, parts related with the sensorial perception are different from the association cortex).

Thus, the high complexity of the brain makes very difficult even to reproduce the same experiment. It is necessary, then, to find a very simple theoretical model able to reproduce these results by using the most simple possible ingredients of Neuroscience.

6.3.2 Theoretical Models for Neuronal Avalanches

What is exactly the origin of the scale-free behavior (if it really exists) in the case of the neural networks? A phenomenological bridge with SOC systems has been built in the previous section but a key ingredient, as conservation is, has been obviated in the discussion. Can exhibit neural networks SOC behavior in the absence of a defined conservation rule? Indeed, what are the basic ingredients to take into account in order to obtain the phenomenology observed in [261, 262]?

To answer these questions, the construction of theoretical models is very useful. As in the case of the Oslo ricepile experiment (see above), a model intended to reproduce the critical behavior of an experiment is necessary.

In the previous section, many SOC related ingredients, experimentally observed in real neural networks, have been enumerated. They are necessary ingredients for a system to exhibit SOC, and therefore they are to be present in any SOC model of neural network. However, it is not clear what kind of conservation is relevant for these systems. Moreover, the recurrent patterns described above point out the presence of a relevant underlying topology in the network. Thus, conservation and topology are the only aspects that will be discussed here [266].

[9] A different origin for the $1/f$ scaling of the power spectra was also stated; however, as said above, the presence or absence of such scaling is not necessarily a consequence of SOC [16].

The Role of Conservation in Neural Networks

In the rich behavior of the brain, some quantities are conserved, at least, on average. If such quantities were relevant for the criticality of the system, a conservation on average could be enough to observe a reasonable scale-free behavior of the measured magnitudes (see section 5.5.2).

It is well known that, in living matter, there exist many regulatory mechanisms due to which a stable environment is achieved, necessary for certain essential functions to be performed. They are called **homeostatic mechanisms**[10].

In the brain, homeostatic mechanisms are, of course, present. For instance, the learning process and memory, inherent of brain, imply structural changes between the connections in the network (**plasticity**); however, when solely implemented in a theoretical model, they make it develop stability problems. A regulatory mechanism, for instance depression and potentiation processes, prevents the real network from being unstable.

These mechanisms can bring associated a conservation, as is the case of the mentioned example, in which total synaptic weight (the strength of the connection between two neurons) is conserved [267].

However, a kind of local conservation law like the typical of sandpiles seems not to be suitable in the brain: if the neural network is identified with an electrical circuit, a perfect conduction without loss of energy is only an idealization. In the case of chemical synapses, also there exist dissipative phenomena like the **leakage**, a loss of potential into the neuron due to the deviation of the cations responsible of the conduction to different channels (leak channels). **A local conservative rule is not realistic for this system**.

Locally Conserved Models

Of course, when local conservation is implemented in a neural system which captures the rest of essential ingredients of SOC, criticality is recovered. In this section, one illustrative example is presented.

In [268], Arcangelis et al. consider a square lattice of neurons connected

[10] A trivial example of homeostatic mechanism is sweating, with which endothermic animals prevent the organism from getting too hot.

by means of *electrical synapses*. A threshold V_{max} is defined for the potential V_i accumulated at any site i. An external driving is imposed and, once the threshold is overcome, an avalanche is triggered. During the relaxation events, the potential of active sites is exactly redistributed only among the neighbors to which it can flows (i.e. a positive electrical current between them can be defined) according to certain synaptic weights, which are also updated. When no more active sites remain in the system, the driving mechanism is again switched on. Thus, the dynamics is as follows:

- Initial activity is obtained by raising the potential of a site up to the threshold level. An avalanche is, thus, started.
- For any active site (i.e. $V_i \geq V_{max}$), V_i is proportionally distributed only between neighbors fulfilling $V_j < V_i$ (i.e. with a positive electrical current $I_{i,j}$ flowing from site i to site j). The fraction received by each site is weighted by the strength of the synapse $g_{i,j}$ (or *conductance*).
- After the firing of a site, the conductance of all the synapses of the active neuron is updated in a quantity $\alpha_g \ I_{i,j}$. As the sign of the increase depends on the sign of the current, active unions are reinforced while passive unions are, in the end, pruned (*plasticity*).
- The two previous steps are repeated for any new active site into the system until there are no more active neurons. Then, a *regulatory reduction* of all the conductances is made.
- After the regulation, a new driving step is performed.

With this dynamics, in the end, a stationary state is achieved. In it, and in the presence of rewiring mechanisms which facilitate a small-world character for the network, the numerically-measured exponent for the avalanche size distribution is the expected $\tau = 3/2$ when a random site is chosen for driving events [268]. Also, scale-free behavior for the power spectra is reported.

However, two important **unrealistic assumptions** have been done in order to obtain this behavior:

i) A local conservation rule for the redistribution of the potential of active sites.

ii) A regulatory mechanism for the conductances imposed "by hand" which needs of a fine tuning of α_g in order to obtain the reported critical behavior. Indeed, α_{g_c} changes with the set of parameters considered.

The control-parameter character of α_g is even clearer when leakage is switched on by means of the equation:

$$\frac{dV_i(t)}{dt} = -\gamma V_i(t). \tag{6.2}$$

In such a case, to maintain the scale-free shape of the power spectra, α_g must be increased one order of magnitude for the case illustrated in [268] ($\gamma = 0.01$). These values correspond to a strong regulatory process for the conductances, similar to the repoblation mechanism studied in the previous chapter, which is able to bring the dynamics to a pseudo-critical state.

In conclusion, the neural network model of Arcangelis et al. achieves criticality by means of somehow unrealistic regulatory mechanisms and local conservation rules which, when broken, need from a strong regulation mechanism to be compensated.

The Repoblation Mechanism in Neural Networks

When realistic *leaking neurons* are considered, local conservation does not hold anymore. Then, it is possible to use mechanisms which compensate in any way the loss of potential.

In [269], the background dynamics already used in the SOBP-BD model (see [231] and the previous chapter) is applied to neural networks. In this adaptation of that model, the neuron can be at one of these three possible states: *i)* dormant state, *ii)* threshold state, and *iii)* excited state, which correspond with the refractory, quiescent and excited states defined in [231].

In the course of an avalanche (see chapter 5 for further details of the rules), part of the information can be lost. Thus, when no more excited sites remain in the system, a compensation mechanism is turned on by means of which some dormant neurons are transformed into threshold neurons and viceversa, with an associated probability. With a convenient tuning of these probabilities, the background of potential is effectively increased to compensate the dissipation.

The background dynamics, which represents fluctuations in the membrane potentials of the neurons, makes the system reach the SOC state for finite values of the system size. But, as in the SOBP-BD (see chapter 5 and [232]), for the sizes with which critical behavior is observed, the effect of dissipation is already negligible. Moreover, the only way to reach this state is by means of

a fine-tuning of the background probabilities. Therefore, this system cannot be SOC in the presence of leakage.

As already explained in the previous chapter, when bulk dissipation (i.e. leakage) is considered, the only way to recover a reasonable SOC stationary state is by means of a compensation mechanism present *during* the course of avalanches, not only between them.

This concept can summarize the mechanisms acting in the model proposed by Levina et al. in [270]. It is based on the model of chemical synapses of Markram and Tsodyks (MT) [271], which considers three variables with which the dynamics of the synapse can be modeled: the potential of each neuron (V_i); the number of neurotransmitters[11] avaliable at the presynaptic neuron j ($J_{i,j}$); and the fraction of such particles to be used for the transmission of the information ($u_{i,j}$).

In a previous adaptation of the model [272], one equation was proposed for each of these three variables, as in the original MT model. The evolution of $u_{i,j}$ entails a potentiation of the transmission (**facilitation**), while the evolution of $J_{i,j}$ contributes to its weakness (**depression**). In this way, the competition between both mechanisms was argued to drive the system towards a self-organized stationary state: when a neuron fires many times, the number of used neurotransmitters increases, which makes decrease the number of neurotransmitters avaliable; on the other hand, when there are no more neurotransmitters avaliable, the neuron must remain inactive and the amount of such proteins increases again. In spite of this regulatory process, in [272] the presence of a standard critical point makes this system not able to be SOC.

However, in [270], Levina et al. perform one simplification in the previous model: the fraction of used neurotransmitters remains constant ($u_{i,j} = u$). Thus, together with the dynamics for the membrane potential, only the depression mechanism is taken into account.

Consider a fully connected network of N neurons. Each neuron is characterized by a membrane potential $0 < V_i(t) < V_{max}$. There exists an external input which applies a current I^{ext} to a randomly selected neuron $\zeta_h(t)$ with a rate h. As time goes on, neurons integrate these external signals until, at one of them, a threshold V_{max} is overcome. Then, this neuron i fires,

[11] Proteins and other chemicals which are stored in vesicles in the synapse. Due to the presence of them in the synaptic gap, the pulse of information is transmitted from the presynaptic to the postsynaptic neuron.

redistributing *part* of its potential among the rest of the system, and it turns to the value $V_i(t_{sp}^+) \rightarrow V_i(t_{sp}^-) - V_{max}$, where t_{sp} is the firing (or spiking) time. Consequently, the number of neurotransmitters of the active sites of the lattice decreases. Also, the membrane potential of all sites of the lattice is affected: the activity of a site makes it decrease, but the potential at the neighbors of such an active site increases. The set of temporal steps during which the system remains active, starting from an initial activation due to the external driving, constitutes an avalanche. After an initial transient level, a stationary state for both V_i and $J_{i,j}$ is achieved.

In a summarized way, the equations which represent the explained dynamics are:

$$\begin{cases} \partial_t V_i = & \delta_{i,\zeta_h(t)} I^{ext} + \dfrac{1}{N} \displaystyle\sum_{j=1}^{N} u J_{i,j} \delta(t - t_{sp}^j - t_d) \\ \partial_t J_{i,j} = & \dfrac{1}{t_J} \left(\dfrac{\alpha_J}{u} - J_{i,j} \right) - u J_{i,j} \delta(t - t_{sp}^j). \end{cases} \tag{6.3}$$

Now, each term will be briefly explained.

a) Equation for the membrane potential V_i: The two terms at the r.h.s. in the upper line of Eqs.(6.3) correspond to (from left to right):

i) The external driving. Only when the site i is randomly selected, the external input I^{ext} is applied to this site.

ii) The result of the firing of the neighbors. Each time a neuron j fires ($t = t_{sp}^j$), and if $t_d \ll h$ (the separation of time scales is fulfilled), the potential is increased a quantity $uJ_{i,j}/N$ at site i.

In addition, an extra term $-V_{max}\delta(t - t_{sp}^i - t_d)$ must be added to the evolution of the potential. It takes into account the reduction of potential at site i due to its relaxation.

b) Equation for the avaliable neurotransmitters $J_{i,j}$: The terms at the r.h.s. in the lower row of Eqs.(6.3) correspond to (from left to right):

i) The recovery of the number of neurotransmitters. Each time, the amount of neurotransmitters at each synapse increases; in the absence of more terms, the maximum level given by α_J/u is achieved. The

time scale for such recovery is given by the product $t_J = \nu h N$, where $1 < \nu \ll N$ and t_J is called the recovery time.

ii) The use of neurotransmitters. Each time the neuron fires, the amount of avaliable neurotransmitters is decreased in $uJ_{i,j}$.

Concerning the similarities with sandpiles, the membrane potential in this model can be seen as the energy stored at each site of a fully connected pile. The external pulses I^{ext} are the driving grains. Thus, the first row of Eqs.(6.3), with the additional term proposed above, can be seen as a sort of regularized[12] equation for the relaxation rules of the pile, with non-conservative dynamics. Only in the limit in which $uJ_{i,j} = V_{max}\ \forall(i,j)$, conservation is recovered (see below).

The equation for $J_{i,j}$ represents in a certain way the repoblation mechanism explained in the previous chapter. When the recovery level given by α_J/u is large enough, a certain degree of compensation is achieved. Now, two important questions arise [266].

i) Which is the stationary value of $\langle J_{i,j}\rangle$ necessary for the system to be critical? In [270], a study of the static limit (i.e. $J_{i,j}$ fixed for all the synapses) is made. First, the set of parameters $u, t_d, t_J, N \ldots$ is chosen; concretely for the threshold, $V_{max} = 1$. By fixing $J_{i,j} = \alpha_{0_J}/u\ \forall(i,j)$, the parameter α_{0_J} is fine-tuned until criticality is obtained. The value at which criticality is recovered for any size N is $\alpha_{0_J} \sim 0.95 \sim V_{max}$. For this value, the amount of potential *transmitted to the neighbors* during a firing is $\sum_j uJ_{i,j}/N \sim V_{max}(N-1)/N \sim V_{max}$ for large N. As the site is decreased to $V_i \to V_i - V_{max}$ after the relaxation, it can be affirmed that the critical point for the static case corresponds to the conservation limit. However, due to the lack of dissipation in the limit of exact conservation[13], the critical point for a finite system is always situated below the $\alpha_{0_J} = V_{max}$ critical value to ensure the existence of a stationary state [266].

ii) Is criticality obtained if the dynamics situates $J_{i,j}$ around this α_{0_J}/u critical value on average? Although the answer to this question is "yes", these evolution equations are not able to achieve such a stationary state (see Eqs.(6.3)). There are two important reasons:

1.- *First*, even considering the fine-tuning of α_J to α_{0_J}, the reach of the conservation limit is always impeded by the depression term associated

[12] Because of the presence of a unique time scale, see chapter 2.

[13] Note that there are no boundaries in this system.

with activity (negative term in $\partial_t J_{i,j}$, see Eqs.(6.3)); only in the absence of activity (or in the static limit), this value could be reached.

2.- *Second*, the presence of a recovery time scale makes, for a certain time, the dynamics subcritical (nonconservative; see chapter 5), and therefore prevents the system from reaching the stationary critical value. Even if α_J is fine tuned to a supercritical value $\alpha_J > \alpha_{0_J}$ in order to compensate dissipation, only when $\nu t_J N \sim 1$ (which implies an unphysical instantaneous recovery for neurotransmitters), criticality could be reached.

Within this scenario, the possibility for this system to exhibit SOC behavior can be rejected. Only when the system is fine-tuned to the unrealistic conservative level in the static, not-self-organized case, a true scale invariance can be observed. Or, by considering the dynamics described by the second equation of Eqs.(6.3), only the unphysical limit of instantaneous recovery together with a fine-tuning of α_J, could make the system reach its critical stationary state.

With the same arguments of a fine-tuning to reach conservation, the more realistic equation with a leaking term for the membrane potential proposed in [270] can be argued not to be SOC [266].

In [270], Levina et al. also claim that any $\alpha_J \geq 1$ ($\alpha_J \geq V_{max}$, indeed), in the thermodynamic limit $N \to \infty$, drives the system to a true SOC state. This result is correct only when two assumptions are made: $I^{ext} \sim N^{-w}$, with $w > 0$, and the average value of the interevent interval IEI$\sim N$. Although it is reasonable to think that, in the thermodynamic limit ($N \to \infty$), the external input represents a negligible quantity for the average potential of the system, and in consequence the IEI also diverges, here the assumption is stronger: they must scale in a specific way with the size of the system. This, which represents a fine-tuning analogous to the double separation of scales of the stochastic forest fire model (see the previous chapter), constitutes a very artificial situation in which many of the units of the neural network remain inactive during large periods of time.

Moreover, this condition seems not to have been applied in the simulations presented in [270], aimed to prove the SOC behavior of the system, where I^{ext} seems to be fixed regardless the system size. Also, the SOC behavior is argued by using a rather arbitrary parameter as is the "deviation from power-law behavior".

In summary, **none of the variations of the MT model** made in [270]

or [272] **are true SOC systems**. The only way in which criticality is recovered is, again (see above and chapter 5), by means of a fine-tuning to the unrealistic conservation limit or double separation of scales; or by means of a fine-tuning to a supercritical value together with the unphysical limit of instantaneous recovery for neurotransmitters.

The Origin of the Scale Invariance in Neural Networks

In light of the results obtained in the previously discussed models it seems clear that, as expected, a system with the basic ingredients of SOC needs of conservation to be critical (see chapter 5). Thus, as local dissipation must be considered for a model of neural network to be realistic, it is necessary to look for the path to criticality by means of another self-organization mechanism different from SOC.

Recall that the ultimate aim of this discussion about neural network models is to obtain one with which the critical features observed in [261, 262] can be observed. So far, the discussion has been focused on the scale-free behavior. But now, it turns to the feature of the recurrence patterns.

The existence of such patterns implies a non-trivial underlying topology for the network; this is a consequence of the learning process in which some synapses are reinforced and others are pruned (i.e. of plasticity). The missing ingredient can be a non-trivial topology for the network able to induce scale-free behavior.

As Grinstein et al. argued in [274], the hierarchical structure of a scale-free network (a network whose node degree distribution follows a power law [264]) can induce, in a non-critical system, a scale free behavior in quantities related with the spreading of an initial seed of activity (i.e. avalanches).

This is due to the presence of large **hubs**, sites which are connected to many nodes at once. Thus, if activity reaches a node with low connectivity, the avalanche is small; and if it hits one of these hubs, the avalanche is large even with only one step of surviving activity. Therefore, avalanches of all sizes are possible in such networks, with a duration which depends on the distance to criticality for the system.

However, observables like $P(s)$ are shown in [274] to inherit the same scale-free behavior exponent of the topology. If this hypothesis is applied to the measurements of [261, 262], the value $\tau = 3/2$ found is, then, explained by *i)* an underlying scale-free topology for the networks, with an identical

degree distribution of exponent 3/2; or *ii)* the topology presents features of small-world networks (see above).

Although work is still in process [266], it is reasonable to think that it is possible to find in the highly heterogeneous structure of the neural networks of the brain a *mixed scale-free network with some subtle small-world characteristics*. This would explain the recurrent patterns and scale-invariant behavior (due to the scale-free network) and the mean-field values (small-world network, which induces a mean-field behavior). Also, the short duration of the avalanches would be explained due to the lack of criticality because of the existence of leakage (i.e. the deviation from conservation). And the lack of scale-free behavior observed in other parts of the brain, that would stem from underlying structural differences.

A model of non-conservative neural networks with the above defined underlying topology, thus, would embrace all the properties observed in the experiments here mentioned [261–263, 265] and would represent a theoretical model with a realistic mechanism for a non-conservative system to reach scale-free behavior in the absence of criticality [266]. But, as long as these statements are conveniently proved, this remains as an open question.

6.4 Concluding Remarks

With the study of theoretical models, SOC can be characterized and its universal features, distinguished. In this way, the relevant universality classes can be identified, and even mesoscopic descriptions for such classes can be found.

However, direct experimental realizations of SOC are very elusive. In real life, together with the usual features of SOC, additional phenomenology can be present.

For the archetypical example of real sandpiles, the inertia of the grains makes large avalanches present an oscillatory relaxation behavior. Only small avalanches, for which this effect is not so pronounced, exhibit scale-free behavior.

This lack of kinetic friction can be circumvented in two ways:

- By using elongated grains (rice grains) with which the friction is increased, allowing the local forces to dominate over inertia.

- By using inertia-free grains, i.e. exploring the realm of superconducting avalanches.

In both examples, experiments have been performed and clean power-laws have been reported. Therefore, the only backward of granular systems which prevents them from being the perfect real systems where SOC must be looked for is the presence of inertia.

In other kind of systems, like neural networks, although some basic ingredients of SOC are present, the lack of one of the necessary ingredients (conservation), avoid the development of critical behavior by means of SOC. The measured scale invariance of some parts of the brain must stem from different mechanisms (as, for instance, a nontrivial underlying topology).

Despite the difficulty of a reliable measurement of its critical observables, the features of SOC can be observed in Nature, as are the systems with absorbing states. However, as stated in this chapter, the fragility of some of its ingredients reduces the extremely wide range of applicability suggested at first moment by BTW.

But, still, one cannot help to be fascinated with how the mechanisms typical of the SOC theory are used by Nature, in a great or lesser extent, to build and keep in balance the world in which we live.

Chapter 7

Conclusions

The Foundations of SOC

Self-Organized Criticality (SOC) is a term coined by Bak, Tang and Wiesenfeld (BTW) aimed to explain the ubiquity of scale invariance observed in Nature. This scale-free behavior (assumed to be a sign of criticality) would be the result of a common generic mechanism, present in all dynamical systems with many interacting degrees of freedom (which Nature is plagued of).

Today, it is well-known that not all the observed scale-free behavior is caused by emergent criticality, but there are many other mechanisms which can generate scale invariance out of criticality.

However, there still are many other systems in which the general features of SOC are present. Concretely, the basic ingredients reported to be essential for SOC are:

- A slow accumulation of a physical quantity (stress, energy, magnetic field, ...). We use here energy for the sake of simplicity.
- A threshold for this energy defined for each of the interacting individuals.
- A conservative rule for redistribution of energy when the threshold is exceeded.
- A rapid (as compared with the accumulation time scale) relaxation of all the sites above threshold.

- Dissipation of energy only possible at the limits of the (finite) system.

These characteristics can be observed in many different systems, from earthquakes to type-II superconductors. The five points commented above give rise to **metastability** and **infinite separation of time-scales** which, together with **conservation**, define the basic ingredients for a system to display SOC.

The behavior of a system with these ingredients is dominated by a burst-like dynamics in which individual avalanches can be defined. By means of these avalanches, the dynamic parameter of the system (in this case, energy), is driven towards a stationary state in which it is maintained around a specific value. Below this value, avalanches can spread their activity only up to a finite distance of the initial seed. Above this value, in the thermodynamic limit, the activity (and, therefore, the avalanche) never dies. Therefore, the above mentioned value is the *critical value* for the **control parameter**, and the activity of an avalanche is the **order parameter** of the system.

Thus, the observables which can be defined in the avalanche (for instance, the avalanche-size/duration probability distributions) follow a power law only limited by the finite size of the system, which introduces a **cutoff** in the spreading of the activity. Systems with a common set of the critical exponents measured from these power laws can be grouped into **universality classes**.

Many different theoretical models, as for instance the archetypical sandpile models, are defined in order to deeply study this behavior. These models allow to identify not only the conditions under which SOC can be expected, but also the basic ingredients defining each universality class.

Therefore, a SOC system can be considered a system out of equilibrium whose dynamics makes it achieve a stationary state in which its control parameter is maintained around the critical point of a second-order phase transition and the relevant observables show scale-free behavior.

SOC as a Second-Order Phase Transition

The phase transition undergone by a SOC system is what is known as an **absorbing state phase transition**, because the critical point separates an overcritical phase, with an ever-lasting activity spreading, and a subcritical phase, in which the system gets trapped once it is reached (**absorbing phase**). Moreover, an avalanche is just an event in which an initial seed of activity is posed into an otherwise absorbing state, and activity-spanning related observables are measured. That is, it is equivalent to the spreading

experiments which are usually performed in absorbing state systems.

Although the paradigmatic universality class of systems with absorbing states is the so-called **Directed Percolation** (DP) class, the conservation present in SOC systems prevents them from showing the same critical behavior defined by this class.

Two different universality classes are usually distinguished in conservative SOC theoretical models:

- The universality class of systems with deterministic relaxation rules (deterministic -or BTW- sandpile class).
- The universality class of systems with stochastic relaxation rules (stochastic -or Manna- sandpile class).

Concretely, when the basic ingredients of the latter are identified, two different main fields can be defined: *i)* an *activity field*, whose evolution is very similar to the one of the order parameter of DP, but which is coupled to *ii)* a *conserved background field* (equivalent to the microscopic sand grains under threshold), whose value defines whether a site is active or not.

With these fields, it is possible to construct a mesoscopic representation for the mentioned universality class. As a previous step, it is necessary to perform a **regularization** procedure of the dynamics, after which only one time scale and translational invariance are present in the system. To this end, the slow-driving is forbidden, and the open boundaries are replaced by periodic boundary conditions. In this way, energy is locally and globally strictly conserved, and the **Fixed-Energy Sandpile** (FES) ensemble is defined.

In this FES ensemble, SOC turns into a standard second order phase transition between a state with non-zero activity and a state with no activity (the absorbing state), in which energy acts as the tuning control parameter, not self-organized anymore.

By using the two fields above-defined and the FES ensemble, the mesoscopic equation which represents to this class can be written as:

$$\begin{cases} \partial_t \rho = & D_\rho \nabla^2 \rho + \mu\rho - \lambda\rho^2 + \omega\rho E + \sigma\sqrt{\rho}\eta(\vec{x},t) \\ \partial_t E = & D_E \nabla^2 \rho, \end{cases} \tag{7.1}$$

where ρ and E are the above-mentioned activity and background fields, respectively, η is a Gaussian white noise and the rest of parameters are constants. The form of the noise is caused by the Poissonian distribution of the

number of microscopic creation and annihilation events which, at a mesoscopic level, is translated into a Gaussian noise with variance proportional to the mean rate of the process (i.e. the activity).

This set of Langevin equations defines a system with an infinite number of absorbing states (states with $\rho = 0$, in which there is no evolution of any of the fields); the evolution of the activity field is, as commented above, very similar to the one of DP, but it is also coupled to a conserved field, whose diffusion (as usual in sandpiles) is limited to the propagation of avalanches. Therefore, the class of the microscopic stochastic sandpiles can be, attending to its mesoscopic characteristics, called **Conserved Directed Percolation** (C-DP) universality class.

Comparison of DP and C-DP Classes

Although DP and C-DP classes are conceptually very different, the closeness of the critical exponents which define both classes (see appendix C) makes, sometimes, difficult to distinguish the true universal behavior of systems with long transients present in the observables.

However, the different response of both classes to the presence of certain perturbations can be useful to discern the universality class of such systems.

It is well known that DP systems are Galilean-invariant, i.e. their critical behavior is not changed when **anisotropy** is present in the dynamics. A preferred direction leaves the critical exponents unchanged, in this case.

On the other hand, anisotropy constitutes a relevant perturbation for the C-DP universality class which, in the presence of such a new ingredient, is transformed into a new universality class, called anisotropic C-DP (A-C-DP) class. This different behavior can be used as a discrimination criterium.

When a surface (for instance, **absorbing** or **reflecting**) is introduced into a DP system next to the seed of activity, whereas bulk properties (properties which are not related with the surviving probability) does not suffer any change and no structure can be observed in the background field, the rest of observables change dramatically. This phenomenology, called surface DP (S-DP) here, is very different from the observed in the case of C-DP systems.

For C-DP systems in the presence of a reflecting wall, although a defined structured landscape is present, all the observables remain as in the surface-free (bulk-driven) case. On the opposite, when an absorbing surface is introduced, not only a structured background arises, but the non-bulk exponents

change as well. Therefore, in the case of C-DP, two different phenomenologies can be observed: C-DP$_{ref}$ (where the critical exponents are identical to bulk-driven C-DP) and C-DP$_{abs}$.

In all the cases, the response of a C-DP system to the presence of a wall clearly distinguishes it from a DP system. Thus, this can be also used as a discrimination criterium.

By using the explained different reactions of DP and C-DP systems to such perturbations, a method to distinguish quantitatively both classes in controversial systems can be defined:

1.- Measure the critical exponents of the isotropic, bulk-driven (or surface-free) system, in the large-time/large-size regime.

2.- Introduce a reflecting wall at one boundary next to the site for the driving events or initial seeds of spreading experiments. If the exponents change, the system belongs to the DP class. In contrast, if it does not alter its critical behavior, the system belongs to the C-DP class.

3.- Change this wall by an absorbing surface. If the exponents change with respect to the isotropic case, and coincide with the ones measured in the previous step, the system belongs to the DP class. In contrast, if they are different from those of any of the above described points, the system belongs to the C-DP class.

4.- Define a preferred direction (anisotropy) for the dynamics. If the measured critical exponents do not vary, the system belongs to the DP class. On the contrary, if they change to the ones of the A-C-DP class, it belongs to the C-DP universality class.

SOC and Elastic Interfaces

It is possible to relate the features of the phase transition present in elastic interfaces into random media, with the absorbing state phase transition of the FES ensemble.

The evolution of elastic manifolds into random media is represented by the **quenched Edwards-Wilkinson** (qEW) equation, which defines the qEW universality class, also called linear interface model (LIM) class.

This equation describes the evolution of systems which undergo a continuous phase transition between an active (interface propagation velocity $v \neq 0$)

and an absorbing ($v = 0$) phase, with a critical value for the external force, which acts as the control parameter of the transition.

Moreover, a conserved background field (the sum of the deterministic forces present in the system) can be defined, and when the boundaries of the system are open, an avalanche-like behavior can be observed if the external force is slowly increased. Eventually, a scale invariant stationary state is reached.

Therefore, not only both FES and SOC ensembles can be recognized in the LIM class, but also the same symmetries and ingredients. Thus, for the LIM class, the same critical exponents of C-DP are measured, stating that linear elastic interfaces into random media and stochastic sandpiles are just two different realizations of the same underlying phenomenon: SOC.

Indeed, it is possible to express the dynamics of a microscopic stochastic sandpile by means of the qEW equation and, conversely, to map the microscopic dynamics of a LIM interface into the C-DP set of Langevin equations.

That both classes represent the same phenomenology can be also shown by directly measuring some functions related with the renormalized (mesoscopic) form of the microscopic random pinning potential. The mesoscopic shape of the potential is the responsible for the burst-like behavior of LIM systems and, therefore, the measured functions must coincide with the C-DP ones.

The spectacular collapse of the functions measured for the qEW equation, microscopic LIM systems and both micro and mesoscopic C-DP examples confirms that LIM and C-DP share the same underlying physics, and therefore are two equivalent languages with which SOC can be described.

The Role of Conservation in SOC

Although conservation has been presented here as a necessary (and sufficient) condition for SOC, there are many non-conservative theoretical models claimed to exhibit it. Moreover, many important examples of SOC in Nature, as for instance earthquakes, are intrinsically non-conserved.

It is necessary to distinguish two different types of conservation: global and local.

- **Global conservation** is that of the FES ensemble, in which energy cannot be lost nor introduced into the system. This type of conservation can be violated on average and criticality still be kept. This is the case of the SOC ensemble, in which the global level of energy is

maintained fluctuating around its critical value.

- **Local conservation** is present in what is defined here as *conserved systems*. Local conservation is fulfilled when the redistribution rules are strictly conservative. This is the conservation claimed to be necessary in order to keep the critical behavior of a SOC system.

When local conservation is present in a SOC system, the only way to dissipate incoming energy, in order to keep the stationary state, is by means of arbitrary large avalanches. Thus, any increase of energy due to the random deposition of an amount of extra energy during the driving process can reach the boundaries. As large dissipation of energy is rarely necessary (compared with small dissipations), a power law shape for, say the avalanche-size distribution, is expected.

However, if local dissipation is present, it is not necessary to reach the borders in order to achieve the stationary state and, therefore, large avalanches are not present anymore. This introduces a relevant characteristic length into the system, a cutoff for the scale-invariant behavior of the observables. Thus, although the system still self-organizes to a stationary state, such state is not critical anymore, but *subcritical*.

This heuristic argument illustrates the observed subcritical behavior for locally-dissipative systems. However, in order to compensate the energy lost during the avalanches, a **background dynamics** can be defined.

If this dynamics is implemented between avalanches, the only change in the system is in the initial conditions, but the evolution of the avalanche remains subcritical. This dynamics must be introduced in the course of the avalanches.

Of course, no extra activity can be created by means of the background dynamics, because it would introduce an extra characteristic length. The only way in which this mechanism can be used to recover a quasi-critical evolution is by defining an **on-average**-locally-conservative propagation for the avalanche. With this kind of propagation, it is possible to control how far to the true critical (strictly conserved) state the system is.

Thus, although true criticality is only reached by means of strict local conservation, "local conservation on average" constitutes the only way in which this condition can be relaxed without losing a reasonable large power-law regime for the observables.

SOC in Real Life

Although many theoretical models can be defined to study SOC, the real experiments in which the critical observables of SOC can be reliably measured are not so numerous.

The reason why this happens is that, in real systems, it is usual to find not only the ingredients of SOC, but also extra ingredients which can blur the scale invariance of the observables.

This is the case of the paradigmatic example of SOC, the sandpiles, which in real experiments are affected by *inertia*, which introduces a characteristic length impeding the measurement of power laws for any of the observables.

Inertia can be prevented in granular systems by using elongated *grains of rice* instead of rounded grains. It can also be avoided by using a different type of systems: *type-II superconductors*. When the latter are posed into an external magnetic field H, vortices are created on the surface of the sample and penetrate into its bulk. These vortices carry a quantum of magnetic field which can be considered an inertial-free grain for this new kind of pile, in which internal magnetic field B is stored and **superconducting avalanches** can be defined. The front of penetrating vortices can also be seen as an interface, which evolves by means of bursts of activity.

For both, ricepiles and type-II superconductors, experiments have been performed and clean power-laws has been measured. These examples constitute the best reported experimental realization of SOC up to the date.

In systems like neural networks, scale-free avalanches have been also observed. Although some of the necessary ingredients of SOC are present, the lack of conservation prevents SOC from being the underlying mechanism responsible for the scale invariance. Instead, other factors, as for instance the topology of the network, can originate this non-critical but still power-law like propagation of activity.

SOC is not, as expected at first moment, a general theory to explain the ubiquitous emergence of scale invariance in real systems. As stated in the last example, not all the scale invariance in Nature is even a sign of criticality. But still exist many different systems in which the catastrophic-like behavior of SOC systems can be observed. The accumulated knowledge about this theory allows to predict under which conditions these systems will exhibit true scale invariance. Even so, it is still far a complete understanding of the point up to which SOC is involved in the processes observed in Nature.

Appendix A

Basic Concepts

In this first appendix, some basic concepts concerning phase transitions are explained. This section is an essential part in this thesis, intended to be absolutely self-sufficient. All these definitions can be found in most of books about Statistical Physics, for instance [A1, A2, A3, A4].

A.1 Phase Transitions

A system undergoes a **phase transition** when it suffers a qualitative change in some thermodynamic magnitudes as the result of the variation of one characteristic parameter of the system. In this way, we can use the reaction of some observables to the tuning of some parameters to detect when the system changes from one phase to another. Conceptually, it is usual to think in a phase transition as a change from order to disorder (or viceversa).

The parameter whose variation induces the phase transition is the so-called **control parameter**. One system can suffer many different transitions, and there is one control parameter associated with each of them. Likewise, there is at least one observable whose behavior, when the control parameter varies, is indicative of the existence of a phase change. It is the **order parameter**. Depending on the behavior of the order parameter, the phase transitions are classified into two families.

A.1.1 First Order Phase Transitions

If the order parameter has a discontinuous dependence on the control parameter, the phase transition is called discontinuous or **first order phase transition**. It is *discontinuous* because of the described behavior of the order parameter, and the *first order* denomination stems from the fact that the first derivative of the Gibbs free energy suffers a discontinuity just at the same point.

In this jump, the order parameter takes two different values at the same point of the control parameter axis. This indicates that the system is in two different phases at the same time. This is the so-called **phase coexistence**. During the coexistence, as the control parameter is varied, one of the phases is growing at the expense of the other, which is disappearing.

The usual example of coexistence is water. Its phase diagram is depicted in Fig.A.1 (see left panel). All the lines in this plot are coexistence lines, i.e. pairs pressure-temperature (P, T) at which there are two phases[1] coexisting.

Consider, for instance, the solid-liquid phase transition of water. In this case, the control parameter is the temperature, and it can be selected as order parameter anyone which measures order in the system. It is straightforward to see that, starting from ice phase up to a temperature $T = 0^-$, the order parameter is in its maximum value due to the ordered structure of ice. As temperature raises up to $T = 0$, any amount of energy given to ice is devoted to melting (latent heat), the order parameter begins to decrease, and the coexistence between water and ice starts. When all the ice has disappeared, transformed into water, the energy applied is used again to increase T, and the order parameter reaches its minimum value.

In the previous example, when the molar entropy (s) is taken as the order parameter, the function $s(T)$ presents a jump just when the phase transition is undergone. A more intuitive representation is the one depicted in the right part of Fig.A.1, where the molar volume v is the order parameter, which at certain $P = P'$ takes two different values, v_1 and v_2 (a value per coexisting phase). This indicates the phase transition.

[1] Three, at the point in which the three coexistence lines cross. This is the so-called **triple point** of water (T_3 in the figure).

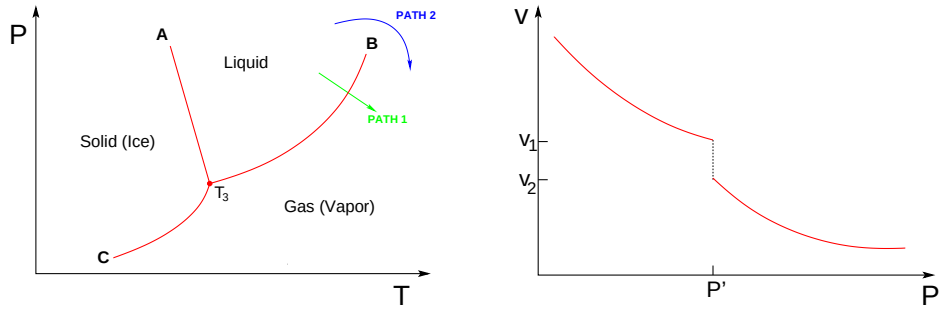

Figure A.1: Left: Water phase diagram. The lines are coexistence lines, indicating a first order phase transition. While, at points A and C, the coexistence lines are not interrumpted, the point B does not entail coexistence; it is the critical point of a second order phase transition. Right: Behavior of the molar volume v of water with the variation of the pressure P; the two values for v at the same P, point to the coexistence of two phases.

A.1.2 Second Order Phase Transitions

But in the same system can occur many different phase transitions. As said above, when one of the coexistence lines is crossed (due to the variation of any of the parameters of the system), a first order phase transition is undergone. However, it is possible to change from one phase to the other avoiding the coexistence.

Recall the phase diagram of the previous example (see left part of Fig.A.1). The point at which a coexistence line ends is a point above which water can pass from one phase to another one continuosly, i.e. the order parameter does not jump at this point, but varies smoothly. This point is called **critical point**, and the transition, second order or **continuous phase transition**. It is *continuous* because of the described behavior of the order parameter, and the *second order* denomination stems from the fact that the first derivative of the Gibbs free energy is continuous, but the second one suffers a discontinuity just at the critical point.

We will use the liquid-vapor continuous phase transition of water to see clearly the difference between both transitions. As explained in the previous section, it is possible to transform liquid water into vapor following path 1 (green line depicted in the phase diagram of the left part of Fig.A.1). Then, when temperature reaches some value posed on the coexistence line, all energy applied to the system is used as latent heat (i.e. to transform liquid into water keeping (P, T) constant) and two phases are coexisting. But it is also possible to follow path 2 (blue line), in which the liquid changes to

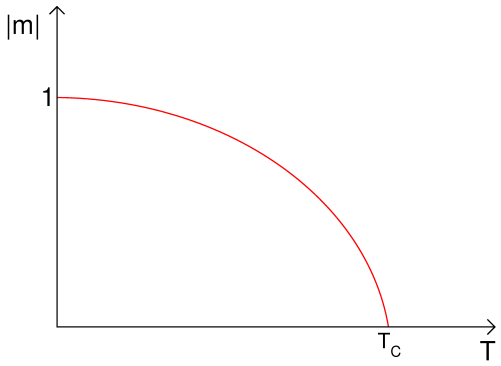

Figure A.2: Second order transition in the Ising model. Above the critical point T_c (the *Curie temperature*), thermal fluctuations make the system be completely disordered.

vapor and the system does not absorb any latent heat, and therefore there is no coexistence.

In equilibrium Statistical Physics, the most instructive example of continuous phase transition is the Ising model. Consider a lattice with N sites, and one spin at each position i which can be oriented only towards two directions. Thus, we can assign the values $s_i = \pm 1$ to each spin. To quantify the order into the system, it is used the *magnetization*, defined as:

$$m(t) = \frac{1}{N} \sum_{i=1}^{N} s_i(t). \tag{A.1.1}$$

In this way, when all the spins are equally oriented, $|m| = 1$ and the system is completely ordered; if any of the spins is oriented towards the opposite direction, $0 < |m| < 1$, and when the system is totally disordered, $|m| = 0$. With this order parameter, it is possible to know whether the system is in its magnetic phase ($m \neq 0$) or in its non-magnetic phase ($m = 0$).

The control parameter is the temperature (T), because thermal fluctuations are the responsibles for changes in the orientation of the spins. The point at which the system undergoes the phase transition (the critical point) is called in this case **Curie temperature**. The phase diagram can be observed in Fig.A.2.

As second order phase transitions are the ones observed in Self-Organized Criticality, we will be focused on them from now on. The phenomenology around and at the critical point is very interesting, and it is what provides

many of the tools needed to study the models described on this thesis.

The Divergence of Correlations

As said before, the behavior of many observables changes in the vicinity of a critical point. One can be interested in observe, in a spatially extended system, how the behavior of one site $\vec{x}_1$ affects to another site $\vec{x}_2$. To this end, it is necessary to define a **two-point spatial correlation function**, $G(\vec{x}_1, \vec{x}_2)$; if the behavior is characterized by, e.g. a spin, this function takes the form:

$$G(\vec{x}_1, \vec{x}_2) = \langle s(\vec{x}_1) s(\vec{x}_2) \rangle \,, \tag{A.1.2}$$

where $\langle . \rangle$ means thermal averaging; or better its **connected** form:

$$G_c(\vec{x}_1, \vec{x}_2) = \langle s(\vec{x}_1) s(\vec{x}_2) \rangle_c = \langle s(\vec{x}_1) s(\vec{x}_2) \rangle - \left\langle s^2 \right\rangle . \tag{A.1.3}$$

When the system is translationally invariant or isotropic, this function depends on distances, and the expression is reduced to:

$$G_c(r) = \langle s(0) s(\vec{r}) \rangle_c = \langle s(0) s(\vec{r}) \rangle - \left\langle s^2 \right\rangle , \tag{A.1.4}$$

where $r = |\vec{x}_1 - \vec{x}_2|$. Away from the critical point ($T \neq T_c$ in this example), this function has the form:

$$G_c(r) \sim e^{-r/\xi}, \tag{A.1.5}$$

that is, correlations decay exponentially fast with the distance, and ξ is a **characteristic length**. This last expression means that the fluctuations at one site $\vec{x}$ can travel a distance up to $r = \xi$, but sites situated far away do not have the information of what happens at $\vec{x}$. This characteristic length ξ is called **correlation length**.

In the proximity of the critical point, and taking the **thermodynamic limit** ($L \to \infty$) and long time limit ($t \to \infty$)[2], this observable behaves in a very special way. Defining $\Delta = T - T_c$, i.e. the distance to the critical point, when $|\Delta| \ll 1$:

[2]The $L, t \to \infty$ limit is called the **hydrodynamic limit**.

$$\xi \sim |\Delta|^{-\nu_\perp}. \tag{A.1.6}$$

This means that, as the control parameter achieves the critical point, this length becomes larger and larger, diverging as a **power law** characterized by the exponent $\nu_\perp$. This affects to the correlation function because, next to the critical point and for large r, it behaves as:

$$G_c(r) \sim \frac{e^{-r/\xi}}{r^{d-2+\eta}} \longrightarrow \frac{1}{r^{d-2+\eta}}, \tag{A.1.7}$$

that is, the correlation function also follows a pure power law, given by the exponent $d-2+\eta$. Both η and $\nu_\perp$ are **critical exponents**, because they characterize the behavior of these observables next to the critical point.

In summary, near the critical point, correlations span throughout the system ($\xi \gg 1$), decaying very slowly as a power law of the distance r.

Similarly, a **temporal correlation function** can be defined, for example, for the order parameter:

$$G_c(t) = \langle \phi(t_0)\phi(t_0+t) \rangle_c = \langle \phi(t_0)\phi(t_0+t) \rangle - \left\langle \phi^2 \right\rangle. \tag{A.1.8}$$

These correlations have as well a characteristic time length (the **correlation time**, ξ_t) which indicates the duration of the correlations or memory effect in the system[3]. This length also follows a power law in the proximity of the critical point:

$$\xi_t \sim |\Delta|^{-\nu_\parallel}. \tag{A.1.9}$$

This means that, as the control parameter is closer to the critical point, the correlations spend more and more time in dissappear. This phenomenon is called **critical slowing down**. Both correlation lengths are linked by the relation:

$$\xi_t \sim \xi^z, \tag{A.1.10}$$

[3]Also, it can be called *decorrelation time length*, because it is the time the system takes to become decorrelated again.

where z is the so-called **dynamical exponent**. This relation allows to link not only the observables, but also the exponents, with the **scaling relation**[4]:

$$z = \frac{\nu_{\parallel}}{\nu_{\perp}}. \tag{A.1.11}$$

Scale Invariance

The relevancy of the power law behavior stems from its underlaying physics. Consider two properties of a system described by the functions $f(x)$ and $g(x)$. Suppose that the first one follows a power law, and the second one, an exponential law. As only dimensionless quantities can be arguments of both functions, a scale length x_0 is to be defined; hence, the functions are:

$$f(x) = \left(\frac{x}{x_0}\right)^{\gamma} \qquad\qquad g(x) = e^{-x/x_0}. \tag{A.1.12}$$

By changing the scale of observation, $x \to \tilde{x} = bx$, the effect on each function is different. For the power law:

$$f(\tilde{x}) = \left(\frac{bx}{x_0}\right)^{\gamma} = b^{\gamma} f(x). \tag{A.1.13}$$

In this way, the new function conserves the shape of the original one (i.e. the selected property of the system conserves the same behavior, a power law characterized by the same exponent) after the change[5]. It is necessary only a linear change in the scale of both axes to recover the original one. In other words, the relative change $f(bx)/f(x) = b^{\gamma}$ is independent of x.

However, the exponential:

$$g(\tilde{x}) = e^{-bx/x_0} = g(x)^b, \tag{A.1.14}$$

that is, the new function has a modified form different from the original one, which cannot be recovered with simple linear changes of scale. Now

[4]These relations reflect symmetries of the system, and therefore they can vary for different systems.

[5]The new function is identical to the original one, but shifted in the f axis by a factor b^{γ}.

$g(bx)/g(x) = g(x)^{b-1}$ depends on x. It also can be seen as a change of the characteristic length (from x_0 to x_0/b). The new function is, thus, *qualitatively* different from the original one, and therefore the property changes its behavior when the scale is varied.

In summary, a property described by a power law remains qualitatively the same regardless the scale of observation, while a property described by an exponential law changes its behavior with the scale of observation. The former phenomenon is known as **scale invariance**. If a system is scale-invariant, the observables defined at the microscopic level of description can be also defined at any other level, and moreover they behave in an identical way. This is an essential property, intimately related to universality (see below).

Dynamic Behavior

Apart from correlation functions, more observables can be used to study the **critical behavior** of a system. Depending on the system and the behavior under study, a certain set of observables must be selected. The previous ones study the behavior *close to* the critical point, but not *just at* the critical point.

Consider a system whose order parameter is given by the number of active sites[6]. Starting from a seed of activity[7] (experiment which is known as **spreading experiment**), it is interesting to measure the temporal behavior of the number of active sites considering only surviving experiments up to time t ($N_s(t)$), considering all the experiments ($N(t)$), the surviving probability ($P_s(t)$) or the mean quadratic distance to the seed of activity considering again only surviving runs ($R^2(t)$); the *average over different experiments* of these quantities, at the critical point ($\Delta = 0$), follows the power laws:

$$N_s(t) \sim t^{\eta+\delta}, \tag{A.1.15}$$

$$N(t) \sim t^{\eta}, \tag{A.1.16}$$

$$P_s(t) \sim t^{-\delta}, \tag{A.1.17}$$

[6]For example, in a simulation of the spreading of diseases in populations: the infected people would be the order parameter and the probability to infect other site or health itself, the control parameter.

[7]One individual infected among the rest of the healthy population.

$$R^2(t) \sim t^{z_{spr}}. \tag{A.1.18}$$

In the same way, it is possible to study how some quantities behave if the initial state is one in which all sites are active. It is interesting, for example, to study the decaying of the density of active sites, ρ, with time; just at the critical point, and averaged over different experiments, it follows the power law:

$$\rho(t) \sim t^{-\theta}. \tag{A.1.19}$$

Static Behavior

Out of the critical point, a stationary density ρ_{st} can be defined. If the control parameter is above its critical value ($\Delta > 0$):

$$\rho_{st} \sim \Delta^{\beta}. \tag{A.1.20}$$

As all these behaviors are valid only in the $L \to \infty$ limit, it is interesting to study how the finite size of any real or simulated system affects to the results. When the system is far from criticality, the correlation length is small, less than the size of the system ($\xi < L$). But, at the critical point, correlations diverge and, for a finite size, $\xi > L$ and correlations are limited by the system size. This is what is called **finite size effect**. In a nutshell, it consists in a shift of the critical point, making Δ larger for a fixed value of the control parameter as the size is reduced. In the opposite way, if the control parameter takes its critical value, this can be expressed with the relation:

$$\Delta(L \to \infty) = 0 \qquad \Longrightarrow \qquad 0 < \Delta(L). \tag{A.1.21}$$

In this way, when the control parameter of a system with finite L takes a value such that $\Delta(\infty) = 0$ (i.e. the critical value of the infinite system), the behavior of the order parameter is supercritical, i.e. it converges to a finite stationary value in a finite time. The value of this time is larger as L increases, and the saturation value fulfills the relation:

$$\rho_{st} \sim L^{-\beta/\nu_{\perp}}. \tag{A.1.22}$$

This behavior is called **finite size scaling**.

A deviation from the power-law behavior of all these quantities shows that the system is close but not at the critical point. Hence, these observables can be used to detect when the system is undergoing a phase transition. As a power law takes a linear form when it is represented in a plot in which both axes are in logarithmic scale, a deviation from a **straight line** in a *log-log plot* indicates a deviation from the critical point. All these exponents also can be linked by using scaling relations like the ones which can be found in chapter 2.

A.2 Universality

In the previous section, many critical exponents have been defined. As can be seen all along the thesis, it is possible, for many different systems with different dynamics (i.e. microscopic rules), to share the same set of values for the critical exponents. This means that, although the microscopic behavior is different, the critical behavior at a higher level of observation is identical. This phenomenon is called **universality**[8].

Universality allows to gather many systems into the same group, characterized by a certain critical behavior. This group is called **universality class**. As it is recalled in the bulk of this thesis, a set of symmetries defines a universality class. Thus, universality is a very powerful concept, because it allows to predict what the critical behavior of a system is just by identifying its symmetries.

Attending to these characteristic symmetries, it is possible to build a continuous equation (a **Langevin equation**) which specifies the behavior of the universality class at a mesoscopic level of description, regardless the microscopic rules of each single system. Due to the scale invariance occurring at the critical point, it makes no difference whether to choose the microscopic or the mesoscopic level to describe the dynamics of the system. As microscopic rules can blur the true asymptotic critical behavior by introducing long transients, it is usually advisable to study the continuous equation, which remains unaffected by these microscopical details.

A very spectacular plot in which the concept of universality is clearly

[8]The set of exponents is identical, but as the microscopic rules are different, the appropriate order or control parameter can be different in each system; due to this, the value of the critical point is not universal.

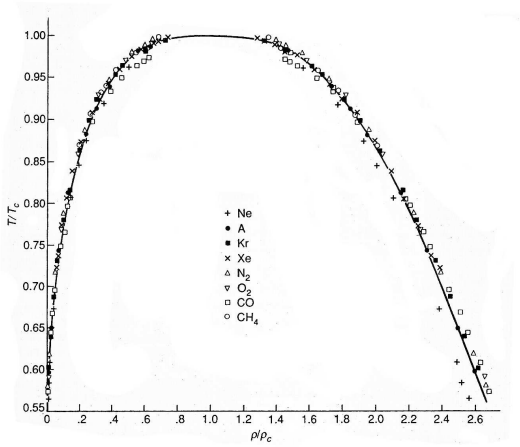

Figure A.3: Liquid-gas coexistence curves for many fluids; observe that temperature and density are scaled by their corresponding critical values, which are non-universal parameters. See [A2] for further details.

depicted is the well-known temperature-density diagram of the liquid-gas coexistence curves of many fluids as noble gases, Fig.A.3. Throughout the thesis, this topic is very recurrent, and thus many plots in which universality is present can be seen. Concretely, Fig.4.8 is recommended.

A.3 Self-Affinity, Self-Similarity, Fractals and $1/f$ Noise

An object is said to be **self-similar** if it looks "roughly" the same on any scale. In other words, when the object is enlarged or reduced, the result is statistically similar to the original one (i.e. it can be superimposed to the original or, if not, at least conserves its shape). The Cantor set is an example of a self-similar object (see Fig.A.4).

On the other hand, if the object has to be rescaled *anisotropically* to recover the shape of the original one, it is said to be **self-affine**.

Fractal Dimension

If $M(L)$ (or mass) is the number of objects of unit length L necessary to fill a *self-similar* object of volume $V(L)$, both magnitudes are related by means

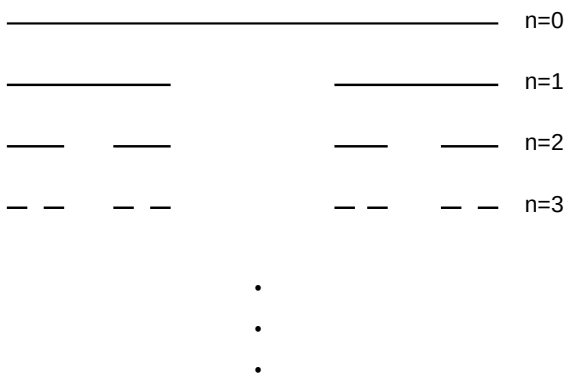

Figure A.4: The one-dimensional Cantor set: starting from a line ($n = 0$), each new generation is obtained by dividing the object of the previous one into three parts and removing the one in the middle.

of the expression:

$$M(L) = V(L) \cdot L^{-d_E}, \tag{A.3.1}$$

which is a power law characterized by the Euclidean dimension of the object, $d_E \in \mathbb{Z}^{0,+}$. The object is said to be a **fractal** if this relation changes to:

$$M(L) \sim L^{-D_f}, \tag{A.3.2}$$

where D_f, the so-called **fractal dimension**, is a non-integer number less than the corresponding Euclidean dimension in which the object is embedded. The presence of this power law implies, as said above, the lack of a characteristic scale of description; therefore, a fractal is a geometrical structure with features of all length scales

$1/f$ Noise

The counterpart of spatial fractals in time domain is the known as $1/f$ *noise*. The spectrum of a temporal signal is defined as the square amplitude of the Fourier transform of the signal or, if a stationary state can be reached, the cosine transform of the temporal correlation function:

$$S(f) = 2 \int_0^\infty dt G(t) \cos(2\pi f t). \tag{A.3.3}$$

Broadly, it can be said that, in many cases, a time-correlation function following a power law implies a scale-free power spectrum:

$$S(f) = 1/f^{\alpha}. \tag{A.3.4}$$

Thus, the presence of $1/f$ noise points out, in many cases (see chapter 6), the divergence of correlations, i.e. some internal temporal structure arising. This is the reason why this noise is said to be a *fractal in time*. The case $\alpha = 1$ is special, because temporal correlations decay in a logarithmic way (very long time correlations).

Appendix B

Field Theory Representation of a Master Equation

In this appendix, some necessary steps to perform a mapping from a reaction-diffusion set of equations to the continuous generating function of the process will be followed. Two species A and B for interacting particles will be considered.

Let $P(m,n;t)$ be the probability for a site i to have m particles of species A and n particles of species B at time t. If $w((m',n') \to (m,n))$ is the transition rate for the changing process from the state (m',n') to the state (m,n), the master equation for this site can be written as:

$$\begin{aligned} \partial_t P(m,n;t) = & \sum_{(m',n')} w((m',n') \to (m,n)) P(m',n';t) \\ - & \sum_{(m',n')} w((m,n) \to (m',n')) P(m,n;t). \end{aligned} \tag{B.1.1}$$

To map the master equation into a field theory, it is necessary to define the state of the system in a *second quantized form*. To this end, it is necessary to introduce the *ket-vector* $|m,n\rangle$, which is the microscopic state for a site i with m particles A and n particles B, and whose scalar product is given by:

$$\langle m',n'|m,n\rangle = m!n!\delta_{m',m}\delta_{n',n}, \tag{B.1.2}$$

which is called *exclusive scalar product* [106]. This defines the orthonormal

basis of a Hilbert space. Creation and annihilation operators are defined for each species:

$$\begin{array}{rl} \hat{a}^\dagger|m,n\rangle = & |m+1,n\rangle \\ \hat{b}^\dagger|m,n\rangle = & |m,n+1\rangle \\ \hat{a}|m,n\rangle = & m|m-1,n\rangle \\ \hat{b}|m,n\rangle = & n|m,n-1\rangle \end{array} \tag{B.1.3}$$

with the commutation rules:

$$\left[\hat{a}_i^\dagger,\hat{a}_j\right]=\delta_{i,j} \quad \left[\hat{b}_i^\dagger,\hat{b}_j\right]=\delta_{i,j} \quad \left[\hat{a}^\dagger,\hat{b}\right]=0 \quad \left[\hat{b}^\dagger,\hat{a}\right]=0; \tag{B.1.4}$$

thus, a Fock space is defined. The *number operator* for each species is given by:

$$\begin{array}{rll} \hat{N}_A = & \hat{a}^\dagger\hat{a}|m,n\rangle & = m|m,n\rangle \\ \hat{N}_B = & \hat{b}^\dagger\hat{b}|m,n\rangle & = n|m,n\rangle. \end{array} \tag{B.1.5}$$

It is convenient to define also the projector state:

$$\langle\ |\ = \langle 0,0|e^{\hat{a}+\hat{b}} \tag{B.1.6}$$

and the identity resolution, given by:

$$\mathbb{I} = \int \frac{d\varphi d\bar{\varphi} d\phi d\bar{\phi}}{(2\pi)^2} e^{i\varphi\bar{\varphi}} e^{i\phi\bar{\phi}} |\varphi,\phi\rangle\langle i\bar{\varphi}, i\bar{\phi}|, \tag{B.1.7}$$

where φ,$\bar{\varphi}$, ϕ and $\bar{\phi}$ are real-valuated, position and time dependent fields. The state $|\varphi,\phi\rangle$ is a **coherent state**, which in its *bra* and *ket* forms can be written as:

$$\begin{array}{rl} |\varphi,\phi\rangle = & e^{\hat{a}^\dagger\varphi}e^{\hat{b}^\dagger\phi}|0,0\rangle = \sum_{m,n}\frac{(\hat{a}^\dagger\varphi)^m}{m!}\frac{(\hat{b}^\dagger\phi)^n}{n!}|0,0\rangle = \sum_{m,n}\frac{\varphi^m}{m!}\frac{\phi^n}{n!}|m,n\rangle \\ \langle\varphi,\phi| = & \langle 0,0|e^{\hat{a}\varphi^*}e^{\hat{b}\phi^*} = \sum_{m,n}\langle 0,0|\frac{(\hat{a}\varphi^*)^m}{m!}\frac{(\hat{b}\phi^*)^n}{n!} = \sum_{m,n}\langle m,n|\frac{(\varphi^*)^m}{m!}\frac{(\phi^*)^n}{n!}. \end{array} \tag{B.1.8}$$

The ket states are eigenvectors of the annihilation operator $\hat{b}\hat{a}$ in this space:

$$\hat{b}\hat{a}|\varphi,\phi\rangle = \varphi\phi|\varphi,\phi\rangle, \tag{B.1.9}$$

and the bra states are eigenvectors of the creation operator $\hat{b}^\dagger\hat{a}^\dagger$:

$$\langle\varphi,\phi|\hat{b}^\dagger\hat{a}^\dagger = \langle\varphi,\phi|\varphi\phi. \tag{B.1.10}$$

The resolution of the identity can be rewritten now as:

$$\mathbb{I} = \int \frac{d\varphi d\bar{\varphi} d\phi d\bar{\phi}}{(2\pi)^2} e^{i\varphi\bar{\varphi}} e^{i\phi\bar{\phi}} e^{\hat{a}^\dagger\varphi} e^{\hat{b}^\dagger\phi} |0,0\rangle\langle 0,0| e^{-i\hat{a}\bar{\varphi}^*} e^{-i\hat{b}\bar{\phi}^*} \tag{B.1.11}$$

Once the Fock space is completely characterized, the rest of the steps of the mapping from the master equation Eq.(B.1.1) to a field theory can be performed. To this purpose, we define now the state of site i at a time t as a superposition of all the possible $|m,n\rangle$ states, each of them with the convenient weight given by the probability $P(m,n;t)$:

$$|\psi_i(t)\rangle = \sum_{(m,n)} P(m,n;t)|m,n\rangle \tag{B.1.12}$$

where the state of the whole system is:

$$|\Psi(t)\rangle = \sum_i |\psi_i(t)\rangle \tag{B.1.13}$$

Thus, if the master equation Eq.(B.1.1) is multiplied by the state $|m,n\rangle$:

$$\begin{aligned} \partial_t P(m,n;t)|m,n\rangle = & \sum_{(m',n')} w((m',n') \to (m,n)) P(m',n';t)|m,n\rangle \\ & - \sum_{(m',n')} w((m,n) \to (m',n')) P(m,n;t)|m,n\rangle, \end{aligned} \tag{B.1.14}$$

and a sum over all possible states is performed:

$$\partial_t \sum_{(m,n)} P(m,n;t)|m,n\rangle = \sum_{(m,n)} \sum_{(m',n')} w((m',n') \to (m,n)) P(m',n';t)|m,n\rangle - \sum_{(m,n)} \sum_{(m',n')} w((m,n) \to (m',n')) P(m,n;t)|m,n\rangle, \tag{B.1.15}$$

With these definitions, the master equation can be written as:

$$\partial_t |\Psi(t)\rangle = -\hat{H}|\Psi(t)\rangle, \tag{B.1.16}$$

where this $\hat{H}$ operator can be written as the contribution of each site and each process separately[1]. It is difficult and not very illustrative to demonstrate this last expression, but it can be easily shown in each concrete example, for example the explained in section 2.7 (see chapter 2).

Eq.(B.1.16) is the imaginary-time Schrödinger equation, which can be integrated to result in:

$$|\Psi(t)\rangle = e^{-\hat{H}t}|\Psi(0)\rangle. \tag{B.1.17}$$

Consider that, at time $t = 0$, the distribution of particles follows a Poissonian distribution; for the whole system, it can be written:

$$P(m,n,0) = \mathcal{C} \prod_i \frac{n_{A_0}^{m_i}}{m_i!} \frac{n_{B_0}^{n_i}}{n_i!}, \tag{B.1.18}$$

where $\mathcal{C}$ is a normalization constant that, for the sake of simplicity, it is assumed to be $\mathcal{C} = 1$; therefore, using the definition of state, Eq.(B.1.12)-Eq.(B.1.13):

[1] Except, of course, the diffusion of particles, which involves two sites.

$$
\begin{aligned}
|\Psi(0)\rangle = & \sum_{m,n}\prod_i \frac{n_{A_0}^{m_i}}{m_i!}\frac{n_{B_0}^{n_i}}{n_i!}|m,n\rangle \\
= & \sum_{m,n}\prod_i \frac{n_{A_0}^{m_i}(\hat{a}_i^\dagger)^{m_i}}{m_i!}\frac{n_{B_0}^{n_i}(\hat{b}_i^\dagger)^{n_i}}{n_i!}|0,0\rangle \\
= & \; e^{n_{A_0}\sum_i \hat{a}_i^\dagger} e^{n_{B_0}\sum_i \hat{b}_i^\dagger}|0,0\rangle.
\end{aligned}
\tag{B.1.19}
$$

The solution of the evolution equation, Eq.(B.1.17), can be used to evaluate the generating function, which is given by:

$$
\begin{aligned}
Z = & \; \langle\, |\Psi(t)\rangle = \langle\, |e^{-\hat{H}t}|\Psi(0)\rangle \\
= & \; \langle 0,0|e^{\sum_i(\hat{a}_i+\hat{b}_i)}e^{-\sum_i \hat{H}_i}|\Psi(0)\rangle.
\end{aligned}
\tag{B.1.20}
$$

For the moment, the contribution of each site i will be considered separately[1]. The subscripts i will be omitted. It is possible to divide the time interval in $K \to \infty$ slices; thus, if Δt is the width of these slices, $t = t_0 + K \cdot \Delta t$, and the exponential of time takes the form:

$$
e^{-\hat{H}t} = \lim_{\Delta t\to 0}(1-\hat{H}\Delta t)^{t/\Delta t} \tag{B.1.21}
$$

and the contribution of site j to the generating function is given by:

$$
Z_j = \lim_{\Delta t\to 0}\langle 0,0|e^{\hat{a}+\hat{b}}(1-\hat{H}\Delta t)^{t/\Delta t}|\psi(0)\rangle. \tag{B.1.22}
$$

Now, introducing the identity resolution between each of the K slices:

$$
\begin{aligned}
Z_j = & \lim_{\Delta t\to 0}\langle 0,0|e^{\hat{a}+\hat{b}}\mathbb{I}_K(1-\hat{H}\Delta t)\mathbb{I}_{(K-1)}(1-\hat{H}\Delta t)\ldots\mathbb{I}_1(1-\hat{H}\Delta t)\mathbb{I}_0|\psi(0)\rangle \\
= & \lim_{\Delta t\to 0}\langle 0,0|e^{\hat{a}+\hat{b}}\left(\int \frac{d\varphi_K d\bar{\varphi}_K d\phi_K d\bar{\phi}_K}{(2\pi)^2} e^{i\varphi_K\bar{\varphi}_K}e^{i\phi_K\bar{\phi}_K}e^{\hat{a}^\dagger\varphi_K}e^{\hat{b}^\dagger\phi_K}|0,0\rangle\right.
\end{aligned}
$$

$$\langle 0,0|e^{-i\hat{a}\bar{\varphi}_K^*}e^{-i\hat{b}\bar{\phi}_K^*}\Big)(1-\hat{H}\Delta t)\dots$$

$$(1-\hat{H}\Delta t)\left(\int\frac{d\varphi_1 d\bar{\varphi}_1 d\phi_1 d\bar{\phi}_1}{(2\pi)^2}e^{i\varphi_1\bar{\varphi}_1}e^{i\phi_1\bar{\phi}_1}e^{\hat{a}^\dagger\varphi_1}e^{\hat{b}^\dagger\phi_1}|0,0\rangle\langle 0,0|e^{-i\hat{a}\bar{\varphi}_1^*}e^{-i\hat{b}\bar{\phi}_1^*}\right)$$

$$(1-\hat{H}\Delta t)\left(\int\frac{d\varphi_0 d\bar{\varphi}_0 d\phi_0 d\bar{\phi}_0}{(2\pi)^2}e^{i\varphi_0\bar{\varphi}_0}e^{i\phi_0\bar{\phi}_0}e^{\hat{a}^\dagger\varphi_0}e^{\hat{b}^\dagger\phi_0}|0,0\rangle\langle 0,0|e^{-i\hat{a}\bar{\varphi}_0^*}e^{-i\hat{b}\bar{\phi}_0^*}\right)|\psi(0)\rangle;$$

by grouping terms:

$$\begin{aligned}Z_j = \lim_{\Delta t\to 0}\langle 0,0|e^{\hat{a}+\hat{b}}\int\left[\prod_{k=0}^{K}\frac{d\varphi_k d\bar{\varphi}_k d\phi_k d\bar{\phi}_k}{(2\pi)^2}e^{i\varphi_k\bar{\varphi}_k}e^{i\phi_k\bar{\phi}_k}\right]\\ \Big[e^{\hat{a}^\dagger\varphi_K}e^{\hat{b}^\dagger\phi_K}|0,0\rangle\langle 0,0|e^{-i\hat{a}\bar{\varphi}_K^*}e^{-i\hat{b}\bar{\phi}_K^*}(1-\hat{H}\Delta t)\\ e^{\hat{a}^\dagger\varphi_{K-1}}e^{\hat{b}^\dagger\phi_{K-1}}|0,0\rangle\langle 0,0|e^{-i\hat{a}\bar{\varphi}_{K-1}^*}e^{-i\hat{b}\bar{\phi}_{K-1}^*}(1-\hat{H}\Delta t)\dots\\ e^{\hat{a}^\dagger\varphi_1}e^{\hat{b}^\dagger\phi_1}|0,0\rangle\langle 0,0|e^{-i\hat{a}\bar{\varphi}_1^*}e^{-i\hat{b}\bar{\phi}_1^*}(1-\hat{H}\Delta t)e^{\hat{a}^\dagger\varphi_0}e^{\hat{b}^\dagger\phi_0}|0,0\rangle\langle 0,0|e^{-i\hat{a}\bar{\varphi}_0^*}e^{-i\hat{b}\bar{\phi}_0^*}\Big]|\psi(0)\rangle.\end{aligned}$$

Thus, three different types of terms can be found into the previous expression:

$$T_1 = \langle 0,0|e^{\hat{a}+\hat{b}}e^{\hat{a}^\dagger\varphi_K}e^{\hat{b}^\dagger\phi_K}|0,0\rangle \tag{B.1.23}$$

$$T_2 = \langle 0,0|e^{-i\hat{a}\bar{\varphi}_l^*}e^{-i\hat{b}\bar{\phi}_l^*}(1-\hat{H}\Delta t)e^{\hat{a}^\dagger\varphi_{l-1}}e^{\hat{b}^\dagger\phi_{l-1}}|0,0\rangle \tag{B.1.24}$$

$$T_3 = \langle 0,0|e^{-i\hat{a}\bar{\varphi}_0^*}e^{-i\hat{b}\bar{\phi}_0^*}|\psi(0)\rangle, \tag{B.1.25}$$

where $\bar{\varphi}^* = \bar{\varphi}$ and $\bar{\phi}^* = \bar{\phi}$, because both are real-valuated fields by definition. Now, each of these three types of terms will be studied separately.

First term, T_1: By using the definitions of the projector, Eq.(B.1.6), and the coherent state, Eq.(B.1.8):

$$T_1 = \langle 0,0|e^{\hat{a}+\hat{b}}e^{\hat{a}^\dagger\varphi_K}e^{\hat{b}^\dagger\phi_K}|0,0\rangle = \langle|\varphi_K,\phi_K\rangle = e^{\varphi_K}e^{\phi_K}. \tag{B.1.26}$$

Second term, T_2: Again, by using Eq.(B.1.8):

$$\begin{aligned} T_2 = & \langle 0,0|e^{-i\hat{a}\bar{\varphi}_l}e^{-i\hat{b}\bar{\phi}_l}(1-\hat{H}\Delta t)e^{\hat{a}^\dagger\varphi_{l-1}}e^{\hat{b}^\dagger\phi_{l-1}}|0,0\rangle \\ = & \sum_{m,n,k,j}\frac{(-i\bar{\varphi}_l)^m(-i\bar{\phi}_l)^n(\varphi_{l-1})^k(\phi_{l-1})^j}{m!\ n!\ k!\ j!}\langle m,n|(1-\hat{H}\Delta t)|k,j\rangle \\ = & \sum_{m,n,k,j}\frac{(-i\bar{\varphi}_l)^m(-i\bar{\phi}_l)^n(\varphi_{l-1})^k(\phi_{l-1})^j}{m!\ n!\ k!\ j!}\Big(\langle m,n|k,j\rangle - \Delta t\langle m,n|\hat{H}|k,j\rangle\Big). \end{aligned} \tag{B.1.27}$$

Thus, by using the definition of the scalar product, Eq.(B.1.2):

$$\sum_{m,n,k,j}\frac{(-i\bar{\varphi}_l)^m(-i\bar{\phi}_l)^n(\varphi_{l-1})^k(\phi_{l-1})^j}{m!\ n!\ k!\ j!}\langle m,n|k,j\rangle = e^{-i\bar{\varphi}_l\varphi_{l-1}}e^{-i\bar{\phi}_l\phi_{l-1}}. \tag{B.1.28}$$

On the other hand, with the operational form for the Hamiltonian:

$$\begin{aligned} \hat{H} = & \sum_{k,j}H_{k,j}\hat{N}_A^k\hat{N}_B^j = \sum_{m,n,k,j}H_{m,n,k,j}\hat{a}^{\dagger\ k}\hat{a}^m\hat{b}^{\dagger\ j}\hat{b}^n \\ = & H(\hat{a}^\dagger,\hat{a},\hat{b}^\dagger,\hat{b}), \end{aligned} \tag{B.1.29}$$

the last part of T_2 can be expressed as:

$$\begin{aligned} & \sum_{m,n,k,j}\frac{(-i\bar{\varphi}_l)^m(-i\bar{\phi}_l)^n(\varphi_{l-1})^k(\phi_{l-1})^j}{m!\ n!\ k!\ j!}\langle m,n|H(\hat{a}^\dagger,\hat{a},\hat{b}^\dagger,\hat{b})|k,j\rangle \\ & = H(\varphi_{l-1},-i\bar{\varphi}_l,\phi_{l-1},-i\bar{\phi}_l)e^{-i\bar{\varphi}_l\varphi_{l-1}}e^{-i\bar{\phi}_l\phi_{l-1}} \end{aligned} \tag{B.1.30}$$

and, therefore:

$$\begin{aligned} T_2 = & e^{-i\bar{\varphi}_l\varphi_{l-1}}e^{-i\bar{\phi}_l\phi_{l-1}}\left[1-H(\varphi_{l-1},-i\bar{\varphi}_l,\phi_{l-1},-i\bar{\phi}_l)\Delta t\right] \\ \sim & e^{-i\bar{\varphi}_l\varphi_{l-1}}e^{-i\bar{\phi}_l\phi_{l-1}}e^{-H(\varphi_{l-1},-i\bar{\varphi}_l,\phi_{l-1},-i\bar{\phi}_l)\Delta t}+O(\Delta t^2). \end{aligned} \tag{B.1.31}$$

Third term, T_3: If the initial state of site j, $|\psi(0)\rangle$, is written as (see Eq.(B.1.19)):

$$|\psi(0)\rangle = e^{n_{A_0}\hat{a}^\dagger} e^{n_{B_0}\hat{b}^\dagger}|0,0\rangle, \tag{B.1.32}$$

then:

$$\begin{aligned} T_3 = \;& \langle 0,0|e^{-i\hat{a}\bar{\varphi}_0} e^{-i\hat{b}\bar{\phi}_0} e^{n_{A_0}\hat{a}^\dagger} e^{n_{B_0}\hat{b}^\dagger}|0,0\rangle \\ = \;& \sum_{m,n,k,j} \langle 0,0|\frac{(-i\bar{\varphi}_0)^m(\hat{a})^m(-i\bar{\phi}_0)^n(\hat{b})^n(n_{A_0})^k(\hat{a}^\dagger)^k(n_{B_0})^j(\hat{b}^\dagger)^j}{m!\; n!\; k!\; j!}|0,0\rangle \\ = \;& \sum_{m,n,k,j} \frac{(-i\bar{\varphi}_0)^m(-i\bar{\phi}_0)^n(n_{A_0})^k(n_{B_0})^j}{m!\; n!\; k!\; j!}\langle m,n|k,j\rangle \\ = \;& e^{-i\bar{\varphi}_0 n_{A_0}} e^{-i\bar{\phi}_0 n_{B_0}} \end{aligned} \tag{B.1.33}$$

With these three contributions, the generating function for a site j takes the form:

$$Z_j = \lim_{\Delta t\to 0} \int \left[\prod_{k=0}^{K} \frac{d\varphi_k d\bar{\varphi}_k d\phi_k d\bar{\phi}_k}{(2\pi)^2} e^{i\Delta\varphi_k\bar{\varphi}_k} e^{i\Delta\phi_k\bar{\phi}_k} e^{-\tilde{H}\Delta t}\right] e^{-i\bar{\varphi}_0 n_{A_0}} e^{-i\bar{\phi}_0 n_{B_0}} e^{\varphi_K} e^{\phi_K}, \tag{B.1.34}$$

where $H = H(\varphi_{k-1}, -i\bar{\varphi}_k, \phi_{k-1}, -i\bar{\phi}_k)$, $\Delta\varphi_k = (\varphi_k - \varphi_{k-1})$, and $\Delta\phi_k = (\phi_k - \phi_{k-1})$.

To obtain the expression of the generating function for the whole d-dimensional system in the continuum limit, some considerations have to be taken into account now:

- The increments of the fields can be expressed as:

$$\Delta\varphi_k = \Delta t\frac{\Delta\varphi_k}{\Delta t} \qquad\qquad \Delta\phi_k = \Delta t\frac{\Delta\phi_k}{\Delta t} \tag{B.1.35}$$

- The redefinition of the differentials:

$$\begin{aligned} \mathcal{D}\varphi_k &= \frac{d\varphi_k}{\sqrt{2\pi}} & \mathcal{D}\phi_k &= \frac{d\phi_k}{\sqrt{2\pi}} \\ \mathcal{D}\bar{\varphi}_k &= \frac{d\bar{\varphi}_k}{\sqrt{2\pi}} & \mathcal{D}\bar{\phi}_k &= \frac{d\bar{\phi}_k}{\sqrt{2\pi}} \end{aligned} \tag{B.1.36}$$

- The change $i\bar{\varphi} \to -i\bar{\varphi}$, and a subsequent **shift** in the response fields $\bar{\varphi} \to 1 + \bar{\varphi}$ and $\bar{\phi} \to 1 + \bar{\phi}$, which only gets rid of the exponentials for the last slice K.

- In the limit $\Delta t \to 0$, $\Delta t \Delta\varphi_k/\Delta t \to dt\partial_t\varphi$, $\Delta t \Delta\phi_k/\Delta t \to dt\partial_t\phi$ and, to the leading orders, $\Delta t H(\varphi_{k-1}, -i\bar{\varphi}_k, \phi_{k-1}, -i\bar{\phi}_k) \sim dt H(\varphi_k, -i\bar{\varphi}_k, \phi_k, -i\bar{\phi}_k)$.

- In a similar way, when the sum over sites is transformed into the continuous space integral, the fields change to *density fields*, due to the (dividing) volume factor appearing in the definition of the integral.

Taking into account these points, the final form for the generating function is:

$$Z = \int \mathcal{D}\varphi\mathcal{D}\bar{\varphi}\mathcal{D}\phi\mathcal{D}\bar{\phi} e^{-S(\varphi,\bar{\varphi},\phi,\bar{\phi})}, \tag{B.1.37}$$

where S is the action, defined as:

$$\begin{aligned} S(\varphi,\bar{\varphi},\phi,\bar{\phi}) = & \int d^dx \int dt \left[i\bar{\varphi}\partial_t\varphi + i\bar{\phi}\partial_t\phi + H(\varphi, 1 + i\bar{\varphi}, \phi, 1 + i\bar{\phi}) \right] \\ - & \int d^dx \left[(1 + i\bar{\varphi}_0) n_{A_0} + (1 + i\bar{\phi}_0) n_{B_0} \right] \end{aligned} \tag{B.1.38}$$

And, with the specific form of the Hamiltonian operator, a continuous equation for each set of original reaction-diffusion processes can be obtained.

Appendix C

Summary of Tables

In the following tables, the main results obtained in this thesis for the Conserved Directed Percolation (C-DP) universality class are collected. In order to easy-compare with Directed-Percolation (DP) class exponents, the critical exponents of this class can also be found in a specific section of this appendix. To check the consistency of the results, the scaling relations of chapters 2-4 can be used.

The appendix is organized in two sections: one devoted to the C-DP class-related exponents, and the other one, to the DP universality class. In each section, four different tables for each class can be found (three, for the DP case).

In the *first table*, are illustrated the exponents of each class itself, measured by means of isotropic bulk-driven (surface-free) experiments (see chapter 2).

Next, two different tables (one for DP) gather the exponents measured when activity spreads in the presence of one of the two different *surfaces* studied in chapter 3 (i.e. absorbing or reflecting walls).

In the last table are shown the critical exponents of the universality class resulting from anisotropy present in the propagation of activity (see chapter 3).

C.1 C-DP Universality Class

In this section, the best results for the C-DP class, obtained with both microscopic models and mesoscopic equations (Eqs.(2.66)), are shown. The critical exponents which take into account the spreading of a seed of activity have been measured by using the SOC and the FES ensemble, indistinctly (see chapter 2).

C-DP	$d = 1$	$d = 2$	Mean-Field†
θ	0.13(2)	0.50(5)	1
η	0.35(2)	0.23(5)	0
δ	0.17(2)	0.48(5)	1
z_{spr}	1.39(2)	1.28(5)	1
τ	1.11(2)	1.26(5)	3/2
τ_t	1.17(2)	1.48(5)	2
D_f	2.18(2)	2.67(5)	4
β	0.24(3)	$0.639(9)^{\dagger}$	1
$\nu_{\perp}$	1.33(3)	$0.799(14)^{\dagger}$	1/2
$\beta/\nu_{\perp}$	0.18(3)	0.85(8)	2
α	1.25(1)	0.75(2)	–
β_W	0.86(3)	0.48(1)	–
κ_W	0.17(3)	0^{+}	–

Table C.1

The exponents of this table have been measured in C-DP systems with periodic boundary conditions or by means of bulk-driven experiments. Due to the equivalence with the class of the quenched Edwards-Wilkinson equation (qEW), Eq.(4.1), (see chapter 4), the roughness-related exponents are taken from own measurements and [164, 171], from interfaces into this class. The exponents labeled with the subscript † are taken from [93, 112].

C.1.1 C-DP in the Presence of a Wall

The results of the following tables are obtained by imposing an absorbing or reflecting boundary condition next to the initial seed of an activity spreading experiment (see chapter 3). Therefore, only the related exponents are shown.

C-DP$_{abs}$	$d=1$
η	$-0.33(2)$
δ	$0.85(2)$
z_{spr}	$1.42(2)$
τ	$1.56(2)$
τ_t	$1.81(2)$
D_f	$2.14(2)$

Table C.2

C-DP$_{ref}$	$d=1$
η	$0.35(3)$
δ	$0.16(3)$
z_{spr}	$1.42(3)$
τ	$1.11(3)$
τ_t	$1.15(3)$
D_f	$2.13(3)$

Table C.3

The exponents of the C-DP reflecting surface (table C.3) coincide, within error bars, with the ones of the bulk-driven case, whereas the exponents of C-DP$_{abs}$ (table C.2) show a very different phenomenology.

C.1.2 C-DP with Anisotropy (A-C-DP Class)

To obtain the following exponents, a preferred direction is considered in the dynamics of a C-DP system. These exponents define a new universality class, *A-C-DP*.

A-C-DP	$d=1$		$d=2$	
η	0	$0.02(3)$	0	$0.03(5)$
δ	$1/2$	$0.45(3)$	$3/4$	$0.80(5)$
z_{spr}	2	$1.98(3)$	2	$2.02(5)$
τ	$4/3$	$1.31(3)$	$10/7$	$1.43(5)$
τ_t	$3/2$	$1.48(3)$	$7/4$	$1.75(5)$
D_f	$3/2$	$1.45(3)$	$7/4$	$1.75(5)$

Table C.4

C.2 DP Universality Class

Due to the high precision of the DP exponents avaliable in the literature, the exponents of the following table are taken from [79, 171, 183] and references therein, but also confirmed with own simulations (see chapters 2-4).

DP	$d = 1$	$d = 2$	Mean-Field
θ	0.15947(3)	0.4505(10)	1
η	0.31368(4)	0.2295(10)	0
δ	0.15947(3)	0.4505(10)	1
z_{spr}	1.26523(3)	1.1325(10)	1
τ	1.108(1)	1.268(1)	3/2
τ_t	1.159(1)	1.451(1)	2
D_f	2.328(1)	2.968(1)	4
β	0.27649(4)	0.583(4)	1
$\nu_\perp$	1.09684(1)	0.733(4)	1/2
$\beta/\nu_\perp$	0.252(3)	0.795(4)	2
α	1.33(1)	0.97(1)	–
β_W	0.839(1)	0.550(5)	–
κ_W	0.4336(4)	0.33(1)	–

Table C.5

C.2.1 Surface DP and Anisotropic DP

The exponents of the following tables are obtained by introducing a surface (left) or anisotropy (right) into the simulation of a DP model. As, in DP, both walls originate identical response for the system (called here surface DP, S-DP), only the results of the absorbing case are shown (see chapter 3 for the results obtained with the reflecting wall).

S-DP	$d = 1$
η	0.05(2)
δ	0.43(2)
z_{spr}	1.28(2)
τ	1.25(3)
τ_t	1.43(2)
D_f	2.31(2)

Table C.6

A-DP	$d = 1$
η	0.33(3)
δ	0.14(3)
z_{spr}	2.00(3)
τ	1.07(4)
τ_t	1.14(4)
D_f	2.30(2)

Table C.7

On the other hand, the DP class is Galilean invariant, and therefore its exponents remain unchanged in the presence of anisotropy.

Appendix D

Resumen en Castellano

Conceptos Básicos de SOC

Criticalidad Auto-Organizada (SOC, por sus siglas en inglés) es un término introducido por Bak, Tang and Wiesenfeld dirigido a explicar la ubicuidad de la invarianza de escala en la Naturaleza. Este comportamiento libre de escala (asumido en un principio como signo de criticalidad) sería el resultado de un mecanismo genérico común, presente en todos los sistemas dinámicos con muchos grados de libertad que interactúan (de los cuales la Naturaleza está plagada).

Hoy en día, es bien conocido que no todo el comportamiento libre de escala que se observa está causado por criticalidad emergente, sino que hay otros muchos mecanismos que pueden generar invarianza de escala fuera del equilibrio.

Sin embargo, aún hay otros sistemas en los cuales las características generales de SOC están presentes. Concretamente, los ingredientes básicos esenciales para la existencia de SOC son:

- Una lenta acumulación de una cierta magnitud física (tensión, energía, campo magnético ...). En este resumen se utilizará la energía, por simplicidad.
- Un nivel máximo para esta energía, definido para cada uno de los individuos que interactúan.
- Una regla conservativa para la redistribución de la energía cuando dicho nivel es superado.

- Una relajación rápida (en comparación con la escala temporal de la acumulación) de todos los sitios con energía por encima de ese nivel.

- Disipación de la energía sólo posible en los límites del sistema (finito).

Estas características pueden ser observadas en muchos sistemas diferentes, desde terremotos a superconductores de tipo II. Los cinco puntos comentados arriba dan lugar a **metaestabilidad** y **separación infinita de escalas temporales**, los dos ingredientes que, junto con la **conservación**, definen los ingredientes básicos de un sistema para mostrar comportamiento SOC.

El comportamiento de un sistema con estos ingredientes está dominado por una dinámica a saltos en la que avalanchas individuales pueden ser definidas. Mediante esas avalanchas, el parámetro dinámico del sistema (en este caso, la energía), es conducido hacia un estado estacionario en el que es mantenido alrededor de un valor específico. Por debajo de ese valor, las avalanchas pueden propagar su actividad sólo hasta una distancia finita de la semilla inicial. Por encima de dicho valor, la actividad (y, por tanto, la avalancha) nunca muere (en el límite termodinámico). Por tanto, el valor mencionado anteriormente es el **valor crítico** para el **parámetro de control**, y la actividad de una avalancha es el **parámetro de orden** del sistema.

Así, los observables que pueden ser definidos en la avalancha (por ejemplo, las distribuciones de probabilidad de su tamaño o duración) siguen una ley de potencias sólo limitada por el tamaño finito del sistema, que introduce un **corte** en la propagación de la actividad. Los sistemas con un conjunto común de exponentes críticos medidos a partir de esas leyes de potencias pueden ser agrupados en **clases de universalidad**.

Existen muchos modelos teóricos distintos, como por ejemplo los arquetípicos modelos de pila de arena, que permiten estudiar en profundidad este comportamiento. En estos modelos es posible identificar no sólo las condiciones bajo las cuales puede esperarse SOC, sino también los ingredientes básicos de cada una de sus clases de universalidad asociadas.

Por tanto, un sistema SOC puede ser considerado un sistema fuera del equilibrio cuya dinámica permite alcanzar un estado estacionario en el que su parámetro de control es mantenido alrededor del punto crítico de un cambio de fase de segundo orden y los observables relevantes muestran comportamiento libre de escala.

SOC como Cambio de Fase de Segundo Orden

El cambio de fase que sufre un sistema SOC es lo que se conoce como un **cambio de fase a estados absorbentes**, porque el punto crítico separa una fase supercrítica, con una propagación infinita de la actividad, y una fase subcrítica, en la que el sistema queda atrapado una vez entra en ella (**fase absorbente**). Y lo que es más, una avalancha es tan sólo un fenómeno en el que una semilla de actividad es colocada en un estado que, por lo demás, es absorbente, y los observables relacionados con la propagación de la actividad son medidos. Esto es, una avalancha es equivalente a los experimentos de propagación de actividad que se suelen llevar a cabo en los sistemas con estados absorbentes.

Aunque la clase de universalidad paradigmática de los sistemas con estados absorbentes es la conocida como **Percolación Dirigida** (DP, por sus siglas en inglés), la conservación presente en los sistemas SOC evitan que muestren el mismo comportamiento crítico definido por esta clase.

Típicamente, pueden distinguirse dos clases de universalidad muy diferentes en los modelos teóricos SOC conservados:

- La clase de universalidad de los sistemas con reglas de relajación deterministas (clase de las pilas de arena deterministas o de BTW).

- La clase de universalidad de los sistemas con reglas de relajación estocásticas (clase de las pilas de arena estocásticas o de Manna).

Concretamente, cuando los ingredientes básicos de ésta última son identificados, dos campos diferentes pueden ser definidos: *i)* un campo de actividad, cuya evolución es muy similar a la del parámetro de orden de DP, pero cuya dinámica está acoplada a *ii)* un campo conservado subyacente (que representa a los granos de arena microscópicos que se encuentran por debajo del nivel máximo antes mencionado), cuyo valor define si un sitio es activo o no.

Con estos campos, es posible construir una representación mesoscópica para la mencionada clase de universalidad. Como paso previo, es necesario antes llevar a cabo un proceso de **regularización** de la dinámica, después de la cual sólo quede una escala temporal e invarianza translacional esté presente en el sistema. Con este objetivo, la lenta adición externa de energía debe ser interrumpida y los bordes abiertos, ser reemplazados por condiciones de

contorno periódicas. De esta manera, la energía se conserva local y globalmente, y un formalismo conocido como de las **Pilas de Arena de Energía Conservada** (FES) queda definido.

En dicho entorno, SOC se vuelve un cambio de fase estándar entre un estado con actividad no-nula y un estado carente de actividad (el estado absorbente), en el que la energía actúa como el parámetro de control ajustable, dejando así de ser un sistema auto-organizado.

Usando los campos antes mencionados y este entorno, la ecuación mesoscópica que representa a esta clase de universalidad puede escribirse como:

$$\begin{cases} \partial_t \rho = & D_\rho \nabla^2 \rho + \mu\rho - \lambda\rho^2 + \omega\rho E + \sigma\sqrt{\rho}\eta(\vec{x},t) \\ \partial_t E = & D_E \nabla^2 \rho, \end{cases}$$

donde ρ y E son los campos de actividad y energía antes definidos, respectivamente, η es un ruido gaussiano y el resto de parámetros son sólo constantes. La forma del ruido se debe a una distribución poissoniana del número de eventos microscópicos de creación y aniquilación, que en este nivel mesoscópico quedan traducidos en un ruido gaussiano cuya varianza es proporcional a la tasa media del proceso (o sea, la actividad).

Este conjunto de ecuaciones de Lagevin define un sistema con un número infinito de estados absorbentes (estados con $\rho = 0$, en los que no hay evolución alguna de cualquiera de los campos) en el que la evolución del campo de actividad es, como ya se ha dicho, muy parecida a la que se encuentra en DP; pero también está acoplada a un campo conservado, cuya difusión (como es habitual en las pilas de arena) está limitada a la propagación de las avalanchas. Por tanto, la clase de universalidad de las pilas de arena microscópicas estocásticas puede ser, teniendo en cuenta estos rasgos mesoscópicos, llamada la clase de **Percolación Dirigida Conservada** (C-DP).

Comparación de las Clases de DP y C-DP

Aunque DP y C-DP son clases conceptualmente muy diferentes, la cercanía del valor de sus exponentes críticos (ver apéndice C) hace que, en ocasiones, sea difícil distinguir el comportamiento crítico real de sistemas que presentan largos transitorios en sus observables.

Sin embargo, la diferente respuesta de ambas clases a la presencia de ciertas perturbaciones puede ser útil para discernir la clase de universalidad de tales sistemas conflictivos.

Es bien conocido que los sistemas DP presentan invarianza galileana, o sea, su comportamiento crítico no es alterado cuando cierta anisotropía está presente en su dinámica. Una dirección privilegiada deja los exponentes críticos sin cambios, en este caso.

Por otro lado, la anisotropía constituye una perturbación relevante para la clase de universalidad de C-DP que, en presencia de este nuevo ingrediente, queda transformada en una nueva clase de universalidad, conocida como clase de C-DP anisotrópico (A-C-DP). Este coportamiento tan distinto puede ser utilizado como criterio de discriminación.

Cuando una superficie (por ejemplo, **absorbente** o **reflejante**) es introducida en un sistema DP al lado de la semilla de actividad inicial, mientras que las propiedades del interior (no relacionadas con la probabilidad de supervivencia) no sufren ningún cambio y no puede apreciarse estructura alguna en el campo de energía subyacente, el resto de observables cambian dramáticamente. Esta fenomenología, llamada aquí DP con superficie (S-DP), es muy distinta de la observada para los casos de C-DP.

Para un sistema C-DP en presencia de una pared reflejante, aunque aparece un perfil estructurado, todos los observables permanecen como en el caso sin superficie presente (dirigidos desde el interior). Por el contrario, cuando una superficie absorbente es introducida, no sólo aparece una estructura, sino que los exponentes relacionados con la probabilidad de supervivencia cambian, de una manera distinta al caso S-DP. Por tanto, en el caso de C-DP, pueden observarse dos fenomenologías diferentes: C-DP$_{ref}$ (donde los exponentes críticos son idénticos a los de C-DP) y C-DP$_{abs}$.

En todos los casos, la respuesta del sistema C-DP en presencia de una pared cláramente lo distinguen de un sistema DP. Así, ésto puede ser también usado como criterio de discriminación.

Usando las ya explicadas distintas reacciones de los sistemas DP y C-DP a tales perturbaciones, puede definirse un método para distinguir cuantitativamente ambas clases en casos conflictivos:

1.- Medir los exponentes críticos para el caso isotropico dirigido desde el interior, para tiempos y tamaños lo más grandes posibles.

2.- Introducir una pared reflejante en uno de los bordes, y la semilla de actividad de las avalanchas al lado de dicha pared. Si el exponente cambia, el sistema pertenece a DP. Por el contrario, si permancen inalterados, el sistema pertenece a C-DP.

3.- Reemplazar el caracter reflejante del muro por absorbente. Si los exponentes cambian respecto al caso isotrópico, y coinciden con los del apartado anterior, el sistema pertenece a DP. Si no, y son distintos a cualesquiera de los medidos hasta ahora, el sistema pertenece a C-DP.

4.- Definir una dirección privilegiada en la dinámica. Si los exponentes críticos no varían, el sistema pertenece a la clase de DP. Por el contrario, si cambian a los de la clase de A-C-DP, el sistema original pertenece a C-DP.

SOC como Cambio de Fase en Superficies

Es posible relacionar las características del cambio de fase presente en interfases elásticas en medios aleatorios, con los cambios de fase a estados absobentes del entorno FES.

La evolución de superficies elásticas en medios aleatorios están representadas por la **ecuación de Edwards-Wilkinson congelada** (qEW), que define la clase de universalidad de qEW, también conocida como clase del modelo de interfase lineal (LIM).

Esta ecuación describe la evoluvión de sistemas que sufren un cambio de fase continuo entre una fase activa (velocidad de propagación de la interfase $v \neq 0$) y una fase absorbente ($v = 0$), con un valor crítico para la fuerza externa que actúa como parámetro de control.

Lo que es más, puede ser definido un campo conservado subyacente (suma de todas las fuerzas deterministas presentes en el sistema) y, cuando los bordes del sistema son abiertos, un comportamiento a saltos con avalanchas puede ser observado si la fuerza externa es aumentada lentamente. Así, finalmente, se alcanza un estado estacionario invariante de escala.

Por tanto, no sólo los entornos FES y SOC pueden ser reconocidos en la clase LIM, sino que también las mismas simetrías e ingredientes pueden encontrarse. Así, para la clase LIM, se obtienen los mismos exponentes de C-DP, estableciendo que las interfases lineales elásticas en medios aleatorios y las pilas de arena estocásticas son sólo dos realizaciones diferentes del mismo fenómeno subyacente: SOC.

De hecho, es posible expresar la dinámica de una pila de arena estocástica microscópica mediante la ecuación qEW y, del mismo modo, traducir la dinámica microscópica de una interfase LIM en el conjunto de ecuaciones de Langevin de C-DP.

Que ambas clases representan la misma fenomenología puede ser mostrado mediante la medida directa de algunas funciones relacionadas con la forma renormalizada (mesoscópica) del potencial aleatorio microscópico de los sistemas LIM. La forma mesoscópica del potencial es la responsable del comportamiento con avalanchas de los sistemas LIM y, por tanto, las funciones que se midan deben coincidir con las de C-DP.

El espectacular colapso de las funciones medidas para la ecuacion qEW, los sistemas microscópicos LIM y ejemplos tanto micro como mesoscópicos de C-DP, confirma que LIM y C-DP comparten la misma física subyacente, y por tanto ambas son lenguajes equivalentes con los que SOC puede ser descrito.

El Papel de la Conservación en SOC

Aunque la conservación ha sido presentada aquí como una condición necesaria (y suficiente) para la existencia de SOC, hay muchos modelos teóricos no-conservados que dicen presentar comportamiento SOC. Es más, muchos ejemplos importantes de SOC en la Naturaleza, como por ejemplo los terremotos, son intrínsecamente no-conservados.

Es necesario distinguir dos tipos diferentes de conservación: global y local.

- **Conservación global** es la que se define en el formalismo FES, en el que la energía no puede ser introducida en ni perdida por el sistema. Este tipo de conservación puede ser violada en media y la criticalidad permanece inalterada. Este es el caso del formalismo SOC, en el que el nivel global de la energía es mantenido fluctuando alrededor de su valor crítico.

- **Conservación local** es la que está presente en lo que se ha definido aquí como sistemas conservados. La conservación local se cumple cuando las reglas de redistribución de la energía son estríctamente conservativas. Ésta es la conservación que se considera aquí necesaria para mantener el comportamiento crítico de un sistema SOC.

Cuando la conservación local está presente en un sistema SOC, la única manera en la que se puede disipar la energía que es introducida en el sistema es mediante avalanchas arbitrariamente grandes. Así, cualquier incremento de la energía debido a la introducción en una posición aleatoria del sistema de energía extra (durante el proceso de acumulación de la misma) puede alcanzar los bordes. Como disipaciones grandes son raramente necesarias en

contraste con las pequeñas, puede esperarse una forma de ley de potencias para, por ejemplo, la distribución de tamaños de avalancha.

Sin embargo, si la disipación local está presente, no es necesario alcanzar los bordes para alcanzar el estado estacionario, y por tanto ya no tendrá sentido que se desarrollen las avalanchas grandes. Esto introduce una longitud característica relevante en el sistema, un corte para el comportamiento invariante de escala de los observables. Así, aunque el sistema todavía se auto-organiza a un estado estacionario, este estado ya no es crítico, sino *subcrítico*.

Este argumento heurístico ilustra el comportamiento subcrítico observado para sistemas localmente disipativos. Sin embargo, para intentar compensar la energía disipada durante las avalanchas, se puede definir una **dinámica para el campo subyacente**.

Si esta dinámica se implementa entre avalanchas, el único cambio en el sistema es en las condiciones iniciales para la dinámica, pero la evolución permanece subcrítica. La implementación debe introducirse en el transcurso de las avalanchas.

Por supuesto, ninguna actividad extra puede ser creada durante la dinámica del campo subyacente, puesto que esto conduciría a la aparición de una escala característica. La única manera en la que este mecanismo puede ser usado para recuperar una evolución cuasi-crítica es definiendo una propagación localmente conservada **en media** para las avalanchas. Con este tipo de propagación, es posible controlar cuán lejos está el sistema de su comportamiento verdaderamente crítico (estrictamente conservado).

Así, aunque la verdadera criticalidad es tan sólo alcanzada mediante conservación local estricta, la conservación local en media constituye la única manera en la que esta condición puede ser relajada sin perder un régimen razonablemente grande de ley de potencias para los observables.

SOC en la Vida Real

Aunque se pueden definir muchos modelos teóricos para el estudio de SOC, no son tan numerosos los experimentos reales en los que los observables críticos en SOC pueden ser medidos con la suficiente seguridad y confianza.

El motivo por el que ésto sucede es que, en los sistemas reales, es normal encontrar no sólo los ingredientes de SOC, sino también ingredientes añadidos que pueden dificultar la observación de la invarianza de escala de los observables.

Este es el caso del ejemplo paradigmático de SOC, las pilas de arena, que en experimentos reales están afectadas por la **inercia**, que introduce una escala característica que impide la medida de leyes de potencia para cualquiera de sus observables.

La inercia puede ser evitada en sistemas granulares mediante el uso de *granos de arroz* en lugar de granos redondeados. También puede evitarse usando sistemas diferentes, como los superconductores de tipo II. Cuando éstos se colocan dentro de un campo magnético H, se crean vórtices en su superficie que penetran en su interior. Estos vórtices portan un cuanto de campo magnético que puede ser considerado un grano libre de inercia en este nuevo tipo de pila, en la que se almacena campo magnético interno (B) y pueden definirse **avalanchas superconductoras**. El frente de penetración de los vórtices puede ser también visto como una interfase, que evoluciona mediante "explosiones" de actividad en forma de avalanchas.

Para ambos (pilas de arroz y superconductores de tipo II), experimentos han sido llevados a cabo, y se han medido nítidas leyes de potencias. Estos ejemplos constituyen la mejor realización experimental de SOC observada hasta la fecha.

En sistemas como las redes neuronales también han sido observadas avalanchas libres de escala. Aunque algunos de los ingredientes necesarios para la existencia de SOC están presentes, la falta de conservación evita que SOC sea el mecanismo responsable de la invarianza de escala observada. En su lugar, otros mecanismos, como por ejemplo la topología de la red, pueden originar esta propagación con ley de potencias pero subcrítica de las avalanchas.

SOC no es, como se esperaba en un primer momento, una teoría general que explica la ubicuidad con la que se observan leyes de potencia en sistemas reales. Como se puede deducir del ejemplo anterior, no toda la invarianza de escala de la Naturaleza es debida a un comportamiento crítico. Sin embargo, aún existen muchos sistemas diferentes en los que puede ser observado el comportamiento en forma de eventos catastróficos de SOC. El conocimiento acumulado sobre esta teoría permite predecir bajo qué condiciones estos sistemas presentarán invarianza de escala. Aun así, todavía se está lejos de comprender exactamente hasta qué punto está SOC involucrado en los procesos que observamos en la Naturaleza, y que conforman el mundo en el que vivimos.

Appendix E

List of Publications

[P1] J. A. Bonachela, J. J. Ramasco, H. Chaté, I. Dornic, and M. A. Muñoz, *Sticky Grains do not Change the Universality Class of Isotropic Sandpiles*, Phys. Rev. E **74**, 050102(R) (2006).

[P2] O. Al Hammal, J. A. Bonachela, and M. A. Muñoz, *Absorbing State Phase Transitions with a Non-Accessible Vacuum*, J. Stat. Mech. P12007 (2006).

[P3] J. A. Bonachela, H. Chaté, I. Dornic, and M. A. Muñoz, *Absorbing States and Elastic Interfaces in Random Media: Two Equivalent Descriptions of Self-Organized Criticality*, Phys. Rev. Lett. **98**, 155702 (2007).

[P4] J. A. Bonachela and M. A. Muñoz, *How to Discriminate Easily Between Directed-Percolation and Manna Scaling*, Physica A **384**, 89 (2007).

[P5] J. A. Bonachela, H. Hinrichsen, and M. A. Muñoz, *Entropy Estimates of Small Data Sets*, J. Phys. A **41**, 202001 (2008).

[P6] J. A. Bonachela and M. A. Muñoz, *Confirming and Extending the Hypothesis of Universality in Sandpiles*, Phys. Rev. E **78**, 041102 (2008).

[P7] J. A. Bonachela, M. Alava, and M. A. Muñoz, *Cusps in Systems with (many) Absorbing States*, arXiv:condmat 0810.4395, *submitted to Phys. Rev. Lett.* (2008).

[P8] J. A. Bonachela and M. A. Muñoz, *Boundary-Induced Heterogeneous Absorbing States*, in *Modeling and Simulation of New Materials: Tenth*

Granada Lectures, Eds. P. L. Garrido, J. Marro and P. I. Hurtado, American Institute of Physics, to be published (2009).

[P9] A. C. Barato, C. E. Fiore, J. A. Bonachela, H. Hinrichsen, and M. A. Muñoz, *The Simplest Nonequilibrium Phase Transition into an Absorbing State*, to be published (2008).

[P10] J. A. Bonachela and M. A. Muñoz, *Non-Conservation in Self-Organized Criticality*, to be published (2008).

[P11] J. A. Bonachela, S. de Franciscis, J. J. Torres, and M. A. Muñoz, in preparation (2008).

Contributions to Conferences

- J. A. Bonachela, J.J. Ramasco, H. Chaté, I. Dornic, and M. A. Muñoz, *Non all Conservation Laws Alter the Directed Percolation Universality Class*, Modeling Cooperative Behavior in the Social Sciences: Eighth Granada Lectures, Eds. P. L. Garrido, J. Marro and M. A. Muñoz, American Institute of Physics (2005).

- J. A. Bonachela, H. Chaté, I. Dornic, and M. A. Muñoz, *Absorbing States and Pinned Interfaces in random media: Two descriptions of the same Phenomenon*, Congreso Nacional de Física Estadística FISES'06, Granada (Spain) (2006).

- C. E. Fiore, J. A. Bonachela and M. A. Muñoz, *Bosonic and Fermionic Descriptions for a Simple Nonequilibrium Model*, in *Modeling Cooperative Behavior in the Social Sciences: Ninth Granada Lectures*, Eds. P. L. Garrido, J. Marro, and J. J. Torres, American Institute of Physics (2007).

Bibliography

[1] P. Bak, *How Nature Works*, Springer-Verlag (1996).

[2] B. Gutenberg and C. F. Richter, *Seismicity of the Earth and Associated Phenomenon*, 2nd Ed., Princeton University Press (1954).

[3] B. Mandelbrot, *The Fractal Geometry of Nature*, Freeman (1982).

[4] M. E. J. Newman, *Power Laws, Pareto Distributions and Zipf's Law*, Contemp. Phys. **46**, 323 (2005).

[5] D. Sornette, *Critical Phenomena in Natural Sciences*, 2nd Ed., Springer (2006).

[6] P. Bak, C. Tang, and K. Wiesenfeld, *Self-Organized Criticality: An Explanation of 1/f Noise*, Phys. Rev. Lett. **59**, 381 (1987).

[7] R. Frigg, *Self-Organized Criticality: What it is and What it isn't*, Stud. Hist. Phil. Sci. **34**, 613 (2003).

[8] J. Horgan, *From Complexity to Perplexity*, Scient. Amer. **272**, 104 (1995).

[9] G. Grinstein, *Generic Scale Invariance and Self-Organized Criticality*, in *Scale Invariance, Interfaces and Non-Equilibrium Dynamics*, Proc. 1994 NATO Adv. Study Inst., Eds. A. McKane et al. (1995).

[10] T. Hwa and M. Kardar, *Avalanches, Hydrodynamics, and Discharge Events in Models of Sandpiles*, Phys. Rev. A **45**, 7002 (1992).

[11] R. Dickman, M. A. Muñoz, A. Vespignani, and S. Zapperi, *Paths to Self-Organized Criticality*, Braz. J. Phys. **30**, 27 (2000).

[12] Z. Olami, H. J. S. Feder, and K. Christensen, *Self-Organized Criticality in a Continuous, Nonconservative Cellular Automaton Modeling Earthquakes*, Phys. Rev. Lett. **68**, 1244 (1992).

[13] P. Bak, K. Chen, and C. Tang, *A Forest-Fire Model and Some Thoughts on Turbulence*, Phys. Lett. A **147**, 297 (1990).

[14] B. Drossel and F. Schwabl, *Self-Organized Critical Forest-Fire Model*, Phys. Rev. Lett. **69**, 1629 (1992).

[15] P. Bak and K. Sneppen, *Punctuated Equilibrium and Criticality in a Simple Model of Evolution*, Phys. Rev. Lett. **71**, 4083 (1993).

[16] H. J. Jensen, *Self-Organized Criticality*, Cambridge University Press (1998).

[17] D. Turcotte, *Self Organized Criticality*, Rep. Prog. Phys. **62**, 1377 (1999).

[18] K. Sneppen, *Self-Organized Pinning and Interface Growth in a Random Medium*, Phys. Rev. Lett. **69**, 3539 (1992).

[19] S. I. Zaitsev, *Robin Hood as Self-Organized Criticality*, Physica A **189**, 411 (1992).

[20] O. Peters, J. D. Neelin, *Critical Phenomena in Atmospheric Precipitation*, Nature Physics **2**, 393 (2006).

[21] O. Peters and K. Christensen, *Rain: Relaxations in the Sky*, Phys. Rev. E **66**, 036120 (2002).

[22] D. Stauffer and D. Sornette, *Self-Organized Percolation Model for Stock Market Fluctuations*, Physica A **271**, 496 (1999).

[23] E. T. Lu and R. J. Hamilton,*Avalanches and the Distribution of Solar Flares*, Astrophys. J. Lett. **380**, L89 (1991).

[24] B. Plourde, F. Nori, and M. Bretz, *Water Droplet Avalanches*, Phys. Rev. Lett. **71**, 2749 (1993).

[25] H. Takayasu and H. Inaoka, *New Type of Self-Organized Criticality in a Model of Erosion*, Phys. Rev. Lett. **68**, 966 (1992).

[26] A. Rinaldo, I. Rodriguez-Iturbe, R. Rigon, E. Ijjasz-Vasquez, and R. L. Bras, *Self-Organized Fractal River Networks*, Phys. Rev. Lett. **70**, 822 (1993).

[27] A. Rinaldo, A. Maritan, F. Colaiori, A. Flammini, R. Rigon, I. Rodriguez-Iturbe, and J. R. Banavan, *Thermodynamics of Fractal River Networks*, Phys. Rev. Lett. **76**, 3364 (1996).

[28] B. Malamud and D. Turcotte, *Self-Organized Criticality Applied to Natural Hazards*, Natural Hazards **20**, 93 (1999).

[29] R. Rigon, A. Rinaldo, and I. Rodriguez-Iturbe, *On Landscape Self-Organization*, Journal of Geophysical Research **99**, 11971 (2004).

[30] S. Hergarten, *Landslides, Sandpiles, and Self-Organized Criticality*, Nat. Hazards Earth Syst. Sci. **3**, 505 (2003).

[31] H. J. Jensen, *Lattice Gas as a Model of* $1/f$ *Noise*, Phys. Rev. Lett. **64**, 3103 (1990).

[32] A. V. Milovanov, K. Rypdal, and J. J. Rasmussen, *E-Pile Model of Self-Organized Criticality*, arXiv: cond-mat 0711.4571v1 (2007).

[33] P. Bak, C. Tang, and K. Wiesenfeld, *Self-Organized Criticality*, Phys. Rev. A **38**, 364 (1988).

[34] D. Dhar, *Self-Organized State of Sandpile Automata Models*, Phys. Rev. Lett.**64**, 1613 (1990).

[35] S. N. Majumdar and D. Dhar, *Height Correlations in the Abelian Sandpile Model*, J. Phys. A **24**, L357 (1991).

[36] S. N. Majumdar and D. Dhar, *Equivalence Between the Abelian Sandpile Model and the* $q \to 0$ *Limit of the Potts Model*, Physica A **185**, 129 (1992).

[37] K. Christensen, *On Self-Organized Criticality in One Dimension*, Physica A **340**, 527 (2004).

[38] E. V. Ivashkevich, D. V. Ktitarev, and V. B. Priezzhev *Critical Exponents for boundary avalanches in Two-Dimensional Abelian Sandpile Model*, J. Phys. A **27**, L585 (1994).

[39] V. B. Priezzhev, D. V. Ktitarev, and E. V. Ivashkevich, *Formation of Avalanches and Critical Exponents in an Abelian Sandpile Model*, Phys. Rev. Lett. **76**, 2093 (1996).

[40] M. De Menech, A. L. Stella, and C. Tebaldi, *Rare Events and Breakdown of Simple Scaling in the Abelian Sandpile Model*, Phys. Rev. E **58**, R2677 (1998).

[41] C. Tebaldi, M. De Menech, and A. L. Stella, *Multifractal Scaling in the Bak-Tang-Wiesenfeld Sandpile and Edge Events*, Phys. Rev. Lett. **83**, 3952 (1999).

[42] D. V. Ktitarev, S. Lübeck, P. Grassberger, and V. B. Priezzhev, *Scaling of Waves in the Bak-Tang-Wiesenfeld Sandpile Model*, Phys. Rev. E **61**, 81 (2000).

[43] B. Drossel, *Scaling Behavior of the Abelian Sandpile Model*, Phys. Rev. E **61**, R2168 (2000).

[44] D. Dhar, *Theoretical Studies of Self-Organized Criticality*, Physica A **369**, 29 (2006).

[45] P. Grassberger and S. S. Manna, *Some more Sandpiles*, J. Phys. (France) **51**, 1077 (1990).

[46] K. Christensen and Z. Olami, *Sandpile Models With and Without an Underlying Spatial Structure*, Phys. Rev. E **48**, 3361 (1993).

[47] Y.-C. Zhang, *Scaling Theory of Self-Organized Criticality*, Phys. Rev. Lett. **63**, 470 (1989).

[48] L. Pietronero, P. Tartaglia, and Y.-C. Zhang, *Theoretical Studies of Self-Organized Criticality*, Physica A **173**, 22 (1991).

[49] R. Pastor-Satorras and A. Vespignani, *Anomalous Scaling in the Zhang Model*, Eur. Phys. J. B **18**, 197 (2000).

[50] V. B. Priezzhev, *The Upper Critical Dimension of the Abelian Sandpile Model*, J. Stat. Phys. **98**, 667 (2000).

[51] D. Dhar and S. N. Majumdar, *Abelian Sandpile Model on the Bethe Lattice*, J. Phys. A **23**, 4333 (1990).

[52] T. E. Harris, *The Theory of Branching Processes*, Springer-Verlag (1963).

[53] L. P. Kadanoff, S. R. Nagel, L. Wu, and S.-M. Zhou, *Scaling and Universality in Avalanches*, Phys. Rev. A **39**, 6524 (1989).

[54] S. S. Manna, *Two-State Model of Self Organized Criticality*, J. Phys. A **24**, L363 (1991).

[55] A. Chessa, A. Vespignani, and S. Zapperi, *Critical Exponents in Stochastic Sandpile Models*, Comp. Phys. Com. **121**, 299 (1999).

[56] D. Dhar, *Some Results and a Conjecture for Manna's Stochastic Sandpile Model*, Physica A **270**, 69 (1999).

[57] V. Frette, K. Christensen, A. Malthe-Sørenssen, J. Feder, T. Jøssang, and P. Meakin, *Avalanche Dynamics in a Pile of Rice*, Nature **379**, 49 (1996).

[58] V. Frette, *Sandpile Models with Dynamically Varying Critical Slopes*, Phys. Rev. Lett. **70**, 2762 (1993).

[59] K. Christensen, A. Corral, V. Frette, J. Feder, and T. Jossang, *Tracer Dispersion in a Self-Organized Critical System*, Phys. Rev. Lett. **77**, 107 (1996).

[60] K. Christensen, N. R. Moloney, O. Peters, and G. Pruessner, *Avalanche Behavior in an Absorbing State Oslo Model*, Phys. Rev. E **70**, 067101 (2004).

[61] A. Ben-Hur and O. Biham, *Universality in Sandpile Models*, Phys. Rev. E **53**, R1317 (1996).

[62] E. Milshtein, O. Biham, and S. Solomon, *Universality Classes in Isotropic, Abelian, and Non-Abelian Sandpile Models*, Phys. Rev. E **58**, 303 (1998).

[63] A. Chessa, H. E. Stanley, A. Vespignani, and S. Zapperi, *Universality in Sandpiles*, Phys. Rev. E **59**, R12 (1999).

[64] R. Dickman and J. M. M. Campelo, *Avalanche Exponents and Corrections to Scaling for a Stochastic Sandpile*, Phys. Rev. E **67**, 066111 (2003).

[65] S. S. Manna and A. L. Stella, *Self-Organized Random Walks and Stochastic Sandpile: From Linear to Branched Avalanches*, Physica A **316**, 135 (2002).

[66] P. Pradhan and D. Dhar, *Probability Distribution of Residence Times of Grains in Models of Rice Piles*, Phys. Rev. E **73**, 021303 (2006).

[67] R. Dickman, A. Vespignani, and S. Zapperi, *Self-Organized Criticality as an Absorbing Phase Transition*, Phys. Rev. E **57**, 5095 (1998).

[68] A. Vespignani and S. Zapperi, *How Self-Organized Criticality Works: An Unified Mean-Field Picture*, Phys. Rev. E **57**, 6345 (1998).

[69] A. Vespignani, R. Dickman, M. A. Muñoz, and S. Zapperi, *Driving, Conservation and Absorbing States in Sandpiles*, Phys. Rev. Lett. **81**, 5676 (1998).

[70] A. Vespignani and S. Zapperi, *Order Parameter and Scaling Fields in Self-Organized Criticality*, Phys. Rev. Lett. **78**, 4793 (1997).

[71] M. Vergeles, A. Maritan, and J. R. Banavar, *Mean-Field Theory of Sandpiles*, Phys. Rev. E **55**, 1998 (1997).

[72] A. Chessa, E. Marinari, A. Vespignani, and S. Zapperi, *Mean-Field behavior of the Sandpile Model Below the Upper Critical Dimension*, Phys. Rev. E **57**, R6241 (1998).

[73] A. Barrat, A. Vespignani, and S. Zapperi, *Fluctuations and Correlations in Sandpile Models*, Phys. Rev. Lett. **83**, 1962 (1999).

[74] C. Tang and P. Bak, *Critical Exponents and Scaling Relations for Self-Organized Critical Phenomena*, Phys. Rev. Lett. **60**, 2347 (1988).

[75] A. Vespignani, R. Dickman, M. A. Muñoz, and S. Zapperi, *Absorbing Phase Transitions in Fixed-Energy Sandpiles*, Phys. Rev. E **62**, 4564 (2000).

[76] M. A. Muñoz, R. Dickman, R. Pastor-Satorras, A. Vespignani, and S. Zapperi, *Sandpiles and Absorbing-State Phase Transitions: Recent Results and Open Problems*, in *Proceedings of the 6th Granada Seminar on Computational Physics*, Eds. J. Marro and P. L. Garrido, Am. Inst. of Phys. **574**, 102 (2001).

[77] P. Grassberger and A. de la Torre, *Reggeon Field Theory (Schlögl's First Model) on a Lattice: Monte Carlo Calculations of Critical Behaviour*, Ann. Phys. (NY) **122**, 373 (1979).

[78] J. Marro and R. Dickman, *Nonequilibrium Phase Transitions in Lattice Models*, Cambridge University Press, Cambridge (1999).

[79] M.A. Muñoz, R. Dickman, A. Vespignani, and S. Zapperi, *Avalanche and Spreading Exponents in Systems with Absorbing States*, Phys. Rev. E **59**, 6175 (1999).

[80] I. Jensen and R. Dickman, *Nonequilibrium Phase Transitions in Systems with Infinitely Many Absorbing States*, Phys. Rev. E **48**, 1710 (1993).

[81] H. Hinrichsen, *Nonequilibrium Critical Phenomena and Phase Transitions into Absorbing States*, Adv. Phys. **49**, 815, (2000).

[82] H. K. Janssen, *On the Nonequilibrium Phase Transition in Reaction-Diffusion Systems with an Absorbing Stationary State*, Z. Phys. B **42**, 151 (1981).

[83] P. Grassberger, *On Phase Transitions in Schlögl's Second Model*, Z. Phys. B **47**, 365 (1982).

[84] P. C. Hohenberg and B. I. Halperin, *Theory of Dynamic Critical Phenomena*, Rev. Mod. Phys. **49**, 435 (1977).

[85] I. Jensen, *Critical Behavior of the Pair Contact Process*, Phys. Rev. Lett. **70**, 1465 (1993).

[86] M. A. Muñoz, G. Grinstein, R. Dickman, and R. Livi, *Critical Behavior of Systems with Many Absorbing States*, Phys. Rev. Lett. **76**, 451 (1996).

[87] M. A. Muñoz, G. Grinstein, and R. Dickman, *Phase Structure of Systems with Infinite Numbers of Absorbing States*, J. Stat. Phys. **91**, 541 (1998).

[88] G. Ódor, *Universality Classes in Nonequilibrium Lattice Systems*, Rev. Mod. Phys. **76**, 663 (2004).

[89] H. Hinrichsen, *Stochastic Lattice Models with Several Absorbing States*, Phys. Rev. E **55**, 219 (1997).

[90] M. Rossi, R. Pastor-Satorras, and A. Vespignani, *Universality Class of Absorbing Phase Transitions with a Conserved Field*, Phys. Rev. Lett. **85**, 1803 (2000).

[91] J. F. F. Mendes, R. Dickman, M. Henkel, and M. C. Marques, *Generalized Scaling for Models with Multiple Absorbing States*, J. Phys. A **27**, 3019 (1994).

[92] R. Dickman, M. Alava, M. A. Muñoz, J. Peltola, A. Vespignani, and S. Zapperi, *Phase transition in one-dimensional stochastic sandpiles* Phys. Rev. E **64**, 056104 (2001).

[93] S. Lübeck, *Universal Scaling Behavior of Non-Equilibrium Phase Transitions*, Int. J. Mod. Phys. B **18**, 3977 (2004).

[94] F. Bagnoli, F. Cecconi, A. Flammini, and A. Vespignani, *Short Period Attractors and Non-Ergodic Behavior in the deterministic Fixed-Energy Sandpile Model*, Europhys. Lett. **63**, 512 (2003).

[95] L. Dall'Asta, *Exact Solution of the One-Dimensional Deterministic Fixed-Energy Sandpile*, Phys. Rev. Lett. **96**, 058003 (2006).

[96] R. Pastor-Satorras and A. Vespignani, *Field Theory of Absorbing Phase Transitions with a Nondiffusive Conserved Field*, Phys. Rev. E **62**, R5875 (2000).

[97] F. van Wijland, K. Oerding, and H. J. Hilhorst, *Wilson Renormalization of a Reaction-Diffusion Process*, Physica A **251**, 179 (1998).

[98] J. E. de Freitas, L. S. Lucena, L. R. da Silva, and H. J. Hilhorst, *Critical Behavior of a Two-Species Reaction-Diffusion Problem*, Phys. Rev. E **61**, 6330 (2000).

[99] R. Pastor-Satorras and A. Vespignani, *Reaction-Diffusion System with Self-Organized Critical Behavior*, Eur. Phys. J. B **19**, 583 (2001).

[100] M. Doi, *Second Quantization Representation for Classical Many-Particle Systems*, J. Phys. A **9**, 1465 (1976).

[101] L. Peliti, *Path Integral Approach to Birth-Death Processes on a Lattice*, J. Physique **46**, 1469 (1985).

[102] B. P. Lee and J. Cardy, *Renormalization Group Study of the $A+B \to \emptyset$ Diffusion-Limited Reaction*, J. Stat. Phys. **80**, 971 (1995).

[103] A. Kamenev, *Keldysh and Doi-Peliti Techniques for out-of-Equilibrium Systems*, arXiv: cond-mat 0109316 (2001).

[104] J. Cardy, *Renormalisation Group Approach to Reaction-Diffusion Problems*, arXiv: cond-mat 9607163v2 (1996).

[105] B. P. Lee, *Critical Behavior in Non-Equilibrium Systems*, Ph.D. Thesis, University of California, U.S.A. (1994).

[106] L. Pechenik and H. Levine, *Interfacial Velocity Corrections Due to Multiplicative Noise*, Phys. Rev. E **59**, 3893 (1999).

[107] P. Grassberger and M. Scheunert, *Fock-Space Methods for Identical Classical Objects*, Fortschritte der Physik **28**, 547 (1980).

[108] A. Díaz-Guilera, *Noise and Dynamics of Self-Organized Critical Phenomena*, Phys. Rev. A **45**, 8551 (1992).

[109] A. Díaz-Guilera, *Dynamic Renormalization Group Approach to Self-Organized Critical Phenomena*, Europhys. Lett. **26**, 177 (1994).

[110] R. Dickman and R. Vidigal, *Path-Integral Representation for a Stochastic Sandpile*, J. Phys. A **35**, 7269 (2002).

[111] I. Dornic, H. Chaté, and M. A. Muñoz, *Integration of Langevin Equations with Multiplicative Noise and the Viability of Field Theories for Absorbing Phase Transitions*, Phys. Rev. Lett. **94**, 100601 (2005).

[112] J. J. Ramasco, M. A. Muñoz, and C. A. da Silva Santos, *Langevin theory of Self-organized-criticality.* Phys. Rev. E **69**, R045105 (2004).

[113] Frédéric van Wijland, *Universality Class of Nonequilibrium Phase Transitions with Infinitely Many Absorbing States*, Phys. Rev. Lett. **89**, 190602 (2002).

[114] Frédéric van Wijland, *Infinitely-Many Absorbing-State Nonequilibrium Phase Transitions*, Braz. J. Phys. **33**, 551 (2003).

[115] S. Lübeck and A. Hucht, *The Mean-Field Scaling Function of the Universality Class of Absorbing Phase Transitions with a Conserved Field*, J. Phys. A **35**, 4853 (2002).

[116] S. Lübeck and P. C. Heger, *Universal Scaling Behavior at the Upper Critical Dimension of Nonequilibrium Continuous Phase Transitions*, Phys. Rev. Lett. **90**, 230601 (2003).

[117] S. Lübeck, *Logarithmic Corrections of the Avalanche Distributions of Sandpile Models at the Upper Critical Dimension*, Phys. Rev. E **58**, 2957 (1998).

[118] S.-D. Zhang, *Universality and Self-Similarity of an Energy-Constrained Sandpile Model with Random Neighbors*, Phys. Rev. E **60**, 259 (1999).

[119] K. -I. Goh, D. -S. Lee, B. Kahng, and D. Kim, *Sandpile on Scale-Free Networks*, Phys. Rev. Lett. **91**, 148701 (2003).

[120] V. Colizza, R. Pastor-Satorras, and A. Vespignani, *Reaction-Diffusion Processes and Metapopulation Models in Heterogeneous Networks*, Nature Physics **3**, 276 (2007).

[121] G. Grinstein, D. -H. Lee, and S. Sachdev, *Conservation Laws, Anisotropy, and "Self-Organized Criticality" in Noisy Nonequilibrium Systems*, Phys. Rev. Lett. **64**, 1927 (1990).

[122] T. Hwa and M. Kardar, *Dissipative Transport in Open Systems: An Investigation of Self-Organized Criticality*, Phys. Rev. Lett. **62**, 1813 (1989).

[123] D. Dhar and R. Ramaswamy, *Exactly Solved Model of Self-Organized Critical Phenomena*, Phys. Rev. Lett. **63**, 1659 (1989).

[124] T. Tsuchiya and M. Katori, *Exact Results for the Directed Abelian Sandpile Models*, J. Phys. A **32**, 1629 (1999).

[125] J. C. Kimball and H. L. Frisch, *Random Walks, Avalanches and Branching Processes*, arXiv: cond-mat 0606454 (2006).

[126] E. Domany and W. Kinzel, *Equivalence of Cellular Automata to Ising to Ising Models and Directed Percolation*, Phys. Rev. Lett. **53**, 311 (1984).

[127] S. Maslov and Y. -C. Zhang, *Exactly Solved Model of Self-Organized Criticality*, Phys. Rev. Lett. **75**, 1550 (1995).

[128] V. B. Priezzhev, E. V. Ivashkevich, A. M. Povolotsky, and C. -K. Hu, *Exact Phase Diagram for an Asymmetric Avalanche Process*, Phys. Rev. Lett. **87**, 084301 (2001).

[129] R. Pastor-Satorras and A. Vespignani, *Critical Behavior and Conservation in Directed Sandpiles*, Phys. Rev. E **62**, 6195 (2000).

[130] R. Pastor-Satorras and A. Vespignani, *Universality Classes in Directed Sandpile Models*, J. Phys. A **33**, L33 (2000).

[131] M. Kloster, S. Maslov, and C. Tang, *Exact Solution of a Stochastic Directed Sandpile Model*, Phys. Rev. E **63**, 026111 (2001).

[132] M. Paczuski and K. E. Bassler, *Theoretical Results for Sandpile Models of Self-Organized Criticality with Multiple Topplings*, Phys. Rev. E **62**, 5347 (2000).

[133] G. Pruessner and H. J. Jensen, *Anisotropy and Universality: The Oslo Model, the Rice Pile Experiment, and the Quenched Edwards-Wilkinson Equation*, Phys. Rev. Lett. **91**, 244303 (2003).

[134] G. Pruessner, *Exact Solution of the Totally Asymmetric Oslo Model*, J. Phys. A **37**, 7455 (2004).

[135] M. Stapleton and K. Christensen, *Universality Class of One-Dimensional Directed Sandpile Models*, Phys. Rev. E **72**, 066103 (2005).

[136] D. Hughes and M. Paczuski, *Large Scale Structures, Symmetry, and Universality in Sandpiles*, Phys. Rev. Lett. **88**, 054302 (2002).

[137] M. Stapleton and K. Christensen, *One-Dimensional Directed Sandpile Models and the Area Under a Brownian Curve*, J. Phys. A **39**, 9107 (2006).

[138] K. Binder, in *Phase Transitions and Critical Phenomena*, Vol. 8, Eds. C. Domb and J. L. Lebowitz, Academic Press (1983).

[139] H. W. Diehl, in *Phase Transitions and Critical Phenomena*, Vol. 10, Eds. C. Domb and J. L. Lebowitz, Academic Press (1986).

[140] H. K. Janssen, B. Schaub, and B. Schmittmann, *The Effects of Surfaces on Directed Percolation and Related Stochastic Evolution Processes*, Z. Phys. B **72**, 111 (1988).

[141] P. Fröjdh, M. Howard, and K. B. Lauritsen, *Directed Percolation and Other Systems with Absorbing States: Impact of Boundaries*, Int. J. Mod. Phys. B **15** 1761 (2001).

[142] K. B. Lauritsen, K. Sneppen, M. Markošová, and M. H. Jensen, *Directed Percolation with an Absorbing Boundary*, Physica A **247**, 1 (1997).

[143] P. Fröjdh, M. Howard, and K. B. Lauritsen, *Directed Percolation with a Wall or Edge*, J. Phys. A **31**, 2311 (1998).

[144] H. Nakanishi and K. Sneppen, *Universal versus Drive-Dependent Exponents for Sandpile Models*, Phys. Rev. E **55**, 4012 (1997).

[145] A. Malthe-Sørenssen, *Tilted Sandpiles, Interface Depinning, and Earthquake Models*, Phys. Rev. E **59**, 4169 (1999).

[146] K. B. Lauritsen, P. Fröjdh, and M. Howard, *Surface Critical Behavior in Systems with Absorbing States*, Phys. Rev. Lett. **81**, 2104 (1998).

[147] J. W. Essam and D. TanlaKishani, *Directed Compact Percolation Near a Wall: I. Biased Growth*, J. Phys. A **27**, 3743 (1994).

[148] Z. Farkas and T. Fülöp, *One-Dimensional Drift Diffusion Between Two Absorbing Boundaries: Application to Granular Segregation*, J. Phys. A **34**, 3191 (2001).

[149] J. A. Bonachela and M. A. Muñoz, *Boundary-Induced Heterogeneous Absorbing States*, in *Modeling and Simulation of New Materials: Tenth Granada Lectures*, Eds. P. L. Garrido, J. Marro and P. I. Hurtado, American Institute of Physics, to be published (2009).

[150] B. Tadić and D. Dhar, *Emergent Spatial Structures in Critical Sandpiles*, Phys. Rev. Lett. **79**, 1519 (1997).

[151] P. K. Mohanty and D. Dhar, *Generic Sandpile Models Have Directed Percolation Exponents*, Phys. Rev. Lett. **89**, 104303 (2002).

[152] A. Vázquez and O. Sotolongo-Costa, *Universality Classes in the Random-Storage Sandpile Model*, Phys. Rev. E **61**, 944 (2000).

[153] A. Vázquez and O. Sotolongo-Costa, *Self-Organized Criticality and Directed Percolation*, J. Phys. A **32**, 2633 (1999).

[154] J. A. Bonachela, J. J. Ramasco, H. Chaté, I. Dornic, and M. A. Muñoz, *Sticky Grains do not Change the Universality Class of Isotropic Sandpiles*, Phys. Rev. E **74**, 050102(R) (2006).

[155] J. A. Bonachela and M. A. Muñoz, *How to Discriminate Easily Between Directed-Percolation and Manna Scaling*, Physica A **384**, 89 (2007).

[156] P. K. Mohanty and D. Dhar, *Critical Behavior of Sandpile Models with Sticky Grains*, Physica A **384**, 34 (2007).

[157] B. Tadić, *Scale-Free Energy Dissipation and Dynamic Phase Transition in Stochastic Sandpiles*, Phys. Rev. E **59**, 1452 (1999).

[158] S. Maslov and Y. -C. Zhang, *Self-Organized Critical Directed Percolation*, Physica A **223**, 1 (1996).

[159] J. A. Bonachela and M. A. Muñoz, *Confirming and Extending the Hypothesis of Universality in Sandpiles*, Phys. Rev. E **78**, 041102 (2008).

[160] T. Halpin-Healy and Y. -C. Zhang, *Kinetic Roughening Phenomena, Stochastic Growth, Directed Polymers and All That. Aspects of Multidisciplinary Statistical Mechanics*, Phys. Rep. **254**, 215 (1995).

[161] J. Koplik and H. Levine, *Interface Moving Through a Random Background*, Phys. Rev. B **32**, 280 (1985).

[162] O. Narayan, D. S. Fisher, *Threshold Critical Dynamics of Driven Interfaces in Random Media*, Phys. Rev. B **48**, 7030 (1993).

[163] T. Nattermann, S. Stepanow, L. -H. Tang, and H. Leschhorn, *Dynamics of Interface Depinning in a Disordered Medium*, J. Phys. II (France) **2**, 1483 (1992).

[164] H. Leschhorn, T. Nattermann, S. Stepanow, and L. -H. Tang, *Driven Interface Depinning in a Disordered Medium*, Ann. der Phys. **6**, 1 (1997).

[165] P. Chauve, P. Le Doussal, and K. J. Wiese, *Renormalization of Pinned Elastic Systems: How Does It Work Beyond One Loop?*, Phys. Rev. Lett. **86**, 1785 (2001).

[166] H. Leschhorn, *Interface Depinning in a Disordered Medium - Numerical Results*, Physica A **195**, 324 (1993).

[167] F. Family and T. Vicsek, *Scaling of the Active Zone in the Eden Process on Percolation Networks and the Ballistic Deposition Model*, J. Phys. A **18**, L75 (1985).

[168] J. Krug, *Turbulent Interfaces*, Phys. Rev. Lett. **72**, 2907 (1994).

[169] J. M. López, *Scaling Approach to Calculate Critical Exponents in Anomalous Surface Roughening*, Phys. Rev. Lett. **83**, 4594 (1999).

[170] M. Jost and K. D. Usadel, *On the Automaton Representation of the Edwards-Wilkinson Model with Quenched Disorder*, Physica A **255**, 15 (1998).

[171] J. Kockelkoren and H. Chaté, *Absorbing Phase Transitions with Coupling to a Static Field and a Conservation Law*, arXiv: cond-mat 0306039 (2003).

[172] A. I. Larkin, *Effect of Inhomogeneities on the Structure of the Mixed State of Superconductors*, Sov. Phys. JETP **31**, 784 (1970).

[173] M. Paczuski, S. Maslov, and P. Bak, *Avalanche Dynamics in Evolution, Growth, and Depinning Models*, Phys. Rev. E **53**, 414 (1996).

[174] O. Narayan and A. A. Middleton, *Avalanches and the Renormalization Group for Pinned Charge-Density Waves*, Phys Rev. B **49**, 244 (1994).

[175] S. F. Edwards and D. R. Wilkinson, *The Surface Statistics of a Granular Aggregate*, Proc. R. Soc. London, Ser. A **381**, 17 (1982).

[176] M. Alava and M. A. Muñoz, *Interface Depinning versus Absorbing-State Phase Transitions*, Phys. Rev. E **65**, 026145 (2002).

[177] M. Paczuski and S. Boettcher, *Universality in Sandpiles, Interface Depinning, and Earthquake Models*, Phys. Rev. Lett. **77**, 111 (1996).

[178] M. Marsili, *Run Time Statistics in Models of Growth in Disordered Media*, J. Stat. Phys. **77**, 733 (1994).

[179] M. Alava and K. B. Lauritsen, *Quenched Noise and Over-Active Sites in Sandpile Dynamics*, Europhys. Lett. **53**, 569 (2001).

[180] M. Alava, *Self-Organized Criticality as a Phase Transition*, in *Advances in Condensed Matter and Statistical Physics*, Eds. E. Korutcheva and R. Cuerno, Nova Science Publishers (2004).

[181] C. M. Aegerter, R. Günter, and R. J. Wijngaarden, *Avalanche Dynamics, Surface Roughening, and Self-Organized Criticality: Experiments on Three-Dimensional Pile of Rice*, Phys. Rev. E **67**, 051306 (2003).

[182] M. Alava, *Scaling in Self-Organized Criticality from Interface Depinning?*, J. Phys. Cond. Mat. **14**, 2353 (2002).

[183] R. Dickman and M. A. Muñoz, *Interface Scaling in the Contact Process*, Phys. Rev. E **62**, 7632 (2000).

[184] G. Pruessner, *Oslo Rice Pile Model is a Quenched Edwards-Wilkinson Equation*, Phys. Rev. E **67**, 030301 (2003).

[185] J. A. Bonachela, H. Chaté, I. Dornic, and M. A. Muñoz, *Absorbing States and Elastic Interfaces in Random Media: Two Equivalent Descriptions of Self-Organized Criticality*, Phys. Rev. Lett. **98**, 155702 (2007).

[186] K. J. Wiese and P. Le Doussal, *Functional Renormalization for Disordered Systems. Basic Recipes and Gourmet Dishes*, Markov Processes and Relat. Fields **13**, 777 (2007).

[187] A. A. Middleton, P. Le Doussal, and K. J. Wiese, *Measuring Functional Renormalization Group Fixed-Point Functions for Pinned Manifolds*, Phys. Rev. Lett. **98**, 155701 (2007).

[188] P. Le Doussal and K. J. Wiese, *How to Measure Functional Renormalization Group Fixed-Point Functions for Dynamics and at the Depinning*, Europhys. Lett. **77**, 66001 (2007).

[189] A. Rosso, P. Le Doussal, and K. J. Wiese, *Numerical Calculation of the Functional Renormalization Group Fixed-Point Functions at the Depinning Transition*, Phys. Rev. B **75**, 220201 (2007).

[190] J. A. Bonachela, M. Alava, and M. A. Muñoz, *Cusps in Systems with (many) Absorbing States*, arXiv: cond-mat 0810.4395, *submitted to Phys. Rev. Lett.* (2008).

[191] T. Hwa and M. Kardar, *Fractals and Self-Organized Criticality in Dissipative Dynamics*, Physica D **38**, 198 (1992).

[192] B. Tadić, U. Nowak, K. D. Usadel, R. Ramaswamy, and S. Padlewski, *Scaling Behavior in Disordered Sandpile Automata*, Phys. Rev. A **45**, 8536 (1992).

[193] B. Tadić and R. Ramaswamy, *Criticality in Driven Cellular Automata with Defects*, Physica A **224**, 188 (1996).

[194] E. Jettestuen and A. Malthe-Sørenssen, *Scaling Properties of a One-Dimensional Sandpile Model with Grain Dissipation*, Phys. Rev. E **72**, 062302 (2005).

[195] E. Noether, *Invariante Variationsprobleme*, Nachr. d. König. Gesellsch. d. Wiss. zu Göttingen, Math-phys. Klasse 235257 (1918).

[196] S. Zapperi, K. B. Lauritsen, and H. E. Stanley, *Self-Organized Branching Processes: Mean-Field Theory for Avalanches*, Phys. Rev. Lett. **75**, 4071 (1995).

[197] K. B. Lauritsen, S. Zapperi, and H. E. Stanley, *Self-Organized Branching Processes: Avalanche Models with Dissipation*, Phys. Rev. E **54**, 2483 (1996).

[198] T. Tsuchiya and M. Katori, *Proof of Breaking of Self-Organized Criticality in a Nonconservative Abelian Sandpile Model*, Phys. Rev. E **61**, 1183 (2000).

[199] C. Vanderzande and F. Daerden, *Dissipative Abelian Sandpiles and Random Walks*, Phys. Rev. E **63**, 030301 (R) (2001).

[200] M. R. Spiegel, *Complex Variables*, Schaum Publishing, McGraw-Hill (1991).

[201] L. E. Blumenson, *A Derivation of n-Dimensional Spherical Coordinates*, Amer. Math. Monthly **67**, 63 (1960).

[202] I. S. Gradshteyn and I. M. Ryzhik, *Table of Integrals, Series, and Products*, 7th Edition, Academic Press (2007).

[203] P. Bak and C. Tang, *Earthquakes as a Self-Organized Critical Phenomenon*, J. Geophys. Res. **94**, 15635 (1989).

[204] K. Chen, P. Bak, and S. P. Obukhov, *Self-Organized Criticality in a Crack-Propagation Model of Earthquakes*, Phys. Rev. A **43**, 625 (1991).

[205] R. Burridge and L. Knopoff, *Model and Theoretical Seismicity*, Bull. Seismol. Soc. Am. **57** 341 (1967).

[206] H. J. S. Feder and J. Feder, *Self-Organized Criticality in a Stick-Slip Process*, Phys. Rev. Lett. **66**, 2669 (1991).

[207] P. Bak, *Self-Organized Criticality in Non-Conservative Models*, Physica A, **191**, 41 (1992).

[208] K. Christensen, Z. Olami, and P. Bak, *Deterministic* $1/f$ *Noise in Nonconservative Models of Self-Organized Criticality*, Phys. Rev. Lett. **16**, 2417 (1992).

[209] K. Christensen and Z. Olami, *Scaling, Phase Transitions, and Nonuniversality in a Self-Organized Critical Cellular Automaton Model*, Phys. Rev. A **46**, 1829 (1992).

[210] J. E. S. Socolar, G. Grinstein, and C. Jayaprakash, *On Self-Organized Criticality in Nonconserving Systems*, Phys. Rev. E **47**, 2366 (1993).

[211] P. Grassberger, *Efficient Large-Scale Simulations of a Uniformly Driven System*, Phys. Rev. E **49**, 2436 (1994).

[212] A. A. Middleton and C. Tang, *Self-Organized Criticality in Nonconserved Systems*, Phys. Rev. Lett. **74**, 742 (1995).

[213] S. Lise and H. J. Jensen, *Transitions in Nonconserving Models of Self-Organized Criticality*, Phys. Rev. Lett. **76**, 2326 (1996).

[214] P. Ghaffari, S. Lise, and H. J. Jensen, *Nonconservative Sandpile Models*, Phys. Rev. E **56**, 6702 (1997).

[215] H. -M. Bröker and P. Grassberger, *Random Neighbor Theory of the Olami-Feder-Christensen Earthquake Model*, Phys. Rev. E **56**, 3944 (1997).

[216] B. D. Malamud, G. Morein, and D. L. Turcotte, *Forest Fires: An Example of Self-Organized Critical Behavior*, Science **281**, 1840 (1998).

[217] G. Caldarelli, R. Frondoni, A. Gabrielli, M. Montuori, R. Retzlaff, and C. Ricotta, *Percolation in Real Wildfires*, Europhys. Lett. **56**, 510 (2001).

[218] K. Chen, P. Bak and M. H. Jensen, *A Deterministic Forest Fire Model*, Phys. Lett. A **149**, 207 (1990).

[219] P. Grassberger, *On a Forest Fire Model with Supposed Self-Organized Criticality*, J. Stat. Phys. **63**, 685 (1991).

[220] K. Christensen, H. Flyvbjerg, and Z. Olami, *Self-Organized Critical Forest-Fire Model: Mean-Field Theory and Simulation Results in 1 to 6 Dimensions*, Phys. Rev. Lett. **71**, 2737 (1993).

[221] B. Drossel, S. Clar, and F. Schwabl, *Exact Results for the One-Dimensional Self-Organized Critical Forest-Fire Model*, Phys. Rev. Lett. **71**, 3739 (1993).

[222] C. Henley, *Statics of a "Self-Organized" Percolation Model*, Phys. Rev. Lett. **71**, 2741 (1993).

[223] P. Grassberger, *On a Self-Organized Critical Forest-Fire Model*, J. Phys. A **26**, 2081 (1993).

[224] S. Clar, B. Drossel, and F. Schwabl, *Forest Fires and Other Examples of Self-Organized Criticality*, J. Phys.: Condens. Matter **8**, 6803 (1996).

[225] K. Schenk, B. Drossel, S. Clar, and F. Schwabl, *Finite-Size Effects in the Self-Organized Critical Forest-Fire Model*, Eur. Phys. J. B **15**, 177 (2000).

[226] R. Pastor-Satorras and A. Vespignani, *Corrections to Scaling in the Forest-Fire Model*, Phys. Rev. E **61**, 4854 (2000).

[227] V. Loreto, L. Pietronero, A. Vespignani, and S. Zapperi, *Renormalization Group Approach to the Critical Behavior of the Forest-Fire Model*, Phys. Rev. Lett. **75**, 465 (1995).

[228] A. Honecker and I. Peschel, *Length Scales and Power Laws in the Two-Dimensional Forest-Fire Model*, Physica A **239**, 509 (1997).

[229] P. Grassberger, *Critical Behaviour of the Drossel-Schwabl Forest Fire Model*, New J. Phys. **4**, 17 (2002).

[230] G. Pruessner and H. J. Jensen, *Broken Scaling in the Forest-Fire Model*, Phys. Rev. E **65**, 056707 (2002).

[231] D. E. Juanico, C. Monterola, and C. Saloma, *Self-Organized Critical Branching in Systems that Violate Conservation Laws*, New J. Phys. **9**, 92 (2007).

[232] J. A. Bonachela and M. A. Muñoz, *Non-Conservation in Self-Organized Criticality*, to be published (2008).

[233] G. Pruessner and H. J. Jensen, *A Solvable Non-Conservative Model of Self-Organised Criticality*, Europhys. Lett. **58**, 250 (2002).

[234] S. S. Manna, L. B. Kiss, and J. Kertész, *Cascades and Self-Organized Criticality*, J. Stat. Phys. **61**, 923 (1990).

[235] K. A. Takeuchi, M. Kuroda, H. Chaté, and M. Sano, *Directed Percolation Criticality in Turbulent Liquid Crystals*, Phys. Rev. Lett. **99**, 234503 (2007).

[236] H. M. Jaeger, C.-H. Liu, and S. R. Nagel, *Relaxation at the Angle of Repose*, Phys. Rev. Lett. **62**, 40 (1989).

[237] H. J. Jensen, K. Christensen, and H. C. Fogedby, $1/f$ *Noise, Distribution of Lifetimes, and a Pile of Sand*, Phys. Rev. B **40**, 7425 (1989).

[238] G. A. Held, D. H. Solina, II, D. T. Keane, W. J. Haag, P. M. Horn, and G. Grinstein, *Experimental Study of Critical-Mass Fluctuations in an Evolving Sandpile*, Phys. Rev. Lett. **65**, 1120 (1990).

[239] S. R. Nagel, *Instabilities in a Sandpile*, Rev. Mod. Phys. **64**, 321 (1992).

[240] M. Bretz, J. B. Cunningham, P. L. Kurczynski, and F. Nori, *Imaging of Avalanches in Granular Materials*, Phys. Rev. Lett. **69**, 2431 (1992).

[241] J. Rosendahl, M. Vekić, and J. Kelley, *Persistent Self-Organization of Sandpiles*, Phys. Rev. E **47**, 1401 (1993).

[242] J. Feder, *The Evidence for Self-Organized Criticality in Sandpile Dynamics*, Fractals **3**, 431 (1995).

[243] C. P. C. Prado and Z. Olami, *Inertia and Break of Self-Organized Criticality in Sandpile Cellular-Automata Models*, Phys. Rev. A **45**, 665 (1992).

[244] E. Altshuler, O. Ramos, C. Martínez, L. E. Flores, and C. Noda, *Avalanches in One-Dimensional Piles with Different Types of Bases*, Phys. Rev. Lett. **86**, 5490 (2001).

[245] L. Corté, P. M. Chaikin, J. P. Gollub, and D. J. Pine, *Random Organization in Periodically Driven Systems*, Nature Physics **4**, 420 (2008).

[246] S. Zapperi, P. Cizeau, G. Durin, and H. E. Stanley, *Dynamics of a Ferromagnetic Domain Wall: Avalanches, Depinning Transition, and the Barkhausen Effect*, Phys. Rev. B **58**, 6353 (1998).

[247] P. G. de Gennes, *Superconductivity of Metals and Alloys*, W. A. Benjamin (1966).

[248] C. P. Bean, *Magnetization of Hard Superconductors*, Phys. Rev. Lett. **8**, 250 (1962).

[249] E. Altshuler and T. H. Johansen, *Experiments in Vortex Avalanches*, Rev. Mod. Phys. **76**, 471 (2004).

[250] K. E. Bassler and M. Paczuski, *Simple Model of Superconducting Vortex Avalanches*, Phys. Rev. Lett. **81** 3761 (1998).

[251] S. Field, J. Witt, F. Nori, and X. Ling, *Superconducting Vortex Avalanches*, Phys. Rev. Lett. **74**, 1206 (1995).

[252] R. J. Zieve, T. F. Rosenbaum, H. M. Jaeger, G. T. Seidler, G. W. Crabtree and U. Welp, *Vortex Avalanches at One Thousandth the Superconducting Transition Temperature*, Phys. Rev. B **53**, 11849 (1996).

[253] M. S. Welling, C. M. Aegerter, and R. J. Wijngaarden, *Self-Organized Criticality Induced by Quenched Disorder: Experiments on Flux Avalanches in NbH_x Films*, Phys. Rev. B **71**, 104515 (2005).

[254] O. Plá, N. K. Wilkin, and H. J. Jensen, *Avalanches in the Bean Critical State: A Characteristic of the Random Pinning Potential*, Europhys. Lett. **33**, 297 (1996).

[255] K. Behnia, C. Capan, D. Mailly, and B. Etienne, *Internal Avalanches in a Pile of Superconducting Vortices*, Phys. Rev. B **61**, R3815 (2000).

[256] C. M. Aegerter, M. S. Welling, and R. J. Wijngaarden, *Self-Organized Criticality in the Bean State in $YBa_2Cu_3O_{7-x}$ Thin Film*, Europhys. Lett. **65**, 753 (2004).

[257] R. J. Wijngaarden, M. S. Welling, C. M. Aegerter, and M. Menghini, *Avalanches and Self-Organized Criticality in Superconductors*, Eur. Phys. J. B **50**, 117 (2006).

[258] V. K. Vlasko-Vlasov, U. Welp, V. Metlushko, and G. W. Crabtree, *Experimental Test of the Self-Organized Criticality of Vortices in Superconductors*, Phys. Rev. B **69**, 140504(R) (2004).

[259] M. S. Welling, C. M. Aegerter, and R. J. Wijngaarden, *Noise Correction for Roughening Analysis of Magnetic Flux Profiles in $YBa_2Cu_3O_{7-x}$*, Eur. Phys. J. B **38**, 93 (2004).

[260] C. M. Aegerter, M. S. Welling, and R. J. Wijngaarden, *Dynamic Roughening of the Magnetic Flux Landscape in $YBa_2Cu_3O_{7-x}$*, Physica A **347**, 363 (2005).

[261] J. M. Beggs and D. Plenz, *Neuronal Avalanches in Neocortical Circuits*, J. Neurosci. **23**, 11167 (2003).

[262] J. M. Beggs and D. Plenz, *Neuronal Avalanches Are Diverse and Precise Activity Patterns That Are Stable for Many Hours in Cortical Slice Cultures*, J. Neurosci. **24**, 5216 (2004).

[263] J. M. Beggs, *The Criticality Hypothesis: How Local Cortical Networks Might Optimize Information Processing*, Phil. Trans. R. Soc. A **366**, 329 (2008).

[264] R. Albert and A.-L. Barabási, *Statistical Mechanics of Complex Networks*, Rev. Mod. Phys. **74**, 47 (2002).

[265] C. Bédard, H. Kröger, and A. Destexhe, *Does the $1/f$ Frequency Scaling of Brain Signals Reflect Self-Organized Critical States?*, Phys. Rev. Lett. **97**, 118102 (2006).

[266] J. A. Bonachela, S. de Franciscis, J. J. Torres, and M. A. Muñoz, in preparation (2008).

[267] S. Royer and D. Paré, *Conservation of Total Synaptic Weight Through Balanced Synaptic Depression and Potentiation*, Nature **422**, 518 (2003).

[268] L. de Arcangelis, C. Perrone-Capano, and H. J. Herrmann, *Self-Organized Criticality Model for Brain Plasticity*, Phys. Rev. Lett. **96**, 028107 (2006).

[269] D. E. Juanico and C. Monterola, *Background Activity Drives Criticality of Neuronal Avalanches*, J. Phys. A **40**, 9297 (2007).

[270] A. Levina, J. M. Herrmann, and T. Geisel, *Dynamical Synapses Causing Self-Organized Criticality in Neural Networks*, Nature Physics **3**, 857 (2007).

[271] H. Markram and M. Tsodyks, *Redistribution of Synaptic Efficacy Between Neocortical Pyramidal Neurons*, Nature **382**, 807 (1996).

[272] A. Levina, J. M. Herrmann, and T. Geisel, *Dynamical Synapses Give Raise to a Power-Law Distribution of Neuronal Avalanches*, in *Advances in Neural Information Processing Systems* **18**, 771 (Eds. Y. Weiss, B. Schölkopf, and J. Platt), MIT Press (2006).

[273] C. W. Eurich, J. M. Herrmann, and U. A. Ernst, *Finite-Size Effects of Avalanche Dynamics*, Phys. Rev. E **66**, 066137 (2002).

[274] G. Grinstein and R. Linsker, *Synchronous Neural Activity in Scale-Free Network Models Versus Random Network Models*, Proc. Natl. Acad. Sci. USA **102**, 9948 (2005).

[A1] J. Biel, *Curso sobre el Formalismo y los Métodos de la Termodinámica*, Ed. Reverté (1998).

[A2] J. J. Binney, N. J. Dowrick, A. J. Fisher, and M. E. J. Newman, *The Theory of Critical Phenomena*, Claredon Press, Oxford (1992).

[A3] A. -L. Barabási, H. E. Stanley, *Fractal Concepts in Surface Growth*, Cambridge University Press (1995).

[A4] L. E. Reichl, *A Modern Course in Statistical Physics*, 2nd Edition, John Wiley and Sons (1998).

[A5] N. G. Van Kampen, *Stochastic Processes in Physics and Chemistry*, 6th Edition, North Holland, Elsevier Science Publishers (1990).